U.PORTO

DOUTORAMENTO EM CIÊNCIAS FARMACÊUTICAS
FITOQUIÍMICA E FARMACOGNOSIA

The natural product chemical space for modulating endoplasmic reticulum stress in chronic diseases

Daniela Correia da Silva

D

2023

U.PORTO

FACULDADE DE FARMÁCIA
UNIVERSIDADE DO PORTO

The natural product chemical space for modulating endoplasmic reticulum stress in chronic diseases

Daniela Correia da Silva

Thesis for Doctor Degree in Pharmaceutical Sciences
Phytochemistry and Pharmacognosy specialty

Under the supervision of:
Prof. Doctor David Pereira

And co-supervision of:
Prof. Doctor Patrícia Valentão

April, 2023

“You should laugh every moment you live,
for you'll find it decidedly difficult afterwards.”

Joe Abercrombie

The work developed throughout this thesis was financially supported by FCT/MCTES through national funds (UIDB/50006/2020 and UIDP/50006/2020). The candidate extends special thanks to the Fundação para Ciência e Tecnologia (FCT) for the doctoral grant (SFRH/BD/130998/2017) and its exceptional extension (COVID/BD/152734/2022).

PUBLICATIONS

The following publications contain the work developed throughout the course of this thesis.

Publications in indexed international peer-reviewed journals:

Correia da Silva D, Valentão P, Andrade PB, Pereira DM. Endoplasmic reticulum stress signaling in cancer and neurodegenerative disorders: Tools and strategies to understand its complexity. Pharmacological Research 2020; 155:104702.

Correia da Silva D, Valentão P, Andrade PB, Pereira DM. A pipeline for natural small molecule inhibitors of endoplasmic reticulum stress. Frontiers in Pharmacology, 2022, 13, 956154.

Correia da Silva D, Valentão P, Pereira DM. A survey of naturally occurring molecules as new endoplasmic reticulum stress activators with selective anticancer activity. Cancers, 2023, 15(1), 293.

Correia da Silva D, Valentão P, Pereira DM. Naturally occurring small molecules with dual effect upon inflammatory signaling pathways and endoplasmic reticulum stress response. (Submitted)

Correia da Silva D, Jervis PJ, Martins JA, Valentão P, Ferreira PMT, Pereira DM. Fisetin derivatives exhibit enhanced anti-inflammatory activity and modulation of endoplasmic reticulum stress. International Immunopharmacology, 2023, 119, 110178.

Oral communications:

Correia da Silva D, Valentão P, Andrade PB, Pereira DM. ER stress and inflammation: towards natural product-derived modulators of ER stress. Natural Products in Drug Discovery and Human Health (NatProdDDH) - PSE Meeting 2019. 28-31 July 2019, Lisbon, Portugal.

Correia da Silva D, Valentão P, Andrade PB, Pereira DM. Polyphenolic modulators of endoplasmic reticulum stress as anticancer agents. International IBERPHENOL Conference: "Advances in the role of phenols in health effects and other uses". 5-6 November 2020, Coimbra, Portugal.

Correia da Silva D, Valentão P, Andrade PB, Pereira DM. A drug discovery pipeline for endoplasmic reticulum stress inhibitors. 14th National Organic Chemistry Meeting & 7th National Medicinal Chemistry Meeting. 20-22 April 2022, Almada, Portugal.

Poster communications:

Correia da Silva D, Valentão P, Andrade PB, Pereira DM. Towards polyphenol modulators of inflammation and endoplasmic reticulum stress. 9th International Conference on Polyphenols and Health. 28 November-1 December 2019, Kobe, Japan.

Correia da Silva D, Valentão P, Andrade PB, Pereira DM. A drug discovery pipeline for endoplasmic reticulum stress inhibitors from natural products. Encontro Ciência '21. 28-30 June 2022, Lisboa, Portugal.

AUTHOR STATEMENT

The author states to have had a major contribution to the technical execution, interpretation of the results and manuscript preparation of all works included in this thesis, with the collaboration of other co-authors.

ACKNOWLEDGEMENTS

O percurso que passa agora pela escrita destas linhas não se teria materializado de igual forma sem a participação e apoio daqueles que irei aqui assinalar.

Em primeiro lugar, expresso a minha gratidão à Fundação para a Ciência e Tecnologia FCT pela atribuição da bolsa de doutoramento que me permitiu percorrer esta jornada.

Estarei sempre grata ao meu Orientador, Prof. Doutor David Pereira, por tudo o que me ensinou, por ser uma parte tão importante deste trabalho, por ter confiado tantas vezes em mim, tendo-me apoiado melhor do que eu soube fazer. Nunca me vou esquecer de si.

À minha Coorientadora, Prof. Doutora Patrícia Valentão, agradeço o interesse demonstrado, a presença, garantida sempre que necessária, e por ter *sempre* algo pertinente a acrescentar.

Agradeço ao Peter Jervis, José Martins e Paula Ferreira, do Centro de Química da Universidade do Minho, pela colaboração na síntese dos derivados da fisetina.

Não poderei deixar de agradecer a toda a equipa do Laboratório de Farmacognosia que me acompanhou durante o percurso no Laboratório, por ter encontrado ajuda sempre que essa necessidade foi sentida. Em especial, agradeço à Vera e ao Renato, que tantas vezes incomodei durante a escrita desta tese.

Todas as contribuições acima mencionadas culminam na escrita destas linhas. No entanto, para a chegada deste dia contribuiu o impacto positivo gerado por aqueles que me rodeiam. Assim, agradeço ainda às minhas gatas, por serem tão boa companhia ao final de mais um dia.

Aos meus amigos, sem os quais seria certamente uma pessoa diferente. A todos os meus Amigos, todos tão especiais, muito obrigada.

A toda a minha família, a todos os que me têm apoiado e também àqueles que não verão este dia, pela oportunidade de ter sido criada com tanto carinho, demonstrado tantas vezes com tantas pequenas coisas, todas elas tão importantes.

Agradeço de forma muito especial aos meus Pais, que são, sem discussão possível, os melhores que há.

Ao Daniel, por conhecer todas as minhas insuficiências e escolher vê-las à melhor luz possível, e, acima de tudo, por ser a melhor coisa do Mundo.

Tenho sorte de vos ter encontrado a todos.

ABSTRACT

ABSTRACT

Homeostasis in eukaryotes is inseverable of that of the endoplasmic reticulum (ER) and proteostasis. The ER performs the synthesis and folding of the majority of the proteome, being also the major reservoir of ionic calcium in the cell. Multiple factors can induce stress upon this organelle. When unresolved, this stress leads to the activation of stress response signaling pathways collectively termed as the unfolded protein response (UPR). This signaling cascade aims to restore homeostasis, but it can, nonetheless, result in deleterious effects upon cells if chronically or intensely activated.

Among molecules capable of modulating ER stress and the UPR, those of natural occurrence are the most common. For this reason, this work addresses a chemical library of over 100 natural products. The compounds were subjected to a battery of assays designed to evaluate their potential to modulate ER stress in different contexts, aiming to describe natural small molecules that can act as ER stress modulators.

Compromised ER function and chronic UPR activation underlie the pathogenesis of neurodegenerative disease. To identify molecules that can counter UPR activation and protein aggregation that characterize this type of illness, their effect upon calcium homeostasis, key gene and protein expression, and levels of protein aggregation in cells were determined. From this effort resulted the identification of several bioactive natural products, with particular emphasis on delphinidin, that displayed a strong potential against protein aggregation in neuronal cells, indicating that it may be a valuable ally in the research and drug development against neurodegeneration.

Chronic activation of ER stress-resolving pathways also occurs concomitantly to the inflammatory response, reason for which this organelle may be a relevant molecular target for treating inflammatory conditions. Aiming to provide building blocks for the development of new strategies to treat chronic inflammatory disorders, this work describes the inflammatory/UPR-related molecular machinery modulated by a panel of natural products. The molecules were analyzed in what regards their NF-κB inhibitory potential, their effect upon ROS generation, inflammasome activation, cytokine release and UPR-related gene expression. This work demonstrates that 5-deoxykaempferol, berberine, luteolin-4'-*O*-glucoside, myricetin, quercetagetin and sennoside B can simultaneously ameliorate inflammatory and UPR signaling.

In the case of cancer, and as consequence of their abnormally high protein synthesis rates, malignant cells present a known vulnerability against ER stress. For this reason, the same library was screened for their selective cytotoxicity against cancer cell lines by triggering ER stress. The molecules that exerted this cytotoxicity were further studied to clarify the involvement of UPR activation in the observed effect, namely by evaluating their

impact upon calcium homeostasis, caspase activation, and UPR-related gene expression. by According to our results, berberine and emodin are characterized as potential leads for the subsequent research and drug development of selective anticancer agents. Berberine was effective against two cells lines, AGS (gastric adenocarcinoma) and A549 (lung adenocarcinoma), disrupting Ca^{2+} homeostasis, upregulating UPR target gene expression and ER-resident caspase-4 activation. For these reasons, it stands out as the most promising molecule against neoplastic disease.

Fisetin was another hit identified in this work. A set of derivatives of this compound was synthesized and tested, along with the parent molecule, to determine their potential against ER stress in the aforementioned contexts. At noncytotoxic concentrations, fisetin was effective against LPS-induced NF-κB signaling, cytokine release, inflammasome activation, ROS generation and UPR gene expression. This activity was shared among some of its derivatives and shows that it is possible to tailor small molecules for improved ER modulation capacity.

Globally, the results presented in this work add to the premise that natural products can offer valuable tools for the discovery and pharmaceutical development of chemical entities to modulate proteostasis and the UPR, as well as the inflammatory response.

Keywords: endoplasmic reticulum, unfolded protein response, inflammation, natural products, fisetin

RESUMO

RESUMO

A homeostasia de um organismo eucarionte é inseparável da do retículo endoplasmático (RE) e da proteostasia. O RE executa a síntese e enovelamento da maior parte do proteoma, sendo também o principal reservatório celular de cálcio iónico. O *stress* neste organelo pode ser induzido por múltiplos fatores. Quando não é resolvido, esse *stress* leva à ativação de vias de sinalização citoprotetoras, coletivamente denominadas de resposta a proteínas mal enoveladas (UPR, do inglês *unfolded protein response*). Esta cascata de sinalização visa restaurar a homeostasia, mas pode, no entanto, resultar em efeitos deletérios sobre a célula se intensa ou cronicamente ativada.

Entre as moléculas capazes de modular o *stress* reticular e a UPR as de ocorrência natural são as mais comuns. Por esta razão, este trabalho foi realizado considerando uma biblioteca química de mais de 100 produtos naturais. Os compostos foram submetidos a uma bateria de ensaios destinados a avaliar seu potencial para modular o *stress* reticular em diferentes contextos, visando descrever pequenas moléculas naturais que possam atuar como moduladores do *stress* reticular.

Uma função reticular comprometida e a ativação crónica da UPR são a base da patogénese das doenças neurodegenerativas. De forma a identificar as moléculas que conseguem contrariar a ativação da UPR e a agregação proteica que caracterizam estas doenças, foi analisado o seu efeito relativamente à homeostasia do cálcio, expressão génica e proteica e níveis de agregação proteica na célula. Deste esforço resultou a identificação de vários produtos naturais bioativos, com particular destaque para a delfinidina, que apresentou um forte potencial contra a agregação de proteínas em células neuronais, indicando que poderá ser um valioso aliado na investigação e desenvolvimento de fármacos contra a neurodegeneração.

A ativação crónica das vias de resolução de *stress* reticular ocorre também concomitantemente à resposta inflamatória, razão pela qual o RE pode ser um alvo molecular relevante para o tratamento de doenças inflamatórias. Com o objetivo de fornecer peças fundamentais para o desenvolvimento de novas estratégias para tratar doenças inflamatórios crónicas, este trabalho descreve a maquinaria molecular relacionada com a inflamação/UPR modulada por um painel de produtos naturais. As moléculas foram analisadas quanto à sua capacidade para inibir o NF-κB, seu efeito na geração de ROS, ativação do inflamassoma, libertação de citocinas e expressão génica relacionada à UPR. Este trabalho demonstra que as moléculas 5-desoxicaempferol, berberina, luteolina-4'-*O*-glicósido, miricetina, quercetagetina e senósido B simultaneamente atenuam a sinalização inflamatória e da UPR.

No caso do cancro, graças ao seu ritmo de síntese proteica anormal, as células malignas apresentam uma conhecida vulnerabilidade ao *stress* reticular. Por esta razão, os produtos naturais foram triados para moléculas seletivamente citotóxicas contra linhas celulares cancerígenas que atuem desencadeando o *stress* reticular. As moléculas que exerceram esta citotoxicidade foram ainda estudadas para esclarecer o envolvimento da ativação da UPR no efeito observado, nomeadamente avaliando o seu impacto na homeostasia do cálcio, ativação de caspases e expressão génica relacionada com a UPR. A berberina e a emodina são caracterizadas pelos nossos resultados como potenciais compostos líder para a subsequente investigação e desenvolvimento de fármacos anticancerígenos seletivos. A berberina foi eficaz contra dois modelos celulares, nomeadamente células AGS (adenocarcinoma gástrico) e A549 (adenocarcinoma pulmonar), perturbando a homeostasia do cálcio, induzindo a expressão génica de biomarcadores da UPR e a ativação da caspase-4, residente no RE. Por esses motivos destaca-se como a molécula mais promissora contra a doença neoplásica.

A fisetina foi outro composto ativo identificado ao longo deste trabalho. Foi sintetizado um conjunto de derivados deste composto, que foi testado juntamente com a molécula-mãe para determinar seu potencial contra o *stress* reticular nos vários contextos mencionados acima. Em concentrações não-citotóxicas, a fisetina foi eficaz contra a sinalização de NF-κB, libertação de citocinas, ativação do inflamassoma, produção de ROS e expressão génica de biomarcadores da UPR induzidos pelo LPS. Esta atividade é partilhada com alguns dos seus derivados e demonstra que é possível desenhar pequenas moléculas com melhor capacidade de modular o RE.

Estes resultados reforçam a premissa de que os produtos naturais podem oferecer ferramentas valiosas para a descoberta e desenvolvimento farmacêutico de entidades químicas para modular a proteostasia e a UPR, bem como a resposta inflamatória.

Palavras-chave: retículo endoplasmático, resposta a proteínas mal enoveladas, inflamação, produtos naturais, fisetina

TABLE OF CONTENTS

Chapter I - Introduction

Chapter IV – Discussion, conclusions and future perspectives

Chapter V - References

FIGURE INDEX

TABLE INDEX

ABBREVIATIONS

AD	Alzheimer's disease
ASK1	Apoptosis signal-regulating kinase 1
ATF4	Activating transcription factor 4
ATF6	Activating transcription factor 6
ATG1	Autophagy-related protein 1
ATG13	Autophagy-related protein 13
ATG5	Autophagy-related protein 5
ATL3	Atlastin GTPase3
ATP	Adenosine triphosphate
$A\beta_{42}$	Amyloid-β_{42}
Bad	Bcl-2-associated agonist of cell death
Bax	Bcl-2-associated X-protein
Bcl-2	B-cell lymphoma-2
Bcl-X	Bcl-2-like protein 1
Bid	BH3 interacting-domain death agonist
Bim	Bcl-2-like protein 11
BiP	Binding immunoglobulin protein
BPTI	Bovine pancreatic trypsin inhibitor
CaMKII	Calcium/calmodulin-dependent protein kinase II
CAMKK2	Calcium/calmodulin-dependent protein kinase 2
CCPG1	Cell cycle progression 1
CHOP	CCAAT/enhancer-binding protein homologous protein
DAMPs	Damage-associated molecular patterns
DAPI	4',6-diamidino-2-phenylindole
DMEM	Dulbecco's Modified Eagle Medium
DMSO	Dimethyl sulfoxide
Drp-1	Dynamin-related protein 1
DTT	Dithiothreitol
EDEM	ER degradation-enhancing α-mannosidase-like protein
eIF2α	Eukaryotic translation-initiation factor 2α
ELISA	Enzyme-linked immunosorbent assay
EOR1α	ER oxidoreductin 1α
ER	Endoplasmic reticulum
ERAD	Endoplasmic reticulum-associated degradation
ERdh4/5	E3 ubiquitin-protein ligases

ERdj3/6	DnaJ homolog subfamily B members
ERp44	Endoplasmic reticulum-resident protein 44
ERp57	Endoplasmic reticulum-resident protein 57
ERp72	Endoplasmic reticulum-resident protein 72
ERSE	Endoplasmic reticulum stress response element
FBS	Fetal bovine serum
FITC	Fluorescein-5-isothiocyanate
GADD34	Growth arrest and DNA damage-inducible protein
GAPDH	Glyceraldehyde 3-phosphate dehydrogenase
GRP75	Glucose-regulated protein 75
GRP78	Glucose-regulated protein 78
GRP94	Glucose-regulated protein 94
HAEC	Human aortic endothelial cells
HBSS	Hanks' Balanced Salt Solution
HRP	Horseradish peroxidase
HSP70	Heat shock protein 70 kDa family
HSP90	Heat shock protein 90 kDa family
HSPs	Heat shock proteins
IFN-γ	Interferon-γ
IgE	Immunoglobulin E
IL	Interleukin
IL-1β	Interleukin-1β
IL-6	Interleukin-6
IP_3R	Inositol 1,4,5-trisphosphate receptors
IRE1	Inositol-requiring enzyme 1
IRE1α	Inositol-requiring enzyme 1α
IRE1β	Inositol-requiring enzyme 1β
ISR	Integrated stress response
IκB-α	Nuclear factor kappa-light-chain-enhancer of activated B cells inhibitor alpha
JNK	c-Jun N-terminal kinase
KDEL	Lys-Asp-Glu-Leu
LC3β	Microtubule-associated protein 1 light chain 3β
MAM	Mitochondria-associated ER membrane
MAPK	Mitogen-activated protein kinases
MDS	Multidimensional scaling
MEFs	Mouse embryonic fibroblasts

MEM	Minimum Essential Medium
MKK4	Mitogen-activated protein kinase kinase 4
MKK7	Mitogen-activated protein kinase kinase 7
mTOR	Mammalian target of rapamycin
mTORC1	Mammalian target of rapamycin complex 1
MTT	(3-(4,5-dimethylthiazol-2-yl)-2,5-diphenyltetrazolium bromide
NF-κB	Nuclear factor kappa-light-chain-enhancer of activated B cells
NK	Natural killer
NO	Nitric oxide
OMM	Outer mitochondrial membrane
PACS-2	Phosphurin acidic cluster sorting protein 2
PAMPs	Pathogen-associated molecular patterns
PCA	Principal component analysis
PD	Parkinson's disease
PDI	Protein disulfide isomerase
PERK	Double-stranded RNA-dependent protein kinase (PKR)-like ER kinase
PI3K	Phosphoinositide-3-kinase
PMA	Phorbol 12-myristate 13-acetate
PP1	Protein phosphatase 1
PRR	Pattern recognition receptor
Puma	p53 upregulated modulator of apoptosis
RETREG1	Reticulophagy regulator 1
RIDD	Regulated IRE1-dependent decay
RNAi	Interfering RNA
RNS	Reactive nitrogen species
ROS	Reactive oxygen species
RPMI	Roswell Park Memorial Institute
RTN3	Reticulon 3
RT-qPCR	Reverse transcription-quantitative polymerase chain reaction
RyR	Ryanodin receptor
SDS-PAGE	Sodium dodecyl sulfate–polyacrylamide gel electrophoresis
SEC63	translocation protein SEC63 homolog
SERCA	Sarco/endoplasmic reticulum Ca^{2+}-ATPase
SOCE	Store-operated calcium entry
Tg	Thapsigargin
Th	T helper cells

ThT	Thioflavin T
TLR	Toll-like receptors
TLR4	Toll-like receptor 4
TNF-α	Tumor necrosis factor-α
TRB3	Tribbles homolog 3
t-SNE	Distributed stochastic neighbor embedding
UMAP	Uniform manifold approximation and projection
UPR	Unfolded protein response
UPRE	Unfolded protein response element
VDAC	Voltage-dependent anion channel
XBP1	X-box-binding protein 1
XBP1s	Spliced XBP1

THESIS OUTLINE

THESIS OUTLINE

This doctoral thesis comprises five main sections:

Chapter I – Introduction

The first chapter contains a review article produced under the scope of this thesis, with the title "*Endoplasmic reticulum stress signaling in cancer and neurodegenerative disorders: Tools and strategies to understand its complexity*". This work provides an overview on the molecular biology of the endoplasmic reticulum, its role in health and disease (emphasizing cancer and neurodegenerative diseases), and methodologies that can be employed to study these topics. It was also necessary to address the topic of inflammation and endoplasmic reticulum stress, reason for which an additional original text on this subject ensues.

Chapter II – Objectives

The objectives that were outlined for this work are disclosed herein.

Chapter III – Results

This section contains the results obtained during this thesis, which are presented by the means of the resulting original research articles.

The first work presented here is titled "*A pipeline for natural small molecule inhibitors of endoplasmic reticulum stress*" (Original Article #1), and describes the potential of a library of natural products against endoplasmic reticulum stress in the context of neurodegeneration. As a result of being the first work to be published, it also includes a description of the chemical library used in this thesis, including from a chemometric point of view.

The second (original article #2), "*A survey of naturally occurring molecules as new endoplasmic reticulum stress activators with selective anticancer activity*", explores the bioactivity of these molecules in what concerns to endoplasmic reticulum stress induction in cancer cells.

The same chemical library was surveyed for anti-inflammatory compounds with simultaneous amelioration of endoplasmic reticulum stress, resulting in the original article #3, "*Naturally occurring small molecules with dual effect upon inflammatory signaling pathways and endoplasmic reticulum stress response*".

Finally, derivatives of fisetin were synthesized and prospected for anti-endoplasmic reticulum stress and anti-inflammatory bioactivities, as described throughout the section and in original article #4, "*Anti-inflammatory activity of fisetin derivatives*".

Chapter IV – Discussion, conclusions and future perspectives

This section contains an integrated interpretation and discussion of the works presented in the previous chapter. The main conclusions are summarized, and perspectives for future endeavors are traced.

Chapter V – References

The final chapter of this thesis provides the bibliographic references that supported its state of the art, discussion and writing.

Chapter I – Introduction

REVIEW ARTICLE

Endoplasmic reticulum stress signaling in cancer and neurodegenerative disorders: Tools and strategies to understand its complexity

Daniela Correia da Silva, Patrícia Valentão, Paula B. Andrade, David M. Pereira

Pharmacological Research, 2020, 155:104702

Abstract

The endoplasmic reticulum (ER) comprises a network of tubules and vesicles that constitutes the largest organelle of the eukaryotic cell. Being the location where most proteins are synthesized and folded, it is crucial for the upkeep of cellular homeostasis.

Disturbed ER homeostasis triggers the activation of a conserved molecular machinery, termed the unfolded protein response (UPR), that comprises three major signaling branches, initiated by the protein kinase RNA-like endoplasmic reticulum kinase (PERK), inositol-requiring enzyme 1 (IRE1) and the activating transcription factor 6 (ATF6). Given the impact of this intricate signaling network upon an extensive list of cellular processes, including protein turnover and autophagy, ER stress is involved in the onset and progression of multiple diseases, including cancer and neurodegenerative disorders. There is, for this reason, an increasing number of publications focused on characterizing and/or modulating ER stress, which have resulted in a wide array of techniques employed to study ER-related molecular events. This review aims to sum up the essentials on the current knowledge of the molecular biology of endoplasmic reticulum stress, while highlighting the available tools used in studies of this nature.

Keywords: unfolded protein response, endoplasmic reticulum stress, PERK, IRE-1, ATF6, autophagy

1.1. Endoplasmic reticulum (ER) function, structure and dynamics

The endoplasmic reticulum (ER) is the largest organelle of eukaryotic cells, comprising an intricate and highly dynamic network of tubules and branches that emerge from the nucleus and are distributed throughout the cytoplasm.

From a structural point of view, the ER comprises the rough ER, constituted by sheets, and the smooth ER, constituted by tubules, each structure being related to the type of processes that takes place at the site. The rough ER is easily distinguished from the smooth ER due to the density of ribosomes it presents on its cytosolic surface, while the smooth ER lodges few ribosomes and presents smoother and more curved surfaces (1-3).

The reticular architecture is highly dynamic, with new tubules being formed at constant rates, as well as their cytoskeletal transport along microtubules and homotypic fusion. New tubules branch from the older ones and slide along the others, being that the microtubule motors govern the expansion of the ER towards the cell membrane, while the inwards movements are microtubule-independent (4). Nonetheless, in the absence of microtubules, peripheral ER tubules may also move along actin filaments. Furthermore, microtubule polymerization may, by itself, push the movement of the ER tubules (4). Altogether, microtubule and actin filament dynamics influence the tubule-to-sheet ratio of the ER, as has been shown by cell imaging/ 3D-electron microscopy techniques (5).

The ER plays a role of the utmost importance in the homeostasis of a wide array of cellular processes, even though it is classically associated to its main function: the *de novo* synthesis and folding of proteins (mainly in the rough ER). It is in the ER that the synthesis of most proteins takes place, mainly secreted and transmembrane proteins, but also some cytosolic ones. In the presence of a signal recognition particle (SRP), ribosomes containing mRNAs to be translated are recruited to bind the surface of the ER and proceed with their translation (1). The next step is protein folding, which encompasses the formation of disulfide bonds between cysteine residues of peptides at the ER lumen. After this, post-translational modifications, such as *N*-linked glycosylation, also take place (6). As discussed later (**Section 7**), the inability to properly conduct this folding step is the basis of a number of proteinopathies, notably several neurodegenerative diseases.

The ER is also involved in the transport of newly-synthesized protein and their delivery to target site through the secretory pathway, which involves the rough ER, ER exit sites, the ER-to-Golgi intermediate compartment, the Golgi apparatus itself and post-Golgi carriers that transport the proteins to their final target site (7). Although on a smaller scale, the synthesis and transportation of phospholipids and steroids also takes place in this organelle, mostly in the smooth ER (1). Furthermore, the ER constitutes the most important reservoir of ionic calcium in the cell, as discussed in depth in **Section 1.5**.

1.1.1. Studying ER morphology

Changes the reticular morphology are commonly evaluated in studies regarding ER stress. Concerning ER labeling, even though the number of selective probes towards the ER is scarce, there are a few commercial options for direct ER imaging. Assessing ER morphology resorting to this sort of probe can be useful to detect ER stress by observing its characteristic traits, such as dilation, expansion, granulation or vacuolization of the organelle (8, 9). For instance, the ER is reported to expand in response to thapsigargin (10) or cyclosporine (11). On the fungus *Pisolithus tinctorius,* ER expansion and modified localization were observed upon treatment with brefeldin (12).

ER trackers include ER-Tracker™ Blue-White, DPX ER-Tracker™ Green (glibenclamide BODIPY® FL) and ER-Tracker™ Red (glibenclamide BODIPY® TR). The green and red options consist of a dye of the selected spectrum bound to glibenclamide, which binds sulfonylurea receptors of ATP-sensitive K^+ channels in the ER, potentially bearing the disadvantage of impairing the normal function of the organelle. On the other hand, the blue-white option is more environmentally sensitive and decreases its quantum yield on the presence of highly polar solvents, which can pose a great disadvantage when working with live cells (13-15). To choose the color of the probe relies solely on the preference of the researcher, being that it should be of a distinct color when the user intends to co-stain with dyes for other organelles.

Another option is CellLight® products, that transfect green or red fluorescent protein-based constructs fused to an ER retention signal that, in both cases, is calreticulin and KDEL, into cells. These options are to be used on live cells only, unlike ER trackers, which allow ER visualization both on live or fixed cells (16, 17). Furthermore, in 2016, McDonald et al. reported the first two fluorescent flavonoids that accumulate in the ER lumen. This accumulation is reported to be selective, as it was comparable with the localization of ER-Tracker™ Red. However, the authors did not evaluate if these molecules accumulated in other cellular compartments, such as mitochondria or the Golgi apparatus, reason for which the there is still room for improving the knowledge regarding the selectivity of these compounds (18). Meinig et al. synthesized analogues of the flurophore rhodol that display the same properties (19).

The number of selective probes towards the ER is quite scarce. Furthermore, they are associated to a few limitations, since they may not be the most specific labeling tool and the manufacturer may not clearly indicate their target, enabling constraints in result interpretation. For these reasons, immunohistochemistry is often used to image the ER. The use of antibodies anti-reticular proteins combined with secondary antibodies with fluorogenic properties are the most frequent instances of this procedure. There are

published examples for several ER proteins, such as PDI (20), calpain-1 (21), calnexin (22, 23), calreticulin (24) or the binding immunoglobulin protein (BiP) (25). The selectivity inherent to this sort of method is higher than that of the previously mentioned ER probes in that it allows visualization of a specific antigen, providing information regarding its expression at the protein level while simultaneously allowing to capture its subcellular localization (26). Differently, some commercially available probes do not always inform on the biological basis of the ER-affinity, which may lead to problems regarding selectivity.

Recently, a promising alternative to conventional antibodies has emerged, namely the use of nanobodies or single-domain antibodies. These are fragments of antibodies that can be used in fluorescence microscopy and in the investigation of protein functions and interactions (27). Such approach has already been used to study the plasma membrane junctions with the ER on mammalian neurons (28) and to analyze retrograde transport to the Golgi apparatus (29). There is also a report concerning the development of a toolkit of functionalized nanobodies to study calcium dynamics (30). Even though currently this is not (yet) a common approach to study ER morphology, it is likely that will be the case in the years to come. This tool offers new possibilities to accurately study and visualize protein function in real time on live cells, posing a set of major advantages when compared to traditional antibodies. Briefly, these single domain antibodies are more stable in the cellular environment, more soluble, more resistant to varying thermal of chemical conditions and possess higher affinity towards the antigen (31). Nanobodies are highly specific due to their size, which allows them to bind cavities on the surface of the antigen, such as ligand-binding sites of receptors or catalytic sites on enzymes, and thus reducing nonspecific background binding. Furthermore, the production yield of this type of antibody considerably higher (32, 33).

1.1.2. Assessing misfolded proteins

Chaperones aid newly synthesized proteins acquire their correct tridimensional conformation (34). In order to fulfill its role in protein folding, the ER relies on three chaperone families: i) the heat shock family, such as BiP, a member of the heat shock protein 70 kDa family (HSP70), also termed glucose regulated protein 78 (GRP78), and the glucose-related protein-94 (GRP94), which belongs to the heat shock protein 90 kDa family (HSP90); ii) lectins, such as calreticulin, calnexin and the ER degradation-enhancing α-mannosidase-like protein (EDEM) and iii) the protein disulfide isomerase family (PDI) (35).

BiP regulates one of the two major chaperone systems by recognizing exposed hydrophobic regions rich in tryptophan, phenylalanine or leucine, typical of misfolded

proteins. This is a monomeric protein that possesses two binding domains, one peptide-binding and one ATP-binding. The second system is led by the two lectin chaperones calnexin (integral membrane protein) and calreticulin (luminal protein) that present glycoproteins to ERp57, a member of the PDI family, for disulfide bond formation and isomerization (35, 36). Whenever the calnexin-calreticulin deglycosylation-glycosylation cycle fails to produce correctly assembled peptides, the aberrant proteins are forwarded to endoplasmic reticulum-associated degradation (ERAD), that involves ubiquitination of targeted proteins and their subsequent degradation by the proteasome (37).

The BiP system differs from calnexin in that it only detects the unfolded regions mentioned above, while calnexin/calreticulin system also detects *N*-linked glycans (36, 38). Hence, BiP is strongly associated to the detection of unfolded non-glycosylated peptides. Furthermore, this chaperone is important for maintaining of the permeability of the ER translocon. Once recognized as misfolded, proteins are directed to the cytosol *via* a protein channel formed by Sec61p, where the 26S proteasome can be found. Substrates recognized by calnexin/calreticulin are transferred to EDEM, while peptides associated to BiP are freed from the folding enzyme ERdj3/6 and bound to ERdh4/5 for degradation (36, 38). Even though the mechanism by which the ER can distinguish and target misfolded proteins from nascent polypeptides is yet to be clarified, chaperone GRP94 is considered to have a role on the process, since its knockdown inhibits the degradation of known ERAD substrates. It is therefore proposed that this chaperone interacts with ERAD sensor proteins (39). Like other members of the HSP90 family, GRP94 displays an *N*-terminal domain, and acidic linker domain, a middle domain and a *C*-terminal domain and functions as a dimer. Being more selective, it possesses a shorter client list than other chaperones (39).

The accumulation of protein aggregates in the ER lumen is a hallmark of ER stress, reason for which its detection and quantification is a powerful tool to detect compromised reticular homeostasis, particularly in fields in which proteotoxicity is pivotal, such as neurodegeneration (40). Thioflavin T (ThT, Ex. 458 nm excitation, Em. 480–520 nm) is a small molecule that issues a fluorescent response when bound to protein aggregates. Techniques based on this molecule can be employed for both imaging and quantitation of misfolded protein accumulation. Nonetheless, this approach does not provide insight into the molecular machinery activated during that disturbance. ThT is reported to have a particular affinity towards β-sheets (41). In a study designed to assess the feasibility of its use to detect ER stress, it was successfully employed in a cell culture system with mouse embryonic fibroblasts (MEFs), human hepatocarcinoma cells (HepG2), and human aortic endothelial cells (HAEC), and also on $ApoE^{-/-}$ mouse liver sections. In thapsigargin (a potent ER stress inducer)-challenged cells (1 μM, 12 h), 5 μM ThT resulted in maximum differences of 5.5 fold against control cells. It also responded to treatments with other known ER stress

inducers, namely dithiothreitol (DTT), glucosamine and palmitate. Increasing thapsigargin concentration (from 0 to 1 μM) revealed a linear response, relatable to the degree of ER stress. This study also develops a staining method employing ThT, which allows visualization of the fluorescent compound in the ER lumen, where misfolded proteins accumulate (42).

Anti-KDEL staining has been used to visualize increased chaperone protein levels under ER stress, using monoclonal antibodies that bind these ER stress biomarkers. KDEL represents the aminoacid sequence Lys-Asp-Glu-Leu, characteristic of ER-synthesized proteins for the secretory pathway (42, 43). The use of this technique is vastly described in the literature, using several ER stress biomarkers (44-49). However, even though KDEL is a retention signal to the ER, it also works as a retrieval signal from the Golgi apparatus, and hence anti-KDEL staining may suffer some interference from peptides that are in the latter organelle to be retrotransported to the ER (50).

Protein disulfide isomerases (PDIs) play a pivotal role in protein folding. For this reason, cell-free enzymatic assays have been developed to analyze the ability of candidate molecules to modulate the activity of these enzymes, which can be a demanding task considering PDIs can mediate up to four distinct reactions. Isomerase activity is measured when substrates presents scrambled disulfide bonds. PDI converts it to its native state, restoring its activity. Oxidase activity occurs when the substrate is in a reduced and PDI performs its oxidative refolding. Reductase activity, on the other hand, occurs when the substrate is oxidized. Finally, chaperone activity can be measured using substrates that do not contain disulfide bonds. This last can be determined through recovery of substrate activity, thus its subsequent determination is required (such as the reductase or isomerase) and also through changes in substrate aggregation (51, 52). A summary of the substrates that are commonly used for the determination of each type of PDI activity can be found in **Table 1**.

Table 1. Common substrates for the determination of each type of PDI activity.

Activity	Substrates	References
Reductase	Insulin along with DTT or glutathione (GSH); di-(*o*-aminobenzoyl)-GSSG (diabz-GSSG); dieosinGSSG (Di-E-GSSG)	(53)
Oxidase	RNAse; bovine pancreatic trypsin inhibitor (BPTI) lysozyme	(51, 52)
Isomerase	Scrambled RNAse; riboflavin-binding protein	(51, 52)
Chaperone	D-glyceraldehyde-3-phosphate dehydrogenase (GAPDH); lactate dehydrogenase; rhodanase or citrate synthase; alcohol dehydrogenase	(54, 55)

1.2. The unfolded protein response

In cases where homeostasis of any of the aforementioned ER-based processes is disturbed, the resulting stress conditions may compromise this organelle's ability to correctly assemble and process peptides. Eventually, the amount of newly synthesized proteins surpasses the amount awaiting folding in the ER, leading to the accumulation and aggregation of misfolded and/or unfolded proteins in the ER lumen. At this point, the unfolded protein response (UPR) is triggered, a chain of molecular events that has evolved to restore homeostatic conditions. Briefly, the UPR i) decreases the rate of protein synthesis to alleviate protein overload, while promoting the correct processing of synthesized proteins and preventing aggregation in the ER lumen, ii) promotes ERAD and iii) boosts the expansion of the ER network. Nevertheless, if the stress upon the ER is of such intensity or duration that it cannot be repaired, the UPR signaling switches from survival to pro-death mechanisms (56). The major molecular events resulting from UPR activation will be discussed hereafter.

BiP, senses the accumulation of misfolded polypeptides in the ER by binding their exposed hydrophobic residues to its *C*-terminal domain, thus acting as a chaperone. When misfolded proteins are sensed on its *C*-terminal domain, ATP is hydrolyzed at the *N*-terminal domain, increasing the affinity of the *C*-terminal domain towards its incorrectly processed substrate, thus keeping it in the ER lumen for a more extended period of time, in order to allow for other mechanism to intervene and correct the mistake. Under homeostatic conditions, BiP localizes on the ER lumen, binding the luminal domain of all of the three major transmembrane proteins that sense ER stress. The classic UPR model indicates that, upon ER stress and increased levels of misfolded proteins, BiP detaches from these sensors, subsequently leading to their activation (57, 58). These sensor proteins are the protein kinase RNA-like endoplasmic reticulum kinase (PERK), inositol-requiring enzyme 1 (IRE1) and the activating transcription factor 6 (ATF6). Their mechanisms of action will be detailed below and are schematized in **Figure 1**.

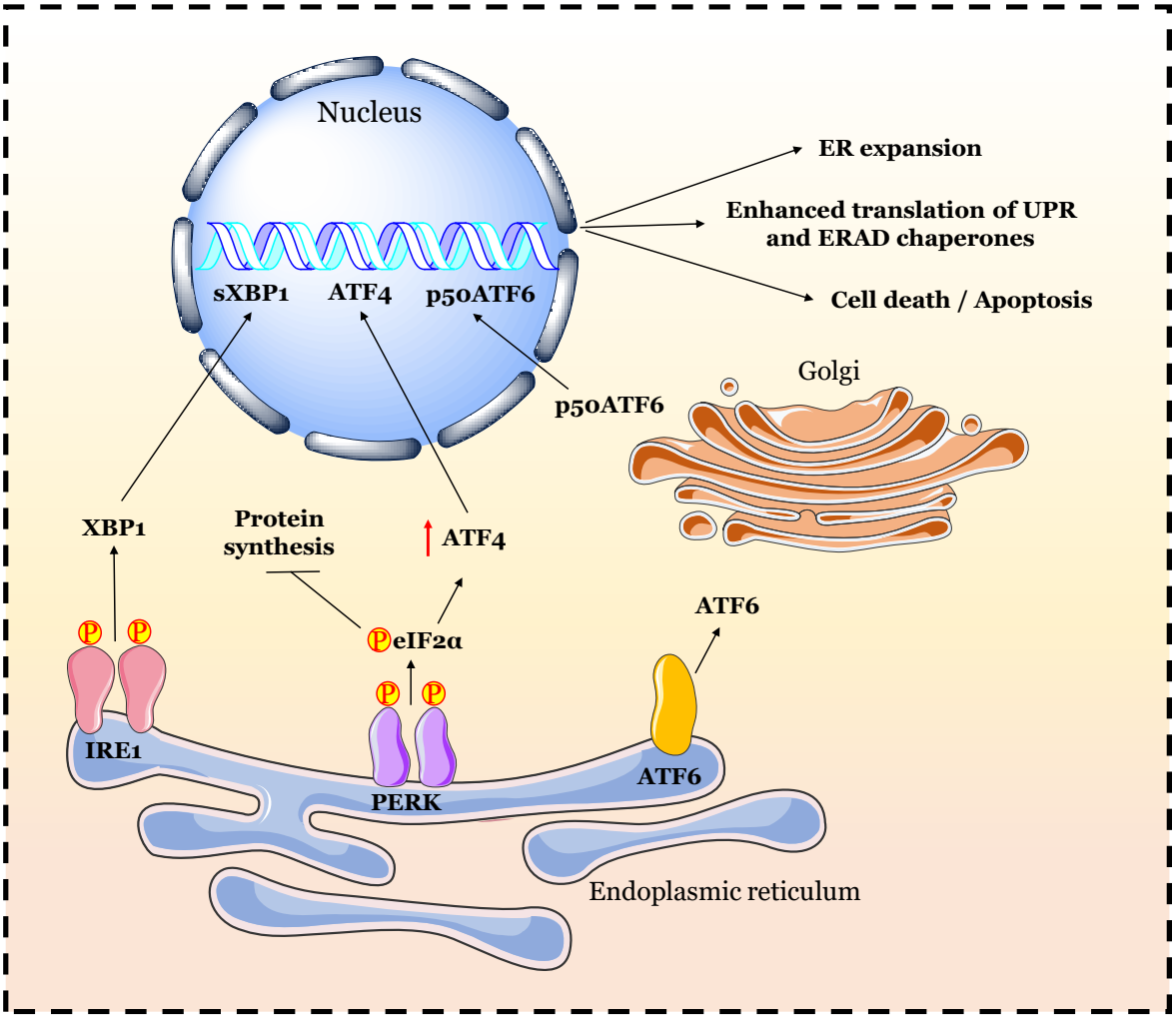

Figure 1. Major molecular machinery involved in the activation of the unfolded protein response (UPR).

By minimizing or even silencing gene expression, interfering RNA (RNAi) is a powerful tool of gene knockdown. An example of one of these instances was developed to study the role of BiP on palate development. Towards this goal, a small RNAi of BiP was inserted on a fluorescent vector and injected on palate explants. This injection resulted, as it was to be expected, on reduced UPR gene expression (59).

1.2.1. PERK branch

The first of the three major branches of the UPR discussed here is initiated by PERK. When BiP dissociates from this sensor, PERK is activated by homodimerization and trans-autophosphorylation. Then, it phosphorylates the α subunit of the eukaryotic initiation factor 2 (eIF2), which, in turn, attenuates protein translation in order to decrease the load of proteins in the ER lumen that await processing. This pro-survival signaling may allow the

cell to cope with the stress conditions it is under, thus helping restore homeostasis. However, if these stress conditions are too severe or last for too long, this branch can switch to pro-apoptotic signaling by activating the activating transcription factor 4 (ATF4). ATF4 is a basic leucine zipper transcription factor responsible for enhancing the expression of genes related to amino acid metabolism, nutrient uptake, anti-oxidation, protein folding and apoptosis, working along with other transcription factor in the UPR (60, 61). This transcription factor induces the expression of genes like the one encoding for the CCAAT-enhancer-binding protein homologous protein (CHOP), which triggers apoptosis (62). Although the mechanisms through which CHOP triggers regulated cell death are still not completely understood, it is accepted that there is a correlation between CHOP-induced cell death and downregulation of the pro-survival protein B-cell lymphoma-2 (Bcl-2), concurrently with upregulation of caspase-3, Bcl-X (Bcl-2 like protein 1), Bax (Bcl-2 associated X-protein), GADD34 (growth arrest and DNA damage-inducible protein), as well as the EOR1α and TRB3 genes (63, 64). GADD34 restores protein synthesis rates by stimulating eIF2α dephosphorylation, which, in turn, results in proteotoxicity by increased reactive oxygen species (ROS) production and ATP depletion (64). The relationship between oxidative stress and ER stress will be more detailed on **Section 1.4.**. TRB3 is another CHOP-induced gene known to be involved in cell death and to downregulate its own expression by repressing CHOP activity (65). Finally, ER oxidoreductin 1 (EOR1) sets off the CHOP-EOR1α-IP_3R-calcium-calcium/calmodulin-dependent protein kinase II (CaMKII) pathway, which culminates in mitochondria permeabilization and release of Bax/Bak (63).

Phosphorylation of eIF2α favors the translation of a few genes, designated by integrated stress response (ISR) genes (66). These genes include ATF4 and CHOP. As is it associated to triggering stress-induced apoptosis, basal levels of CHOP are usually low. However, they quickly rise upon ATF4 activation, even though it can also be induced in a PERK-, IRE1- or ATF6-dependent manner. This transcription factor is crucial for ensuing ER stress-induced apoptotic signaling (67). Molecular events ensuing the activation of the PERK branch of the UPR are schematized in **Figure 2**.

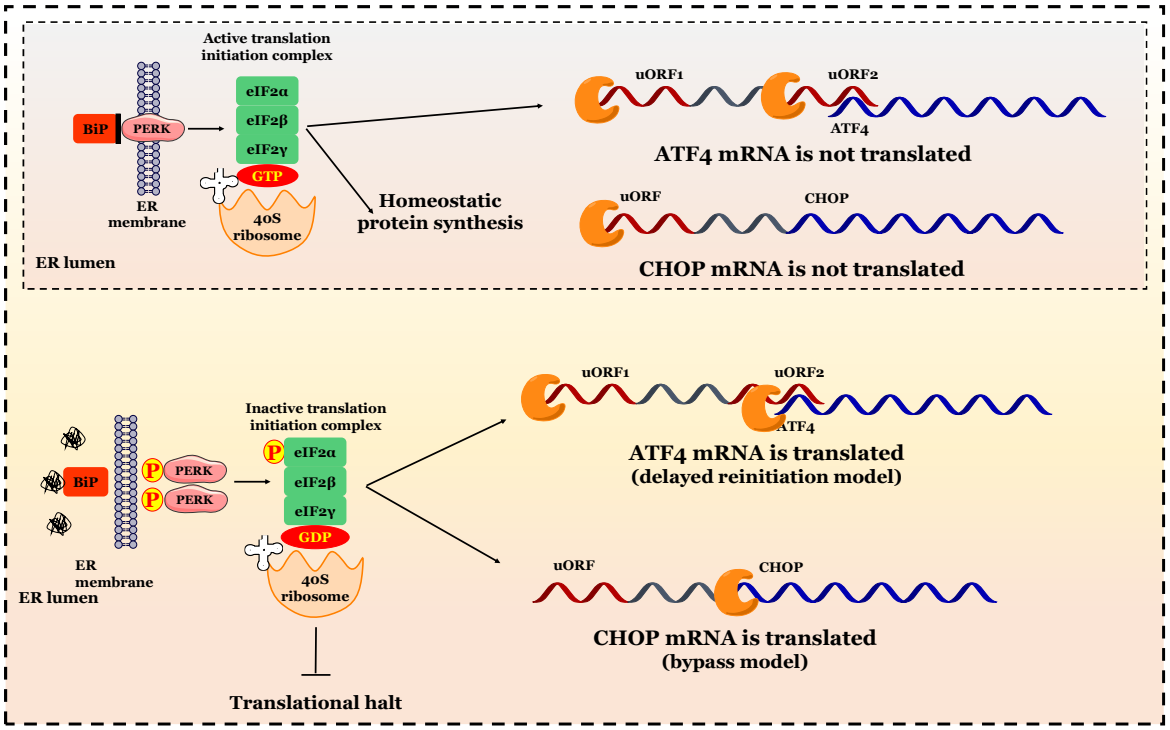

Figure 2. Molecular events ensuing the activation of the PERK branch of the UPR.

Badr et al. employed Western Blotting to analyze UPR activation by assessing ATF4 protein levels and distinguish between phosphorylated and unphosphorylated eIF2α, using a specific antibody for the phosphorylated form and a pan-eIF2α antibody (68). In brief, this sort of technique is robust and widespread throughout the literature regarding ER stress.

In order to infer about the role of a given pathway in in the UPR, some selective pharmacological inhibitors are available. Most of these molecules have been discovered or developed in the attempt to create drugs acting specifically in the ER, yet their toxicity deemed their use for research only.

GSK2606414 is a selective inhibitor of PERK. In *in vivo* models of prion-disease, GSK2606414 restored protein synthesis, resulting in neuroprotection and prevention of disease onset. However, the compound presented marked toxicity, inducing weight loss and hyperglycemia (69). Salubrinal is a pharmacological inhibitor of eIF2α dephosphorylation that acts by blocking the activity of the protein complex growth arrest and GADD34/protein phosphatase 1 (PP1) (70). There is a considerable number of studies indicating that salubrinal is able to protect cells against a set of toxic compounds that act by triggering ER stress. Multiple studies rely in the co-incubation of cells with a toxic compound in the presence of salubrinal and subsequently measure cell viability or death pathways. Concentrations of salubrinal used are usually in the 5-100 μM range and, in some cases, this molecule is pre-incubated one to two hours before the target toxic compound (70-75).

Salubrinal has also been tested *in vivo*, being injected *via* intracerebral ventricle to study the impact of ER stress in autophagy induced by brain ischemic preconditioning. The concentrations of salubrinal tested in this study are considerably lower (75-150 pM) than usually reported (76). In different reports, however, salubrinal was administrated through intraperitoneal injection at 1 mg/kg (77, 78), in the intra-articular space at 1.5 mg/kg (73) or intravenously at 2.0 mg/kg (75). This significant variation in protocols calls for a standard in the field which can contribute to improve the benchmarking between distinct studies. There are also *in vivo* studies that reported the high toxicity of the compound, reason for which its use is currently reserved for research purposes (69, 79).

1.2.2. IRE1 branch

The IRE1 branch of the UPR is initiated upon activation of the kinase through autophosphorylation and homodimerization or oligomerization. Of all the UPR transducers, IRE1 is the most conserved (80).

Not unlike PERK, this branch can also promote survival or trigger cell death, as summarized in **Figure 3**. In addition to its kinase function, IRE1 also has RNAse activity and it splices the mRNA encoding for X-box binding protein 1 (XBP1), removing its introns and thus leading to the formation of spliced XBP1 (XBP1s) and its subsequent translation into a transcription factor.

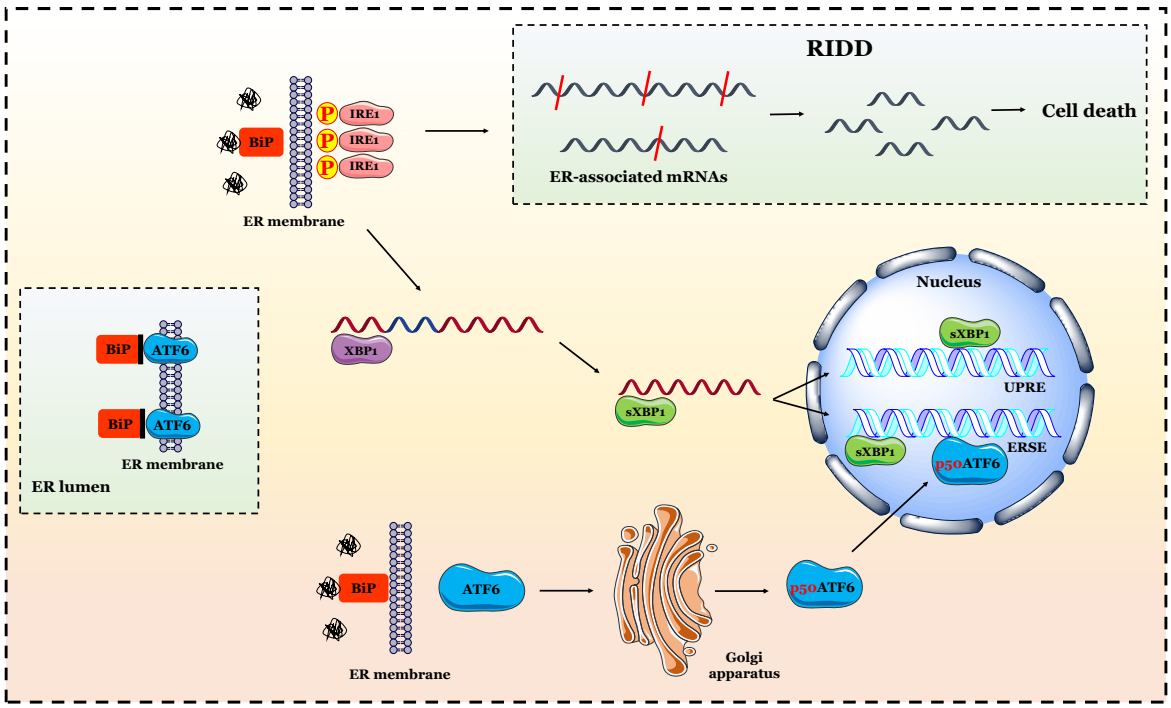

Figure 3. Molecular events ensuing the activation of the IRE1 and ATF6 branches of the UPR.

This requires the cooperation of IRE1 units and is involved in its pro-survival action (80-84). Its pro-death action, however, can be carried out by a single unit of the enzyme, and consists of a process termed regulated IRE1-dependent decay (RIDD), ultimately resulting in cell death. RIDD involves the preferential cleavage of ER-associated mRNAs encoding for growth-promoting proteins, the resulting fragments being rapidly degraded by the action of exoribonucleases (80-82). It is worth mentioning that IRE1 occurs in two different isoforms (IRE1α and –β) and, even though both are activated upon ER stress conditions, IRE1α is the most relevant, since it occurs ubiquitously in the organism, unlike IRE1β, which is restricted to gastrointestinal and respiratory epithelial cells (80, 85, 86).

XBP1s is a potent transcription factor that binds the endoplasmic reticulum stress response element (ERSE) and unfolded protein response element (UPRE) and, consequently, enhances the expression of genes comprised in the ER machinery, such as BiP. Although its cleavage is associated to the IRE1 pathway, its expression can also be induced by ATF6 (87, 88).

A luminescence-based high-throughput IRE1 activity assay has been designed to identify its potential modulators. The authors identified peptides derived from the kinase domain of IRE1 that can modulate its activity and performed *in vitro* (in human hepatocellular carcinoma cells) and *in vivo* (in *Caenorhabditis elegans*) experiments that conclude that these peptides can enhance IRE1 oligomerization and promote cell survival upon ER stress conditions by enhancing XBP1 splicing but simultaneously limiting JNK activation and RIDD. This poses the possibility of selectively modulating of IRE1 activity, being that the establishment of modulators of the pro-survival activity of this protein may build a new strategy against the nefarious effects of ER stress (89, 90).

In the case of *xbp-1*, to simply determine total mRNA amounts by qPCR is not illustrative of its activity, since its activation as a transcription factor involves mRNA splicing. As so, experimental frameworks should compare the amounts of spliced and unspliced *xbp1* mRNA to be able to draw any conclusions (87). There is a report on a spliced-*xbp1* specific RT-PCR technique, which allows to separate spliced and unspliced mRNA in a human monocytic cell line (THP-1) (87).

Gene expression levels of *ern1* (IRE1 gene) may also be misleading, since it is more assertive to infer about its activation by determining its phosphorylation status by Western Blotting. There are numerous IRE1-specific antibodies available, not only to determine the whole IRE1 protein but also to specifically analyze the phosphorylated portion of the latter (91, 92). For this reason, researchers have resorted to the determination of mRNA levels of genes like *erdj4*, which is an ERAD-related gene downstream of *xbp1* (93).

Reporter genes assays have also been employed to study the IRE1 branch of the UPR. One such instance are Venus-based constructs, a variant of green fluorescent protein. By

fusing it to XBP1, it is possible to analyze its splicing by IRE-1 under ER stress conditions, by detecting the fluorescence of the translated protein (94). Furthermore, XBP-1 has been implied in the antimyeloma activity of bortezomib *via* RNAi knockdown in cell lines (95). This type of technique has also been used on XBP-1 and IRE1 to study the mechanism of RIDD (96). There are also reports of dominant-negative IRE1 transgenes expressed in cell lines, as well as IRE1 knockout mice models (97).

4μ8C is one of the pharmacological inhibitors available that acts upon the IRE1 branch of the UPR. It inhibits both the kinase and RNAse activity of IRE1 by binding its kinase domain at K^{599} and its RNAse domain at K^{907} (98, 99). *In vitro*, the concentration in which 4μ8C is used is quite wide (72, 100-102), including a report of 150 nM as its IE_{50} (50% inhibition efficacy) towards XBP1 splicing inhibition in macrophages (103), to concentrations as high as 100 μM described for the same cell type (92). *In vivo*, it has been used at 10 mg/kg, administrated by intraperitoneal injection (104).

STF083010, like 4μ8C, acts as an IRE1 inhibitor. However, it inhibits only its RNAse domain, thus allowing it to retain its kinase activity while preventing XBP1 mRNA splicing and RIDD. *In vitro*, it is commonly used at 50 or 60 μM (92, 104-106). *In vivo*, it has been used at 30 mg/kg *via* intraperitoneal injection (104, 107).

1.2.3. ATF6 branch

The transcription factor ATF6 is embedded in the ER membrane, being released upon accumulation of misfolded proteins in the ER lumen. Once activated, it translocates to the Golgi apparatus, where it is cleaved by site-1 and site-2 proteases, originating p50ATF6. It then translocates to the nucleus, where it is responsible for inducing the transcription of ER chaperones by binding ERSE in an attempt to restore homeostasis (108-111). Under optimal conditions, ATF6 is maintained in the ER binding BiP, which inhibits Golgi localization signals (112). The events resulting from the activation of this transcription factor are depicted in **Figure 3**.

Not unlike other UPR transducers, simply assessing gene expression levels of ATF6 may not provide enough information, being that it is important to determine its activation by analyzing its cleavage and localization. Another possible approach is to determine gene expression levels of its downstream genes, such as *HYOU1* and *HERPUD* (113). There are also several reports of green fluorescent protein constructs with ATF6 that can be useful in assessing its subcellular localization, and therefore infer about its activation status (114).

There are not many examples in the literature of the use of pharmacological inhibitors towards the ATF6 branch of the UPR. However, in 2016, Gallagher et al. discovered that a class of pyrazole amides named ceapins can inhibit ATF6 signaling, without affecting other

proteins involved in the UPR, and thus allowing for the analysis of the impact of all the three major UPR branches separately. The IC_{50} of ceapins are 4.9 μM for ceapin A1 and 2.6 μM and 0.59 μM for ceapin A6 and ceapin A7, respectively (115). There have not been noteworthy advances since this, and thus there is still a significant need for new ATF6 modulators. There are, however, reports of a pharmacological inducer of this transcription factor, discovered among a library of over 600,000 molecules (116), and subsequent studies on knockout mice models. The discovery of an ATF6 inducer led to the hypothesis that stimulation of this signaling branch may greatly benefit proteostasis under pathological conditions in which it is compromised (117).

Mice models have been an important tool to the achievement of the current knowledge of ER stress and the UPR. There are available *in vivo* knockout models to study multiple UPR transducers, like *atf6*, *ern1*, *xbp1*, *perk*, *eif2α*, *atf4* and *ddit3*, as reviewed elsewhere (118).

A brief summary of the functions of the major proteins involved in the UPR can be found in **Table 2**.

Table 2. Description of the activation and mechanisms of action of the major proteins involved in the UPR.

Protein	Class	Mechanism of action	References
ATF4	Transcription factor	Upregulates pro-apoptotic genes such as CHOP or activating transcription factor 3 (ATF3) / upregulates pro-survival genes like BiP	(68)
ATF6	Transcription factor	Upregulation of UPR machinery and CHOP	(119, 120)
BiP	Chaperone	Binding of unfolded/misfolded proteins,	(57)
CHOP	Transcription factor	Triggers apoptosis *via* Bcl-2 downregulation	(67)
eIF2α	Translation initiation factor	Impairment of translation initiation, selectively upregulation of a few UPR proteins	(121)
IRE1	Kinase and RNAse	Splicing of the XBP1mRNA	(81)
PERK	Kinase	Phosphorylation of eIF2α	(122, 123)
XBP1s	Transcription factor	Binding of ERSE and UPRE, upregulating UPR machinery	(88)

Assessment of changes in the mRNA levels of UPR target genes is one of the strategies most commonly found in the literature (44, 45, 48, 68, 124-127). **Table 3** presents the most relevant UPR genes, which expression is often evaluated in ER stress-related studies.

Table 3. Name, NCBI reference sequence, chromosomal location and function of the most widely-used UPR genes, according to the GenBank database.

Gene/Protein	NCBI Reference Sequence	Chromosomal Location	Expression/Function
***atf4*/ATF4**	Var1: NM_001675.4 Var2: NM_182810.2	22q13.1	Ubiquitous expression. Broadly expressed in bone marrow.
***atf6*/ATF6**	NM_007348.4	1q23.3	Ubiquitous expression, particularly high on thyroid, placenta, brain, kidneys and appendix.
***ddit3*/CHOP**	Var1: NM_001195053.1 Var2: NM_001195054.1 Var3: NM_001195055.1 Var4: NM_001195056.1 Var5: NM_004083.5 Var6: NM_001195057.1	12q13.3	Expressed in virtually every type of tissue, notably on thyroid and bone marrow.
***eif2ak3*/PERK**	Var1: NM_004836.6 Var2: NM_001313915.1	2p11.2	Higher expression in thyroid, stomach, colon and bone marrow.
***eif2s1*/eIF2α**	NM_004094.5	14q23.3	Expressed in all tissues, highlighting testis and esophagus.
***ern1*/IRE1**	NM_001433.5	17q23.3	Ubiquitously expressed. Broadly expressed in adrenal glands and pancreas
***hspa5*/BiP**	NM_005347.5	9q33.3	Broadly expressed in every tissue, particularly in thyroid, bone marrow and placenta.
***xbp1*/XBP1**	Var1: NM_005080.3 Var2: NM_001079539.1	22q12.1; 22q12	Ubiquitous expression, albeit especially high in salivary glands, liver and urinary bladder.

In the case of several key mediators of the UPR, mRNA expression by itself does not provide sufficient information. For example, in the case of IRE1, PERK or eIF2α, the phosphorylation status should also be determined, in order to correctly infer about their activity. Analogously, the gene expression of ATF6 or XBP1 provides little information about its activity as a transcription factor, since it depends on proteolytic or mRNA cleavage, respectively. Thus, it is necessary to distinguish between the native and cleaved forms, rather than just assessing total mRNA amount.

In order to understand and modulate ER stress, several molecules of different origins were established as modulators of one or more of its signaling pathways. The most commonly used molecules on research are listed on **Table 4**, along with a brief description of their mechanism of action, in order to provide insights about their use on assays aiming

to analyze ER stress. For a deeper insight on the subject of ER stress modulators, the reader is referred to a few available reviews (128-132).

Table 4. ER stress modulators classified according to their respective mechanism of action.

Molecule	Effect	Mechanism of action	References
4-Phenylbutyric acid	Protector	Chemical chaperone.	(125, 133-135)
Salubrinal	Protector	Inhibition of eIF2α dephosphorylation	(70, 71, 76, 136, 137)
Brefeldin	Inducer	Inhibition of ER-Golgi transport.	(138-140)
DTT	Inducer	Impairment of protein folding	(141)
Palmitate	Inducer	Activation of caspase-4 and JNK, induction of ATF4 and CHOP.	(142, 143)
Thapsigargin	Inducer	Irreversible SERCA pump inhibition.	(144, 145)
Tunicamycin	Inducer	*N*-linked glycosylation inhibition.	(146)

1.3. The ER-mitochondria axis

The ER and mitochondria mutually communicate through zones collectively termed mitochondria-associated ER membrane (MAM). Both organelles are dynamic structures that can relocate within the cytoplasm by moving through the cytoskeleton according to the needs of the cell. For this reason, under ER stress MAM surface increases, particularly on the perinuclear region. MAM encloses a significant portion of the outer mitochondrial membrane (OMM), up to 20%. At these sites, there are direct channels for calcium transfer from the ER lumen into the mitochondria, since chaperone GRP75 directly links IP_3-R on the ER membrane and the voltage-dependent anion channel (VDAC) on the OMM. Under ER stress, this transfer may be overwhelming for mitochondria, leading to the depolarization of the inner mitochondrial membrane (IMM) and potentially triggering regulated cell death mechanisms, as depicted on **Figure 4** (147). Currently, it is possible to isolate MAMs resorting to subcellular fractionation techniques (148).

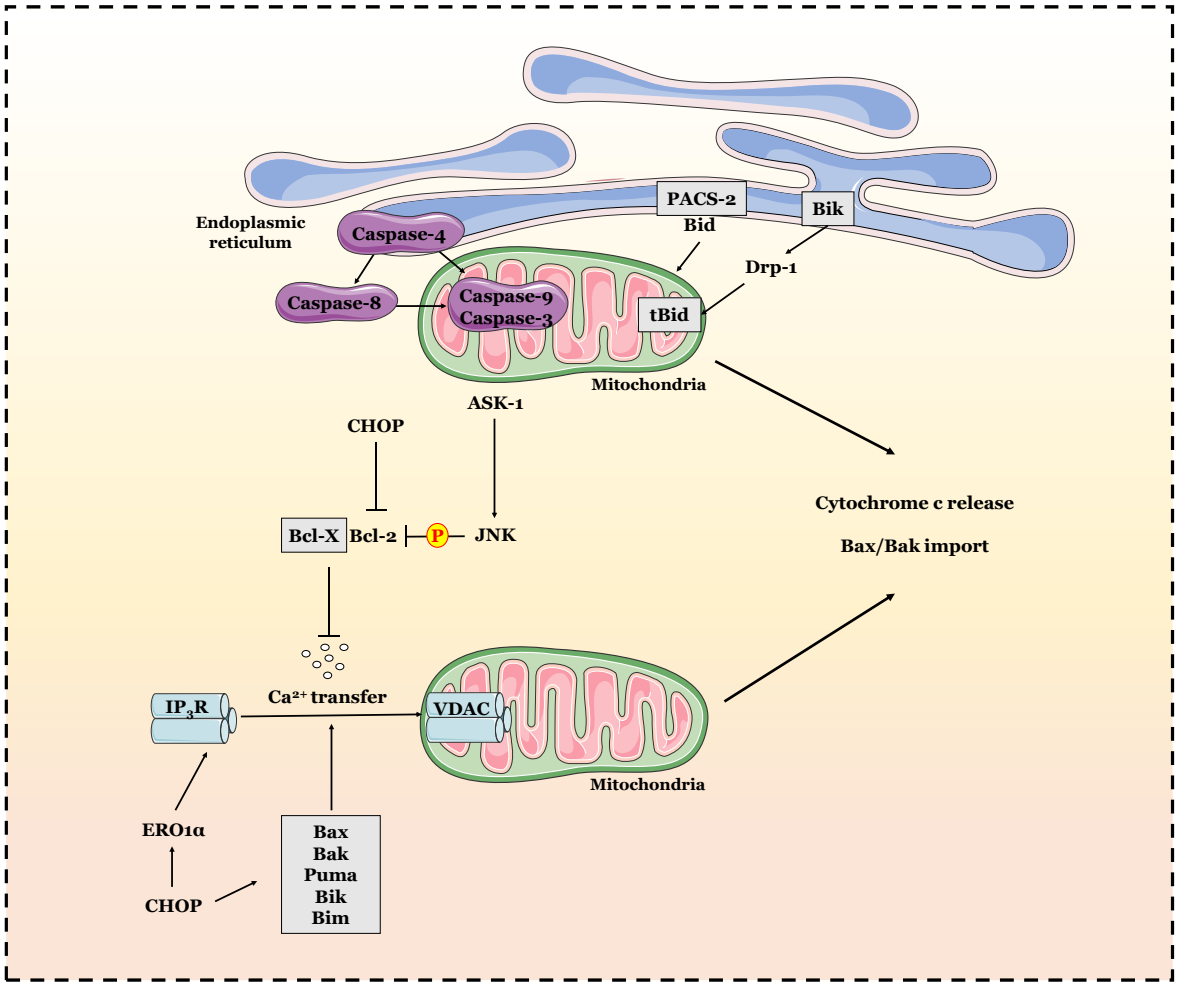

Figure 4. ER-induced mitochondria-dependent regulated cell death. Dynamin-related protein 1 (Drp1) mediates mitochondrial membrane fission. Phosphofurin acidic cluster sorting protein 2 (PACS-2) is necessary for the connection between the ER and mitochondria. Apoptosis signal-regulating kinase 1 (ASK1) is a member of the mitogen-activated protein kinase MAPK family, as well as dual specificity mitogen-activated protein kinase kinases -4 and -7 (MKK4/7).

Depolarization of IMM disrupts its otherwise low permeability and results in the release of cytochrome *c* and other pro-apoptotic factors. Such proteins include the BH3-only proteins of the Bcl-2 family; Bid, Bad, Bim and Puma, which bind other proteins of the Bcl-2 and block their pro-survival action (149, 150). Apoptotic cell death is classically divided in two pathways: the intrinsic, or mitochondrial, and the extrinsic, or death receptor pathway. While ER stress is known to trigger the intrinsic pathway, ER stress-mediated pathway have been associated to distinct apoptotic models, namely the cell death receptor-mediated apoptosis (151). ER stress-induced regulated cell death involves the activation of the inflammatory caspase-4 in humans (caspase-12 in rodents (152)), which resides in the ER in homeostatic conditions (127, 153). Shortly, the involvement of the UPR in the process is known to involve changes on PERK and IRE1α signaling, as well as calcium release from

the ER lumen, elements of the Bcl-2 family and MAPK-kinases, namely the c-Jun *N*-terminal kinase (JNK) (64, 154).

In order to study the communication between the ER and the mitochondria, the most extensively used techniques have been electron microscopy, calcium dynamics and ROS production (155).

1.4. Crosstalk between ER stress and ROS

Recent research has established that oxidative stress can trigger ER stress, the opposite event also being possible (156). In fact, it is currently known that protein folding and generation of ROS are inseparable events. As mentioned before, protein folding implicates the formation of disulfide bonds between cysteine pairs and allows the protein to acquire its correct tertiary structure. The highly oxidizing redox potential of the ER is pivotal for oxidative protein folding to take place, namely disulfide bond formation, and thus the accumulation of unfolded proteins on the ER lumen is accompanied by changes on its redox status, beyond UPR activation. The redox status of this organelle is actively regulated by a number of thiol oxidoreductases and low-molecular weight redox-active electron carriers, which regulate the activities of the ER-resident oxidases peroxiredoxin 4 and ERO1 (157). ROS are physiologically present in the ER as a product of the transference of electrons between PDI and ERO1. When the ER is overloaded with misfolded proteins, ROS are overproduced and interact with ER enzymes, chaperones and calcium channels, leading to the leakage of ionic calcium into the cytosol, leading the mitochondria to generate more ROS and disrupting the mitochondrial membrane potential and thus inducing programmed cell death events or triggering autophagy (158-160). In a thapsigargin-induced model of cell death, overexpression of antioxidant enzymes like superoxide dismutase has been observed to protect neuronal cells, thus evidencing the role ROS in ER-mediated cell death (161). *In vitro* and *in vivo* studies with *Chop -/-* mice have elucidated that this gene is required for the response to oxidative stress and subsequent progression of apoptosis, since its knockout protects against the induction of UPR related genes, such as EDEM1, while simultaneously reducing the expression of ERO1 (159, 162). Furthermore, CHOP contributes to oxidative stress by inhibiting the expression of Bcl-2 and enhancing JNK signaling (163).

Redox-sensitive green fluorescent proteins (GFP) have been successfully employed to evaluate redox changes on the ER both *in vitro* and *in vivo*. These reporters, termed eroGFP (ER-targeted redox-sensitive GFP), possess a cysteine pair that becomes disulfide-linked when in and oxidizing environment, changing its fluorescence excitability maximum from 490 to 400 nm. These reporters are therefore advantageous in that they allow the

determination of the ratio between the fluorescence excitation of both wavelengths, hence allowing to minimize interferences such as photobleaching or operator errors. Combining this reporter with a red fluorescent protein-based construct designed to evaluate UPR activation, the authors conclude that unfolded protein accumulation induced by ER stressors results in reduction of the ER redox potential and UPR activation (164). This construct contained KDEL, the mammalian ER retrieval signal, on the C-terminus of the reporter, and the sequence of BiP on its N-terminus. It was observed that, *in vivo*, the probe is nearly completely oxidized under homeostatic conditions, and that impaired ERO1 or peroxiredoxin 4 activities compromise the oxidizing potential of the ER (165). Subsequent reports mention green fluorescent protein-based constructs (roGFP1-iL) detect oxidizing and reducing changes between -190 and -130 mV (as determined in 3T3-L1 fibroblasts) by glutathione (GSH)-mediated formation of disulfide bonds and dimerization, significantly increasing the molecule's reduction potential (157). A similar green-fluorescent protein probe for measuring the ER redox potential has been developed by Hoseki et al. by substituting specific amino acids in order to increase folding efficacy of the protein. This new probe was named ER-targeted roGFP-S4 and was tested in HeLa cells. Like the previously mentioned reporter, this probe presents two excitations maxima depending on the surrounding redox status. This study reports that an enhanced ERO1 redox cycle increases ER oxidation. Consequently, protein folding is enhanced, since this enzyme generates H_2O_2 *via* transference of electrons to H_2O molecules. As expected and like in the previously mentioned studies, the ER redox state was found to reduce after treatment with reference ER stress inducers (thapsigargin and tunicamycin) (166).

1.5. Role of the ER in calcium homeostasis

Maintenance of proteostasis is not the only role that the ER plays in the cellular upkeep. This organelle is the main calcium reservoir of the cell and is involved in the tight regulation of its levels, which in turn are involved in processes such as cell proliferation, differentiation, metabolism, apoptosis and gene expression (167). The normal concentration of calcium outside the cell can be as high as 2 mM, while in the cytosol it is estimated to be around 100 nM (167, 168).

Fundamental mechanisms of calcium concentration upkeep in the ER involve three types of proteins: i) pumps to import Ca^{2+} ions from the cytosol, ii) luminal proteins to bind calcium and iii) channels to release these ions according to the cellular context, controlled by an electrochemical gradient. Several calcium-binding ER proteins are involved on calcium buffering, like BiP and other chaperones, such as GRP94 and calreticulin, as well as proteins from the PDI family. One of the best-known pumps involved in this process is

the sarco/endoplasmic reticulum Ca^{2+}-ATPase (SERCA). This ATPase, regulated by calnexin and calreticulin, is in charge of calcium uptake by the ER, importing two calcium ions from the cytosol for each ATP molecule hydrolyzed (169). On the other hand, the release of calcium ions into the cytosol requires the inositol 1,4,5-triphosphate receptor (IP_3R) and the ryanodine receptor (RyR) (170). The relationship between ionic calcium levels and proteostasis is further established, since insufficient calcium on the ER will impair the function of these proteins.

Binding of calcium to chaperones results in two major consequences: i) buffering ER calcium levels and ii) regulation of the calcium-dependent function of these proteins. GRP94 represents 5 to 10% of the pool of luminal proteins in the ER and possesses 19 calcium binding sites. BiP has a lower capacity to bind calcium (1 to 2 mol of calcium per mol). However, due to its high expression, it contributes to about 25% of the calcium storage capacity of the ER. This monomeric protein possesses two binding domains, one peptide-binding and one ATP-binding. PDI and PDI-like proteins also contribute to calcium buffering in the reticular environment. Examples of such PDI-like proteins are calcistorin, calsequestrin, ERp72 and ERp44 (37).

Evidently, intracellular calcium levels are tightly regulated within the cell, being that the occurrence of ER stress may lead to its displacement from the ER lumen into the cytosol. It also works on the opposite direction, i.e., temporal and/or spatial imbalances on calcium upkeep may lead to ER stress. For this reason, disturbances in calcium homeostasis are frequently analyzed in ER stress studies. Fura-2-acetoxymethyl ester or Fura-2/AM, a membrane-permeable derivative of the original calcium dye Fura-2, is the most commonly employed calcium probe in the ER-related literature nowadays. It is a ratiometric dye that is used both for intracellular calcium imaging and quantitation; the fact that it is ratiometric confers it a high reliability, due to decreased errors brought by uneven pipetting, photobleaching, or differences in cell lines. Once in the cell, cellular esterases cleave the acetoxymethyl group; then, the calcium-bound molecule will display its excitation wavelength at approximately 340 nm, while the free form is centered around 380 nm, being that the emission is maximum at 510 nm in both cases. Hence, the amount of intracellular calcium is presented as the $F_{340/510}/F_{380/510}$ ratio (171-173).This fluorescent dye has been used extensively in a wide set of cell lines in the 3-5 μM range (72, 174-176).

There are other fluorescent calcium probes commercially available. One example is Fura-PE3/AM, a variant of Fura-2/AM that is designed to avoid possible compartmentalization in the cell. Suppliers report that hydrolysis of this molecule by esterases will trap it inside the cytosol and make it cell membrane impermeable (177, 178). Other methodologies available include quantitation of radiolabeled $^{45}Ca^{2+}$ in ER microsomes and whole cells (168).

Assays to determine SERCA pump activity are not found in the literature quite as often as other less direct approaches to infer about changes on calcium homeostasis. A reason for this may be the technical difficulties posed by direct measurements of its activity. There are, however, a few reports concerning the indirect determination of SERCA activity. Towards this goal, McMullen and co-workers developed a 96-well plate colorimetric assay to quantify the amount of inorganic phosphate that is released by the pump following ATP hydrolysis, which then complexes with ammonium molybdate and malachite green. The authors proceeded to isolate microsomes from brain tissue and prepared an inorganic phosphate quantification reagent that binds with inorganic phosphate, whereas the resulting complex issues a green color that can be measured at 660 nm in a spectrophotometer (168).

Another approach for the analysis of SERCA pump activity *in vitro* is based on the chemiluminescent calcium-binding protein aequorin targeted to the ER. This allows for the analysis of the rate of calcium import into the ER lumen, which is related to SERCA activity. The same authors propose a protocol for determining SERCA activity *in vivo*, through isolation of ER vesicles and their analysis of their calcium uptake resorting to the fluorescent calcium dye Fluo-3 (46).

1.6. A role for ER stress and the UPR in autophagy

Autophagy, a highly conserved catabolic mechanism, is critical for organism development and cellular homeostasis by assuring the protein turnover of the cell, refurnishing it with the amino acids that result from the breakdown of intracellular components like soluble peptides, protein aggregates or even organelles. The process begins with the formation of the phagophore, often arising from the ER membrane, and comes to an end with the elimination of the autophagosome (179).

Autophagy is involved on the pathogenesis of several diseases. This process progressively subsides with age, leading to the reduced formation of autophagic vesicles and their impaired fusion with lysosomes (180). In fact, the accumulation of toxic protein aggregate that are characteristic of some neurodegenerative diseases is connected to unsuccessful autophagy following the cell's inability to properly fold these proteins. However, on the case of neoplastic disease, a dual role is attributed to the autophagic pathway: on one hand, it suppresses initial tumor development, on the other hand, it may protect it from the immune response (181).

Autophagy can be sorted in three different types, i. e. i) macroautophagy, that implies the enclosure of cytoplasmic content in double-walled vesicles destined to fuse with lysosomes and is generally referred to simply as autophagy, ii) microautophagy, that occurs when the cytoplasmic content, labeled with a signal peptide, is directly gorged by the

lysosome and iii) selective autophagy, that eliminates mitochondria, endoplasmic reticulum, lipid droplets and invading pathogens (181). Autophagy is triggered by mammalian target of rapamycin *(*mTOR*)* inactivation, resulting in activation of the autophagy-related protein 1 (ATG1) and that phosphorylation of ATG13, which in turn recruits other ATG proteins, ultimately leading to the formation of the autophagosome. Detailed insights on the molecular and cell biology of autophagy surpasses the scope of this article and thus the reader is referred to comprehensive reviews on the subject (182-184).

Early in the current century, the crosstalk between this catabolic process and the UPR was first reported, when it was noticed that ER stress inducers could trigger the formation of autophagosomes (185, 186). Activation of any of the three major signaling branches of the UPR can impact the autophagic process. Activated IRE1 induces autophagy by phosphorylating the MAPK8, that in turn promotes the activity of the downstream autophagy mediator Beclin-1. In addition, UPR-mediated JNK activation (either by the IRE1 or PERK branch) also results in MAPK8 phosphorylation by this kinase. JNK itself has a direct effect on autophagy by stimulating the expression of ATG5. Furthermore, this kinase activates c-Jun, which plays a role in increasing the expression of the autophagosome initiator Beclin-1 by interacting with its promoter. Finally, JNK also prevents the association of Beclin-1 to Bcl-2 by phosphorylating the latter. This will result in complexation of Beclin-1 with the phosphoinositide-3-kinase-kinase (PI3K) and leads to autophagosome formation. IRE1/JNK/-cJun signaling pathway is, for this reason, a major mechanism by which the UPR influences autophagy. A role for XBP1 in autophagy, by indirectly regulating Bcl-2 and directly inducing Beclin-1 expressions, is also in place (187-191).

The involvement of the PERK branch of the UPR on the autophagic process is mediated its transcription factors ATF4 and CHOP, which increase the expression of autophagic proteins such as ATG5, ATG12 and Beclin-1. Furthermore, as a result of overall impaired protein synthesis induced by the activation of the PERK branch, Bcl-2 levels are reduced and, consequently, Beclin-1 is released. In addition, ATF4 induces the expression of microtubule-associated protein 1 light chain 3β (LC3β), a structural protein in autophagosomes (188-190, 192-194). Since it leads to the expansion of the ER machinery, including CHOP and XBP1, ATF6 activation can also result in the occurrence of autophagy (188-190, 195, 196).

The exit of ionic calcium from the ER lumen into the cytosol leads the activation of autophagic enzymes, such as the on calcium/calmodulin-dependent protein kinase kinase 2 (CAMKK2), that leads to the inhibition of mTORC1, consequently resulting in autophagy initiation. In fact, this is the mechanism behind the calcium-induced autophagy elicited by thapsigargin (197, 198). In recent years many paths connecting ER stress, the UPR and autophagy have been described (184). Learning how to modulate ER stress may constitute

a strategy to fine-tune autophagy, and consequently pave the way for new therapeutic strategies, particularly given the increasingly recognized potential of autophagy modulation in pathologies such as immune diseases, cancer and neurodegenerative diseases (180, 184, 189). This interplay between the UPR and autophagy is summarized in **Figure 5**.

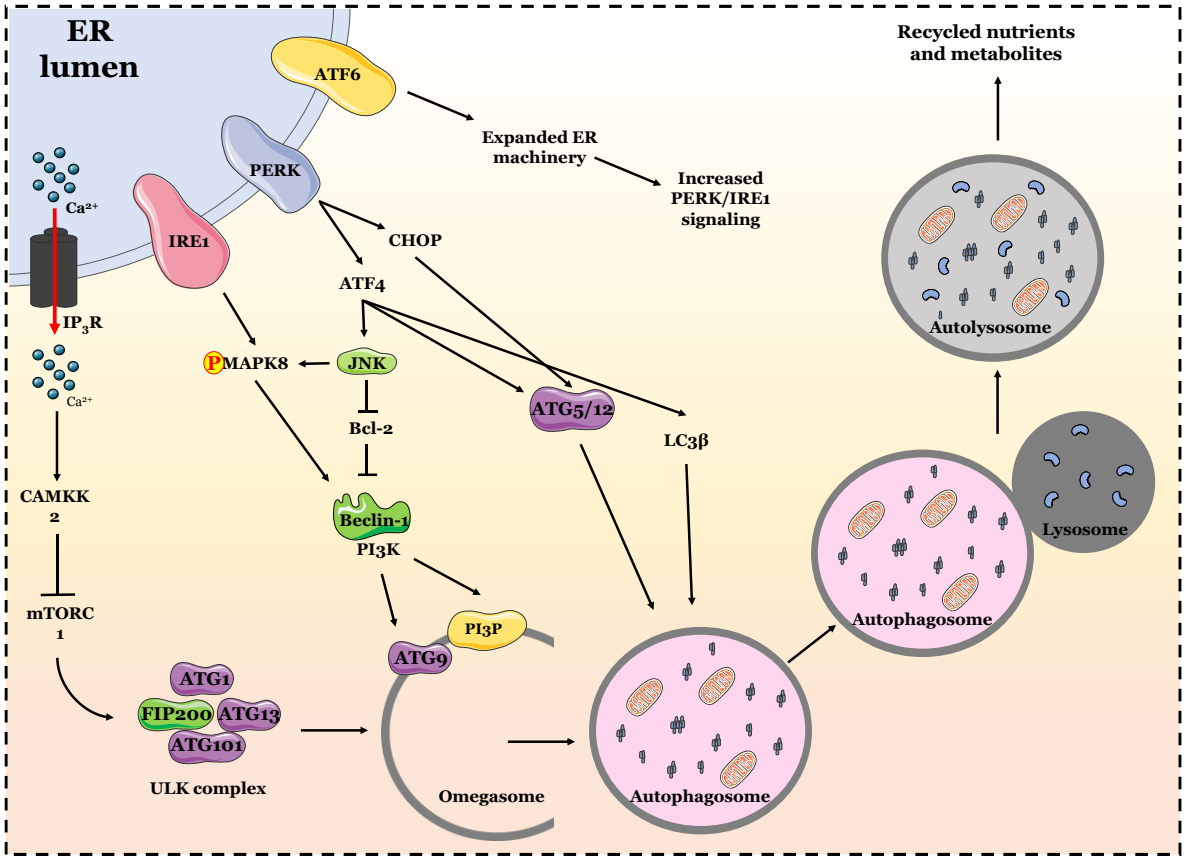

Figure 5. Molecular crosstalk between the UPR and autophagy.

The analysis of autophagy incorporated the identification of autophagic structures and measuring of the autophagic flux, as reviewed elsewhere (199).

The selective lysosomal degradation of ER fragments and/or protein aggregates is termed reticulophagy (200). Together with the UPR and ERAD, reticulophagy is another major quality control pathway that bridges ER turnover and homeostasis. FAM134B (family with sequence similarity 134, member B)/RETREG1 is a reticulophagy receptor, and thus its inhibition enhances proteotoxicity. In malignant cells, it is reported that this receptor inhibits tumoral growth. Concurrently, it is known that aggressive cancers often carry mutations on the corresponding gene. It may also play a role on several other types of chronic disease and on viral infection. For these reasons, it is a potential biomarker of disease (201). Its expression has been evaluated at gene and protein level through through qPCR and Western Blotting, respectively (202), while knockout mouse embryonic

fibroblasts are currently available (203, 204). Recently, an increasing number of such receptors have been identified, including the cargo receptor Atlastin GTPase3 (ATL3), translocation protein SEC63 homolog (SEC63), the long splice variant of RTN3 (RTN3L and CCPG1) (205).

1.7. ER stress in health and disease

ER stress has been observed throughout the pathogenesis of a number of severe diseases of considerable prevalence worldwide, such as cancer, neurodegenerative diseases, cardiovascular diseases, obesity and diabetes mellitus. Furthermore, the link between ER stress and inflammation has already been established.

The latest numbers available show that in 2015 there were some staggering 17.5 million cancer cases worldwide and 8.7 million deaths (206). The enhanced metabolic rates of cancer, resulting from aberrant proliferation under a low vascularized state, results in an adverse microenvironment that includes acidic pH, low oxygen and also and low glucose, as well as other nutrient deficiencies (126). These conditions result in the accumulation of misfolded proteins, reason for which cancer cells depend heavily in adequate proteostasis. For this reason, acute states of the UPR may benefit tumor progression by enhancing the protein folding capacity of malignant cells, hence maintaining proteostasis. However, if the UPR fails to restore ER proteostasis, or if it is augmented beyond a tolerability threshold, tumor cell apoptosis ensues (207).

Building on this information, the pivotal role of the UPR in tumor survival can be exploited from the standpoint of diagnosis and treatment. For example, GRP78 is frequently found to be highly expressed in breast, lung cancer and prostate, as well as other cancers (208-210), being clinically associated to poor prognosis (211, 212). Interestingly, this overexpression of GRP78 in the surface of cancer cells is not found in non-cancer cells (213), which may pave the way for a UPR-guided sorting of cancer cells. Other branches of the UPR are equally known to be involved. For example, increased XBP1 expression and splicing have been described in breast cancer and hepatocellular carcinoma (214-216), which can in turn be a consequence of its regulatory function over GRP78. We refer the reader to previous works that have reviewed the evidence of ER stress and UPR activation in various human cancers (216, 217). There are promising results that suggest this role of UPR branches in tumor progression can be exploited as a therapeutic strategy. For example, the XBP1 splicing inhibitor MKC-3946 has reduced the growth of MM and potentiate the pro-apoptotic effect of the anticancer drug bortezomib (218), a result also found for the IRE1 endonuclease inhibitor STF-083010 (106).

There is sufficient evidence in literature suggesting that triggering ER stress in cancer cells can be an effective strategy for eliciting cancer cell death, both with stand-alone ER stress inducers (72, 219-221) and in combination with well-established anticancer drugs (222, 223).

A significant number of neurodegenerative diseases are, from a pathophysiological point of view, proteinopathies which symptoms arise from upstream protein aggregation or misfolding. Each disease has its typically-involved proteins, such as huntingtin in Huntington's disease, amyloid-β in Alzheimer's (AD) or α-synuclein in Parkinson's disease (PD). AD and PD are the two neurodegenerative disorders of highest incidence worldwide.

For many neurodegenerative diseases ER stress and the activation of the UPR have been established as hallmarks of the aforementioned disorders, being also biomarkers of these conditions (56). Increased levels of phosphorylated PERK and IRE1α have been found in the hippocampus of patients with AD, where they colocalize with phosphorylated tau, one of the hallmarks of the disease (224, 225). In cultured human neurons, exposure to amyloid-β_{42} ($A\beta_{42}$), the major component of amyloid plaques, induces CHOP expression, while treatment with CHOP antisense RNA results in increased survival, thus suggesting a role for the ER in $A\beta_{42}$-mediated cell death and hence a potential pharmaceutical target (225, 226). The involvement of ER stress in neuronal death in AD is further strengthened if we consider that administration of $A\beta_{42}$ results in activation of the ER-resident caspases-4/12, which are involved in ER stress-induced apoptosis (227). Promisingly, co-incubation with the ER protector salubrinal results in decreased toxicity of Aβ42 in primary neurons (209).

Disturbances in the secretory pathway are known to be significant to the onset and progression of PD (228, 229). A few *in vivo* reports establish a relationship between UPR activation and the progression of PD. A number of works show that α-synuclein accumulation at the ER of dopaminergic neuros is accompanied by UPR activation and that ER protectors, such as salubrinal, improve motor performance, alleviate α-synuclein accumulation at the ER and ultimately improve the lifespan of PD models (230).

Even though the existence of a relationship between ER stress and neurodegenerative disorders is fairly documented in the literature, a lot remains to be described in what seems to be a vicious cycle of cause-effect in which ER stress triggers and is triggered by the progression of these diseases. Regardless, the fact that pharmacological intervention with molecules capable of alleviating ER stress show clinical gains in animal models (209, 224, 225) may represent an exciting and promising strategy.

1.8. Conclusions and future perspectives

The performance and UPR signature of the ER are crucial to the physiology of the cell and to its built-in stress response mechanisms. Its importance towards stress recognition and response relies on complex signaling processes that have evolved in eukaryotic organisms.

Regardless of the intense research that has focused in the signaling pathways of the ER and its involvement in disease onset, it is clear that no universal biomarker of UPR activation is currently known. This is to be expected, considering the distinct branches of the UPR and the myriad of pathways that connect the events taking place during the UPR to many other cellular events. Specific UPR signatures have already been identified in cancer cells and have been used as a prognostic marker and as a tool to predict response to chemotherapy. When considering the tight interconnection of cancer to upregulated UPR signature markers, a provocative line of research could be the clarification of potentially oncogenic nature of misfolded proteins.

Likewise, brain tissue of AD and PD patients have shown to overexpress a number of UPR proteins. Are these proteins a consequence of the diseases, or can they perhaps be involved in their very onset? This is still unclear nowadays, however the next few years are expected to shed a light on this apparent cause-effect cycle. It could be the case that both hypotheses are correct and that the explanation lies in the kinetics of the UPR, with different functions in different moments of the cellular fate.

From a pharmacological point of view, there is an increasing number of small molecules known to modulate ER function. Unfortunately, several of those molecules have displayed high toxicity and their use remains in the domain of biochemical tools. Furthermore, it was only in 2016 that one of the first classes of selective ATF6 modulators was described, which furthers the need for more specific and non-toxic ER modulators.

Nonetheless, increasing knowledge of the ER stress molecular network, as well as the establishment of more and more high-throughput techniques that allow testing dozens or even hundreds of molecules at the same time will certainly lead to the identification of novel bioactive molecules on a short term. Furthermore, the field requires more information regarding the impact of the model under study to the stress pathways investigated. For example, ER stress responses in 3D and heterotypic systems are still mostly lacking, as is the detailed knowledge on the kinetics of UPR responses. In a near future, new ER-based strategies will hopefully evolve and add to the current pharmacological arsenal for countering ER stress in disease and, perhaps, establish the ER as a drug target.

1.9. Inflammation

The occurrence of inflammation has been acknowledged since the 1st century in Ancient Rome, where it was documented by Celsus as a set of phenomena that include redness, swelling, heat and pain upon tissue injury. The 19th century witnessed the addition of organ dysfunction to this list, as well as phagocytosis (231). Today, inflammation is regarded as the response to tissue injury or infection by invading pathogens, while also regarded as pathological if the inflammatory signaling is chronical (231). Evolution has carved out inflammatory signaling axes over millions of years to perceive and respond to danger signals that are widespread in the tree of life, with some ranging from mammals to jawless fish, invertebrates, and even the plant kingdom (232). Currently, our knowledge of inflammation remains in steady evolution, allowing us to identify the cell types and the signaling mechanisms involved in its course (231).

As a response to harm, resulting either from pathogen infection, cell or tissue damage, harmful xenobiotics or radiation, the immune system triggers inflammation. Aiming to eliminate the harmful factor and heal the resulting injury, the occurrence of inflammation is crucial in the maintenance of homeostasis (233). When the harmful stimulus is detected, the ensuing signaling cascade involves the release of multiple inflammatory mediators, including cytokines, free radicals, and hormones, as well as leukocyte chemotaxis (234). The signaling machinery that is activated will be detailed hereafter; however, in brief, inflammatory signaling initiates when cellular receptors recognize a threat, leading to the release of inflammatory mediators and, finally, leucocyte recruitment from the blood into tissue (233).

1.9.1. Immune responses and cell types

Even though there is crosstalk between both lines of defense, classically we divide immune responses in two different types, namely the innate and the adaptive.

The innate immune response is responsible for the recognition of pathogen-associated molecular patterns (PAMPs), in order to rapidly respond to the trigger. In this sort of response, a second exposure to the same insult results in the same stereotyped response (235). Briefly, innate immune cells are able to synthesize multiple types of inflammatory mediators upon activation and even perform the phagocytosis of pathogens (236).

On the other hand, the adaptive immune response is activated at a lengthier pace. However, unlike in innate responses, effector cells have their molecular memories altered

to act upon specific triggers, relying on antigen receptor production towards specific molecular patterns (235).

Both types of immune response involve the recruitment of several cell types. This section enumerates the cell types involved in the innate immune response. **Monocytes** and **macrophages**, along with dendritic cells, integrate the mononuclear phagocytic system. These cell types share common traits and differentiate from hematopoietic stem cell monoblasts. Once they differentiate into monocytes, they enter the blood stream, differentiating into macrophages later on, in tissues. Besides their roles in development and homeostasis, macrophages are pivotal cells for both innate and adaptive immune response, and they can differentiate into two opposing phenotypes, a pro-inflammatory type (or M1) and an anti-inflammatory one (or M2). M1 macrophages are essential to eliminate pathogens and perform phagocytosis of their components, as well as to produce pro-inflammatory mediators and induce the differentiation of T cells. Differently, M2 macrophages, are vital to the resolution of inflammation and tissue repair (237, 238). Monocytes can also give rise to **dendritic cells** (238). Dendritic cells are innate immune cells that provide an interface between adaptive immune responses. While they recognize PAMPs and damage-associated molecular patterns (DAMPs), they also interact with T cells as antigen-presenting cells, inducing their activation (239). Recognition of PAMPs and/or DAMPs, as well as the presence of endogenous inflammatory *stimuli*, induce their maturation and migration (240). Similarly, **mast cells** also derive from the myeloid lineage and are implied in innate and adaptive defenses. Notably, these cells mediate inflammation and allergic reactions, like anaphylaxis. Mast cells are thought to have evolved before antibodies, since urochordates present homologous cells (241). Like dendritic cells, mast cells migrate and mature upon the presence of endogenous inflammatory *stimuli*, and can be activated upon recognition of PAMPs or DAMPs. Furthermore, they can undergo antigen-specific immunoglobulin E (IgE)-mediated activation. These cells harbor pre-formed secretory granules containing proteases and inflammatory mediators, being also capable of producing newly-synthesized mediators. These mediators include pro- and anti-inflammatory cytokines, chemokines, leukotrienes, prostaglandins and eicosanoids (242, 243). **Natural killer (NK) cells** are short-lived granular cells that belong to the innate lymphoid cell family. These cells possess cytolytic activity against infected, malignant and activated immune cells, which produce ligands that are recognized by cell surface receptors. Furthermore, these cells can secrete pro-inflammatory cytokines. Thus, NK cells are capable of upregulating or downregulating immune responses, thereby keeping homeostasis (244). The recruitment of NK cells involves chemotaxis and the expression of adhesion molecules, for instance, by mast cells or dendritic cells. However, it is possible for these cells to act upon their targets without priming of any kind, albeit their cytolytic activity is strongly

enhanced upon activation by cytokines (245). In spite of being considered innate immune cells, it has been established that NK cells can acquire immunological memory like adaptive immune cells (246). Another kind myeloid cells that are front-line responders of the innate immune system are **neutrophils**, that comprise half or more of circulating leukocytes. These cells are associated to the innate response to pathogen infection, which can cause their production to increase ten-fold (247). Neutrophils present strategies against pathogen infection that include degranulation (since, like mast cells, they possess secretory granules), phagocytosis or neutrophil extracellular traps. The latter are built from proteins and DNA from neutrophils into extracellular fibers (248, 249). Even though these cells were once considered a homogeneous population, evidence arises that there are discrete populations of neutrophils, even though they are yet to be precisely defined (248, 250). Generally, 1-5% of leukocytes in the blood are **eosinophils**, that are traditionally associated to parasitic infections and allergy. These bone marrow-derived cells release both stored and newly-synthesized inflammatory mediators upon recruitment and activation. The referred mediators comprise cytokines, chemokines, lipids and cytotoxic granule proteins (251, 252).

The defensive capacity of **epithelial cells** goes beyond the physical barrier they constitute against the entry of pathogens into the organism, since they can produce cytokines to mount immune responses and counter the invasion (245). That is also the case of **endothelial cells** (236). Other cell types that are not classically associated to immune responses but have also been observed to be involved in innate immunity are **fibroblasts** (253), **keratinocytes** (254) and **smooth muscle cells** (255). Finally, **natural killer T cells** present a hybrid nature between innate and adaptive immune cells. They received their designation due to the fact that they present cell receptors of NK cells along with a T cell (adaptive cells) receptor (256).

On the other hand, the adaptive immune response relies on **T** and **B lymphocytes**. While both are hematopoietic cells, T cells have the peculiarity of maturing in the thymus. Both cell types can be further divided in subsets; briefly, T lymphocytes are in charge of the cytotoxic immunity, while B lymphocytes take the role of producing antibodies and other macromolecules (257). T-cells may originate two types of T helper (Th) cells, being that Th1 cells produce cytokines, including interferon-γ (IFN-γ), and Th2 cells elicit B-cell maturation (231).

Upon infection or tissue damage, immune cells undergo chemotaxis towards the affected site. Neutrophils are the first to reach the site, ahead of monocytes, NK cells, T and B cells, and mast cells (233).

1.9.2. Inflammatory signaling

DAMPs are endogenous biomolecules, like ATP, DNA or heat shock proteins (HSPs), that are released upon cell or tissue damage (258). PAMPs are components from pathogens, including lipopolysaccharides, heat shock proteins, peptidoglycans and cytosine phosphate-guanin units (232). DAMPs and PAMPs are recognized by pathogen recognition receptors (PRRs), that include toll-like receptors (TLRs), mannose binding lectin (MBL) and nucleotide-binding oligomerization domain (NOD)-like receptors (NLRs). The response to DAMPs and PAMPs allows the organism to differentiate endogenous threats from pathogen infection (232).

PRRs are expressed by innate immune cells and are activated upon detection of PAMPs or DAMPs, in immune cells and also in other cell types, initiating both infectious and noninfectious inflammatory signaling. Activation of these receptors results in the activation of signaling cascades that will be discussed herein, namely the nuclear factor kappa-B (NF-κB), mitogen-activated protein kinase (MAPK) and Janus kinase-signal transducer and activator of transcription (JAK-STAT) pathways. These are the main signaling pathways of inflammation, which will be discussed throughout this section and schematized in **Figure 6**. Impaired function of one or more of them can lead to disease development (233).

1.9.2.1. NF-κB

The inflammatory process is largely mediated by NF-κB, a transcription factor that is activated upon many different insults, from infection to physical damage, and is pivotal for both innate and adaptive immune responses. This transcription factor was first observed in human B cells and has been a subject of intense research ever since, given its pivotal role in commanding innate immune cells (259).

When inactive, NF-κB remains in the cytoplasm, where it is kept in this form by binding NF-κB inhibitors (IκBs) (158). The active form of the NF-κB is a dimer comprising a combination of two of the five Rel family proteins, namely p65 (or RelA), RelB, c-Rel, p105/p50 (or NF-κB1) and p100/52 (or NF-κB2), being that p65, RelB or c-Rel have to be present to render it active. This occurs because, even though all five mentioned proteins possess a Rel Homology Region (RHR) that includes a DNA-binding domain in the N-terminal region, a dimerization domain in the C-terminal region, and a nuclear localization signal (NLS), only p65, RelB and c-Rel display a transcription activation domain (158, 259). NF-κB1 p50 and NF-κB2 p52 form homodimers that have an inhibitory effect, unlike the other NF-κB Rel proteins (259). The units that are assembled into an active transcription factor, and thus its transcriptional outcome, depend on the cell type and environment. For

instance, c-REL is of particular relevance to macrophages and, on the other hand, dimers containing RelA/p50 are abundant in fibroblasts. Elimination of c-Rel and p50 in mice macrophages result in disabled phagocytosis and antimicrobial protein synthesis, and thus impaired response towards bacterial infection (259).

NF-κB activation may occur through canonical on non-canonical pathways. The canonical pathway consists in the activation of cytokine receptors, antigen receptors and PRRs, leading to IκB phosphorylation (158). Once IκB is phosphorylated, it is degraded by the proteasome and results in the release of NF-κB, its translocation to the nucleus and subsequent DNA binding. At this point, this transcription factor will govern cytokine synthesis and cell recruitment (233). The NF-κB essential modulator (NEMO or IKKγ), along with IKKβ, constitute the IKK2 complex. IKK2 is phosphorylated upon cytokine or PRR signaling, and phosphorylates IκB, tagging it for ubiquitination and subsequent degradation. This process makes up the canonical NF-κB signaling pathway. Upon translocation to the nucleus, the active transcription factor promotes the expression of primary response genes such as *TNF* and *IL1B* (259). IκB proteins block the DNA-binding sites on the Rel proteins, while also preventing the translocation of the transcription factor into the nucleus, until they are degraded by the proteasome. *De novo* IκB synthesis leads to the establishment of a negative feedback loop that modulates the dynamics of NF-κB signaling. New IκB will promote the inactivation of NF-κB and its translocation to the cytoplasm, where it can be reactivated (259). The noncanonical NF-κB pathway integrates with the canonical pathway in the adaptive immune response. Briefly, it implies p100 (NF-κB2 precursor protein) processing, being activated in the presence of ligands of tumor necrosis factor superfamily receptors (TNFRs). This is a signaling pathway that lasts longer than the canonical pathway, albeit taking longer to activate (260). Activated NF-κB acts as a transcription factor, upregulating the expression of pro-inflammatory genes, including cytokines and chemokines (260). Different transcriptional outcomes may be due to the diversity of ligands and receptors that result in NF-κB activation (259). The importance of NF-κB signaling comprises both innate and adaptive immunity. The canonical NF-κB pathway is of particular relevance to the innate immune response, given that it is quickly initiated in the involved cells, like macrophages (259).

Canonical NF-κB activation induces the expression of a battery of pro-inflammatory genes, including genes coding for cytokines, chemokines, enzymes and other inflammatory mediators, that either are direct players of the inflammatory response or indirect, promoting immune cell differentiation. Furthermore, NF-κB regulates the function of T cells and inflammasome activation (260). Among the activators of NF-κB we can include pathogen-derived ligands, cytokines and enzymes (233). NF-κB can be activated by PRRs, including TLRs and NOD-like receptors, T and B cell receptors, cytokine receptors such as

TNFRs and IL1Rs, and others (259). TLR4 activation leads to NF-κB activation via MyD88 (259). TLRs are the most broadly studied of all the PRRs. These receptors engage in inflammation initiation, mediating the transmission of PAMPs and DAMPs and ensuing the activation a signaling cascade (233).

LPS binds the TLR4 receptor on the macrophage membrane. This can occur through two adapters. When it occurs through the MyD88 adapter, it induces the polarization of the macrophage towards the M1 phenotype and results in the expression of pro-inflammatory genes. On the other hand, activation *via* the TRIF adapter results in the induction of IFNs and, consequently, of genes that are upregulated in the presence of IFNs (260).

1.9.2.2. JAK-STAT and MAPK

Besides NF-κB signaling, there are other signaling cascades that govern inflammatory signaling. The Janus kinase/signal transduction and activator of transcription (JAK-STAT) signaling pathway implicates extracellular factors (namely cytokines and growth factors) that regulate gene expression by inducing the activation of STATs, which are cytoplasmic transcription factors. JAKs are associated with receptors, and, upon the presence of their ligands, they phosphorylate each other, leading to the formation of docking sites for STATs. After recruitment, STATs are phosphorylated and then dimerize. Translocation to the nucleus ensues, where they perform their function as transcription factors (233). This signaling pathway can be initiated by anti- or pro-inflammatory cytokines.

The serine/threonine protein kinases known as MAPKs comprise the c-Jun N-terminal kinase (JNK), the extracellular-signal-regulated kinase (ERK) and the p38 MAPK. Each of these can occur in different isoforms. MAPKs regulate many cellular processes. In the event of TLR signaling, JNK and p38 MAPK are activated (233, 261). The MAPK pathway is activated along with the interferon regulatory factors 5 (IRF5) and 3 (IRF3), leading to the expression of antiviral genes such as the ones encoding interferons (IFNs) (259).

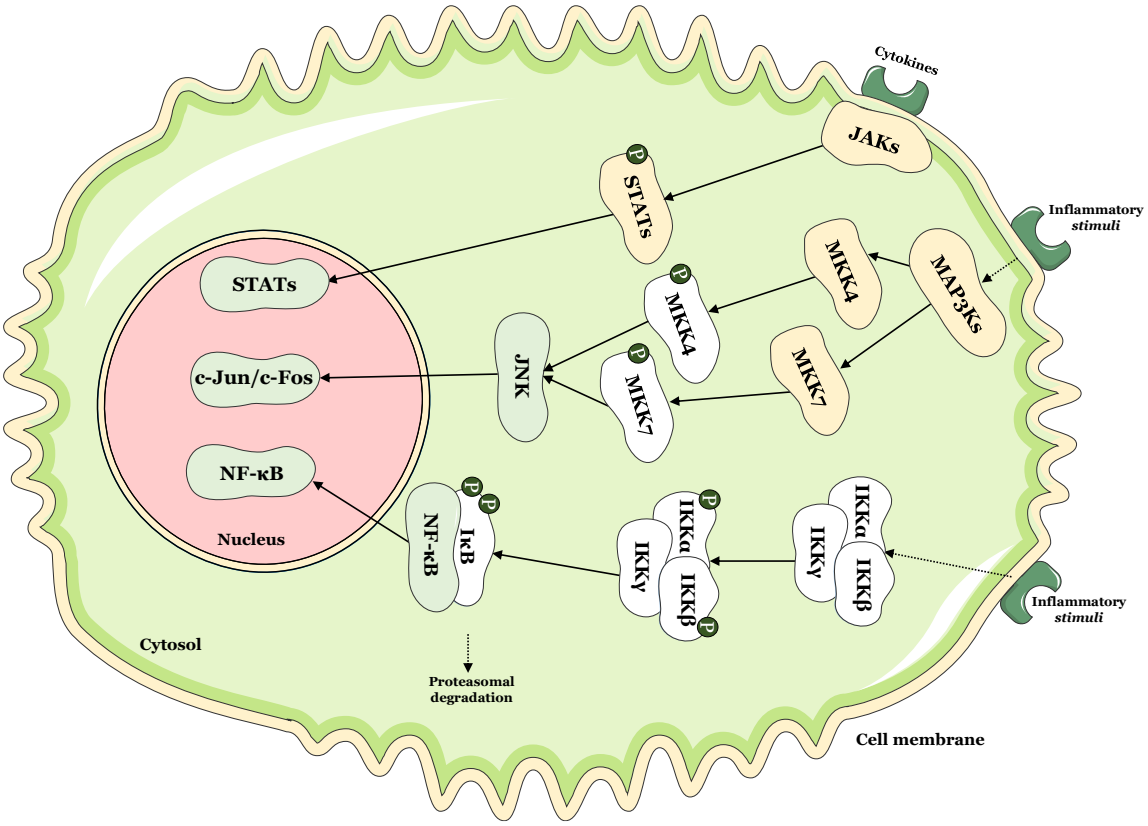

Figure 6. Scheme of the signaling cascades underlying inflammatory signaling, namely NF-κB, MAPK and JAK-STAT pathways.

1.9.3. Cytokines

Upon injury or infection, multiple cell types can produce and secrete cytokines in order to modulate the immune response and activate immune cells. Depending on the cell type they are targeting, cytokines can be pleiotropic, redundant or synergistic (232, 262). Essentially, cytokine release constitutes a communication network among innate immune cells and between innate and adaptive immunity, regulating inflammatory signaling and mediating the activation of T and B cells (236). According to whether they elicit or inhibit inflammation, cytokines can be pro- or anti-inflammatory. Pro-inflammatory cytokines are, as mentioned before, secreted by M1 macrophages. Conversely, anti-inflammatory cytokines are released by macrophages displaying the M2 phenotype (260). Just like pathogen products, cytokines are primary inflammatory *stimuli*. Primary inflammatory *stimuli* are defined as products that can mediate inflammatory signaling by activating inflammatory receptors, like TLRs, the IL-6 receptor (IL-6R), the tumor necrosis factor (TNF) receptor or the IL-1 receptor (IL-1R) (233). The release of cytokines may occur in a constitutive or inducible manner. One instance of the latter is when it occurs in response to TLR signaling and cytokine receptor activation. After synthesis, that takes place in the ER, most cytokines are translocated to the Golgi apparatus in order to be directed to their site

of storage within the cell or to be released by exocytosis, even though some cytokines are released by different mechanisms (e. g. IL-18) (236).

Interleukin-6 (IL-6), TNF-α and IL-1β are the major proinflammatory cytokines. **IL-6** has a major role in acute phase inflammatory signaling and B cell differentiation (263). **TNF-α** is predominantly secreted by Th1 cells and induces the activation of macrophages towards the M1 phenotype (237). The TNF-α activates the TNFR through NF-κB signaling. It can trigger Fas and caspase-mediated regulated cell death. **IL-1β** is produced upon PRR activation of macrophages and dendritic cells. Its activation involves the proteolysis of the IL-1β precursor, that can be carried out, by caspase-1 upon inflammasome activation (232). Nonetheless, there are many other proinflammatory cytokines and chemokines, such as the **IL-8**, also referred to as chemokine ligand 8 or CXCL-8. This is a strong chemokine that induces neutrophil and T cell chemotaxis (e. g. recruitment to target site), and is synthesized and released upon TLR signaling *via* NF-κB and JNK signaling (232). On the other hand, anti-inflammatory cytokines include ILs like IL-4 and -10, that are secreted by Th2 cells and differentiate macrophages to the M2 anti-inflammatory phenotype (237).

Macrophages synthesize cytokines and inflammatory mediators upon activation, releasing them immediately upon synthesis by constitutive exocytosis *via* recycling endosomes and small secretory vesicles. Differently, mast cells, eosinophils and neutrophils are granulocytes. This means that they synthesize and store cytokines from early on to release upon activation. Prior to release, cytokines may be stored in the Golgi apparatus, in secretory granules or vesicles, and undergo regulated exocytosis upon receptor activation in the cell membrane (236).

1.9.4. Reactive oxygen species (ROS)

ROS are byproducts of aerobic metabolism that are partly reduced and present a strong oxidizing potential. They comprise the **singlet oxygen** ($^1O_2$), **superoxide anion** ($O_2\bullet^-$), **hydroxyl** ($HO\bullet$), **hydrogen peroxide** (H_2O_2), **hydroperoxyl** ($HO\bullet_2$) and **hypochlorous acid** (HOCl), being that the latter five occur the most frequently (264, 265).

Generation of ROS as byproducts of metabolic function can occur in the cytoplasm, cell membrane, ER, mitochondria and peroxisome (266). The majority of ROS are generated by the electron transport chain (ETC) in the mitochondria (265). The ETC and a proton gradient to drive ATP production govern mitochondrial respiration, producing ROS as a byproduct. For this reason, inflammatory and metabolic diseases implicate overproduction of mitochondrial ROS. Macrophage activation implicates mitochondrial hyperpolarization and succinate oxidation, shifting towards glycolysis-derived ATP

production and enhanced ROS production (266). As a consequence, inflammatory signaling shifts the ratio of reduced/oxidized GSH in favor of the oxidized form (264).

Nonetheless, the mitochondria also produces ROS by enzymatic activity, such as by action of the dehydrogenases that reside in the matrix (264). Other than this, the activity of multiple enzymes that reside in other locations can result in ROS production, as is the case of the activities of cyclooxygenases, lipoxygenases, nicotinamide adenine dinucleotide phosphate (NADPH) oxidases and cytochrome P450 enzymes (264). In fact, a significant amount of cellular ROS is the direct result of the activity of NADPH oxidase (265, 266). Given their role in aerobic metabolism, peroxisomes are another major source of ROS. These organelles possess several enzymes that result in the generation of hydrogen peroxide, such as xanthine oxidase, acyl-CoA oxidases (ACOX) and polyamine oxidase (266).

There are several roles for ROS in the inflammatory process. Upon inflammation initiation, phagocytic cells, such as macrophages, phagocytize invading pathogens and cellular debris that are to be eliminated, resulting in NADPH oxidase activation and reduction of molecular oxygen, that ultimately leads to more ROS production, in a process that is known as the "oxidative burst". Generated ROS are then released, directly killing invading pathogens by oxidation of several biomolecules. ROS contribute to pathogen elimination in a multitude of other mechanisms, including enzymatic or autophagy (264, 267). ROS also play a part in the performance of phagocytosis and efferocytosis by macrophages, being that these functions require efficient oxidative signaling, for example, in order for lysosomal fusion and phagosomal clearance of apoptotic cells to occur (266).

Increased ROS levels resulting from inflammation further regulate NF-κB activation, inflammasome activation and cytokine release, as well as proteasome activity and transcription of genes of the antioxidant machinery (266).

ROS regulate blood leukocyte migration through the expression of intercellular adhesion molecules on the endothelial surface of the target site (268). In fact, one of the factors that governs leukocyte migration is the emergence of a H_2O_2 gradient (264). Furthermore, ROS mediate inflammation indirectly by promoting the generation of reactive nitrogen species (RNS), which also play a pro-inflammatory part (265). Mitochondrial ROS regulate LPS-mediated NF-κB activation, release of cytokines, NLRP3 inflammasome priming and activation, activator protein 1 (AP-1) activity (266). Finally, the apoptosis of neutrophils and other granulocytes, a major event in the resolution of inflammation, is governed by ROS-dependent signaling pathways (264).

1.10. Inflammation and ER stress

The architecture of the ER comprises the rough ER, the smooth ER and the nuclear envelope. The latter composes another domain of the ER itself, being contiguous and structurally similar to the rough ER (269). As mentioned before, the ER carries out protein biosynthesis and transport to target sites, protein folding, biosynthesis of lipids and steroids, calcium storage, and also carbohydrate metabolism. This variety of functions leads to a complex architecture of the peripheral ER, that varies between different cell types, according to their necessities, since each function is related to a respective physical domain within the organelle. In a general manner, cells that present higher protein synthesis rates present a more developed rough ER, while cells specialized in lipid biogenesis exhibit a larger smooth ER (1). Specifically, plasma and beta cells synthesize large amounts of proteins for the secretory pathway, and therefore present a highly developed rough ER. On the other hand, smooth ER is more abundant in the liver (158). Furthermore, the ER possesses specialized areas that communicate with other cellular organelles, such as the Golgi apparatus and mitochondria, that are dubbed membrane contact sites (270, 271). The synthesis of proteins within the ER is mainly of proteins for the secretory pathway and membrane proteins, but also includes proteins destined to the cytosol. This occurs in the rough ER, since it requires the presence of ribosomes to the cytosolic surface of the organelle (1). The function of this organelle, as well as the molecular machinery that underlies its stress response, were detailed in **Section 1.1.**.

Both inflammation and ER stress signaling have evolved and are activated as protective and coping mechanisms. However, when triggered in an intense or prolonged manner, both can lead to organized cell death (158). Notably, both processes occur concomitantly in multiple settings, which prompts the introduction to the relationship between them in this section. In fact, chronic diseases are often characterized by the concomitance of inflammation and ER stress (158, 233). For instance, it has been shown that ER stress aggravates inflammatory processes in pancreatic cells, stimulating the pathogenesis of type I diabetes (158).

Even though, in most cases, whether ER stress is a cause or consequence of a particular disease is yet to be defined, there is a consensus in that it can be a therapeutic target. Notably, mitigating ER stress associated to inflammation has proven to result in few undesirable side effects (158).

1.10.1. Inflammatory signaling

Known ER stressors, such as thapsigargin and tunicamycin, are known to activate NF-κB, which can result from the activation of any of the three major signaling branches of the UPR. ER stress inhibition proved efficient in reducing inflammation in several *in vitro* and *in vivo* models (158).

Phosphorylated eIF2α, as mentioned in **Section 1.2.1.**, leads to a halt in global protein synthesis rates. The mechanism through which the PERK branch of the UPR can trigger NF-κB lies in this fact, since this halt exerts a crisp effect upon short-lived proteins, as is the case of IκB (158). In fact, it was observed that the knockdown of PERK resulted in impaired NF-κB activation in astrocytes (272). Nonetheless, it selectively enhances the translation of genes that possess internal ribosome entry sites, such as ATF4. One example of this is that PERK-ATF4 signaling is reported to promote cell survival in hibernating bats by inducing NF-κB activation, as well as Nrf2 activation and modulation of Akt signaling (273). Nrf2 relates to redox homeostasis, while Akt promotes cell growth and survival (274, 275).

Concurrently, the kinase activity of IRE1 maintains the activity of IKK (276). Moreover, the IRE1-XBP1 signaling axis governs NK cell proliferation (277). Relevantly, ER stress leads to JNK activation *via* IRE1 signaling. Upon activation, IRE1 binds the TNF receptor-associated factor 2 (TRAF2) that will, in turn, recruit ASK1, ultimately activating JNK (278). At this point, JNK will phosphorylate the transcription factor activator protein 1 (AP-1), promoting the expression of pro-inflammatory genes (234). Furthermore, IRE1 activation results in ERK activation (158). Other than its established functions in innate immunity, interleukin-1 receptor-associated kinase-2 (IRAK2) is an amplifier of the IRE1 branch of the UPR (158).

Similarly, activation of the ATF6 signaling branch of the UPR has also been observed to induce NF-κB and Akt activation and cytokine release, and also enhance cytokine synthesis (279, 280).

1.10.2. Oxidative stress

As mentioned before, protein folding is carried out by the ER. This process is responsible for up to 25% of the generation of ROS within a cell, as the organelle needs to maintain an oxidizing environment for the formation of disulfide bonds. The formation of this disulfide bonds is catalyzed by the protein disulfide isomerase (PDI) by thio-disulfide oxidation, reduction and isomerization between cysteine residues of newly synthesized peptides. The ER membrane-associated oxidoreduction (ERO1) is then in charge of

transferring the electrons from reduced PDI to O_2 molecules, resulting in ROS production. Furthermore, disulfide bonds that are to be eliminated are reduced by GSH leading to a decreased ratio of GSH to oxidized glutathione (GSSG). While in the cell the average GSH:GSSG ratio is anywhere between 30:1 and 100:1, in the ER this ratio oscillates between 1:1 and 3:1. Additionally, the activity of the ER transmembrane protein NADPH oxidase complex (Nox4) leads to the production of superoxide anion and hydrogen peroxide (158).

1.10.3. Calcium homeostasis

As mentioned before, the ER stores the majority of the cellular Ca^{2+}. The organelle has evolved to be capable of regulating its extracellular concentration in a millimolar range (10-100 mM) and maintaining a concentration of Ca^{2+} in its lumen in the µM range (100-800 µM), while the cytosolic concentrations can be as low as 100 nM. This is achieved through a network of channels, pumps, sensors and calcium-buffering proteins (1, 158, 169). This second messenger is released into the cytosol when necessary, through inositol 1,4,5-triphosphate receptors (IP_3Rs). Conversely, Ca^{2+} reuptake occurs through the the Sarco/ER calcium-ATPase (SERCA) pump (169). In the ER lumen, Ca^{2+} is buffered predominantly by proteins of low affinity but high capacity to bind Ca^{2+} like calreticulun and calsequestrin. In the cytosol, calcium buffers present high affinity but low capacity to bind Ca^{2+}, like parvalbumin or calbinidin. Ca^{2+} sensors include calmodulin. This and other sensors can, however, also buffer Ca^{2+} (169).

Ca^{2+} transfer from the ER to the mitochondria (*via* MAMs) is essential for healthy mitochondrial function. However, upon severe ER stress, misfolded protein accumulation provokes the efflux of Ca^{2+} from the ER stores, *via* IP_3Rs. These ions will influx into the mitochondria, resulting in ATP depletion and ROS accumulation, leading to cell death. On the other hand, Ca^{2+} induces the depolarization of the mitochondrial membrane, resulting in the opening of pores, fragmentation of the mitochondrial and release of cytochrome *c* and other proteins, this triggering the mitochondrial pathway of apoptosis (281).

Activation of T-cell receptors (TCR) results in inositol phosphate generation and Ca^{2+} release from the ER stores. The efflux of Ca^{2+} is recognized by the N-terminal domain of the luminal Ca^{2+} sensors EF-handed stromal interaction molecules 1 and 2 (STIM-1 and -2), ultimately inducing its translocation to the plasma membrane to engage in the activation of Ca^{2+} release-activated Ca^{2+} channels (CRAC) on the cell membrane by store-operated Ca^{2+} entry (SOCE) and consequent and influx of extracellular ions into the cell (282). SOCE also plays a part in ROS production by NADPH oxidase, since the activation of the latter is Ca^{2+}-dependent (282). Moreover, stimulation of TCRs by Ca^{2+} signaling leads to the activation of nuclear factor of activated T cells (NFAT), that regulates T cell activation (282-286).

Excess intracellular Ca^{2+} increases cytokine expression and activates calcineurin, that dephosphorylates NFAT, leading to its activation. This renders an active transcription factor that governs cytokine expression. It can also activate the calmodulin-dependent protein kinase II (CaMKII), that promotes NF-κB signaling by phophorylating IκB (282).

Increases in intracellular Ca^{2+} correlates with the process of degranulation and cytokine release in neutrophils, and this increase is possibly enough to trigger exocytosis by itself (282). Ca^{2+} regulates not only macrophage activation but also their polarization towards the M1 phenotype and phagocytic activity, as documented in *in vivo* studies in mice (287, 288). In zebrafish, Ca^{2+} was identified as the first signal for macrophage recruitment and activation upon wounding, as well as regulating phagocytosis, cytokine expression and polarization of macrophages towards the M1 phenotype (289).

Abnormal ROS production and abnormal Ca^{2+} generate a positive feedback loop between each other, given that excess ROS can also promote the cellular uptake of Ca^{2+} (290). Finally, as will be discussed below, Ca^{2+} signaling impacts inflammasome activation.

1.10.4. Inflammasome

Upon the recognition of PAMPs and DAMPs, inflammatory caspase activation and the assembly of intracellular multi-protein complexes may occur. These complexes are labeled inflammasomes and are most extensively present in macrophages, but also in dendritic cells, neutrophils and non-hematopoietic cells involved in inflammatory signaling, integrating the innate immunity (291). Inflammasomes are constituted by three parts: a receptor (the sensor), caspase-activation recruitment domain (apoptosis associated speck-like protein containing CARD (ASC), the adaptor), and the cysteine protease caspase-1 (the effector).

The receptor is a member of the NLR family, either NLRP1, NLRP3 or NLRC4, or AIM2, being that the NLRP3 inflammasome is the most studied among these complexes (260). The adapter is the ASC. The ligand-sensing receptor oligomerizes when activated, hereupon the pro-caspase-1 is recruitment occurs, mediated by the ASC. Pro-caspase-1 endures proteolytic cleavage to originate the active form of caspase-1, that in turn processes the precursors of IL-1β and IL-18. Both cytokines are subsequently released in their mature forms. Inflammasome activation also requires binding of NIMA-related kinase 7 (NEK7), a regulatory protein, to NLRP3 (292).

NLRP3 inflammasome activation implies two signaling steps: the first relies on NF-κB signaling and is termed priming; the second leads to assembly and activation of the inflammasome, resulting in caspase-1 activation and maturation and release of IL-1β (293). Priming enhances the expression of the genes corresponding to NLRP3 and pro-IL-1β, as

well as post translational modifications including the deubiquitination of NLRP3. Activation can be induced by any NLRP3 agonist, like the efflux of K^+ or Ca^{2+} ions, ROS or proteases, resulting in caspase-1 activation and maturation and release of IL-1β (260) (294).

Cellular organelles, namely the ER and mitochondria, participate in NLRP3 inflammasome activation. The influx of Ca^{2+} from the ER stores into the mitochondria leads to the leakage of mitochondrial contents and results in NLRP3 activation. Furthermore, the area between the ER and mitochondria provides a platform for NLRP3 inflammasome assembly, since the inactivated NLRP3 locates mainly in the ER but translocates to this interface upon activation (295).

A brief overview of the relationship between inflammation and ER stress is schematized in **Figure 7**.

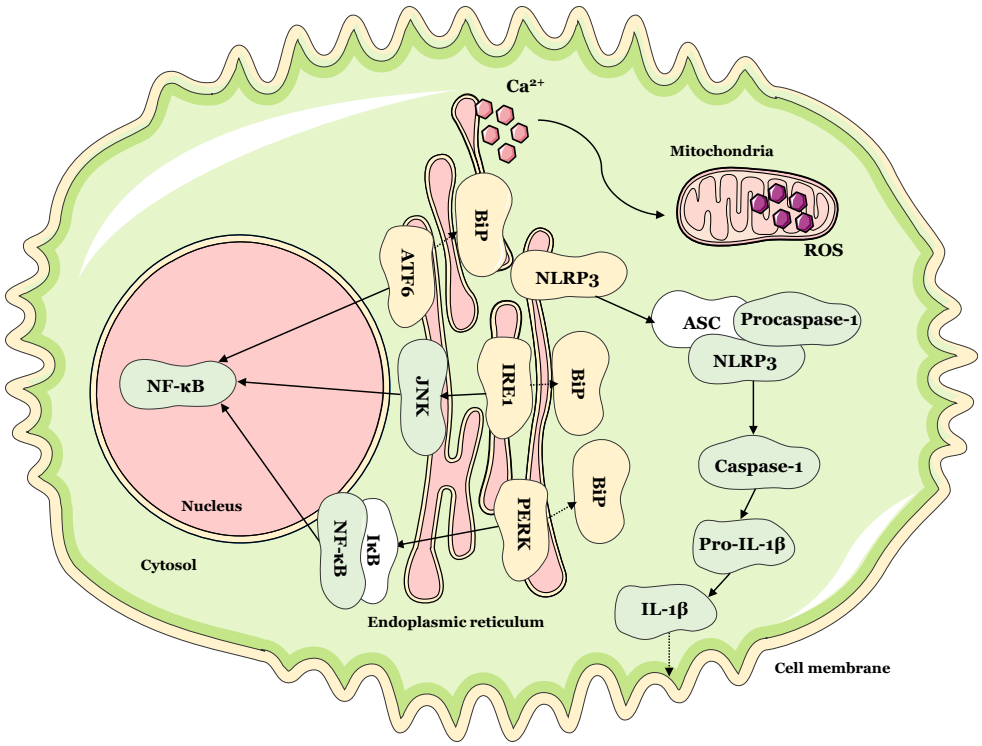

Figure 7. Overview of the interplay between inflammatory signaling and the UPR.

1.11. Naturally occurring ER stress modulators

Humans have resorted to Nature as a source of medicine from immemorial times. For millennia, it was the sole provider of medicine, being that the oldest records found so far date back to 2600 BC in Mesopotamia and include the use of *Papaver somniferum* L. oil, still used nowadays to obtain morphine. Today, it is estimated that roughly 80% of the global population still relies on traditional medicine, specifically on plant products, to obtain health care (296). Plant extracts and plant-derived drugs, often arising from the

knowledge of traditional medicine, still play an important part in the health care provided to the population of developed countries. Despite the remarkable contribution of Nature to the modern pharmacological arsenal, most of its value is yet to be uncovered. The percentage of higher plants that have been analyzed for the presence of bioactive natural products is estimated at only 5-15%, the percentage of fungus is thought to be under 5% and bacteria under 1% (296). The potential of most of the world's biodiversity remains untapped, especially that of extreme environments, where a lot of potential may lie. Currently, endangered ecosystems may be lost, along with some of this biodiversity and its underlying potential (296).

Figure 8 illustrates the relevance of natural products in the bulk of new approved drugs over the last 40 years. We see that the portion of pure natural products approved for pharmacological use is rather small (<5%). Nonetheless, natural product derivatives represent a larger percentage of these drugs. Natural products, their derivatives and the so-called botanical drugs account for nearly 25 % of all approved drugs in this time frame. Other than this, it is worth mentioning that some synthetic drugs are designed to incorporate a known pharmacophore from a natural product. Taking this into account, only 36% of all the drugs approved in this time period are truly synthetic, and a portion of those is designed to mimic a natural product, i.e., to compete with an endogenous substrate of a given target. The importance of natural products to modern medicine is therefore insurmountable.

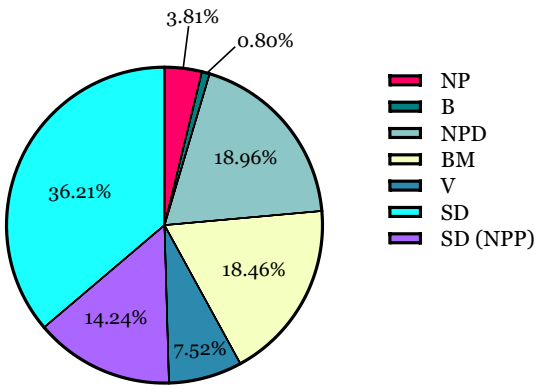

Figure 8. Origin of the approved drugs over the last four decades. Adapted from (297). **NP**: natural product, **B**: botanical drug, **NPD**: natural product derivative, **B**: biological macromolecule, **V**: vaccine, **SD**: synthetic drug, **SD (NPP)**: synthetic drug with natural product pharmacophore.

Relevantly, the scientific literature attributes the ability to modulate ER stress to multiple natural products, as reviewed elsewhere (128, 298). A few examples are referred below, and their chemical structures are presented in **Figure 9**.

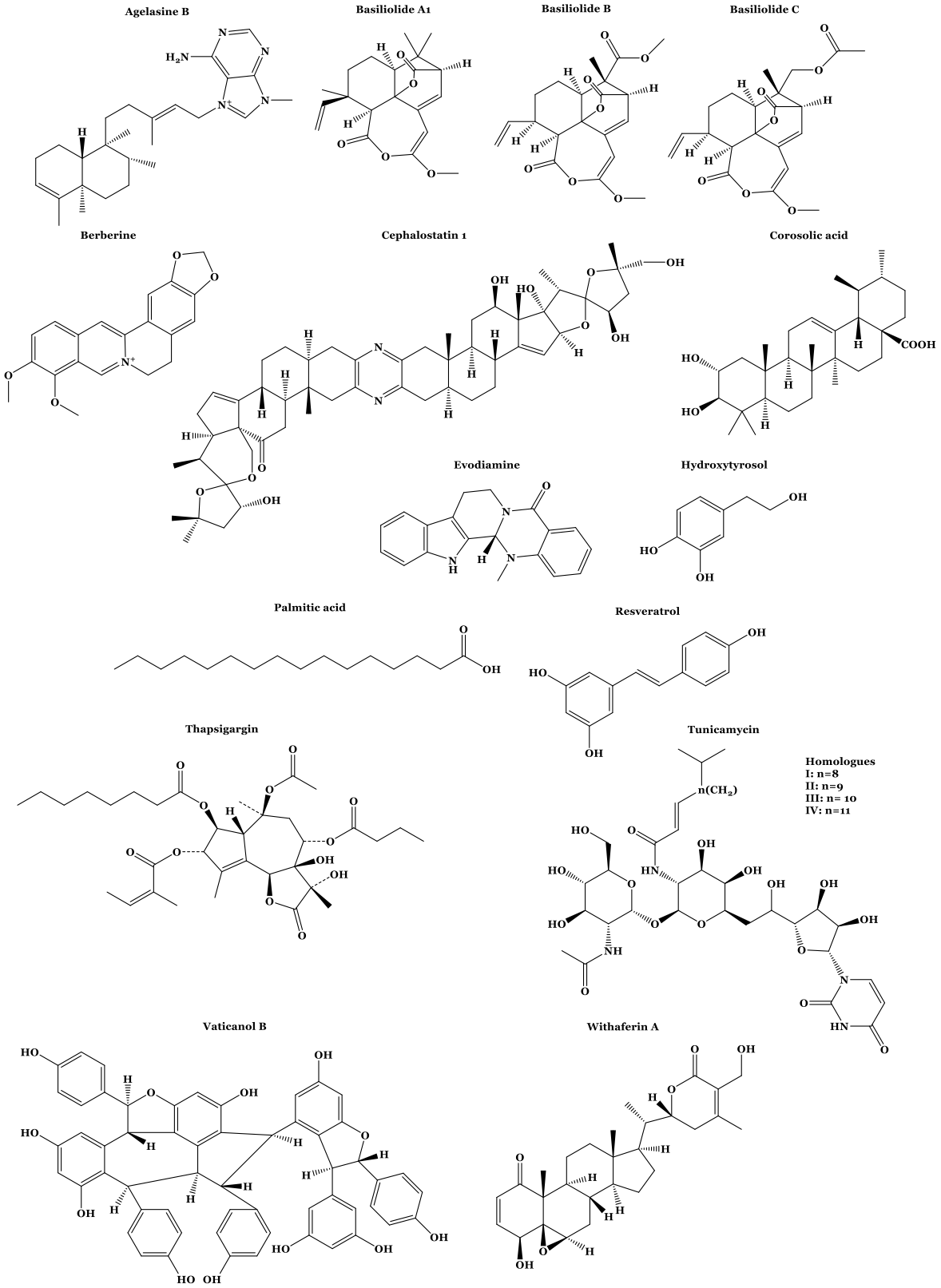

Figure 9. Chemical structures of the natural products with known ability to modulate ER stress that are discussed in this section.

Thapsigargin, a sesquiterpene lactone, occurs naturally in the poisonous plant *Thapsia garganica* L., which is spread throughout the Mediterranean area (299). It has been extensively employed in ER stress research since its characterization as a selective SERCA pump inhibitor in the early 1990's (144, 145). The SERCA pump is in charge of uptaking Ca^{2+} ions from the cytosol and store them in the ER lumen, and thus its function is essential in keeping Ca^{2+} homeostasis in the cell. Its inhibition leads to a rise on Ca^{2+} levels in the cytoplasm, which, in turn, depolarize mitochondrial membranes, leading to their disruption and triggering programmed cell death, resulting from the release of factors like the cytochrome c, which resides in the mitochondria (300, 301).

Along with thapsigargin, **tunicamycin**, a mixture of nucleoside homologues isolated from *Streptomyces* sp., is one of the most common agents to be used by researchers as an ER stress inducer (302). Tunicamycin triggers ER stress by inhibiting N-linked glycosylation of newly synthesised proteins, leading to the build-up of unfolded protein aggregates in the ER lumen and consequent triggering of the UPR. By now, this mechanism of action has been observed in an extensive set of *in vitro* and *in vivo* models (146). In that list is the developing brain of rats, where tunicamycin has induced UPR activation and apoptosis (146). In the human monocyte line THP-1, tunicamycin increased resistin mRNA, through activation of the PERK-ATF4-CHOP branch of the UPR (303). The same had been previously reported in 3T3-L1 mouse adipocytes (304). In the breast cancer cells MCF7, tunicamycin impacted selected cells with cancer stem cell phenotype, specifically increasing XBP-1 splicing, translocation of ATF6 to the nucleus, and CHOP mRNA expression. It inhibited invasion and suppressed cell proliferation on these cells (305). This is one of the studies available pointing out the possibility of the application of tunicamycin against malignancies. Another of these instances was performed by Guha et al., who analysed whole genome expression in tunicamycin treated PC-3 (prostate cancer) cells, concluding that this molecule induces prostate cancer cell death *via* activation of mTORC1 complex (306).

Resveratrol, among other stilbenes, is commonly present in our diet through sources like berries, grapes or peanuts, even though its bioavailability in the organism is thought to be very low (307). In mice and in 3T3-L1 mice adipocytes, resveratrol displayed the capacity to ameliorate obesity-induced insulin resistance and ER stress (308). Furthermore, it was reported that, in an *in vivo* model of Parkinson's disease, resveratrol was also able to alleviate ER stress, namely by lowering mRNA levels of CHOP and GRP78 (309). On the other hand, there is a considerable amount of research concerning the ER stress-inducing potential of resveratrol on cancer cells. One study aimed to combine glycolysis inhibition with 2-deoxy-D-glucose and resveratrol on neuroblastoma cell lines, and observed that the latter enhanced the ER stress caused by glycolysis inhibition (47). In the colon carcinoma cell line HT29 resveratrol induced caspase-4-dependent apoptosis,

through ER stress induction. It was observed the upregulation of GRP78 and CHOP, increased eIF2α phosphorylation, and augmented XBP-1 splicing (310).

A tetramer of resveratrol, **vaticanol B**, has also displayed protective activity against ER stress in the macrophage cell line RAW 264.7, namely by preventing the upregulation of GRP78 and CHOP. Furthermore, this compound inhibited the production of key inflammation mediators, namely tumor necrosis factor-α (TNF-α), nitric oxide, and prostaglandin E2 (311).

Basiliolides have a lot in common with thapsigargin, despite the unrelatedness of their chemistries. Besides sharing their natural origin, being tetracyclic C_{19} lactones that occur in *T. garganica*, they also induce ER stress by disturbing Ca^{2+} homeostasis through inhibition of the SERCA pump. However, there are some differences in the underlying mechanism of action, since, in Jurkat cells, basiliolides failed to induce apoptosis, unlike thapsigargin. Ranked in decreasing order, the most potent of these compounds are basiliolides A1, B and C, the latter being much weaker than the others (312).

Withaferin A, a C_{28}-steroidal triterpenoid lactone of the category of withanolides, naturally occurs in the solanaceous species *Withania somnifera* (L.) Dunal (313). It was reported that this molecule induced ER stress associated cell death in the human renal cancer cell line Caki, where it induced eIF2α phosphorylation, induced XBP-1 splicing and increased GRP78 and CHOP levels (314). A different study observed increases on BiP and GRP94 on withaferin A-treated *Xenopus laevis* kidney epithelial cells, and also proteasomal inhibition (315). In a mouse model of chronic renal disease, withaferin A (3 mg/kg/day, orally administered) decreased the expression of inflammatory mediators (phospho-NF-κB-p65, IL-1β and COX-2) and ER stress-related proteins (BiP, GRP94, ATF4, CHOP, phospho-eIF2α and caspase-12) (316).

Agelasine B is a *trans*-clerodane diterpene isolated from the marine sponge *Agelas clathrodes* (Schmidt, 1870). The toxicity of this molecule was evaluated against human fibroblasts and MCF-7, SKBr3 (breast cancer cell lines) and PC-3 (prostate cancer cell line) cells, where it showed higher toxicity towards all the malignant cells (IC_{50}s of 2.99 μM, 3.22 μM and 6.86 μM, respectively) than towards fibroblasts (IC_{50} = 32.91 μM). It was further determined that the mechanism underlying this toxicity relies on inhibition of the SERCA pump and consequent increase of cytosolic amounts of Ca^{2+}, which were quantified with the aid of the Fura-2-AM fluorescent probe. Also, Ca^{2+} signalling was visualized through confocal microscopy, incubating the cells with Rhod-2/AM and BODIPY-FL-Ryanodine (317).

Cephalostatin 1 is a marine bis-steroidal pyrazine that was identified in extracts of *Cephalodiscus gilchristi* Ridewood, 1908, a marine worm that dwells in Southeast Africa, along with several other cephalostatins. This molecule has caught the attention of

researchers due to its striking activity against the 60 cell line *in vitro* screening of the National Cancer Institute, in which it exhibited a mean panel 50% growth inhibition concentration of ≈ 1nM (318). Subsequent studies have determined that cephalostatin 1 induces ER stress, increasing GRP78 and CHOP expressions, inducing eIF2α phosphorylation and leading to caspase-4 and, then, caspase-9 activation (319). The fact that the amounts of this molecule that can be found in Nature are very limited and its synthesis is complicated, efforts have been made to synthesise analogues that can mimic its activity. Two stereospecific analogues have shown promising results *in vitro*, since their cytotoxicity seems to be fairly cancer-specific. In non-cancer cells, namely white blood cells, retinal pigmented epithelial cell line ARPE-19 and skin fibroblasts GM2149, both compounds resulted in no more than 15% of cell viability loss at 10 μM, while in six different malignant cell lines, that concentration resulted in virtually 100% cell viability loss (namely against breast cancer cell line MCF-7, cervical cancer cells HeLa, prostate cancer cell line DU-145, osteosarcoma cells SAOS-2 and U2OS and chronic myelogenous leukemic cell line K562) (320).

Hydroxytyrosol is a phenolic compound that can be extracted in large amounts from *Olea europaea* L. leaves (321). It was reported that, in HepG2 cells, this molecule exerts a protective effect against tunicamycin-induced ER stress. This was observed through RT-PCR and Western Blot analysis of UPR markers, which confirmed that hydroxytyrosol lowered eIF2α phosphorylation and downregulated the gene expression of *hspa5*, *atf6* and *atf4* (322).

Palmitic acid is a quite common fatty acid in our diet and widely distributed in Nature (323). In the liver cancer cell line H4IIE, palmitic acid induced calcium flux-dependent apoptosis, even though the expression of ER stress markers such as BiP or CHOP was not increased (324). In 3T3-L1 adipocytes, palmitic acid triggered ER stress, as demonstrated by increased JNK phosphorylation and CHOP, BiP and ATF4 expressions. This stress response culminated in JNK-dependent triggering of autophagy (142). **Evodiamine**, a quinolone alkaloid from *Evodia rutaecarpa* (Juss.) Benth, is reported to induce apoptotic cell death in multiple ovarian cancer cell lines at concentrations of 1-4 μM, upregulating the phosphorylation of PERK and eIF2α (325). The triterpenoid **corosolic acid**, from *Eriobotrya japonica* (Thunb.) Lindl., induces regulated cell death in prostate cancer cell lines PC-3 and DU145 by activating PERK and IRE1 signaling. The effect was observed in the presence of the compound at 5 μM (326).

Unlike most compounds discussed on this section, **berberine** has been proposed to prevent ER stress. One study aimed to determine whether or not the insulin-sensitizing potential of berberine is due to ER stress prevention. Towards this goal, the authors pre-treated HepG2 (liver cancer cell line) cells with berberine before incubation with

tunicamycin to induce ER stress. Under these conditions, JNK activation was blocked and PERK and eIF2α phosphorylation was inhibited, while Akt phosphorylation was higher (327). Moreover, there is evidence that this potential against ER stress may turn berberine useful in precluding the progression of hepatic steatosis to more serious conditions like steatohepatitis or fibrosis. Both in primary hepatocytes and hepatocyte cell lines, berberine was effective against tunicamycin-induced ER stress, lowering protein aggregation and preventing lipogenesis through the ATF6/SREBP-1c pathway. *In vivo*, namely on leptin resistant *db/db* mice and methionine-choline-deficient diet fed mice, triglyceride and collagen deposition was diminished, while hepatic inflammation was alleviated (328).

Considering that natural products remain a valuable source of new drugs, and that the scientific literature conveys a multitude of possibilities among the chemical space of natural products to find new modulators of ER stress, it is likely that the future sees the approval of new natural product-based strategies to modulate ER stress and UPR activation in the context of disease.

Chapter II – Objectives

2. Objectives

Considering that Nature remains a source of bioactive molecules, and that, as pointed out in the previous section, modulation of ER stress response can be of interest to counter several chronic diseases, the purposes of this thesis were outlined as follows:

- Exploit a set of naturally occurring molecules for compounds that can **counter ER stress** in the context of neurodegeneration;

- Identify, among this library, molecules that can induce selective toxicity on malignant cells by **inducing ER stress** signaling;

- Describe bioactive molecules against **inflammation and ER stress**, exploring the correlation between the anti-inflammatory activity and prevention of UPR activation;

- Exploit some of the most promising and accessible molecules and obtain semi-synthetic derivatives towards enhanced bioactivity.

- Confirm the role of natural molecules as potential ER stress modulators, contributing to the discovery of new chemical entities capable of acting upon ER signaling pathways.

Chapter III – Results

ORIGINAL ARTICLE #1

A pipeline for natural small molecule inhibitors of endoplasmic reticulum stress

Daniela Correia da Silva, Paula B. Andrade, Patrícia Valentão, David M. Pereira

Frontiers in Pharmacology, 2022, 13, 956154

Abstract

The homeostasis of eukaryotic cells is inseverable of that of the endoplasmic reticulum (ER). The main function of this organelle is the synthesis and folding of a significant portion of cellular proteins, while it is also the major calcium reservoir of the cell. Upon unresolved ER stress, a set of stress response signaling pathways that are collectively labeled as the unfolded protein response (UPR) is activated. Prolonged or intense activation of this molecular machinery may be deleterious. It is known that compromised ER homeostasis, and consequent UPR activation, characterizes the pathogenesis of neurodegenerative disease.

In an effort to discover new small molecules capable of countering ER stress, we subjected a panel of over 100 natural molecules to a battery of assays designed to evaluate several hallmarks of ER stress. The protective potential of these compounds against ER stress was evaluated at the levels of calcium homeostasis, key gene and protein expressions, and levels of protein aggregation in fibroblasts. The most promising compounds were subsequently tested in neuronal cells. This framework resulted in the identification of several bioactive molecules capable of countering ER stress and deleterious events associated to it. Delphinidin stands out as the most promising candidate against neurodegeneration. This compound significantly inhibited the expression of UPR biomarkers, and displayed a strong potential to inhibit protein aggregation in the two aforementioned cell models. Our results indicate that natural products may be a valuable resource in the development of an effective therapeutic strategy against ER stress-related diseases.

Keywords: endoplasmic reticulum stress, unfolded protein response, proteostasis, drug discovery, natural products, chemical library

3.1.1. Introduction

The endoplasmic reticulum (ER) plays a substantial role in the upkeep of the proteostasis of any eukaryotic cell. Upon unresolved ER stress, several stress response signaling pathways are activated in this organelle. These pathways are collectively termed as the unfolded protein response (UPR) and aim to restore reticular homeostasis, but may be deleterious upon sustained or intense activation. Shortly, the UPR relies on three major signaling branches, each initiated by its respective sensor: the protein kinase RNA-like endoplasmic reticulum kinase (PERK), inositol-requiring enzyme 1 (IRE1) or the activating transcription factor 6 (ATF6) (128, 329).

Disturbances in the secretory pathway of proteins and consequent stress upon the ER are hallmarks of several disease etiologies, including those of neurodegenerative nature. Presently, neurodegenerative diseases have a high prevalence around the world, and their incidence is expected to increase as the population ages (329-331). Pharmacological intervention by modulating ER stress has shown promising results against neurodegeneration *in vitro* and *in vivo* (116, 332-334). Accordingly, we consider the development of ER-based strategies against neurodegenerative diseases a necessary step to overcome the burden that these diseases represent to society.

Natural products have been used as medicinal agents from immemorial times and remain the best source of lead compounds and new drugs to modern medicine (296). This chemical space has been gifted with immense structural diversity and has been evolutionarily tailored to provide drug-like molecules, displaying multiple chemotypes and pharmacophores (296, 335). Furthermore, it is known that the time when pharmaceutical companies decided to reduce natural product research projects correlates with decreased numbers of new drugs entering the market (335). A literature survey on nature-derived ER modulators (128) shows the importance of the natural product chemical space for this end, including molecules as distinct as basiliolides (312), fisetin (336-338), berberine (327, 328, 339), withaferin A (314, 315), agelasine B (317), cephalostatin 1 (319, 320), and hydroxytyrosol (322). Notably, most of these molecules are associated to ER stress induction, while hydroxytyrosol and berberine are reported to ameliorate ER stress.

Herein we propose a pipeline for the identification of potential ER stress inhibitors among a library of natural products.

3.1.2. Materials and Methods

3.1.2.1. Chemical library and reagents

The compounds 5,7,8-trihydroxyflavone, 5-deoxykaempferol, acacetin, apigenin, apigetrin, β-escin, chrysoeriol, chrysophanol, coumarin, cyanidin, delphinidin, diosmetin, diosmin, ellagic acid, eriocitrin, eriodictyol, eriodictyol-7-O-glucoside, eupatorin, ferulic acid, fisetin, flavanone, galangin, gallic acid, genkwanin, gentisic acid, guaiazulene, herniarin, hesperidin, homoeriodictyol, homoorientin, homovanillic acid, hyoscyamine, isorhamnetin, isorhamnetin-3-O-glucoside, isorhamnetin-3-O-rutinoside, isorhoifolin, juglone, kaempferide, kaempferol, kaempferol-3-O-rutinoside, kaempferol-7-O-glucoside, kaempferol-7-O-neohesperidoside, linarin, liquiritigenin, lutein, luteolin, luteolin tetramethylether, luteolin-3',7-di-O-glucoside, luteolin-4'-O-glucoside, luteolin-7-O-glucoside, malvidin, mangiferin, maritimein, myricetin, myricitrin, myrtillin, naringenin-7-O-glucoside, narirutin, oleuropein, orientin, pelargonidin, pelargonin, phloroglucinol, pyrogallol, quercetin-3-O-(-6-acetylglucoside), quercetagetin, quercetin-3,3',4',7-tetramethylether, quercetin-3,4'-dimethylether, quercetin-3-methylether, quercetin-3-O-glucuronide, rhoifolin, robinin, saponarin, scopolamine, sennoside A, sennoside B, sulfuretin, tectochrysin, tiliroside, verbascoside and vitexin were purchased from Extrasynthese (Genay, France). The molecules (-)-norepinephrine, (+/-)-dihydrokaempferol, 1,4-naphtoquinone, 18α-glycyrrhetinic acid, 3,4-dihydrobenzoic acid, 3,4-dimethoxycinnamic acid, 3-hydroxybenzoic acid, 4-hydroxybenzoic acid, 5-methoxypsoralen, ajmalicine, berberine, betanin, betulin, boldine, catechol, cholesta-3,5-diene, chrysin, cynarin, daidzein, emodin, galanthamine, genistein, guaiaverin, hesperetin, hydroquinone, lupeol, myristic acid, naringenin, naringin, p-coumaric acid, phloridzin, pinocembrin, plumbagin, quercetin, quercetin-3-O-β-D-glucoside, quercitrin, rosmarinic acid, rutin and silibinin were acquired from Sigma-Aldrich (St. Louis, MO, USA). 5,8-Dihydroxy-1,4-naphtoquinone and caffeine were from Fluka (Buchs, Switzerland), vanillin was supplied by Vaz Pereira (Santarém, Portugal), vicenin-2 was purchased from Honeywell (Charlotte, NC, USA). Chlorogenic acid was from PhytoLab (Vestenbergsgreuth, Germany). Cinnamic acid was obtained through Biopurify (Chengdug, China). Swertiamarin was from ChemFaces (Wuhan, China).

Minimum Essential Medium (MEM), Dulbecco's Modified Eagle Medium/Nutrient Mixture F-12 (DMEM/F-12), fetal bovine serum, penicillin/streptomycin solution (penicillin 5000 units/mL and streptomycin 5000 μg/mL), trypsin-EDTA (0.25%), Qubit® RNA IQ assay kit and Qubit® RNA HS assay kit, the SuperScriptTM IV VILOTM MasterMix, the Qubit® Protein Assay Kit, the anti-BiP mouse monoclonal antibody

(Catalog # MA5-15619, lot WI3375321) and the anti-mouse secondary antibody (Catalog # 61-6520, lot WB319554) were obtained from Invitrogen (Grand Island, NE, USA). Dimethyl sulfoxide (DMSO) was acquired from Fisher Chemical (Loughborough, UK). Isopropanol was obtained from Merck (Darmstadt, Germany). 3-(4,5-Dimethylthiazol-2-yl)-2,5-diphenyltetrazolium Bromide (MTT), calcium ionophore A23187, thapsigargin, RNAzol®, chloroform, isopropanol, diethyl pyrocarbonate (DEPC), KAPA SYBR® FAST qPCR Kit Master Mix (2X) Universal, Aβ25-35, 2-(4-amidinophenyl)-6-indolecarbamidine dihydrochloride (DAPI), protease inhibitor cocktail, phosphatase inhibitor cocktail, acrylamide/bis-acrylamide 30% solution, bromophenol blue, glycerol, sodium dodecylsulfate (SDS), glycine, Trizma® base, Trizma® hydrochloride, sodium deoxycholate, sodium chloride, potassium phosphate monobasic, potassium chloride, sodium phosphate dibasic, sodium bicarbonate, D-glucose and Triton X-100 were purchased from Sigma-Aldrich (St. Louis, MO, USA), while formaldehyde was from Bio-Optica (Milan, Italy). The fluorescent probe Fura-2/AM, as well as the anti-GAPDH (Catalog # ab181602) rabbit monoclonal antibody and the anti-rabbit secondary antibody (Catalog # ab6721, lot GR172025-6), were obtained from Abcam (Cambridge, UK). Thioflavin T was from Alfa Aesar (Kandel, Germany). The WesternBright® ECL HRP was supplied by Advansta (Menlo Park, CA, USA). Trans-Blot Turbo Mini 0.2 μm Nitrocellulose Transfer Packs were acquired from Bio-Rad (Hercules, CA, USA).

3.1.2.2. Chemometric analysis

Since it is the most detailed and up to date database of annotated natural products (340), we started from the COCONUT database (https://coconut.naturalproducts.net), and created a data frame comprising all the molecules under study, where each row corresponded to a different molecule and columns to features. Among all the original features, we have decided to keep only 48, as the remaining ones did not contain relevant information for this work (SMILE notation, fragments, among others). **Supplementary Table S1** contains a list of all variables kept and their description. All data was cleaned and explored using Python 3.9. For preprocessing data, we have used Simple Imputer, Standard Scaler, Ordinal Encoder and Label Encoder from Scikit-learn (341). Dimensionality reduction was conducted using Scikit-learn (341) library (Principal Component Analysis [PCA], Multidimensional Scaling [MDS], t-distributed Stochastic Neighbor Embedding [TSNE] and Uniform Manifold Approximation and Projection (UMAP) used the UMAP library (342). For t-SNE we have used number of neighbors of 5, 13 and 45 and minimum distance of 0.01, 0.1 and 0.5. In the case of UMAP we have iterated through perplexity of 5, 20, 50 and 100 and number of iterations of 300, 900, 1500 and 2000. Unless otherwise

specified, specifications of each algorithm were set for default. Graphics in **Figures 10**, **16**, **17** and **Supplementary Figure S4** were created using Seaborn or MatPlotLib and the remaining ones in GraphPad Prism 8.

3.1.2.3. Cell culture conditions

MRC-5 fibroblasts (European Collection of Authenticated Cell Cultures, Porton Down Salisbury, UK) were cultured in MEM and SH-SY5Y (American Type Culture Collection, LGC Standards S.L.U., Spain) cells were cultured in DMEM/F-12. Both mediums contained 10% FBS and 1% penicillin/streptomycin and both cell lines were maintained at 37 ºC with 5% CO2.

3.1.2.4. Viability assays

For viability assessment, MRC-5 fibroblasts were seeded at a density of 2 x 10^4 cells/well. After 24 h the cells were incubated with the compounds of interest. 24 h later, the wells are aspirated, the medium was replaced by MTT at 0.5 mg/mL and incubated for 2 h. At the end of this period, the solution was discarded and the formazan crystals in the wells dissolved in 200 µL of a 3:1 DMSO:isopropanol solution. The absorbance at 560 nm was read in a Thermo Scientific™ Multiskan™ GO microplate reader.

Results are presented as the percentage of control and correspond to the mean ± SEM of at least three independent experiments, each of them performed in triplicate.

3.1.2.5. Cytosolic calcium level determination

MRC-5 fibroblasts were plated on black bottomed-96-well plates at the density of 2 x 10^4 cells/well. After 24 h, the fluorescent probe Fura-2/AM was added at 5 µM and incubated for 1 h. Then these were incubated with the selected nontoxic compounds in HBSS. The calcium ionophore A23187 was added at a final concentration of 5 µM after 2 h. Finally, 2 h later the fluorescence was read at 340/505 and 380/505 on a Cytation™ 3 (BioTek (Vermont, MA, USA)) multifunctional microplate reader. Data analysis was performed considering the ratio $F_{340/505}/F_{380/505}$. Results are presented as fold decrease *vs* positive control and represent the mean ± SEM of at least three independent experiments, each of them performed in triplicate.

3.1.2.6. RNA extraction and quantification, cDNA synthesis and RT-qPCR reaction

Cells were seeded at 1.6 x 105 cells/well in 12-well plates, left at 37 ºC for 24 h and then incubated with the compounds that displayed positive results in previous assays. After 2 h, thapsigargin (Tg) was used as a positive control and added at a final concentration of 3 µM, and a period of 16 h of incubation ensued. The cells were lysed by aspirating the culture medium and adding 500 µL of PureZOL RNA isolation reagent, pipetting up and down multiple times. The lysate was kept at room temperature for 5 min and then RNA extraction ensued.

The extraction was performed by phase separation, by adding 100 µL of chloroform, shaking, incubating for 5 min and centrifuging at 12000 g for 15 min at 4 ºC. The aqueous phase was collected and 250 µL of isopropyl alcohol were added, following 5 min of incubation and new centrifugation at 12000 g for 10 min, at 4ºC. The supernatant was then discarded, and the pellet was washed with 75% ethanol, vortexed, centrifuged at 7500 g for 5 min at 4 ºC, air dried and resuspended in DEPC-treated water. The RNA in the sample was quantified resorting to the Qubit® RNA HS assay kit. Sample integrity was then evaluated with the Qubit® RNA IQ assay kit, and, if in appropriate conditions, 1 µg was converted to cDNA using the SuperScriptTM IV VILO™ MasterMix.

RT-qPCR reaction was performed in the following thermal cycling conditions: 3 min at 95 ºC, 40 cycles of 95 ºC for 3 s (denaturation), gene-specific temperature for 20 s (annealing temperatures listed on **Table 5**) and 20 s at 72 ºC (extension). The employed mastermix was KAPA SYBR® FAST qPCR Kit Master Mix (2X) Universal. The reaction was conducted on a qTOWER3 G (Analytik Jena AG, Germany), and the data were analyzed on the software supplied along with the equipment (qPCRsoft 4.0). Primers for target genes were designed on Primer BLAST (NCBI, Bethesda, MD, USA) and synthesized by Thermo Fisher (Waltham, MA, USA). The respective nucleotide sequences are presented on **Table 5**. Product specificity was checked with melting curves. *Gapdh* was selected as the reference gene for normalization of expression. All the RT-qPCR reactions were performed in duplicate, and the experiments were repeated, at least, four times. Results are presented as mean ± SEM.

Table 5. Data concerning analyzed genes and designed primer sequences.

Gene	Accession number	Primers	Annealing Temperature (ºC)	Amplicon length (bp)
gapdh (GAPDH)	NM_002046.6	F: AGGTCGGAGTCAACGGATTT R: TGGAATTTGCCATGGGTGGA	60	157
hspa5 (GRP78)	NM_005347.4	F: ACTCCTGAAGGGGAACGTCT R: TTTTCAACCACCTTGAACGGC	59.5	161
ddit3 (CHOP)	NM_001195053.1	F: AAGTCTAAGGCACTGAGCGT R: TTGAACACTCTCTCCTCAGGT	59	93
hsp90β1 (GRP94)	NM_003299.2	F: GCTCTATGTGCGCCGTGTAT R: ATCTGAGTCCACCACACCCTT	60.5	91
atf4 (ATF4)	NM_001675.4	F: ACAACAGCAAGGAGGATGCC R: CCAACGTGGTCAGAAGGTCA	60	135
edem1 (EDEM1)	NM_014674.2	F: GCGGGGACCCTTCAAATCT R: CGGCTTTCTGGAACTCGGAT	60	117

3.1.2.7. Quantification and imaging of protein aggregates

On black bottomed-96-well plates, MRC-5 and SH-SY5Y cells were seeded at the densities of 2 x 10^4 and 3 x 10^4 cells/well, respectively. In the following day, they were incubated with the selected molecules in the presence of $A\beta_{25-35}$ at 10 μM. After an incubation period of 24 h, cells were washed with HBSS and incubated for 30 min with thioflavin T at 5 μM (prepared in HBSS). At this point, fluorescence was read at 450/482 nm on a CytationTM 3 (BioTek (Vermont, MA, USA)) multifunctional microplate reader. Results represent the fold decrease on fluorescence compared to the positive control. We present the mean ± SEM of, at least, three independent assays, individually performed in triplicate.

To image protein aggregates, cells were seeded on clear bottomed-96-well plates at the aforementioned density and treated with the molecules of interest for 24 h in the presence of $A\beta_{25-35}$ at 10 μM. Cells were fixed on 4% formaldehyde at room temperature for 15 min and incubated with 10 μM thioflavin T for 60 min. The counter staining was performed with DAPI at 0.25 μg/mL, for 30 min. Finally, three washing steps with HBSS for 5 min were carried out and cells were imaged under an Eclipse Ts2R-FL (Nikon) fluorescence microscope equipped with a Retiga R1 camera. A FITC filter was employed to observe thioflavin T and DAPI staining was imaged using a DAPI filter. Images were analyzed resorting to the CellProfiler software version 4.2.1 (Broad Institute of MIT and Harvard, Cambridge, MA).

3.1.2.8. Western blotting analysis

MRC-5 and SH-SY5Y cells were seeded in 6-well plates at the densities of 3.2 x 10^5 and 4.8 x 10^5 cells/well. After 24 h, they were incubated with compounds selected as promising in previous experiments. After 2 h, Tg at 3 μM was added, and the plates were left in the incubator for another 22 h. Ended this time frame, cell samples were lysed in RIPA buffer containing 1% protease inhibitor cocktail and 1% phosphatase inhibitor cocktail for 15 min at 4 ºC, and subsequently centrifuged at 14000 g for 15 min to remove cell debris. The supernatant was then collected, and the protein content was determined resorting to the Qubit® Protein Assay Kit.

The following step was to submit 30 μg of each sample, previously denatured at 76 ºC for 10 min, to 10% SDS-PAGE electrophoresis, in a gel containing 10 % acrylamide/bisacrylamide. The proteins were then transferred to a nitrocellulose membrane on a Trans-Blot® Turbo (Bio-Rad; Hercules, CA, USA). The membrane was blocked in a PBS solution containing 5% non-fat milk and 0.1% Triton X-100 for 1 h with orbital agitation. Hereupon, the membrane was incubated with the primary antibody overnight, at 4 ºC, with agitation. The anti-BiP mouse monoclonal antibody was used at a working dilution of 1:1250, while the anti-GAPDH rabbit monoclonal antibody was used at a dilution of 1:10000. A washing step was then performed with PBS 0.1% Triton X-100 for 30 min. Then, the secondary antibody was incubated for 2 h at room temperature. The anti-mouse secondary antibody was used at 1:2000, and the anti-rabbit secondary antibody at 1:3000. At this point, two more washing steps were performed with PBS 0.1% Triton X-100 for 15 min and then with PBS, again twice for 15 min. Finally, bands were detected by addition of a chemiluminescent substrate, WesternBright ECL HRP. The resulting bands were visualized on a ChemiDoc™ Imaging System (Bio-Rad, Hercules, CA, USA). Their relative optical density was calculated by densitometry resorting to the Fiji/ImageJ software version 1.51 (Fiji, Madison, WI, USA) and normalized against the loading control (GAPDH). Results are presented as mean ± SEM of, at least, three independent experiments.

3.1.2.9. Statistical analysis

The statistical analysis was performed using GraphPad Prism 8 software. We resorted to unpaired Student's t-tests to compare every single individual treatment to the control group. Values of $p < 0.05$ were considered statistically significant. Outliers were identified and excluded by the Grubbs' test.

3.1.3. Results

3.1.3.1. Chemical space of the library

We compiled a library of 134 molecules of natural origin (**Supplementary Table S2**). The average molecular weight was 358 g/mol, the inferior limit being 110.1 g/mol (catechol and *p*-hydroquinone) and the upper limit 1131.3 (β-escin) (**Figure 10**). The computed natural product-likeness score, a parameter that tries to quantify how much a given molecule is "natural product-like" (343) had an average of 1.29 (min: -0.4, max: 2.72, **Figure 10**). Over 50% of the molecules displayed no violations of Lipinski's Rule of 5 with over 30% displaying 2 or more (**Figure 10**), a relevant trait for candidate drugs.

For chemical ontology, we have used the computed chemical classes generated by ClassyFire (344). From a chemical point of view, the distribution of the molecules by chemical superclass can be found in **Figure 10**. Phenylpropanoids and polyketides corresponded to the majority of the entries (65.9%), followed by benzenoids (14.4%) and lipids or lipid-like molecules (6.1%). Within phenylpropanoids, flavonoids were the most prevalent molecules (**Figure 10**), followed by cinnamic acids and their derivatives. In the case of benzenoids, simple phenols were predominant, while in the case of lipids, prenol lipids were the most representative (**Figure 10**). The chemical structures of all of the molecules are represented in **Supplementary Figure 1 A-H**, separated according to the herein mentioned chemical superclasses.

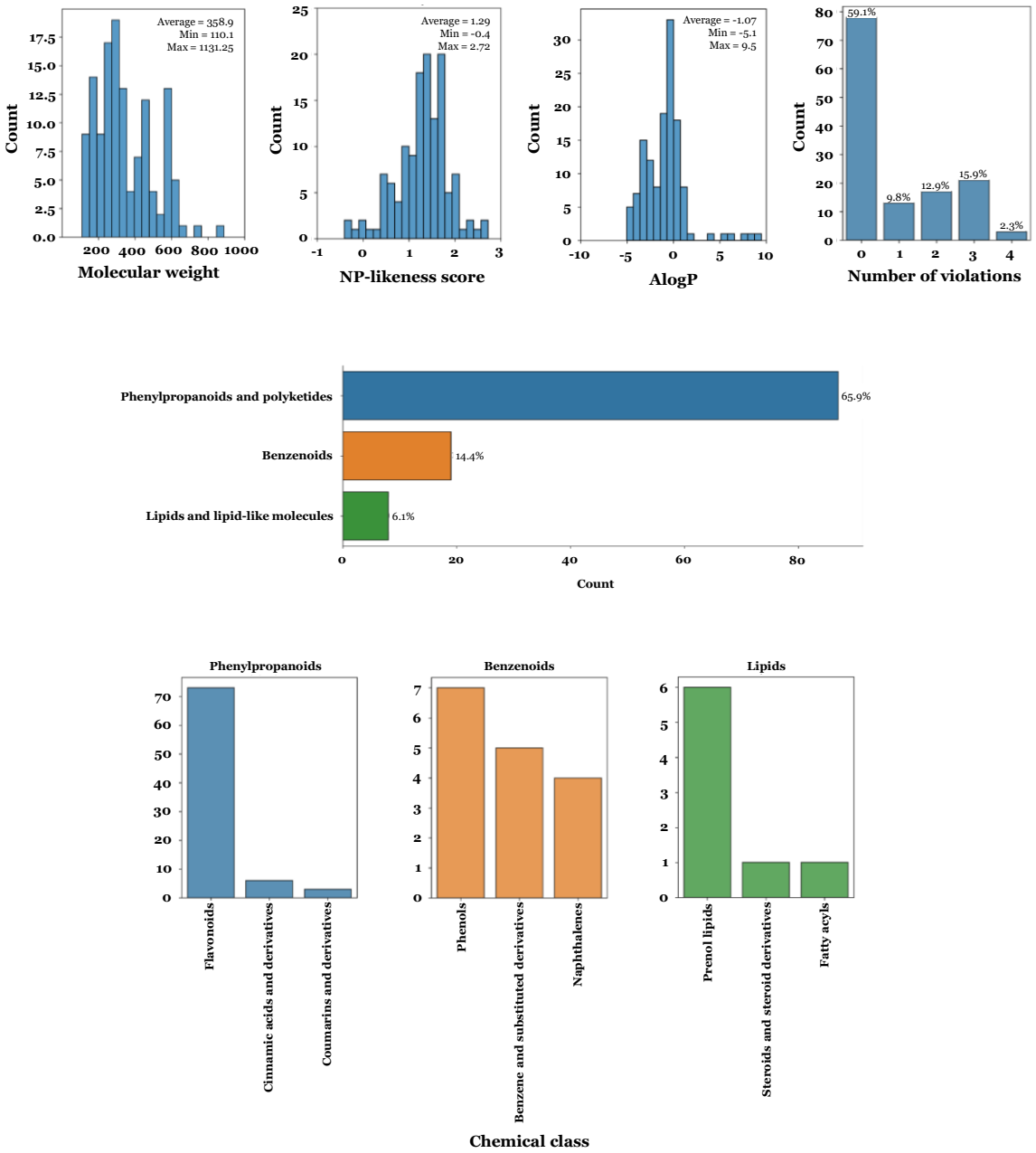

Figure 10. Physico-chemical properties of the library used, and distribution of the chemical (super)classes of the molecules present in the library.

3.1.3.2. Impact of molecules upon cell viability

Given the high number of molecules involved, all compounds were tested at a single concentration (50 µM). Statistically significant decreases in MTT reduction were interpreted as negative impact on cellular viability and the corresponding molecules excluded from subsequent experiments. As evidenced by **Figure 11**, 37 molecules (depicted in **Supplementary Table 2**) were dropped from the pipeline for their toxicity.

The remaining 97 compounds were screened for potentially protective capacity against ER stress. The legend for the heatmap presented in **Figure 11** can be consulted in **Supplementary Table S2**, while **Supplementary Figure 2** contains the individual results for each molecule represented in the bar charts.

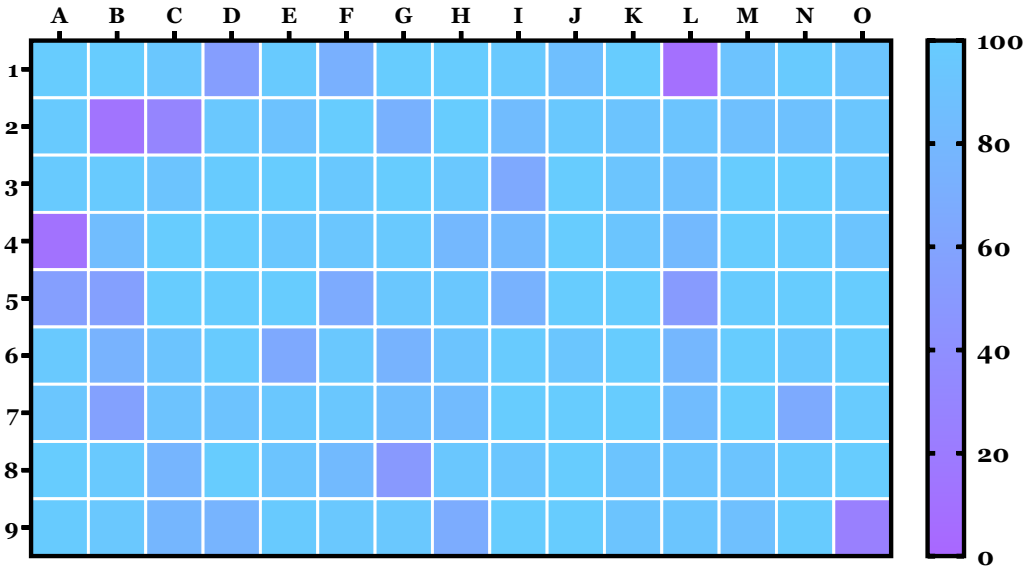

Figure 11. Impact of a library of natural products on MRC-5 fibroblasts viability, as determined by MTT reduction assay. Results represent the percentage of the control and correspond to, at least, three independent experiments, each performed in triplicate.

3.1.3.3. Effect of the library upon cytosolic calcium levels

The next step involved the screening of the nontoxic molecules for potential protection against the onset of ER stress. Towards this goal, and considering the high number of molecules still in the pipeline, we selected changes on calcium levels as an indicator of compromised ER homeostasis. The maintenance of the high concentration of calcium in the ER lumen creates an appropriate environment for protein folding, and thus changes on its levels heavily impact ER function (37, 345). This organelle is able to maintain its calcium levels due to the abundance of resident calcium-buffering proteins, like calnexin and calreticulin (346). Under stress conditions, the ER may release calcium through channels, such as IP_3R and RyRs. Eventually, this may lead to increased calcium in mitochondria, indirectly inducing the generation of ROS and triggering the dissipation of the mitochondrial membrane potential, ultimately leading to the release of resident proapoptotic factors (347).

To evaluate the potential protective effect of the molecules under study, we conducted experiments with the fluorescent probe Fura-2/AM. Calcium ions were detected employing

the divalent cation ionophore A23187 (5 μM) as a positive control for calcium leakage into the cytosol and molecules that could inhibit or counter its effect were searched. Calcium ionophore A23187, or calcimycin, is a calcium-binding molecule that increases the cellular permeability of ionic calcium (348). There are multiple examples in the literature of the use of this molecule to increase cytosolic calcium levels, inducing ER stress, UPR activation and eventual apoptosis or autophagy (349-351).

Under these experimental conditions, we were able to identify several molecules that significantly prevented or ameliorated the calcium overload caused by A23187, as displayed in **Figure 12**. Such molecules included six polyphenols (5-deoxykaempferol, delphinidin, fisetin, naringenin, naringin, quercetin-3-*O*-β-D-glucoside), one anthraquinone (sennoside B), one fatty acid (myristic acid) and one biogenic polyamine (spermine). The full list of molecules tested in this assay can be consulted in **Supplementary Table 3** while **Supplementary Figure 3** represents these data in the bar charts.

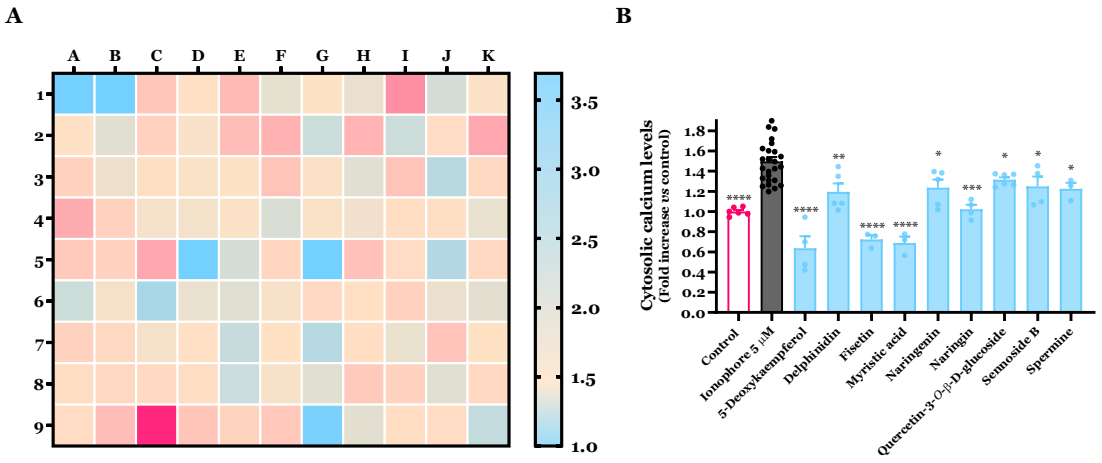

Figure 12. Cytosolic calcium levels in MRC-5 fibroblasts in response to co-incubation of calcium ionophore A23187 at 5 μM and nontoxic molecules (50 μM), as determined by the fluorescence of the probe Fura-2/AM. **A**) Heatmap representing all molecules tested; **B**) Molecules that caused a statistically significant decrease in calcium levels when compared to the positive control. Results correspond to the mean of, at least, three independent experiments, each performed in triplicate. *$p < 0.05$, **$p < 0.01$, ***$p < 0.001$, ****$p < 0.0001$.

3.1.3.4. ER stress counter candidates inhibit thapsigargin-induced UPR signaling in MRC-5 fibroblasts

The non-toxic molecules that successfully lowered Ca^{2+} levels were considered potential candidates for countering ER stress. As so, they were evaluated for their effect upon UPR signaling pathways.

Thapsigargin, a natural sesquiterpene lactone that is widely used as UPR inducer, was the positive control. This molecule acts as an irreversible SERCA pump inhibitor, leading to an impaired calcium homeostasis and subsequent onset of organized cell death mechanisms (128). Accordingly, as evidenced by **Figure 13**, we can see that thapsigargin (3 μM) significantly increased the expression of all the genes of interest, namely the transcription factors *ddit3* and *atf4*, the chaperones *hspa5* and *hsp90β1* (BiP and GRP94 proteins, respectively), and *edem1*, a gene coding for the ER degradation-enhancing alpha-mannosidase-like protein 1, an enzyme involved in ER-associated degradation.

5-Deoxykaempferol at 50 μM inhibited the expression of *ddit3*, *hsp90β1*, *edem1* and *hspa5*, even though it did not significantly decrease *atf4* expression. Fisetin was the only molecule to prevent the increase of all target genes in a significant manner. Delphinidin negatively impacted the expression of *atf4*, *hsp90β1* and *edem1*. Myristic acid and quercetin-3-*O*-β-D-glucoside displayed a similar pattern in the protection against UPR activation, by modulating *hsp90β1* and *edem1* expressions. Sennoside B acted upon *atf4* and *edem1*, while naringenin, naringin and spermine failed to inhibit any of the selected genes.

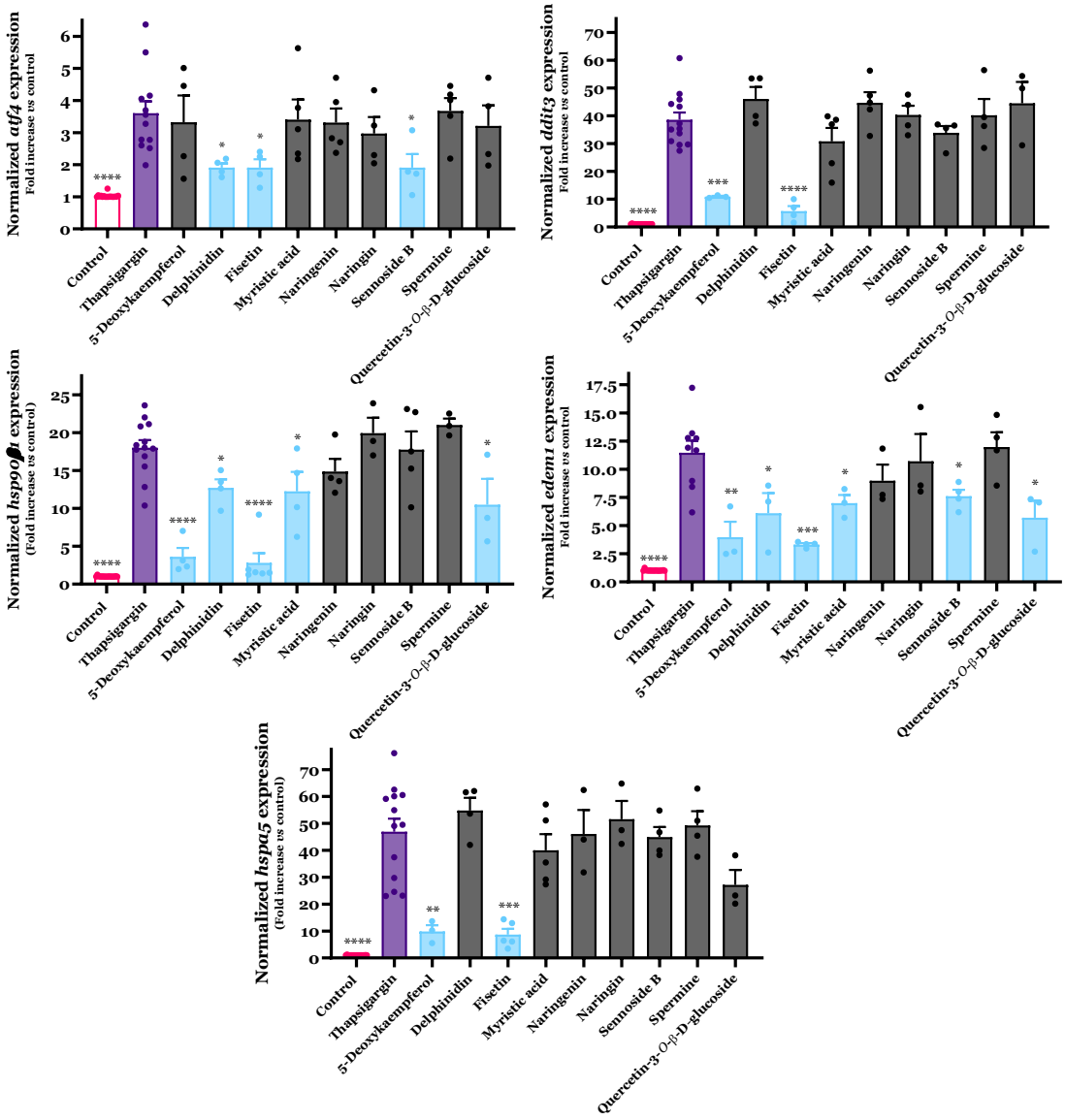

Figure 13. Effect of 5-deoxykaempferol, delphinidin, fisetin, myristic acid, naringenin, naringin, sennoside B, spermine and quercetin-3-*O*-β-D-glucoside on Tg-induced UPR signaling, as determined by RT-qPCR. Results correspond to the mean ± standard error of the mean of, at least, four independent experiments, each performed in duplicate. *Gapdh* was used as a reference gene for normalization of expression. *$p < 0.05$, **$p < 0.01$, ***$p < 0.001$, ****$p < 0.0001$.

3.1.3.5. Molecules that counter ER stress ameliorate protein aggregation in MRC-5 fibroblasts and attenuate UPR activation at the protein level

As discussed earlier, activation of the UPR affects the capacity of cells to fold proteins properly, which frequently results in the formation of protein aggregates and may lead to proteinopathies (56, 352). Conversely, several diseases, notably those of neurodegenerative nature, are associated with these aggregates (353). As so, new molecules capable to

countering ER stress are expected to be able to prevent or lower the amounts of protein aggregates in a biological context. To confirm this, we proceeded to an experimental model of ER stress-triggered protein aggregation using $A\beta_{25-35}$ as a protein aggregation inducer. $A\beta_{25-35}$ is an active fragment of $A\beta_{42}$ (354), a peptide that is associated to the pathogenesis of Alzheimer's disease (AD) and has been characterized in experimental models, where it can lead to the formation of protein aggregates *in vitro* and AD *in vivo* (355).

As shown in **Figure 14 A**, incubation of MRC-5 cells with $A\beta_{25-35}$ elicits protein aggregation, as assessed with thioflavin T, a benzothiazole that presents high fluorescence when bound to β-sheet-rich structures common in protein aggregates, both in a microplate-based (**Figure 14 A**) and an immunocytochemistry method (**Figure 14 B**). In the same conditions, delphinidin, fisetin, myristic acid, sennoside B and quercetin-3-*O*-β-D-glucoside significantly inhibited this effect.

Our Western blotting results show that the exposure of Tg-insulted MRC-5 cells to delphinidin and fisetin clearly reduced BiP expression, and, consequently, we presume that the UPR activation in the presence of these molecules is mitigated.

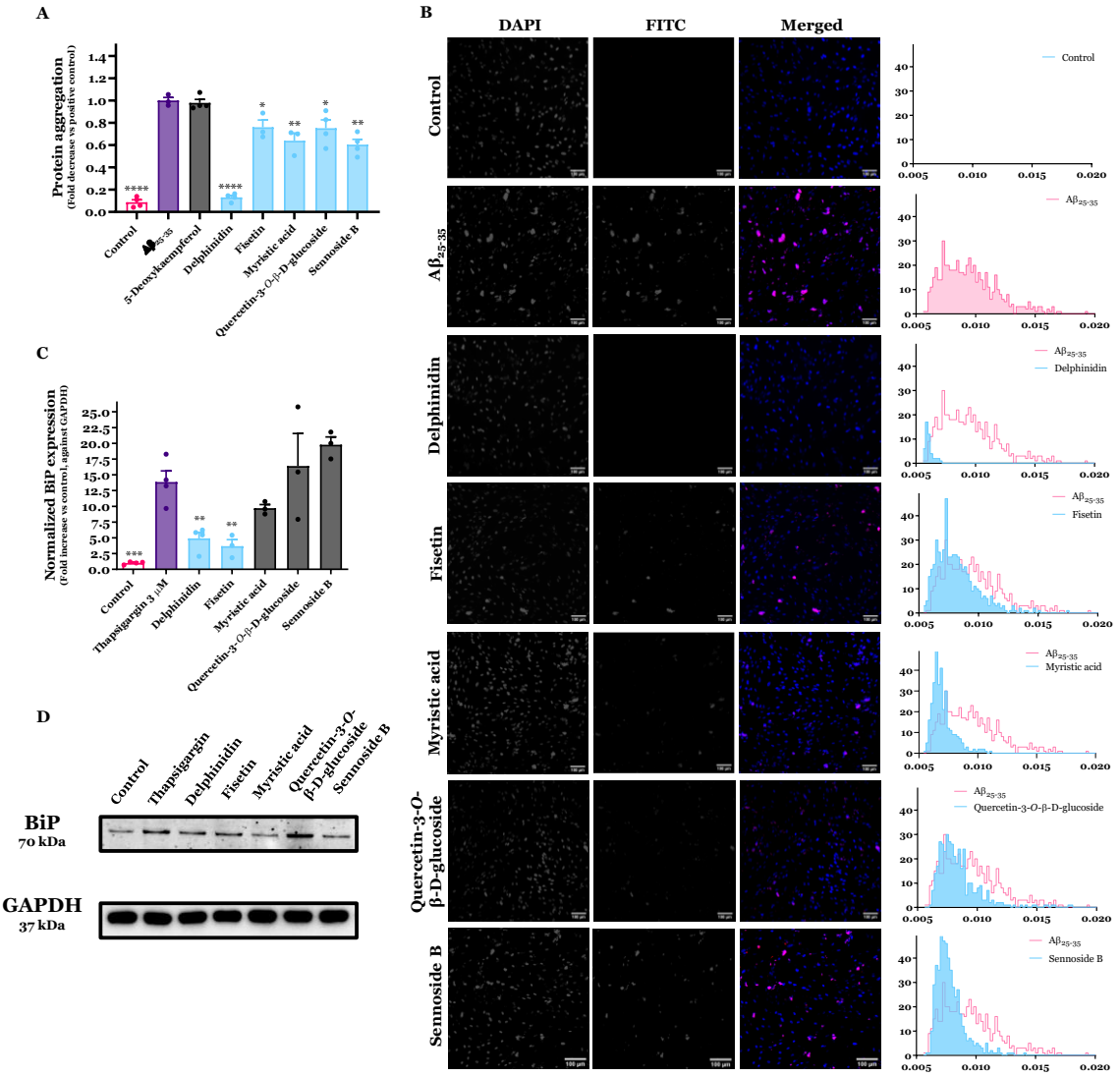

Figure 14. A: Impact of delphinidin, fisetin, myristic acid, sennoside B and quercetin-3-*O*-β-D-glucoside on $A\beta_{25\text{-}35}$-induced protein aggregation in MRC-5 cells, determined by the fluorescence of thioflavin T. Results correspond to the mean ± standard error of the mean of, at least, three independent experiments, individually performed in triplicate. *$p < 0.05$, **$p < 0.01$, ****$p < 0.0001$. **B:** The protective effect of bioactive molecules was captured under a fluorescence microscope. The fluorescent signal of thioflavin T is represented in the histograms. **C:** Effect of delphinidin on Tg-induced BiP expression in MRC-5 cells, as evaluated by Western blotting. Results correspond to the mean ± standard error of the mean of, at least, three independent experiments. **$p < 0.01$, ***$p < 0.001$. **D:** Images obtained through Western blotting analysis.

3.1.3.6. Selected molecules counter protein aggregation and UPR activation at the translational level in neuronal cells

For this assay, the concentrations of the molecules under study had to be adjusted to the highest nontoxic concentration towards this cell line. Fisetin was tested at 25 μM, while the remaining molecules were tested at the concentrations used in MRC-5 cells (50 μM). The

effect of this compound was not replicated on SH-SY5Y cells. We hypothesize that this may be due to the reduction of the concentration that was necessary in order not to impact cell viability in this model. On the other hand, the effect of delphinidin translates to these cells, virtually nullifying the advent of protein aggregates, as evidenced by **Figure 15 A** and **B.**

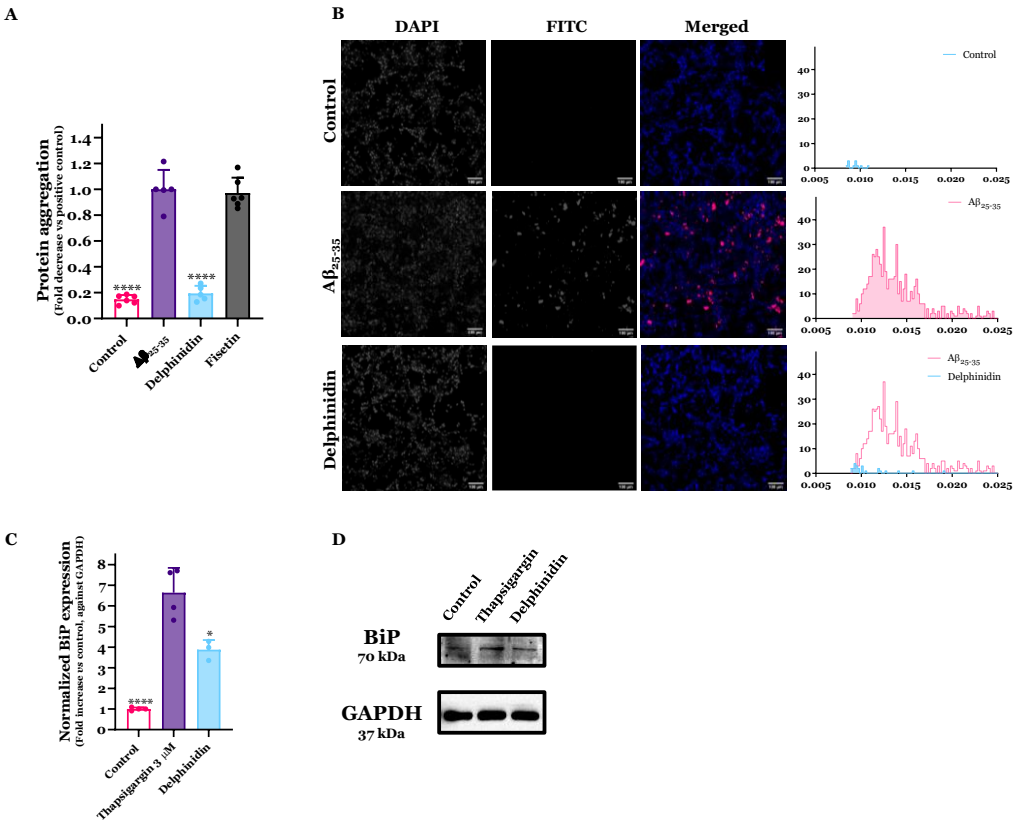

Figure 15. A: Effect of delphinidin and fisetin on $A\beta_{25-35}$-induced protein aggregation in SH-SY5Y cells, as evaluated by determination of the fluorescence of thioflavin T. Results correspond to the mean ± standard error of the mean of, at least, three independent experiments, each performed in triplicate. ****$p < 0.0001$. **B:** The effect of bioactive molecules was observed under a fluorescence microscope. The fluorescent signal of thioflavin T is represented in the histograms. **C:** Effect of delphinidin on Tg-induced BiP expression in SH-SY5Y cells, as evaluated by Western blotting. Results correspond to the mean ± standard error of the mean of, at least, three independent experiments. *$p < 0.05$. **D:** Example of the obtained Western blotting results.

3.1.3.7. Defining a chemical space for future drug development

Considering all the information generated during this work, together with the chemical, structural and topographical information available for the molecules under study, we were interested in understanding if the physico-chemical properties of the library could, *per se*, be a good indicator for its activity. To this end, we took all the molecules used and computed multiple pairs of their properties, sorting them as active or inactive according to the results

of the aggregation assays depicted in **Figure 14**. While there seemed to be a tendency of active molecule to be apart from inactive molecules in some cases (**Supplementary Figure 4**), it soon became apparent that a pairwise comparison could leave behind important features of the molecules, as it reduces high dimensional data to just two dimensions. As so, we have decided to use other methodologies that could take into account all the features of the library, namely dimensionality reduction algorithms, which allows the combination of different features into principal components that can be more easily graphed and understood. We first conducted a correlation study in order to identify molecular features that were highly correlated, which could negatively impact the performance of the statistical analysis given the redundancy it would add. **Figure 16** shows the original features, where it is clear that many are highly correlated, for example, the features "total atom number" and "number of carbons" (0.98), as one directly affects the other. Such features were dropped, and the remaining ones were used. We also decided to assess the robustness of the methods in identifying the chemical space occupied by the molecule that was shown to be active in both cell lines, namely delphinidin.

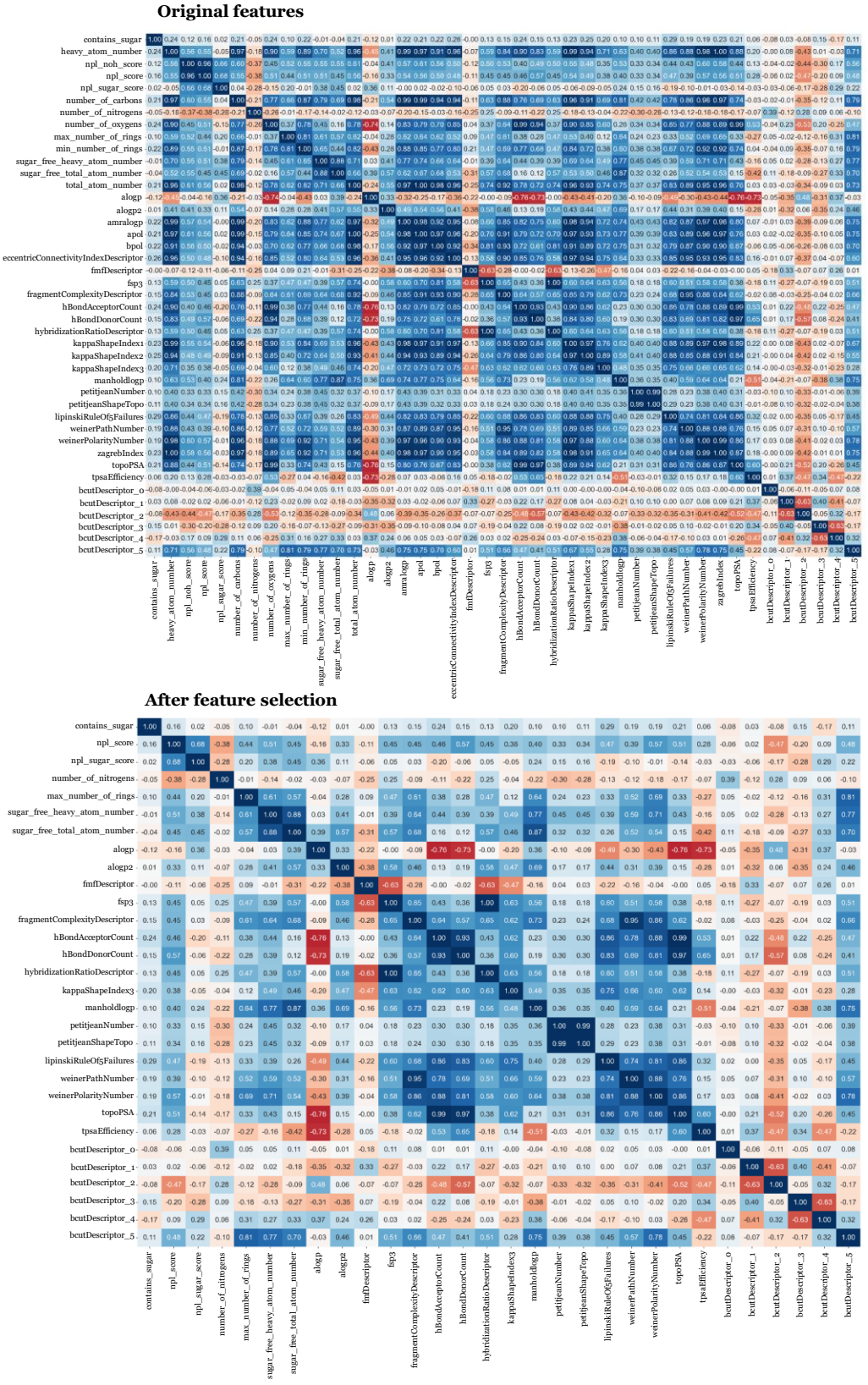

Figure 16. Correlation matrix for the features used for the chemical library used in this work.

We initially used the classical algorithm for principal component analysis (PCA), which is widely used both for chemometric and biological data (356, 357). As shown, PCA was unable to identify a chemical space occupied solely by the molecule that was shown to be active in all the assays used (**Figure 17 A**), the same being true for multidimensional scaling (MDS, **Figure 17 B**). In light of this, we applied a suite of other algorithms, both individually and in tandem with PCA, namely uniform manifold approximation and projection (UMAP) and t-distributed stochastic neighbor embedding (t-SNE).

Differently from PCA and MSD, the combined used of PCA+UMAP led to a 2-principal component-based space, in which delphinidin clearly occupies an outlier space. We have tried distinct combinations of parameters, as stated in the Materials section, the number of neighbors of 45 giving the best performance, both for minimum distance of 0.01 and 0.1. In order to confirm this result, we have employed an additional algorithm, namely PCA+t-SNE. Again, it was shown that delphinidin, together with an outlier, occupies a space that is distinct from over 98% of the library.

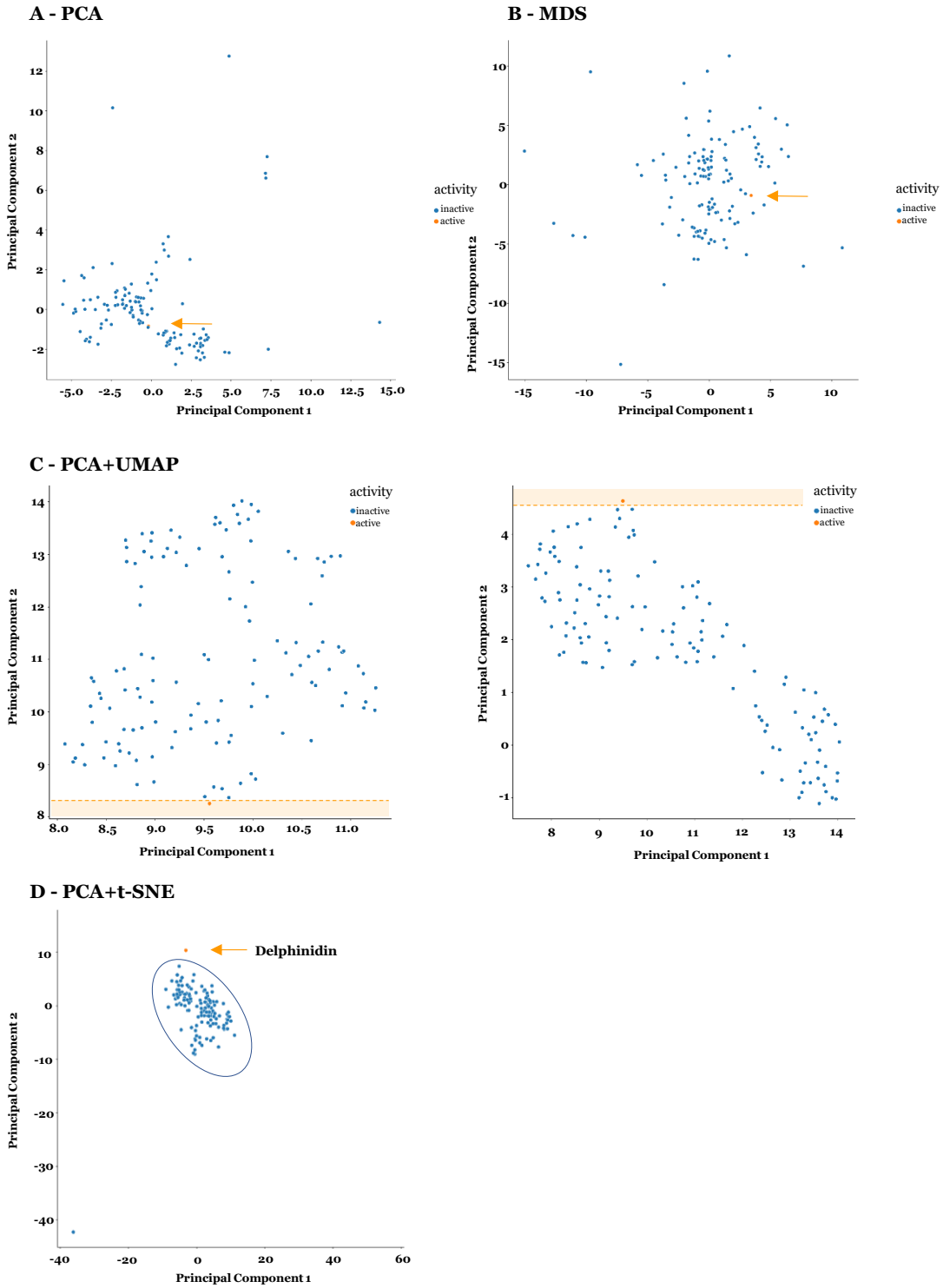

Figure 17. Different dimensionality reduction methods applied to chemical library under study. The active molecule delphinidin is presented in orange and inactive molecules in blue.

3.1.4. Discussion

Having performed the characterization of our in-house library of over 130 natural products, considering that new candidates for countering ER stress should be devoid of toxicity, we proceeded to the evaluation of the impact of all the molecules in the viability of fibroblasts, as assessed by the MTT reduction assay. Fibroblasts present a highly developed endoplasmic reticulum, since their function relates to the production of components of the extracellular matrix, and thus are particularly susceptible to ER stress, reason for which they were chosen as experimental model in this work (358).

The maintenance of the high concentration of calcium in the ER lumen creates an appropriate environment for protein folding, and thus changes on its levels heavily impact ER function (37, 345). This organelle is able to maintain its calcium levels due to the abundance of resident calcium-buffering proteins, like calnexin and calreticulin (346). Under stress conditions, the ER may release calcium through channels, such as IP_3R and RyR. Eventually, this may lead to increased calcium in mitochondria, indirectly inducing the generation of ROS and triggering the dissipation of the mitochondrial membrane potential, ultimately leading to the release of resident proapoptotic factors (347). We were able to identify molecules with the capacity to ameliorate ionic calcium leakage into the cytosol, namely 5-deoxykaempferol, delphinidin, fisetin, naringenin, naringin, quercetin-3-*O*-β-D-glucoside, sennoside B, myristic acid and spermine, and thus deemed these molecules with potentially protective against ER stress, and selected them to subsequent assays.

Regarding the RT-qPCR results, we show that 6 out of the 9 molecules that effectively countered the calcium overload were, simultaneously, capable of downregulating UPR-associated genes, which suggests that the assessment of cytosolic calcium levels is a reliable method to screen of the capacity to counter ER stress in this experimental model. Considering that 5-deoxykaempferol, delphinidin, fisetin, myristic acid, sennoside B and quercetin-3-*O*-β-D-glucoside were capable of significantly preventing the Tg-induced increased expression of, at least, two UPR-related genes, they were selected for subsequent studies. Among this molecules, fisetin displayed the strongest bioactivity at the mRNA expression level since it significantly inhibited the expression of all target genes. In contrast, naringin, naringenin and spermine failed to inhibit the expression of any of the analyzed genes, thus they were dropped from the pipeline.

Taking into account that increased UPR-related gene expression characterizes ER stress, many natural products have been described as ER stress modulators (either inducers or inhibitors) upon observation of their impact on the expression of these genes (128). Most of the molecules that here displayed the potential to ameliorate UPR signaling have not been

described before as ER stress modulators. However, fisetin has already been reported as an ER stress inhibitor, reducing *hspa5* (BiP) mRNA expression in hepatocytes (359). Relevantly, fisetin has already been described as neuroprotective by inhibition of protein aggregation and neuroinflammation in mice (360). There are also several reports of its bioactivity as an UPR inducer in different contexts (338, 361).

On MRC-5 fibroblasts, we show that the molecules that had been selected on the basis of their ability to attenuate UPR pathways were able to act upon the endpoint biological effect of this cascade, namely protein aggregation. As mentioned before, the UPR relies on three major signaling branches. They are all governed by the major chaperone BiP, coded by the gene *hspa5*. Under homeostatic conditions, BiP remains bound to the three major UPR players (PERK, IRE1 and ATF6), releasing them whenever it recognizes the presence of misfolded proteins. This extends the permanence of these proteins in the ER lumen, in order to promote their correct processing. For these reasons, BiP is a key regulator of UPR signaling and its activation prevents protein aggregation (362). In light of our results, we conclude that the UPR activation in the presence of delphinidin and fisetin is mitigated, as they clearly reduced BiP expression. Since both molecules significantly decreased the occurrence of protein aggregates in the cells, we conclude that the observed BiP levels, closer to the basal levels of the control group, are a consequence of a decreased UPR activation. This implies that ER stress levels on the presence of a stress inducer are restored by the presence of delphinidin or fisetin, whether the inducer is thapsigargin or protein aggregation. We can therefore assume that both molecules contribute to a homeostatic protein folding environment in the ER lumen.

It is described that the expression of this chaperone is increased throughout the course of neurodegenerative disease (363). In human brains of AD patients, it was observed a significant increase in BiP expression when compared to samples of non-demented patients (364, 365). It is known that this increased expression emerges early in the pathogenesis of AD and, at this stage, correlates with the adaptive response of the UPR; however, the sustained UPR activation that underlies the disease results in neurodegeneration (224). Additionally, there is considerable amount of evidence indicating the neuroprotective effect of UPR inhibition (69, 366, 367). This is, to the extent of our knowledge, the first report of the protective effect of delphinidin against ER stress and UPR activation.

Given the promising results on MRC-5 fibroblasts, we repeated the experiment, this time with SH-SY5Y cells, in order to analyze whether these compounds could also be protective on this neuronal cell line. The SH-SY5Y cell line has been widely used and described as a good *in vitro* model for the study of protein aggregation (368-371), a process that has been shown to be both consequence and cause of misfolded proteins in the ER and subsequent activation of the UPR (225). Relevantly, in the case of AD it has been shown that

increased levels of phosphorylated PERK and IRE1α are found in the hippocampus of the patients and that they colocalize with phosphorylated tau. Furthermore, treatment of cells with $A\beta_{42}$, the major component of amyloid plaques, induces CHOP expression, which is a product of the PERK and ATF6 branches of the UPR (363, 372, 373). The literature already conveys reports of the bioactivity of naturally occurring small molecules as pharmacological chaperones, for instance, flavonoid glycosides that were protective against protein aggregation in cell-based experiments (374). In murine cells, a study of over 200 naturally occurring molecules of discrete chemical classes concluded that flavonoids displayed the strongest potential to decrease the formation of protein aggregates in the context of AD (375).

The final step in this work was the attempt to define a chemical space where to search for bioactive molecules. Again, it was shown that delphinidin, together with an outlier, occupies a space that is distinct from over 98% of the library. Taken together, these results show that chemometric tools, in tandem with biological data generated from significant number of samples, can be used for future selection of drug candidates relying on data science-based approaches. As so, the composition of the principal components identified can be used for the subsequent selection of novel molecules capable of countering ER stress by screening large databases of molecules for ideal chemical descriptors.

Our framework blending data science-based methods to biological data resulted in the identification of several potentially active molecules against the onset of ER stress. Delphinidin stood out as the most promising candidate against UPR activation and protein aggregation in a cellular model of neurodegenerative disease, being capable to simultaneously modulate calcium levels and downregulate UPR pathways with meaningful biological endpoints.

In light of our results, it is safe to assume that the natural product chemical space may provide molecules that ultimately lead to the development of novel pharmacological strategies to counter ER stress-related pathologies, as is the case of neurodegenerative diseases.

Supplementary Material

Supplementary Table S1. Variables used in the chemometric analysis.

Variable	Description
coconut_id	Identifier used in the COCONUT database
contains_sugar	Bolean for the presence of sugars
heavy_atom_number	Number of heavy atoms
Name	Name of the molecule
contains_ring_sugars	Bolean for the presence of sugars
molecular_formula	Molecular formula
molecular_weight	Molecular weight
npl_noh_score	Natural product-likeness score without taking into account any hydrogen in the molecular structure
npl_score	Natural product-likeness score
npl_sugar_score	NP-likeness score computed on the glycosylated molecule
number_of_carbons	Number of carbons
number_of_nitrogens	Number of nitrogens
number_of_oxygens	Number of oxygens
max_number_of_rings	Maximal number of rings
min_number_of_rings	Minimal number of rings
sugar_free_heavy_atom_number	Heavy atoms number, excluding sugars
sugar_free_total_atom_number	Total atom number, excluding sugars
total_atom_number	Total atom number
Alogp	AlogP
alogp2	AlogP squared
Amralogp	AMR - molar refractivity
Apol	Sum of the atomic polarizabilities
Bpol	BPol descriptor
eccentricConnectivityIndexDescriptor	Eccentric Connectivity Index Descriptor
fmfDescriptor	fmf Descriptor
fsp3	fsp3
fragmentComplexityDescriptor	Fragment Complexity Descriptor
hBondAcceptorCount	Hydrogen bond acceptor count
hBondDonorCount	Hydrogen bond donor count
hybridizationRatioDescriptor	Hybridization Ratio Descriptor (fraction of sp3 carbons to sp2 carbons)
kappaShapeIndex1	First kappa shape index
kappaShapeIndex2	Second kappa shape index
kappaShapeIndex3	Third kappa shape index
manholdlogp	LogP descriptor (Mannhold version)
petitjeanNumber	Petit Jean Number
petitjeanShapeTopo	Petitjean geometrical shape index
lipinskiRuleOf5Failures	Number of Lipinski Rule of 5 violations
vertexAdjMagnitude	Vertex adjacency information
weinerPathNumber	Wiener Path Number
weinerPolarityNumber	Wiener Polarity Number
zagrebIndex	Zagreg Index
topoPSA	Topological polar surface area descriptor
tpsaEfficiency	Fractional polar surface area descriptor
iupac_name	IUPAC name
chemicalClass	Chemical Class
chemicalSubClass	Chemical SubClass
chemicalSuperClass	Chemical SuperClass
directParentClassification	Classification of parent molecule

Supplementary Table S2. Molecules tested in the cell viability assays. Molecules in purple were excluded given their toxicity.

	A	B	C	D	E
1	Control	5,7,8-Trihydroxyflavone	Betanin	Chrysophanol	Ellagic acid
2	(-)-Norepinephrine	5,8-Dihydroxy-1,4-naphtoquinone	Betulin	Cinnamic acid	Emodin
3	(+/-)-Dihydrokaempferol	5-Deoxykaempferol	Boldine	Coumarin	Eriocitrin
4	1,4-Naphtoquinone	5-Methoxypsoralen	Caffeine	Cyanidin	Eriodictyol
5	18α-Glycyrrhetinic acid	Acacetin	Catechol	Cynarin	Eriodictyol-7-*O*-glucoside
6	3,4-Dihydrobenzoic acid	Ajmalicine	Chlorogenic acid	Daidzein	Eupatorin
7	3,4-Dimethoxycinnamic acid	Apigenin	Cholesta-3,5-diene	Delphinidin	Ferulic acid
8	3-Hydroxybenzoic acid	Apigetrin	Chrysin	Diosmetin	Fisetin
9	4-Hydroxybenzoic acid	Berberine	Chrysoeriol	Diosmin	Flavanone
	F	**G**	**H**	**I**	**J**
1	Galangin	Hesperetin	Isorhamnetin-3-*O*-rutinoside	Liquiritigenin	Mangiferin
2	Galanthamine	Hesperidin	Isorhoifolin	Lupeol	Maritimein
3	Gallic acid	Homoeriodictyol	Juglone	Lutein	Myricetin
4	Genistein	Homoorientin	Kaempferide	Luteolin	Myricitrin
5	Genkwanin	Homovannilic acid	Kaempferol	Luteolin tetramethylether	Myristic acid
6	Gentisic acid	Hydroquinone	Kaempferol-3-*O*-rutinoside	Luteolin-3',7-di-*O*-glucoside	Myrtillin
7	Guaiaverin	Hyoscyamine	Kaempferol-7-*O*-glucoside	Luteolin-4'-*O*-glucoside	Naringenin
8	Guaiazulene	Isorhamnetin	Kaempferol-7-*O*-neohesperidoside	Luteolin-7-*O*-glucoside	Naringenin-7-glucoside
9	Herniarin	Isorhamnetin-3-*O*-glucoside	Linarin	Malvidin	Naringin
	K	**L**	**M**	**N**	**O**
1	Narirutin	Plumbagin	Quercetin-3-*O*-*β*-*D*-glucoside	Sennoside B	Tiliroside
2	Oleuropein	Pyrogallol	Quercitrin	Silibinin	Trigonelline
3	Orientin	Quercetagetin	Rhoifolin	Spermine	Vanillin
4	*p*-Coumaric acid	Quercetin	Robinin	Sulfuretin	Verbascoside
5	Pelargonidin	Quercetin-3,3',4',7-tetramethylether	Rosmarinic acid	Swertiamarin	Vicenin-2
6	Pelargonin	Quercetin-3,4'-dimethylether	Rutin	Taxifolin	Vitexin
7	Phloroglucinol	Quercetin-3-methylether	Saponarin	Tectochrysin	Vitexin-2-*O*-rhamnoside
8	Pinocembrin	Quercetin-3-*O*-(-6-acetylglucoside)	Scopolamine	Theobromine	Xanthone
9	Pyrogallol	Quercetin-3-*O*-glucuronide	Sennoside A	Theophylline	ß-escin

Supplementary Table S3. Molecules screened for their ability to preserve cytosolic calcium levels. Molecules in blue were selected for subsequent studies.

	A	B	C	D	E
1	Control	5-Deoxykaempferol	Cinnamic acid	Eriocitrin	Gentisic acid
2	Ionophore	Apigetrin	Coumarin	Eriodictyol	Guaiaverin
3	(-)-Norepinephrine	Berberine	Cyanidin	Eriodictyol-7-*O*-glucoside	Herniarin
4	(+/-)-Dihydrokaempferol	Betanin	Cynarin	Ferulic acid	Hesperetin
5	3,4-Dihydrobenzoic acid	Boldine	Daidzein	Fisetin	Homoeriodictyol
6	3,4-Dimethoxycinnamic acid	Caffeine	Delphinidin	Flavanone	Homoorientin
7	3-Hydroxybenzoic acid	Catechol	Diosmetin	Galanthamine	Homovannilic acid
8	4-Hydroxybenzoic acid	Chlorogenic acid	Ellagic acid	Gallic acid	Isorhamnetin-3-*O*-glucoside
9	5,7,8-Trihydroxyflavone	Cholesta-3,5-diene	Emodin	Genistein	Isorhamnetin-3-*O*-rutinoside
	F	**G**	**H**	**I**	**J**
1	Isorhoifolin	Malvidin	Narirutin	Pyrogallol	Saponarin
2	Juglone	Maritimein	Oleuropein	Quercetin-3-*O*-ß-D-glucoside	Scopolamine
3	Kaempferol	Myricetin	Orientin	Quercetin-3-*O*-(-6-acetylglucoside)	Sennoside B
4	Kaempferol-3-*O*-rutinoside	Myricitrin	*p*-Coumaric acid	Quercetin-3-*O*-glucuronide	Silibinin
5	Kaempferol-7-*O*-neohesperidoside	Myristic acid	Pelargonidin	Quercitrin	Spermine
6	Liquiritigenin	Myrtillin	Pelargonin	Rhoifolin	Sulfuretin
7	Luteolin-3',7-di-*O*-glucoside	Naringenin	Phloridzin	Robinin	Swertiamarin
8	Luteolin-4'-*O*-glucoside	Naringenin-7-glucoside	Phloroglucinol	Rosmarinic acid	Taxifolin
9	Luteolin-7-*O*-glucoside	Naringin	Pinocembrin	Rutin	Theobromine
	K				
1	Theophylline				
2	Tiliroside				
3	Trigonelline				
4	Vanillin				
5	Verbascoside				
6	Vicenin-2				
7	Vitexin				
8	Vitexin-2-*O*-rhamnoside				
9	Xanthone				

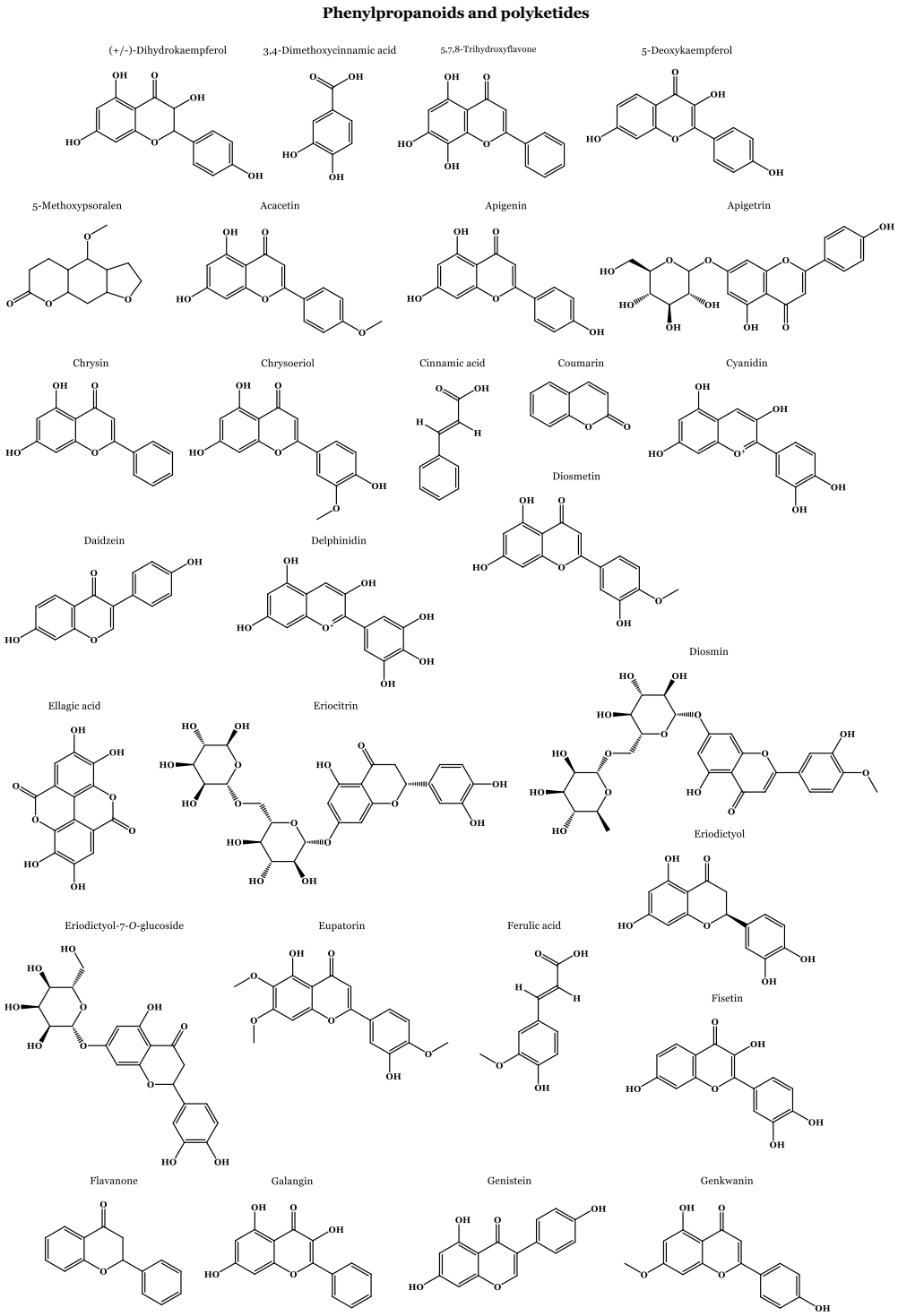

Supplementary Figure S1-A. Chemical structures of all tested molecules, grouped according to the respective chemical superclass according to ClassyFire.

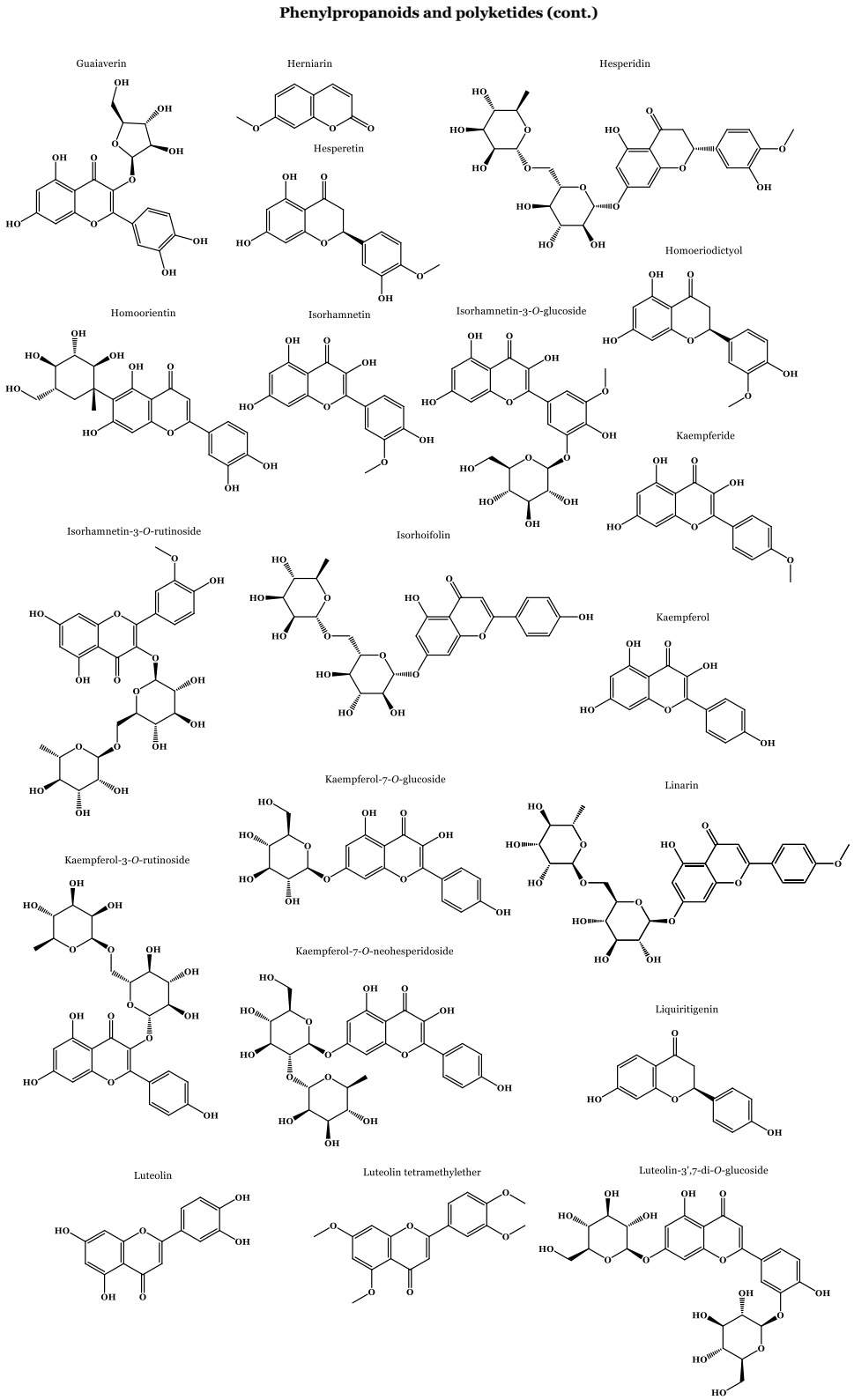

Supplementary Figure S1-B. Chemical structures of all tested molecules, grouped according to the respective chemical superclass according to ClassyFire (cont.).

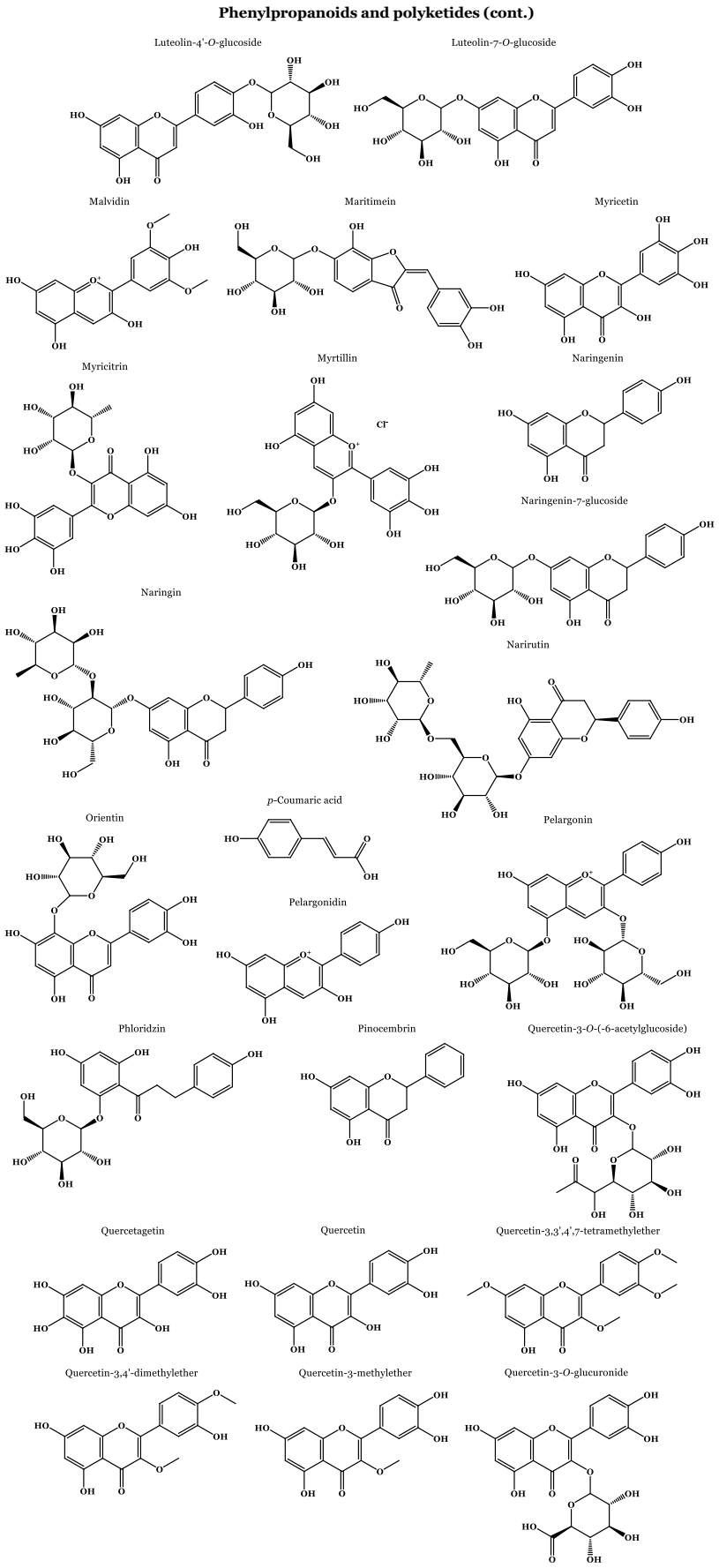

Supplementary Figure S1-C. Chemical structures of all tested molecules, grouped according to the respective chemical superclass according to ClassyFire (cont.).

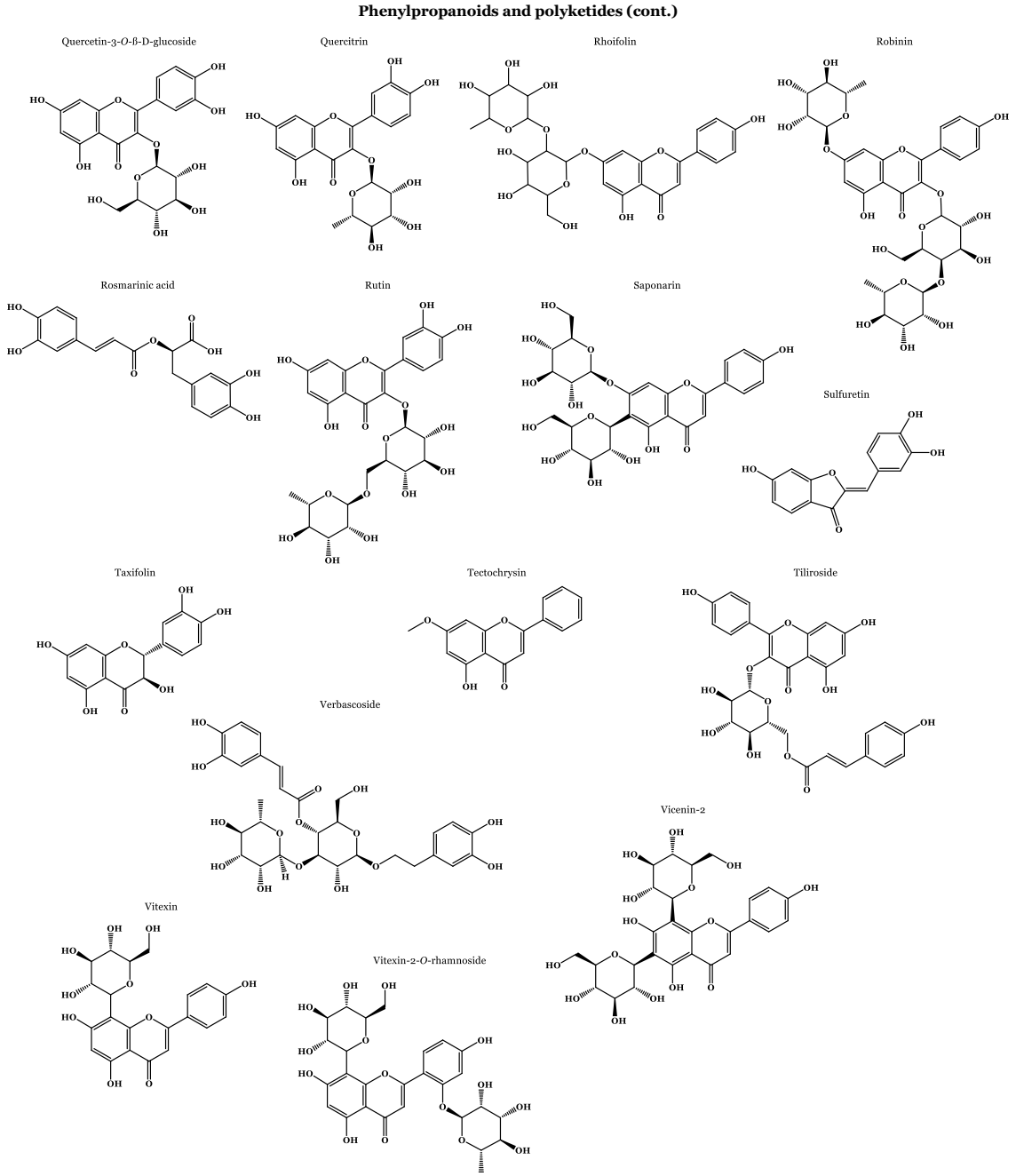

Supplementary Figure S1-D. Chemical structures of all tested molecules, grouped according to the respective chemical superclass according to ClassyFire (cont.).

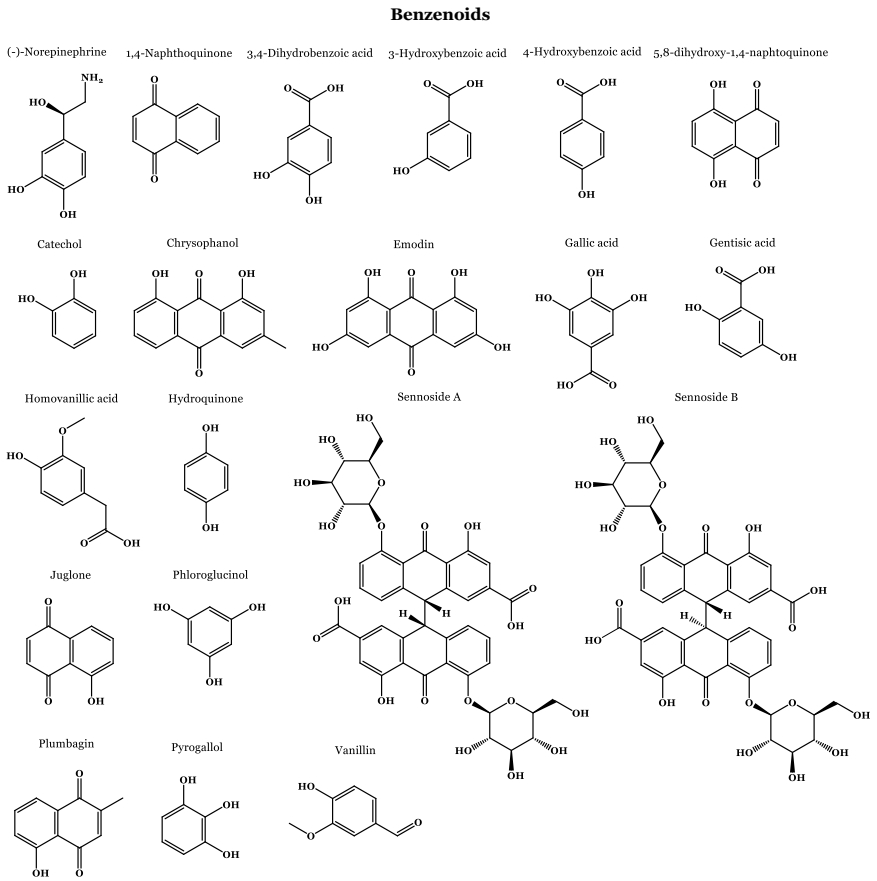

Supplementary Figure S1-E. Chemical structures of all tested molecules, grouped according to the respective chemical superclass according to ClassyFire (cont.).

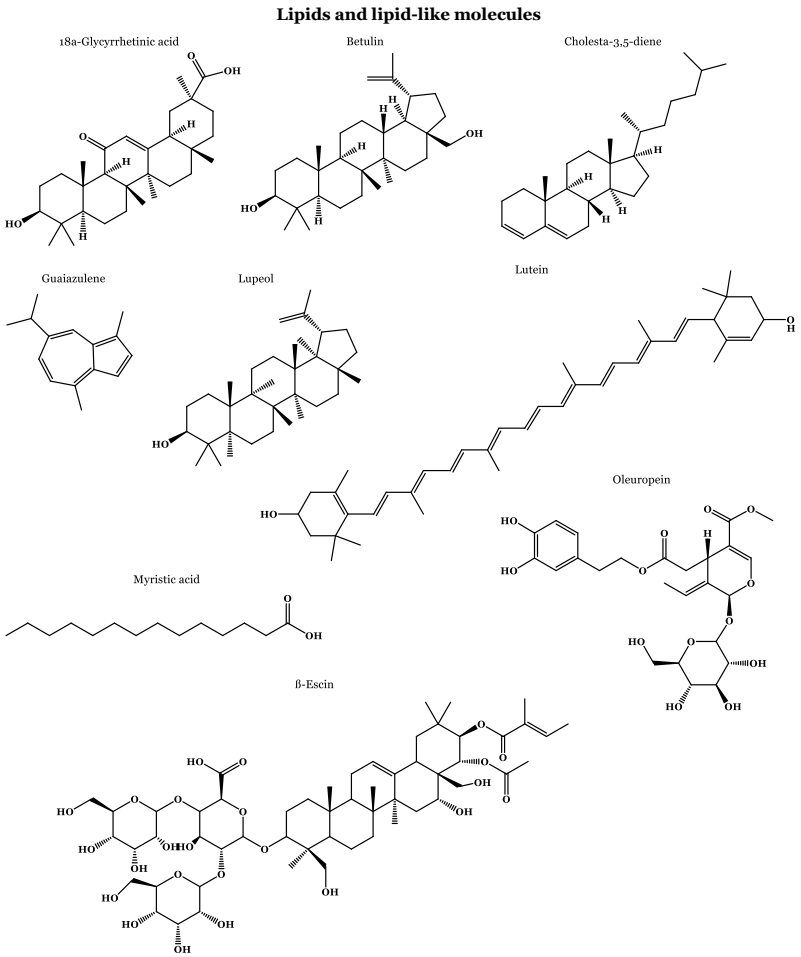

Supplementary Figure S1-F. Chemical structures of all tested molecules, grouped according to the respective chemical superclass according to ClassyFire (cont.).

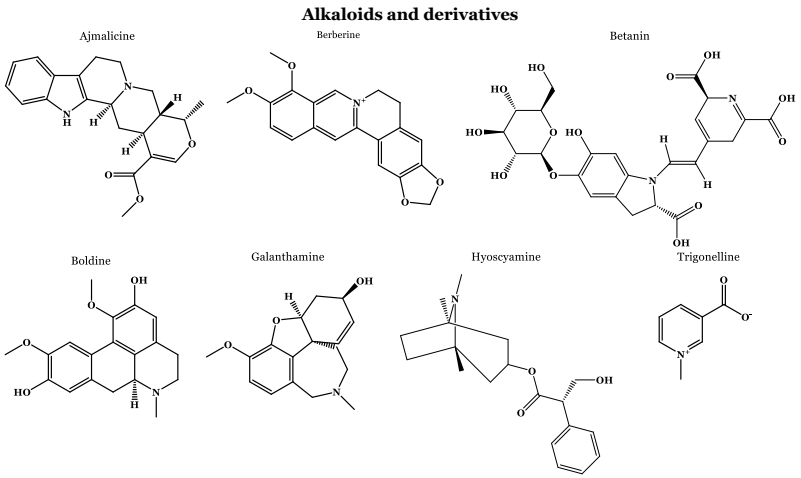

Supplementary Figure S1-G. Chemical structures of all tested molecules, grouped according to the respective chemical superclass according to ClassyFire (cont.).

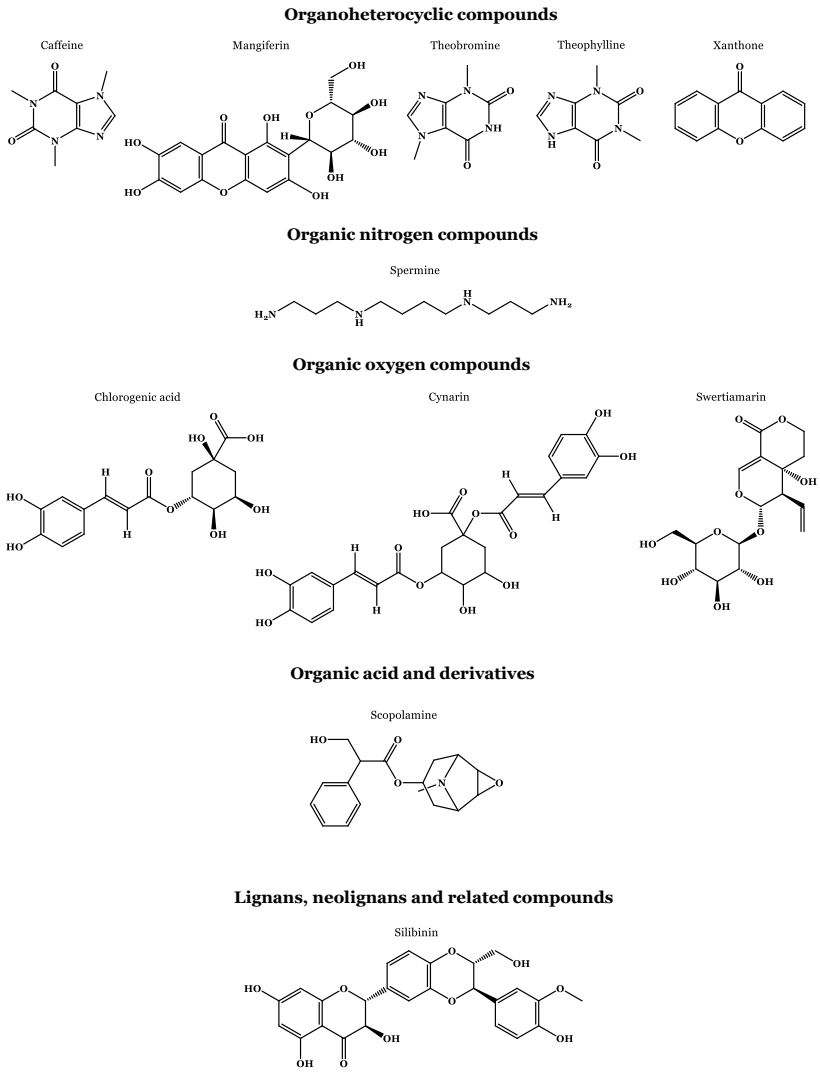

Supplementary Figure S1-H. Chemical structures of all tested molecules, grouped according to the respective chemical superclass according to ClassyFire (cont.).

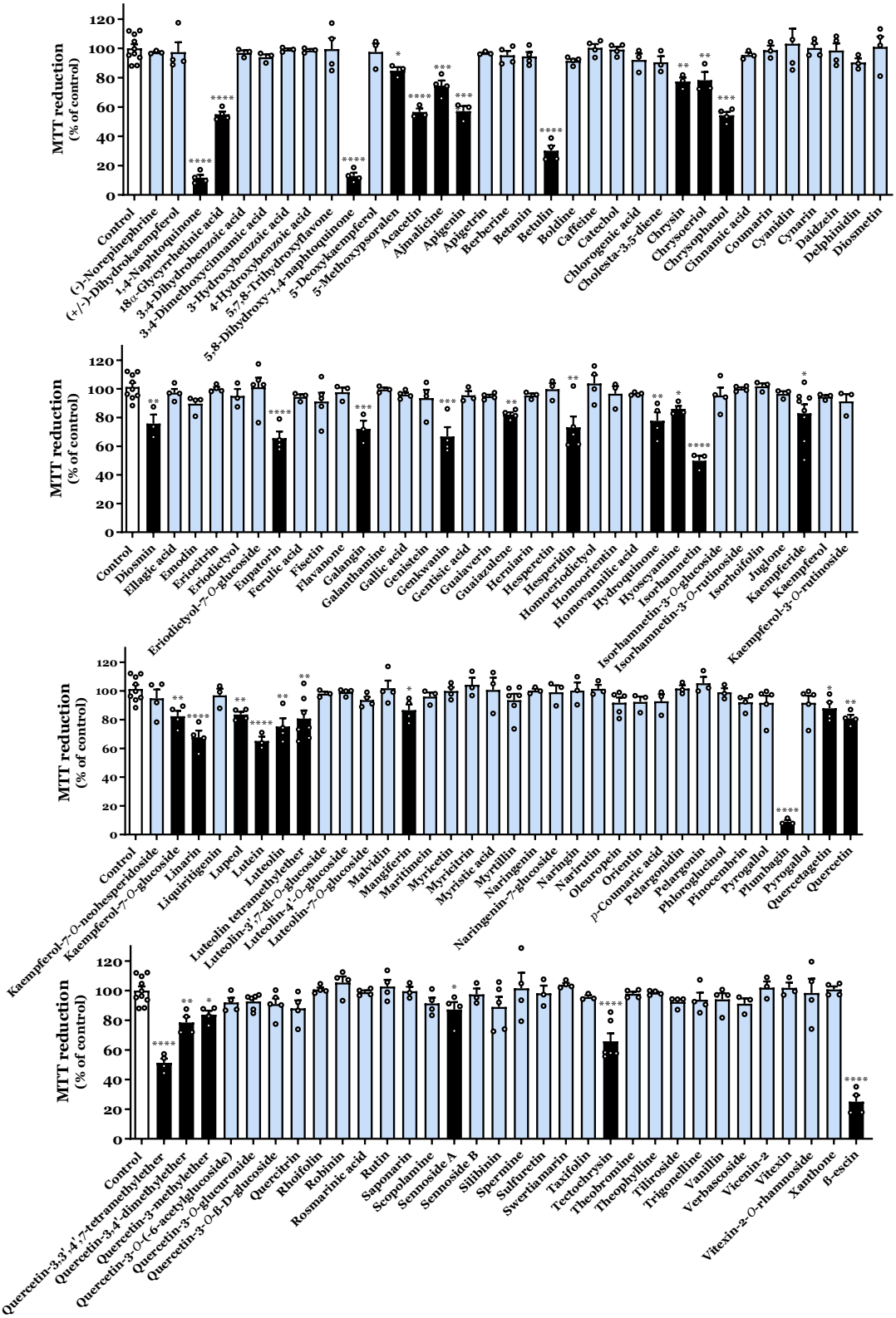

Supplementary Figure S2. Impact of a library of natural products on MRC-5 fibroblasts upon cell viability, as determined by MTT reduction assay. All compounds were tested at 50 μM. Results correspond to the mean ± standard error of the mean and represent, at least, three independent experiments, each performed in triplicate. *$p < 0.05$, **$p < 0.01$, ***$p < 0.001$, ****$p < 0.0001$.

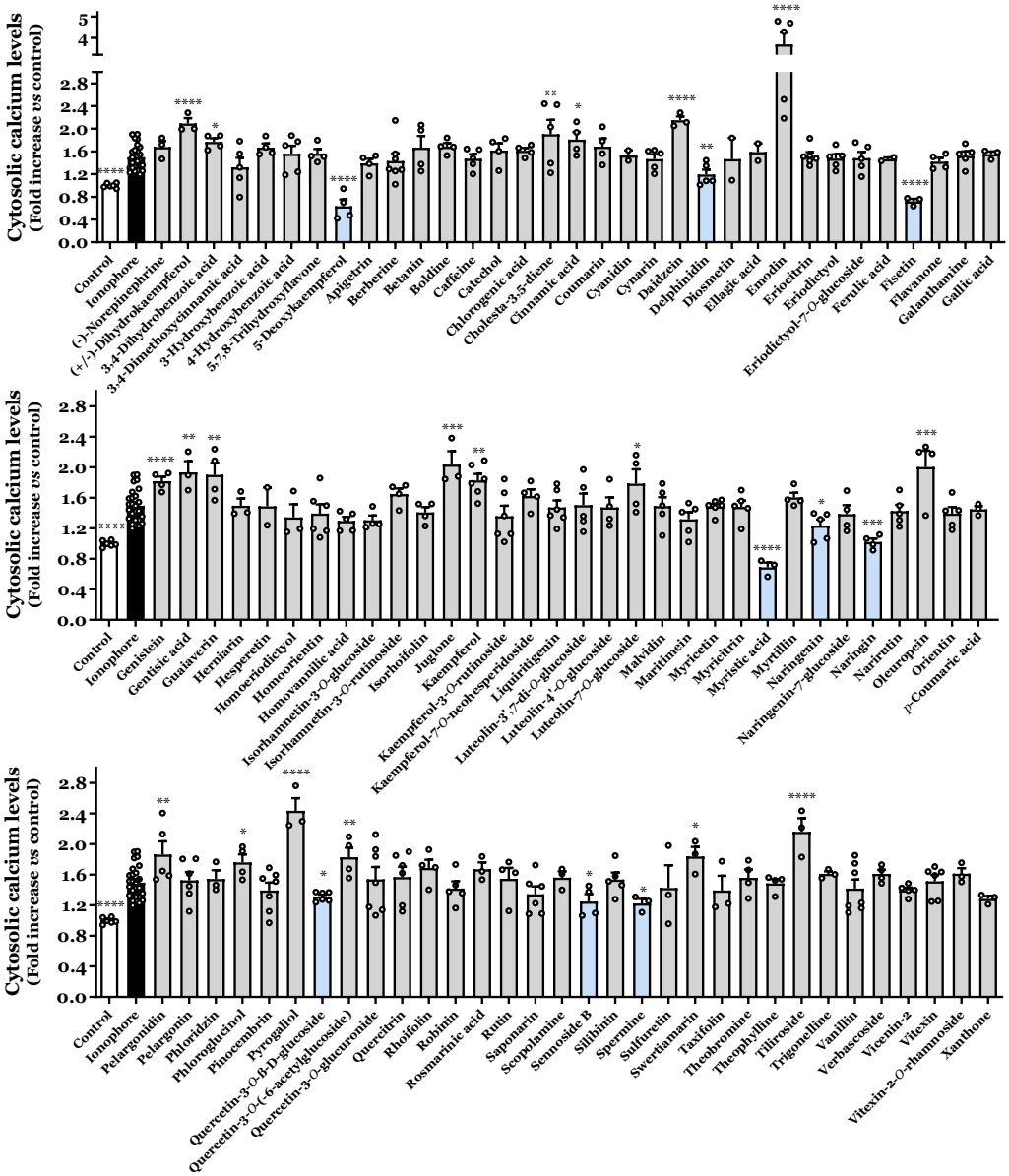

Supplementary Figure S3. Cytosolic calcium levels in MRC-5 fibroblasts in response to co-incubation of calcium ionophore A23187 at 5 μM and nontoxic molecules, as determined by the fluorescence of the probe Fura-2/AM. Results correspond to the mean ± standard error of the mean and represent, at least, three independent experiments, each performed in triplicate. *$p < 0.05$, **$p < 0.01$, ***$p < 0.001$, ****$p < 0.0001$.

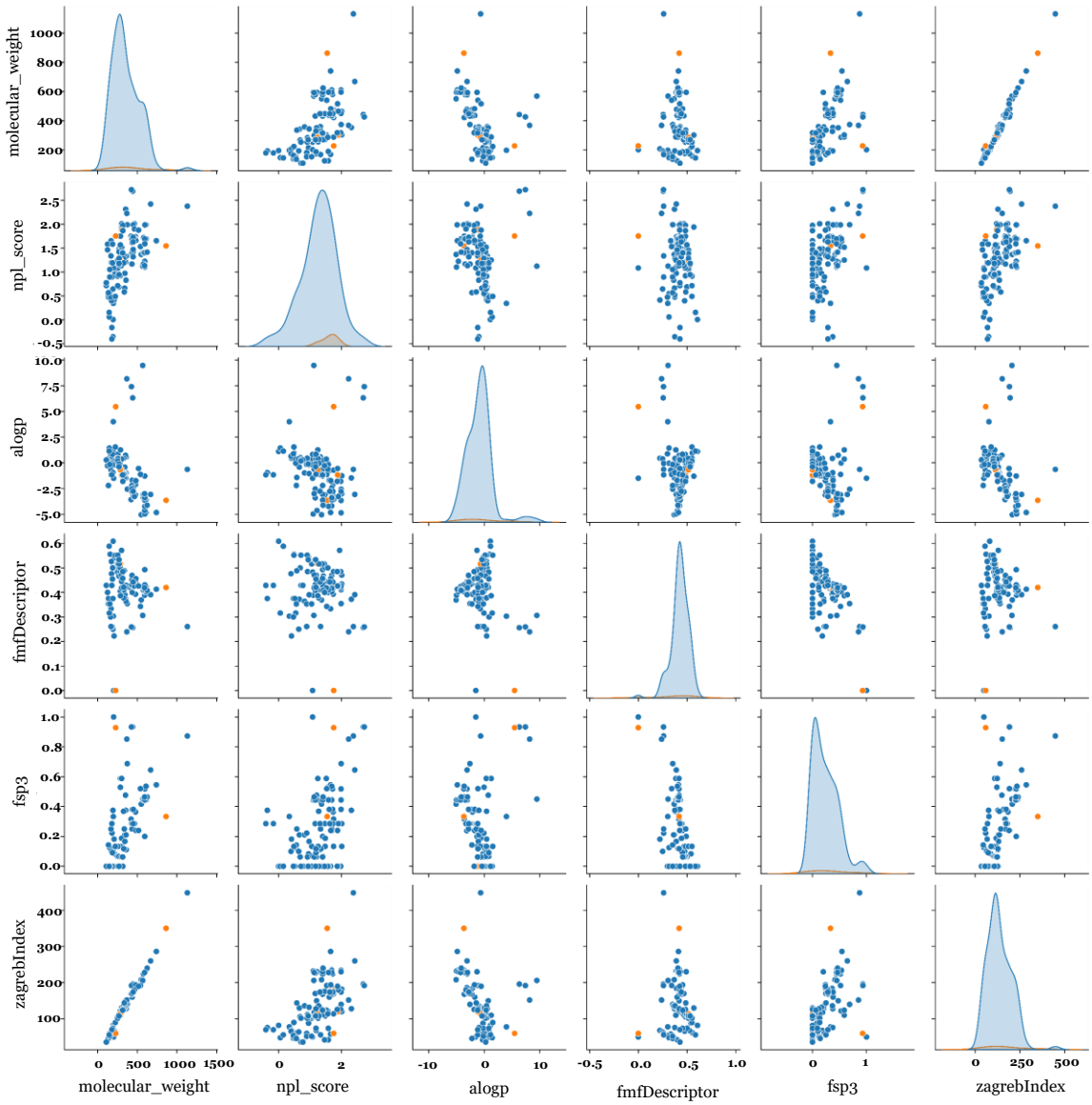

Supplementary Figure S4. Pairwise comparison of different features of the dataset. Blue = inactive molecules, orange = active molecules as *per* the results of **Figure 14 A**.

ORIGINAL ARTICLE #2

A survey of naturally occurring molecules as new endoplasmic reticulum stress activators with selective anticancer activity

Daniela Correia da Silva, Patrícia Valentão, David M. Pereira

Cancers, 2023, 15(1), 293

Abstract

The last century has witnessed the establishment of neoplastic disease as the second cause of death in the world. Nonetheless, the road towards desirable success rates of cancer treatments is still long and paved with uncertainty. This work aims to select natural products that act via endoplasmic reticulum (ER) stress, a known vulnerability of malignant cells, and display selective toxicity against cancer cell lines. Among an in-house chemical library, nontoxic molecules towards noncancer cells were assessed for toxicity towards cancer cells, namely the human gastric adenocarcinoma cell line AGS and the lung adenocarcinoma cell line A549. Active molecules towards at least one of these cell lines were studied in a battery of ensuing assays to clarify the involvement of ER stress and unfolded protein response (UPR) in the cytotoxic effect. Several natural products are selectively cytotoxic against malignant cells, and that the effect often relies on ER stress induction. Berberine was the most promising molecule, being active against both cell models by disrupting Ca^{2+} homeostasis, inducing UPR target gene expression and ER-resident caspase-4 activation. Our results indicate that berberine and emodin are potential leads for the development of more potent ER stressors to be used as selective anticancer agents.

Keywords: unfolded protein response, endoplasmic reticulum stress, natural products, chemical library, drug discovery, ATF4, CHOP, EDEM1, caspase-4, calcium homeostasis

3.2.1. Introduction

Recent decades have witnessed an increase in favorable outcomes of cancer patients. There is, however, a long road until high success rates in cancer treatments (376). In fact, neoplastic diseases remain one of the major causes of death worldwide, second only to cardiovascular disease. Furthermore, the incidence of this type of disease has been increasing (377).

In the eukaryotic cell, protein synthesis and folding, as well as stress response, are inseverable of the endoplasmic reticulum (ER) function. This organelle possesses robust signaling networks that evolved towards recognition and mitigation of disturbances in proteostasis, which, globally, trigger the unfolded protein response (UPR) (378). The UPR encompasses three major signaling branches, each activated with one of three leading sensors, namely the i) protein kinase RNA-like ER kinase (PERK), the ii) inositol-requiring protein 1 (IRE1), and the iii) activating transcription factor 6 (ATF6) (147, 378, 379). UPR activation decreases the protein load to be processed in the ER lumen by bringing the secretory pathway to a halt. It globally impairs protein synthesis, while enhancing ER-associated degradation of misfolded proteins (ERAD). Whenever it cannot restore proteostasis, UPR activation conducts to programmed cell death events (379).

Given their aberrant protein synthesis rates , cancer cells endure chronic ER stress, and their survival strongly relies on UPR activation (329). Notably, expression of UPR biomarkers is associated to multiple types of cancers, often implying therapy resistance and poor prognosis (329). The types of neoplasm in which this has been observed includes lung, breast, colon, gastric, pancreas, liver, prostate, kidney, skin, lymphoblastic leukemias, and β-cell lymphoma (216).

One increasingly promising anticancer strategy is the use of molecules capable of triggering ER stress in cancer cells (380). Relevantly, ER stress inducers often display selective cytotoxic activity against malignant cells, which may be central to the development of safer pharmacological strategies against cancer (381). When the UPR tolerance threshold is reached in cancer cells, it leads to the occurrence of organized cell death (380).

The natural product chemical space, due to its immense structural variability, is a prolific source of ER stress and UPR modulators (128, 219, 382). Two remarkable examples of such molecules are thapsigargin (Tg) and tunicamycin, commonly used as research tools to induce ER stress (144-146, 299, 302, 303). Nonetheless, most reports on selective cytotoxic molecules describe cytotoxicity to non-cancer cells, even though milder than towards cancer cells (383). Others are reported as selectively cytotoxic, due to their specific cytotoxicity towards few types of cancer cells, but they were not, however, compared to non-cancer cells (384).

Lung and stomach cancers represent a significant fraction of cancer incidence and death worldwide (377). Here we report several natural products that are more toxic against a lung cancer cell line than towards lung fibroblasts, most of them being also toxic against a gastric cancer cell line. This work aims to report cytotoxic compounds against cancer cells, among a library of non-toxic natural products, that act by triggering ER stress, a known vulnerability of malignant cells (385, 386).

3.2.2. Materials and Methods

3.2.2.1. Chemical library and reagents

The compounds 5,7,8-trihydroxyflavone, 5-deoxykaempferol, apigetrin, coumarin, cyanidin, delphinidin, diosmetin, ellagic acid, eriocitrin, eriodictyol, eriodictyol-7-*O*-glucoside, ferulic acid, fisetin, flavanone, gallic acid, gentisic acid, herniarin, homoeriodictyol, homoorientin, homovanillic acid, isorhamnetin-3-*O*-glucoside, isorhamnetin-3-*O*-rutinoside, isorhoifolin, juglone, kaempferol, kaempferol-3-*O*-rutinoside, kaempferol-7-*O*-neohesperidoside, liquiritigenin, luteolin-3',7-di-*O*-glucoside, luteolin-4'-*O*-glucoside, luteolin-7-*O*-glucoside, malvidin, maritimein, myricetin, myricitrin, myrtillin, naringenin-7-*O*-glucoside, narirutin, oleuropein, orientin, pelargonidin, pelargonin, phloroglucinol, pyrogallol, quercetin-3-*O*-(-6-acetylglucoside), quercetin-3-*O*-glucuronide, rhoifolin, robinin, saponarin, scopolamine, sennoside B, sulfuretin, tiliroside, verbascoside and vitexin were purchased from Extrasynthese (Genay, France). The molecules (-)-norepinephrine, (+/-)-dihydrokaempferol, 3,4-dihydrobenzoic acid, 3,4-dimethoxycinnamic acid, 3-hydroxybenzoic acid, 4-hydroxybenzoic acid, berberine, betanin, boldine, catechol, cholesta-3,5-diene, cynarin, daidzein, emodin, galanthamine, genistein, guaiaverin, hesperetin, myristic acid, naringenin, naringin, *p*-coumaric acid, phloridzin, pinocembrin, quercetin-3-*O*-β-D-glucoside, quercitrin, rosmarinic acid, rutin and silibinin were acquired from Sigma-Aldrich (St. Louis, MO, USA). Caffeine was from Fluka (Buchs, Switzerland), vanillin was supplied by Vaz Pereira (Santarém, Portugal), vicenin-2 was purchased from Honeywell (Charlotte, NC, USA). Chlorogenic acid was from PhytoLab (Vestenbergsgreuth, Germany). Cinnamic acid was obtained from Biopurify (Chengdug, China). Swertiamarin was from ChemFaces (Wuhan, China).

Dulbecco´s Modified Eagle Medium (DMEM), Dulbecco's Modified Eagle Medium/Nutrient Mixture F-12 (DMEM/F-12), fetal bovine serum, penicillin/streptomycin solution (penicillin 5000 units/mL and streptomycin 5000 µg/mL), trypsin-EDTA (0.25%), Qubit™ dsDNA HS assay kit, Qubit™ RNA IQ assay kit, Qubit™ RNA HS assay kit,

SuperScript™ IV VILO™ MasterMix, and the Qubit™ Protein Assay Kit were acquired from Invitrogen (Grand Island, NE, USA). Dimethyl sulfoxide (DMSO) was acquired from Fisher Chemical (Loughborough, UK). Isopropanol was obtained from Merck (Darmstadt, Germany). 3-(4,5-Dimethylthiazol-2-yl)-2,5-diphenyltetrazolium Bromide (MTT), calcium ionophore A23187, thapsigargin, RNAzol®, chloroform, isopropanol, diethyl pyrocarbonate (DEPC), KAPA SYBR® FAST qPCR Kit Master Mix (2X) Universal, Trizma® base, sodium chloride, potassium phosphate monobasic, potassium chloride, sodium phosphate dibasic, sodium bicarbonate, D-glucose, phorbol 12-myristate 13-acetate (PMA), 4μ8C and Triton X-100 were obtained through Sigma-Aldrich (St. Louis, MO, USA). The fluorescent probe Fura-2/AM and caspase-4 assay kit (fluorometric) were purchased from Abcam (Cambridge, UK). Promega Caspase-Glo™ 3/7 Assay Kit was obtained from Promega Corporation (Madison, WI, USA). Salubrinal and JC-1 iodide were acquired from Santa Cruz Biotechnology (Dallas, TX, USA). Irestatin 9398 was acquired through Axon Medchem (Groningen, Netherlands).

3.2.2.2. Cell culture conditions

AGS human gastric adenocarcinoma cell line (American Type Culture Collection, LGC Standards S.L.U., Spain) was cultured in Dulbecco's Modified Eagle Medium (DMEM) + GlutaMAX™ containing 10% FBS and 1% penicillin/streptomycin. A549 human lung adenocarcinoma cell line (American Type Culture Collection, LGC Standards S.L.U., Spain) was cultured in Dulbecco's Modified Eagle Medium/F12 (DMEM) + GlutaMAX™ containing 10% FBS and 1% penicillin/streptomycin. Both were maintained at 37 ºC with 5% CO_2. In order to obtain spheroids, AGS and A549 cells were seeded in hydrophobic round-bottomed 96-well plates, in appropriate cell culture medium containing collagen (0.3 μg/mL), at a density of 5 x 10^3 cells/well. Under these conditions, spheroids were fully formed after 72 h at 37 ºC.

3.2.2.3. Monolayer and 3D cell viability assays

For the determination of cellular viability in monolayer cell culture, AGS cells were seeded at a density of 1.5 x 10^4 cells/well, while A549 were seeded at 1 x 10^4 cells/well. Afterwards, the cells were maintained at 37 ºC for 24 h. After this growth period, the wells were incubated with the compounds under study (100 μL/well) for another 24 h. The medium was aspirated and replaced by fresh medium containing MTT at 0.5 mg/mL. Cells were incubated for 90 (AGS) or 120 min (A549). Finally, the MTT solution was discarded, the resulting formazan crystals dissolved in a 3:1 DMSO:isopropanol solution (200 μL/well)

and the absorbance at 560 nm read in a Thermo Scientific™ Multiskan™ GO microplate reader. All experiments were performed in triplicate. Results are presented as the percentage of the control value and correspond to the mean ± SEM of, at least, three independent experiments.

To determine the viability of cells under 3D culture conditions, the compounds of interest were incubated on the spheroids for a period of 7 days. After this, the Presto Blue™ reagent was added according to the instructions from the manufacturer and incubated for 4 h at 37 ºC, for both cell lines. Finally, fluorescence at 560/590 nm was read on a Cytation™ 3 (BioTek) multifunctional microplate reader.

3.2.2.4. Evaluation of the mitochondrial membrane potential ($\Delta\Psi_m$)

Cells were seeded at the previously referred densities on 96-well plates. 24 h later they were incubated with the compounds of interest for another 24 h at 37 ºC. Afterwards, the medium was replaced by HBSS containing the ratiometric probe JC-1 at 7 µM. After 45 min at 37 ºC, the wells were carefully washed three times with HBSS. Fluorescence was read at 485/530 nm and at 530/590 nm in a Cytation™ 3 (BioTek) multifunctional microplate reader. The effect upon mitochondrial membrane potential was inferred from the ratio $F_{530/590}/F_{485/530}$. PMA at 100 nM was resorted to as a positive control for the disruption of the mitochondrial membrane, while molecules under study were tested at 50 µM. All determinations were performed in triplicate. Results are presented as fold decrease *vs* control, representing the mean ± SEM of, at least, three independent experiments.

3.2.2.5. RNA sample preparation, conversion to cDNA and RT-qPCR analysis

AGS were seeded at 1.2 x 10^5 cells/well and A549 at 8 x 10^4 cells/well, in 12-well plates. The plates were then kept at 37 ºC for 24 h prior to the incubation with compounds of interest (50 µM) for other 16 h. Tg at 3 µM was used as a positive control for upregulated UPR gene expression. Cells were lysed by replacing the culture medium by 500 µL of PureZOL RNA isolation reagent in each well. The lysate was pipetted up and down several times and the PureZOL reagent transferred to the duplicate well. The process was repeated, and the lysates maintained at room temperature for 5 min.

The RNA was extracted by phase separation, by adding 100 µL of chloroform to each sample and thoroughly mixing, followed by 5 min at room temperature and 15 min centrifugation at 12,000 *g*, at 4 ºC. The resulting aqueous phase was transferred to a new

tube and mixed with 250 µL of isopropyl alcohol. Again, the mixture was left to stand for 5 min at room temperature and then centrifuged at 12,000 *g* for 10 min, at 4ºC. The supernatant was discarded, and the RNA pellet washed with 500 µL of 75 % ethanol and centrifuged for 5 min at 7,500 *g* (4 ºC). Finally, the supernatant was again discarded, and the pellet was air-dried for a few minutes and resuspended in 25 µL of DEPC-treated water.

RNA quantification was performed using a Qubit™ RNA IQ assay kit and its integrity assessed with the Qubit™ RNA IQ assay kit, according to the instructions provided by the manufacturer. Conversion to cDNA was performed with the SuperScript™ IV VILO™ MasterMix, using 1 µg of RNA sample. The primers were designed on Primer BLAST (NCBI, Bethesda, MD, USA) and synthesized by Thermo Fisher (Waltham, MA, USA). The RT-qPCR reaction was performed with the KAPA SYBR® FAST qPCR Kit Master Mix (2X) Universal in the following thermal cycling conditions: 3 min at 95 ºC, 40 cycles of 95 ºC for 3 s, gene-specific temperature for 20 s (specified on **Table 6**), and 20 s at 72 ºC. The reactions took place in a qTOWER3 G (Analytik Jena AG, Germany), and the results were viewed on the software supplied with the equipment (qPCRsoft 4.0). *Gapdh* was selected as a reference gene for expression normalization. The results correspond to, at least, four independent experiments and every reaction was performed in duplicate.

Table 6. Data relative to the selected UPR-related genes and respective primers.

Gene	Accession number	Primers	Annealing Temperature (ºC)	Amplicon length (bp)
gapdh	NM_002046.6	F: AGGTCGGAGTCAACGGATTT R: TGGAATTTGCCATGGGTGGA	60	157
hspa5	NM_005347.4	F: ACTCCTGAAGGGGAACGTCT R: TTTTCAACCACCTTGAACGGC	59.5	161
ddit3	NM_001195053.1	F: AAGTCTAAGGCACTGAGCGT R: TTGAACACTCTCTCCTCAGGT	59	93
hsp90β1	NM_003299.2	F: GCTCTATGTGCGCCGTGTAT R: ATCTGAGTCCACCACACCCTT	60.5	91
atf4	NM_001675.4	F: ACAACAGCAAGGAGGATGCC R: CCAACGTGGTCAGAAGGTCA	60	135
edem1	NM_014674.2	F: GCGGGGACCCTTCAAATCT R: CGGCTTTCTGGAACTCGGAT	60	117

3.2.2.6. Cytosolic Ca^{2+} level determination

AGS and A549 cells were plated at the aforementioned densities on black bottomed-96-well plates and incubated at 37 ºC for 24 h. Then, the medium was replaced by the fluorescent probe Fura-2/AM at 5 µM in HBSS and incubated for 1 h. The molecules under

study (50 μM) were then prepared in HBSS and added to the plate. Two hours later the wells were washed three times with HBSS and fluorescence was read at 340/505 and 380/505 on a Cytation™ 3 (BioTek) multifunctional microplate reader. Data analysis was conducted considering the ratio $F_{340/505}/F_{380/505}$. Each experiment was performed in triplicate. Results are presented as fold increase *vs* control and represent the mean ± SEM of, at least, three independent experiments.

3.2.2.7. Caspase-3 and -4 activities

To determine the activity of caspase-4, cells were plated in 6-well plates at 2.4 x 10^5 cells/well for AGS cells and 1.6 x 10^5 cells for A549, and incubated at 37 ºC overnight. The compounds of interest were then added at 50 μM and cells were incubated for 6 h. After this period, cells lysates were prepared in the lysis buffer provided by the manufacturer of the caspase-4 assay kit, using a volume of 50 μL for each sample. The protein was quantified resorting to the Qubit™ Protein Assay. The assay was conducted in black-bottomed 96-well plates, using 100 μg of protein for each determination. The protein samples were incubated with the reaction buffer and the caspase-4 substrate LEVD-AFC at 50 μM, for 2 h at 37 ºC and, finally, the fluorescent signal was read at 400/505 nm in a Cytation™ 3 (BioTek) multifunctional microplate reader. The experiments were individually performed in duplicate, and the results represent the mean ± SEM of, at least, three independent experiments.

The activation of caspase-3 was evaluated using the Caspase-Glo® 3/7 kit assay. Cells were seeded as described above, on white bottomed-96-well plates. 24 h elapsed, the cells were incubated with the molecules under study for a new period of 24 h. Staurosporine at 100 nM was employed as a positive control for caspase-3 activation. Afterwards, 60 of the 100 μL of medium contained in each well were discarded and replaced by 40 μL of the Caspase-Glo® 3/7 buffer, containing Caspase-Glo® 3/7 substrate. The plate was incubated for 30 min at 22 ºC and the luminescent signal was measured in a Cytation™ 3 (BioTek) multifunctional microplate reader. All measurements were performed in duplicate. Results are presented as fold increase *vs* control and represent the mean ± SEM of, at least, three independent experiments.

The obtained results were normalized for the DNA amounts present after 24 h incubation with the molecules. After 24 h, cells were incubated with ultra-pure water at 37 ºC, for 30 min, and subsequently frozen at -80 ºC. DNA was quantified with the Qubit™ dsDNA HS Assay Kit. Caspase activity results were then normalized with the determined DNA amounts.

3.2.2.8. Study of the involvement of the PERK and IRE-1 branches of the UPR on cell viability

Cells were seeded as described for the MTT reduction assay and incubated with the toxic compounds (50 μM) in the presence or absence of salubrinal (1 μM), an inhibitor of eIF2α dephosphorylation and, thus, of PERK signaling, irestatin 9398 (5 μM), an inhibitor of the IRE-1 endonuclease activity, or 4μ8C (2 μM), an inhibitor of both endonuclease and kinase activities of IRE-1. Prior to the incubation of the molecules under study in the presence of the mentioned UPR inhibitors, a pre-incubation of 1 h with these inhibitors was conducted. The medium was then replaced by a solution containing the molecule and the inhibitor at the aforementioned concentrations. Cell viability was determined 24 h later *via* MTT reduction assay.

3.2.2.9. Statistical analysis

Statistical analysis was carried out on the GraphPad Prism 8 software. In order to compare single treatments with control groups, we employed the unpaired Student's t-test, and values of $p < 0.05$ were considered statistically significant. The Grubbs' test was used to detect outliers.

3.2.3. Results

3.2.3.1. Cytotoxicity evaluation

The physico-chemical properties of the compound library used herein, as well as information on the toxicity of the molecules in non-cancer cells, were reported in our previous work (387). Considering the results obtained with the 97 molecules (**Supplementary Table S4**, **Supplementary Figures S5 and S6**), **Figure 18 A/B** shows the molecules that caused loss of viability of the two cancer cells lines used, AGS (gastric carcinoma) and A549 (lung adenocarcinoma), at a single concentration (50 μM). Most of the hits revealed toxicity to both cells lines, with three exceptions: boldine and spermine were toxic only for AGS cells, while emodin displayed a cytotoxic effect only towards A549 cells. On the other hand, 5-deoxykaempferol, diosmetin, fisetin, berberine, genistein and kaempferol were toxic towards both studied cell lines (**Figure 18 C**). All the results are presented in bar charts in **Supplementary Figure S5** and **Supplementary Figure S6**.

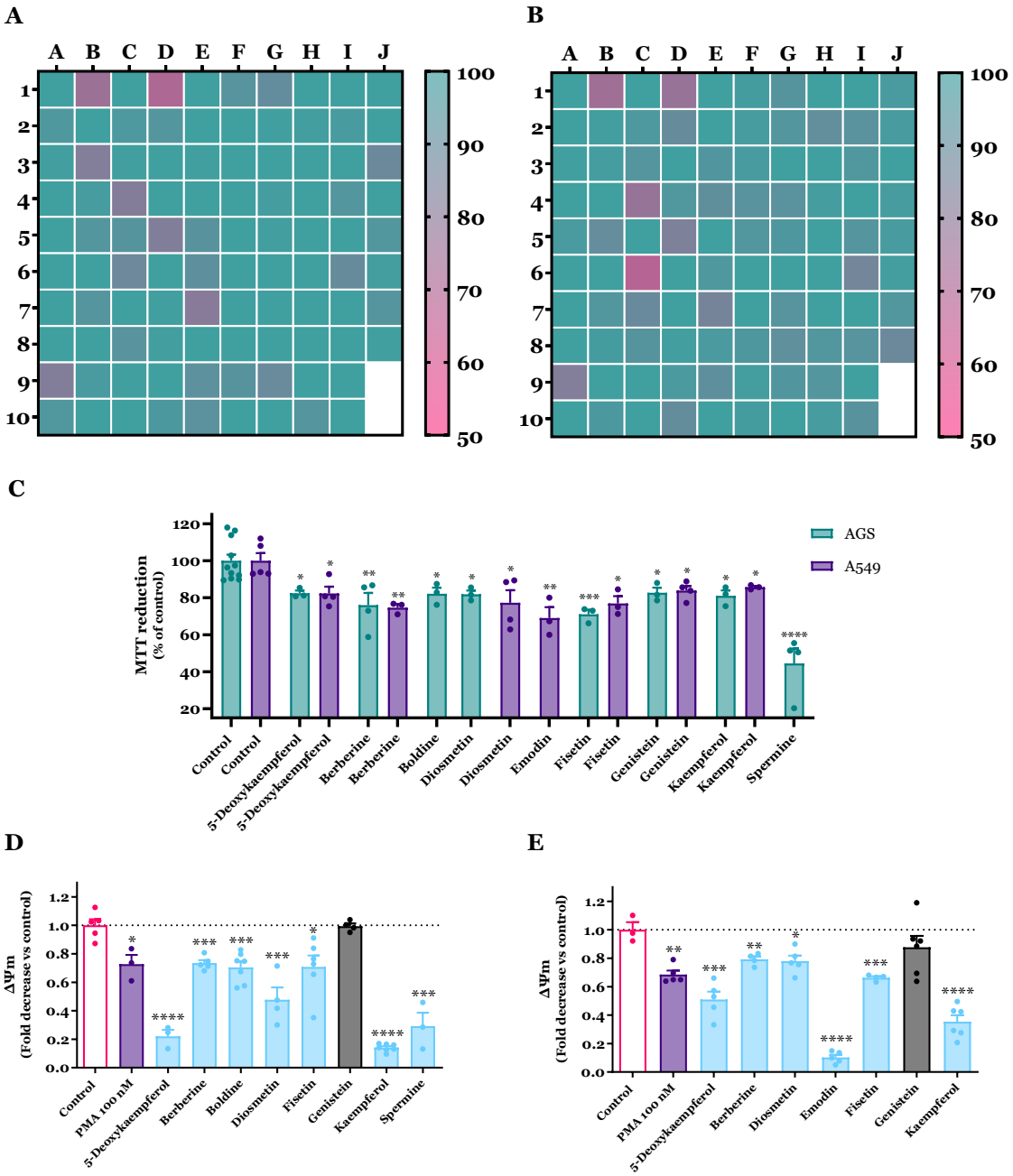

Figure 18. A/B: Impact of each compound on the viability AGS (A) or A549 (B) cells after 24 h, as determined by the MTT reduction assay. Every molecule was tested at 50 μM. Results are presented as the percentage of the control value and correspond to the mean of, at least, three independent experiments. **C:** Impact of each of the selectively cytotoxic molecules on the viability of AGS and A549 cells, representing the mean of, at least, three independent experiments ± SEM. **D/E:** Impact of the selected cytotoxic molecules on the mitochondrial membrane potential ($\Delta\Psi_m$) of AGS (D) and A549 (E) cells. Results consider $F_{530/590}/F_{485/530}$ and express the mean ± SEM of at least three independent assays, all the latter conducted in triplicate. *$p < 0.05$, **$p < 0.01$, ***$p < 0.001$, ****$p < 0.0001$.

As shown in **Figure 18 D/E**, all molecules caused a reduction of $\Delta\Psi_m$ on both cell lines, with the exception of genistein, which was for this reason dropped from the pipeline

(**Figure 18 D/E**). It is reported in the literature that PMA causes the disruption of the $\Delta\Psi_m$ at very low concentrations, alongside increased ROS production, by being and agonist of protein kinase C (PKC), as well as inducing its mitochondrial translocation, and hence it was used here as a positive control (72, 388). We have observed that many of our active molecules at 50 μM could exert a stronger effect at this level than PMA, even though the latter was used at 100 nM. This was observed with both kaempferol and 5-deoxykaempferol on both cell lines. Furthermore, emodin displayed a potent effect on the $\Delta\Psi_m$ dissipation in A549 cells.

3.2.3.2. Effect of cytotoxic molecules on UPR activation

The activation of the UPR involves the increased expression of multiple target genes, representing definitive evidence of stress upon the ER. Representative genes from multiple UPR branches and chaperones (*atf4*, *hspa5*, *ddit3*, *hsp90β1* and *edem1*) were selected and their expression following treatment with the cytotoxic molecules was studied.

As shown in **Figure 19 A**, both AGS and A549 cells had a similar response in terms of *atf4* and *edem1* expression when challenged with Tg, increasing the expression of these genes by around 3/4-fold. In the case of the remaining genes, namely *hspa5*, *ddit3*, and *hsp90β1*, the response was different between the two cell lines, A549 exhibiting a stronger response than AGS. These results show that the genes selected are adequate for assessing the UPR.

After assessing the genetic response in the context of UPR, all the molecules selected as cytotoxic were evaluated in the same conditions. As shown in **Figure 19 B/C**, all molecules were able to upregulate the expression of at least one of the target genes, with the exception of boldine in the case of AGS cells. As so, we hypothesized that the toxicity exerted by this molecule does not involve the UPR, reason for which it was dropped from the pipeline. In these cells, diosmetin and fisetin upregulated all of the analyzed target genes, while kaempferol and spermine upregulated only *edem1* and *ddit3*, respectively. The action of 5-deoxykaempferol resulted in upregulated *ddit3* and *hspa5* expression, while berberine increased the transcription factors *atf4* and *ddit3* and also *edem1*. In what concerns to A549 cells, 5-deoxykaempferol increased the expression of all target genes, berberine and emodin increasing the expression of *atf4, hspa5*, and *ddit3*. Fisetin upregulated all genes but *edem1*. Kaempferol upregulated *atf4*, *hspa5*, and *edem1*. Diosmetin treatment resulted in increased expression of both chaperones.

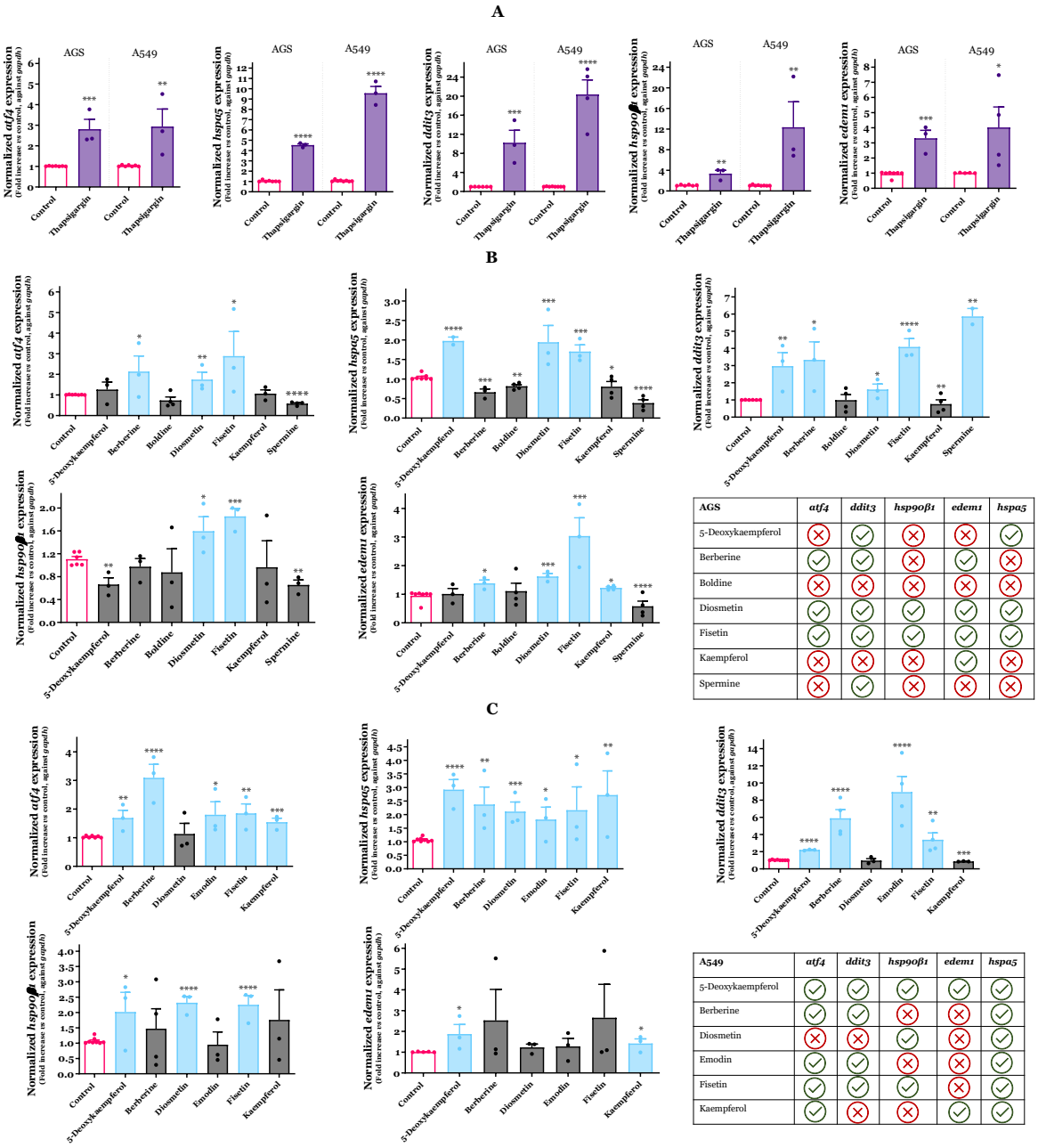

AGS	*atf4*	*ddit3*	*hsp90β1*	*edem1*	*hspa5*
5-Deoxykaempferol	✗	✓	✗	✗	✓
Berberine	✓	✓	✗	✓	✗
Boldine	✗	✗	✗	✗	✗
Diosmetin	✓	✓	✓	✓	✓
Fisetin	✓	✓	✓	✓	✓
Kaempferol	✗	✗	✗	✓	✗
Spermine	✗	✓	✗	✗	✗

A549	*atf4*	*ddit3*	*hsp90β1*	*edem1*	*hspa5*
5-Deoxykaempferol	✓	✓	✓	✓	✓
Berberine	✓	✓	✗	✗	✓
Diosmetin	✗	✗	✓	✗	✓
Emodin	✓	✓	✗	✗	✓
Fisetin	✓	✓	✓	✗	✓
Kaempferol	✓	✗	✗	✓	✓

Figure 19. A: Effect of Tg (3 μM) on the expression of UPR-related genes in AGS and A549 cells, as determined by RT-qPCR. **B:** Effect of the selected cytotoxic molecules on the expression of UPR-related genes in AGS cells, as determined by RT-qPCR. **C:** Effect of the selected cytotoxic molecules on the expression of UPR-related genes in A549 cells, as determined by RT-qPCR. In both cell lines, *gapdh* was selected as a reference gene for the normalization of gene expression. Results portray the mean ± SEM of three independent assays individually conducted in duplicate. *$p < 0.05$, **$p < 0.01$, ***$p < 0.001$, ****$p < 0.0001$.

3.2.3.3. Selected molecules impact Ca^{2+} homeostasis and caspase activity

Berberine, diosmetin and kaempferol caused Ca^{2+} to flow from the ER into the cytosol on the AGS cell line (**Figure 20 A**). Regarding A549 cells (**Figure 20 B**), only berberine and emodin increased the amounts of cytosolic Ca^{2+}.

Berberine elicited caspase-4 activation in both cell lines, being the only molecule that could do so in concomitance with impacting Ca^{2+} homeostasis under the selected experimental conditions. Fisetin could also significantly induce caspase-4 activation in both cell lines, while 5-deoxykaempferol and diosmetin only exerted a visible effect on AGS cells. Regarding caspase-3 activation, fisetin was the only compound that could trigger this effect in both cell lines (**Figure 20 A** and **Figure 20 B**). Other than this, 5-deoxykaempferol triggered caspase-3 activation on A549 cells (**Figure 20 B**).

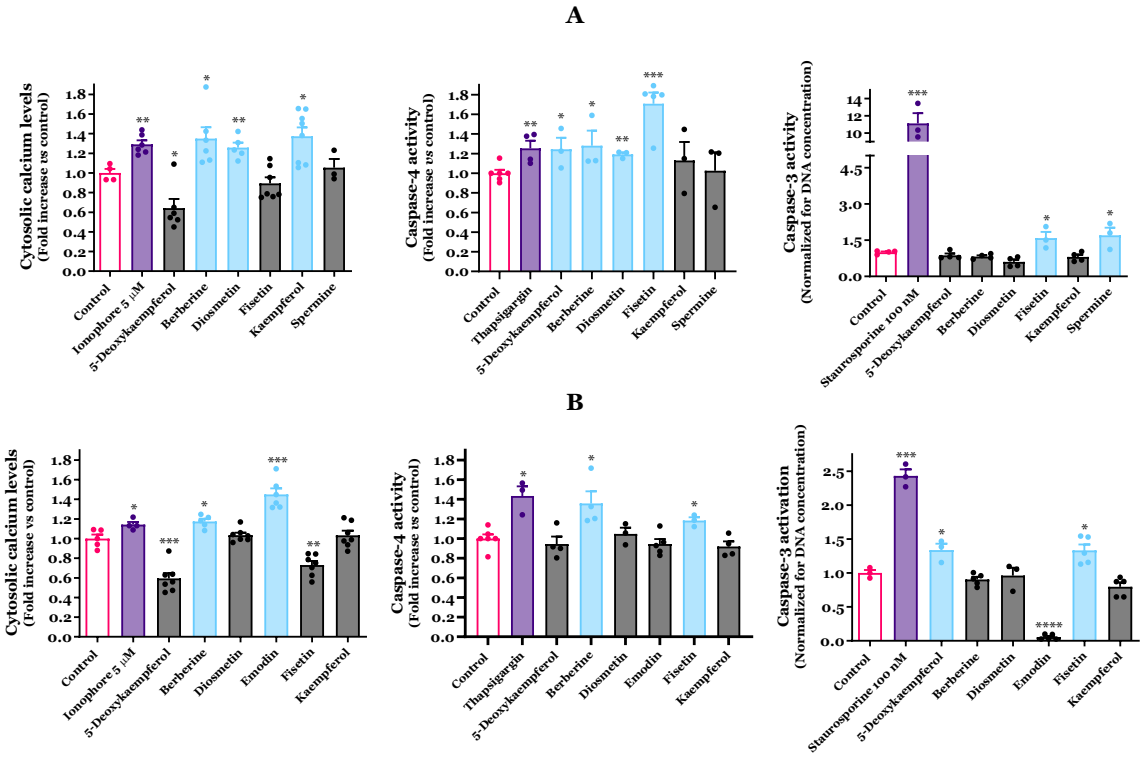

Figure 20. Effect of the molecules under study on the amounts of cytosolic Ca^{2+} in AGS (**A**) and A549 (**B**) cells, as determined with the fluorescent probe Fura-2/AM. Results are calculated considering $F_{340/505}/F_{380/505}$ and represent the mean ± SEM of, at least, three independent assays, individually performed in triplicate. Impact of the selected cytotoxic molecules activities of caspase-4 and caspase-3 in AGS cells (**A**) and in A549 cells (**B**). The displayed results represent the mean ± SEM of, at least, three independent experiments**.** *$p < 0.05$, **$p < 0.01$, ***$p < 0.001$, ****$p < 0.0001$.

3.2.3.4. Pharmacological modulation of UPR impacts cytotoxicity of ER stressors

In AGS cells, pre-incubation with salubrinal (1 μM) resulted in reduced toxicity of berberine (**Figure 21 A**). As for A549 cells, the same effect was observed in the cases of berberine and emodin (**Figure 21 B**). Berberine was the only of these molecules to be tested on both cells lines, and the results show that its effect extends to both. Furthermore, the salubrinal-induced increase on PERK phosphorylation enhances the toxicity of spermine in AGS cells.

Unlike what was verified in the presence of salubrinal, IRE1 inhibitors failed to prevent the toxicity of berberine on AGS cells (**Figure 21 A**). Regarding A549 cells, both irestastin 9398 and 4μ8C could prevent cell death induced by berberine and emodin (**Figure 21 B**).

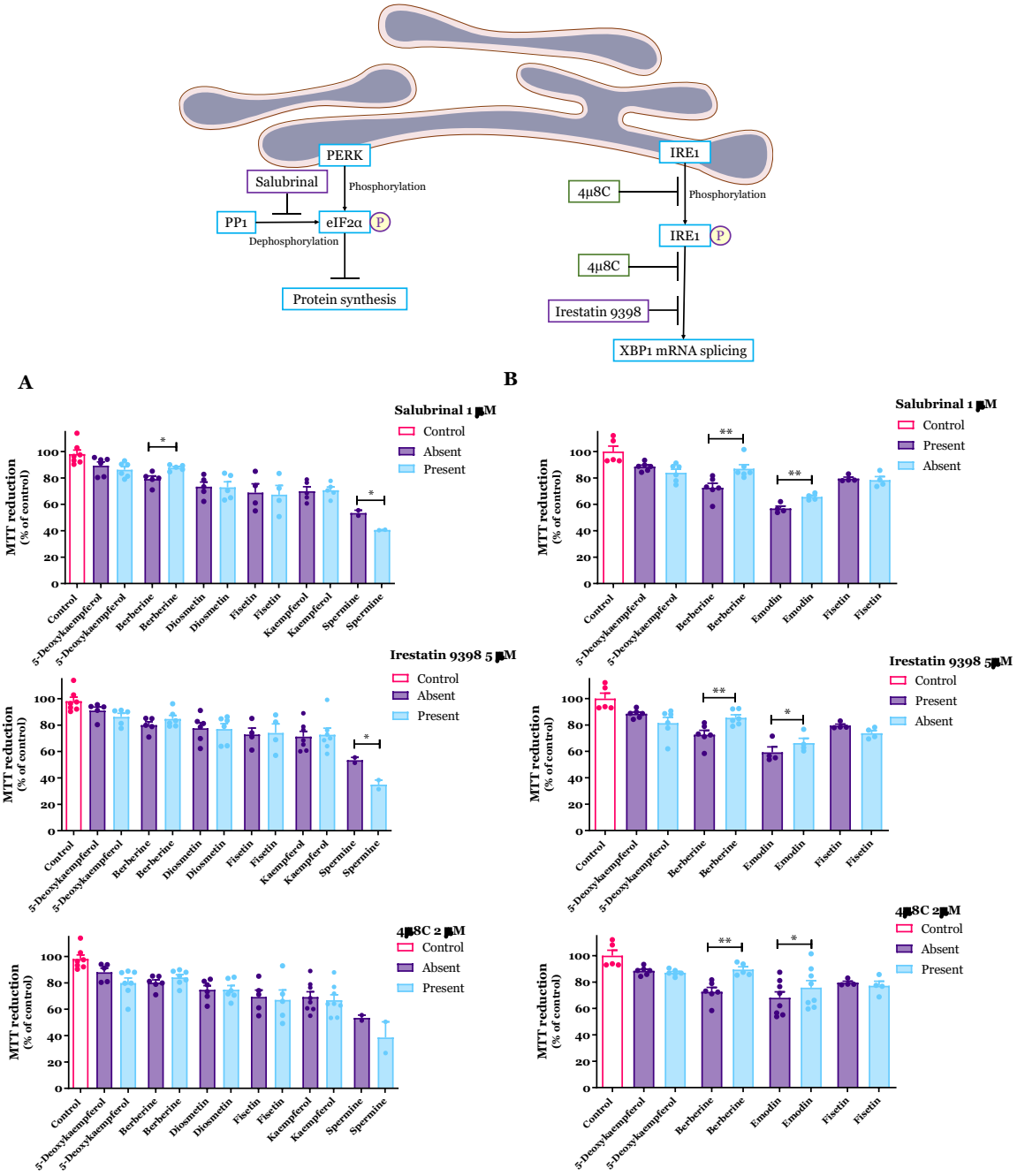

Figure 21. Effect of UPR inhibitors salubrinal, irestatin 9398 and 4μ8C on the impact on cell viability provoked on AGS (**A**) and A549 (**B**) cells by selected natural products. Results express the mean ± SEM of, at least, three independent experiments, all performed in triplicate. *$p < 0.05$, **$p < 0.01$.

3.2.3.5. Cytotoxic effect of ER stressors is retained in 3D models

A 3D cell culture system was implemented to test the selected compounds (**Figure 22**). In AGS cells (**Figure 22 A**), berberine retained the cytotoxic effect. In the case of A549

cells (**Figure 22 B**), both berberine and emodin were active in this regard. Notably, berberine and emodin present a stronger effect than that of the positive control.

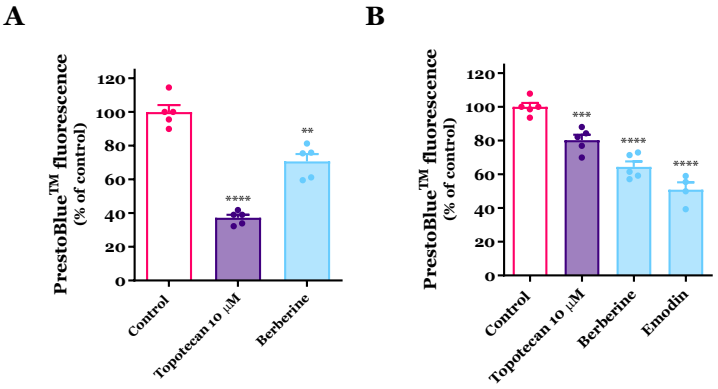

Figure 22. Effect of the molecules under study on the viability of AGS (**A**) and A549 (**B**) cells, in 3D cell culture conditions, as determined by the fluorescence of PrestoBlue™. Results are calculated considering F560/590 nm and represent the mean ± SEM of, at least, three independent assays, individually performed in triplicate. $^{**}p < 0.01$, $^{***}p < 0.001$, $^{****}p < 0.0001$.

3.2.4. Discussion

3.2.4.1. Selection of cytotoxic molecules towards cancer cells

Aiming to avoid the development of anticancer molecules lacking selectivity towards cancer cells, in this work we have used only non-toxic compounds towards human non-cancer cells. It is widely reported that, even though the search for molecules that do not exert undesirable side effects on healthy cells is fierce, the vast majority of attempts at discovery of such molecules has fallen short (389).

Considering that most novel cytotoxic cancer drugs are capable of triggering an array of events that are classified as organized cell death (OCD), we were interested in further filtering the results from cell viability. We have chosen to evaluate the impact of these molecules in the mitochondrial membrane potential ($\Delta\Psi_m$), since loss of $\Delta\Psi_m$ is involved in most processes of OCD, its dissipation being also a hallmark of ER stress, as consequence of the upregulation of BH3-only proteins (390). As so, molecules that have displayed selective cytotoxicity along with decreased $\Delta\Psi_m$ have been studies in the following assays.

3.2.4.2. The selected molecules are capable of triggering UPR activation

The onset of ER stress leads to the upregulation of the expression of a battery of genes, including genes encoding chaperones and transcription factors downstream of the activation of any of the major signaling branches of the UPR.

The *atf4* gene encodes the activating transcription factor-4 (ATF4), a transcription factor inducible by UPR activation, specifically of the PERK signaling branch. Even though PERK signaling leads to an overall decrease of the protein synthesis rate, though enhanced translation of a discrete group of proteins, including ATF4, occurs (391). In turn, ATF4 upregulates genes like *ddit3*, which encodes the C/EBP homologous protein (CHOP). This transcription factor is pivotal in the process of ER stress-induced apoptosis, and its transcription may also be induced by IRE1 or ATF6 signaling, the other two major signaling branches of the UPR (392). The *hspa5* gene corresponds to the binding immunoglobulin protein (BiP) or 78-kDa glucose-regulated protein (GRP78), while *hsp90β1* encodes the 94-kDa glucose-regulated protein (GRP94). Both genes correspond to Ca^{2+} binding proteins and the most abundantly expressed chaperones in the ER. In fact, BiP is firmly established as the major gatekeeper of UPR activation (393). Furthermore, the expression of both genes is known to be upregulated upon ATF6 activation (394). Under homeostatic conditions the mRNA encoding the transcription factor X-box-binding protein 1 (XBP1) is found in the cell in its unspliced form. IRE1 activation leads to its splicing and activation, resulting in the increased expression of genes such as the *edem1*, that generates the ER degradation-enhancing alpha-mannosidase-like protein 1 (EDEM1) (395). This well-known target of XBP1 is involved in ERAD (396). The involvement of these genes in ER stress is schematized in **Figure 23**.

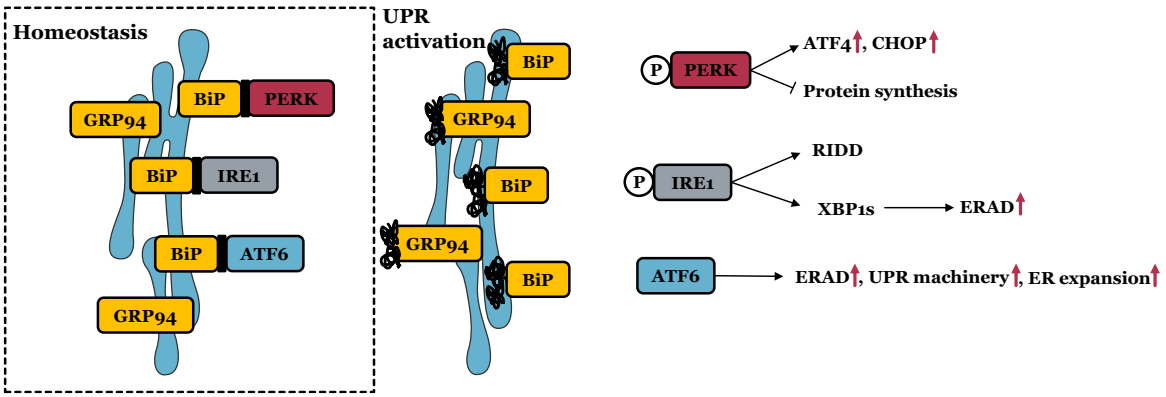

Figure 23. Involvement of the genes analyzed by RT-qPCR in ER stress signaling.

Tg was used as a positive control for the upregulation of the aforementioned target genes in each cell line, accounting for cell-specific differences in the cellular response, as displayed in **Figure 19 A**. This compound has been extensively employed as a positive control for the occurrence ER stress and the activation of the UPR ever since its characterization as a selective SERCA pump inhibitor in the early 1990's (144, 145). The SERCA pump oversees uptaking Ca^{2+} ions from the cytosol and their storage in the ER lumen, and thus its function is essential in keeping Ca^{2+} homeostasis in the cell.

The obtained results indicate that 5-deoxykaempferol, diosmetin, fisetin, berberine, emodin and kaempferol are eliciting the activation of one or more signaling branches of the UPR, reason for which they were considered for subsequent assays. Other than this, the results make clear that UPR activation by the same molecule occurs differently in each cell model, hinting at the relevance of studying each cell type individually, since UPR activation depends on the ER capacity and function of the respective cell (397). This is also ascertained by **Figure 19 A**, evidencing that the same Tg treatment induces different expression of target genes in each cell line.

3.2.4.3. ER stressors disturb Ca^{2+} homeostasis and elicit caspase activation

The ER is the largest Ca^{2+} reservoir of the cell, being in charge of keeping appropriate concentrations of this second messenger. Tight regulation of these concentrations is essential to the upkeep of cellular homeostasis. The ER possesses an intricate network of transporters, channels, and pumps to govern Ca^{2+} homeostasis. Disturbances on this, leading to Ca^{2+} efflux into the cytosol, are a hallmark of ER stress (37, 169). Furthermore, this efflux leads to the dissipation of the $\Delta\Psi_m$ (398). For all this, spatial and temporal changes in this ion are of pivotal relevance when studying ER modulators. As a positive control, we used the calcium ionophore A23187, that has been observed to trigger Ca^{2+} depletion from the ER (399, 400).

The literature shows that, even though organized cell death is inseverable from the dissipation of the $\Delta\Psi_m$, it does not always trigger caspase activation. However, caspase activation is known as a possible downstream event of ER stress (401). Caspase-4 resides in the ER and is activated by ER stress activators such as Tg and tunicamycin (227). As such, Tg was used as a positive control for caspase-4 activation. In turn, caspase-4 can cleave procaspase-9, rendering it active and inducing the subsequent caspase-3 activation (152, 402). Regarding caspase-3, we used staurosporine as positive control, since it is extensively reported to induce caspase activation (72, 403, 404).

The fact that molecules, such as emodin, seem to trigger every hallmark of UPR activation except for caspase activation may be due to the experimental conditions here employed in what concerns, for example, time period, since it is known that caspase expression and activation can change over time (405). Alternatively, there are reports of ER stress triggering organized cell death independently of caspase activation, which is an hypothesis for the mechanism of action of emodin in A549 cell, as well as other molecules that failed to induce caspase activation (406). Similarly, free Ca^{2+} concentrations may be time-dependent, reason for which changes can be overlooked. Moreover, ions may be relocated to the mitochondria instead of remaining in the cytosol (167).

3.2.4.4. Cytotoxic molecules disturb ER homeostasis at different levels

After showing that the cytotoxicity of the molecules under study was mediated by the ER, we were interested in detailing the UPR branch that might have been involved, specifically the PERK and IRE1 pathways. Briefly, PERK signaling results in increased phosphorylation of the eukaryotic initiation factor 2 alpha (eIF2α), leading global protein synthesis to a halt, while selectively enhancing the synthesis of proteins like ATF4 (66). Salubrinal is a cell-permeable selective inhibitor of eIF2α dephosphorylation that acts by inhibiting protein phosphatase 1 (PP1). The effect of salubrinal protects cells against ER stress by preventing the halt in mRNA translation caused by phosphorylated eIF2α (70). As mentioned before, phosphorylated eIF2α selectively upregulates the expression of ATF4 that, in turn, induces the expression of target genes responsible for ER stress-induced OCD mechanisms, such as *ddit3* (66, 70). Thus, it is to be expected that, if cells are undergoing OCD events related to insufficient PERK signaling, salubrinal may relieve the cytotoxicity, allowing to infer the role of this pathway in the mechanism of action of target compounds (72).

The toxicity of berberine is shown to be decreased when enhancing PERK-mediated UPR signaling (**Figure 21 A**). On the other hand, in the case of spermine, it is likely that enhancing eIF2α phosphorylation resulted in increased translation of pro-apoptotic genes, and consequently, increased toxicity.

The IRE1 enzyme possesses both kinase and endonuclease activities. It is activated by transautophosphorylation and plays a dual role on the UPR signaling, being able to promote cell death or survival, like PERK. On one hand, its endonuclease activity results in the splicing of the mRNA corresponding to the transcription factor XBP1, that promotes cell survival by inducing the expression of ER-related genes. On the other hand, it can lead to cell death through increased IRE1-dependent decay of RNA (RIDD) (80, 329). 4μ8C is

capable of inhibiting both activities of IRE1 by binding both its kinase and RNAse domains, simultaneously halting mRNA splicing and RIDD (98, 99, 329). Irestatin 9398, on the other hand, inhibits only its RNAse domain, thus preventing XBP1 mRNA splicing (407). Co-incubation of target molecules with these specific inhibitors may therefore shed a light in the involvement of IRE1 signaling on their effect.

In brief, regarding the active molecules, namely berberine towards AGS cells and berberine and emodin towards A549 cells, the selective inhibitors of PP1 and IRE1, were effective in preventing cell death. These results show that the molecules induce ER stress, leading to a collective activation of at least two of the three major branches of the UPR machinery. However, these results prove the involvement of the UPR in the effects of berberine and emodin, but they do not refute the involvement of the UPR in the cytotoxic effect of the remaining molecules, as the UPR signaling branches are often redundant and can potentially be overactivated once one of them is inhibited (207, 408, 409).

3.2.4.5. Cytotoxic effect of ER stressors is retained in 3D models

Traditional monolayer cell cultures are, to this day, a powerful and the most extensively employed tool in the discovery of drug candidates and subsequent characterization of their mechanism of action (410). However, the surrounding environment of a cell cultured in monolayers differs considerably from an *in vivo* situation. These cells attach to the polystyrene surface of cell culture plates, losing their three-dimensional conformation, lacking normal cell-to-cell interactions, and growing in the absence of extracellular matrix. The deprivation of a natural microenvironment often leads to misleading results (411, 412). 3D cell culture systems recreate the natural microenvironment of the cells more closely (410). On monolayer cell cultures, the test subjects are proliferating cells, while, in these systems, the test subjects are spheroids, that retain natural cell morphology, cell-cell and cell-matrix interactions, and include proliferating, apoptotic and necrotic cells. The proliferating cells are present in the outer areas, whereas the core of the spheroid remains under the pressure of receiving less oxygen and nutrients, and, therefore, may be in a quiescent, hypoxic or necrotic state (412, 413).

Berberine induced UPR activation in both cell models analyzed, and it was confirmed that its cytotoxic effect translates into a 3D cell model. Emodin was active specifically against A549 cells in previous assays, and it retained its cytotoxic potential in a 3D cell model based on this cell line.

3.2.5. Conclusions

The occurrence of selective cytotoxic effect among a group of natural products was described. The cytotoxicity of some of these molecules was shown to rely on the induction of ER stress. The future may provide opportunities for further studies with both compounds, expanding the tested concentrations and increasing the diversity of employed cell models to clarify whether the potential of the molecules is broader than the types of cancer here represented.

Berberine induced the expression of UPR target genes, as well as disturbing Ca^{2+} homeostasis and promoting ER-resident caspase-4 activation. UPR activation was further confirmed upon experiments with selective pharmacological inhibitors of key UPR mediators. Emodin resulted in increased expression of the same genes as berberine in A549 cells, namely *atf4*, *ddit3* and *hspa5*, disturbed cytosolic Ca^{2+} levels, and its toxicity was mitigated by co-incubation with UPR modulators. Relevantly, both molecules were effective on decreasing the viability of a 3D cell model of the cell lines against which they were active.

Being active against the two evaluated cell models, berberine is ascribed as the most promising compound to develop a selectively cytotoxic drug that induces ER stress on cancer cells.

Supplementary Material

Supplementary Table S4. Legend of the heatmap, containing the molecules that were tested in cell viability assays.

	A	B	C	D	E
1	Control	Berberine	Cynarin	Fisetin	Homoorientin
2	(-)-Norepinephrine	Betanin	Daidzein	Flavanone	Homovannilic acid
3	(+/-)-Dihydrokaempferol	Boldine	Delphinidin	Galanthamine	Isorhamnetin-3-*O*-glucoside
4	3,4-Dihydrobenzoic acid	Caffeine	Diosmetin	Gallic acid	Isorhamnetin-3-*O*-rutinoside
5	3,4-Dimethoxycinnamic acid	Catechol	Ellagic acid	Genistein	Isorhoifolin
6	3-Hydroxybenzoic acid	Chlorogenic acid	Emodin	Gentisic acid	Juglone
7	4-Hydroxybenzoic acid	Cholesta-3,5-diene	Eriocitrin	Guaiaverin	Kaempferol
8	5,7,8-Trihydroxyflavone	Cinnamic acid	Eriodictyol	Herniarin	Kaempferol-3-*O*-rutinoside
9	5-Deoxykaempferol	Coumarin	Eriodictyol-7-O-glucoside	Hesperetin	Kaempferol-7-*O*-neohesperidoside
10	Apigetrin	Cyanidin	Ferulic acid	Homoeriodictyol	Liquiritigenin
	F	**G**	**H**	**I**	**J**
1	Luteolin-3-7-*di*-glucoside	Naringenin-7-glucoside	Pinocembrin	Saponarin	Tiliroside
2	Luteolin-4'-*O*-glucoside	Naringin	Pyrogallol	Scopolamine	Trigonelline
3	Luteolin-7-*O*-glucoside	Narirutin	Quercetin-3-*O*-(-6-acetylglucoside)	Sennoside B	Vanillin
4	Malvidin	Oleuropein	Quercetin-3-*O*-glucuronide	Silibinin	Verbascoside
5	Maritimein	Orientin	Quercetin-3-ß-D-glucoside	Spermine	Vicenin-2
6	Myricetin	*p*-Coumaric acid	Quercitrin	Sulfuretin	Vitexin
7	Myricitrin	Pelargonidin	Rhoifolin	Swertiamarin	Vitexin-2-*O*-rhamnoside
8	Myristic acid	Pelargonin	Robinin	Taxifolin	Xanthone
9	Myrtillin	Phloridzin	Rosmarinic acid	Theobromine	
10	Naringenin	Phloroglucinol	Rutin	Theophylline	

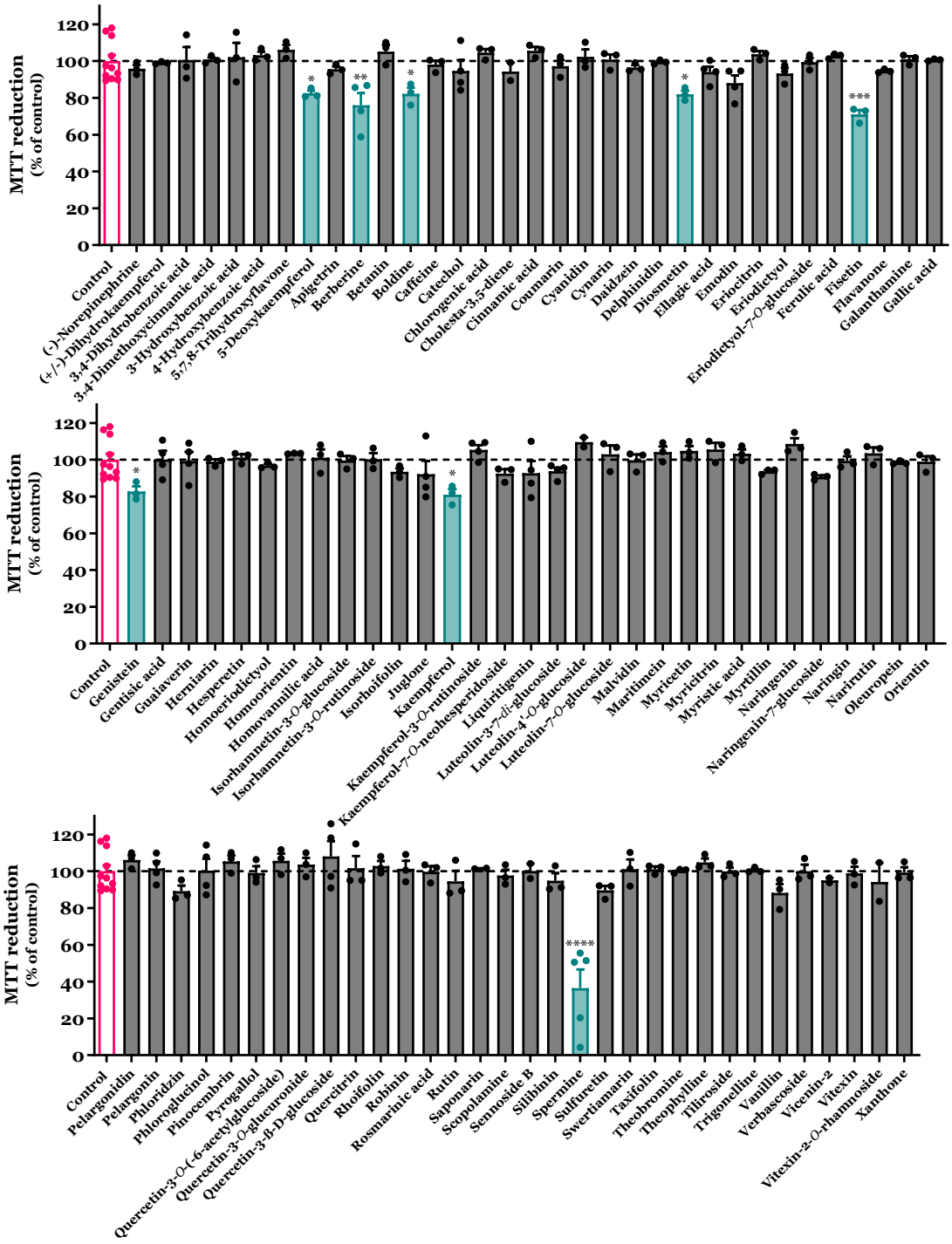

Supplementary Figure S5. Effect of a library of natural products upon AGS cell viability, as determined by MTT reduction assays. All compounds were tested at 50 μM. Results correspond to the mean ± standard error of the mean and represent, at least, three independent experiments, each performed in triplicate. *$p < 0.05$, **$p < 0.01$, ***$p < 0.001$, ****$p < 0.0001$.

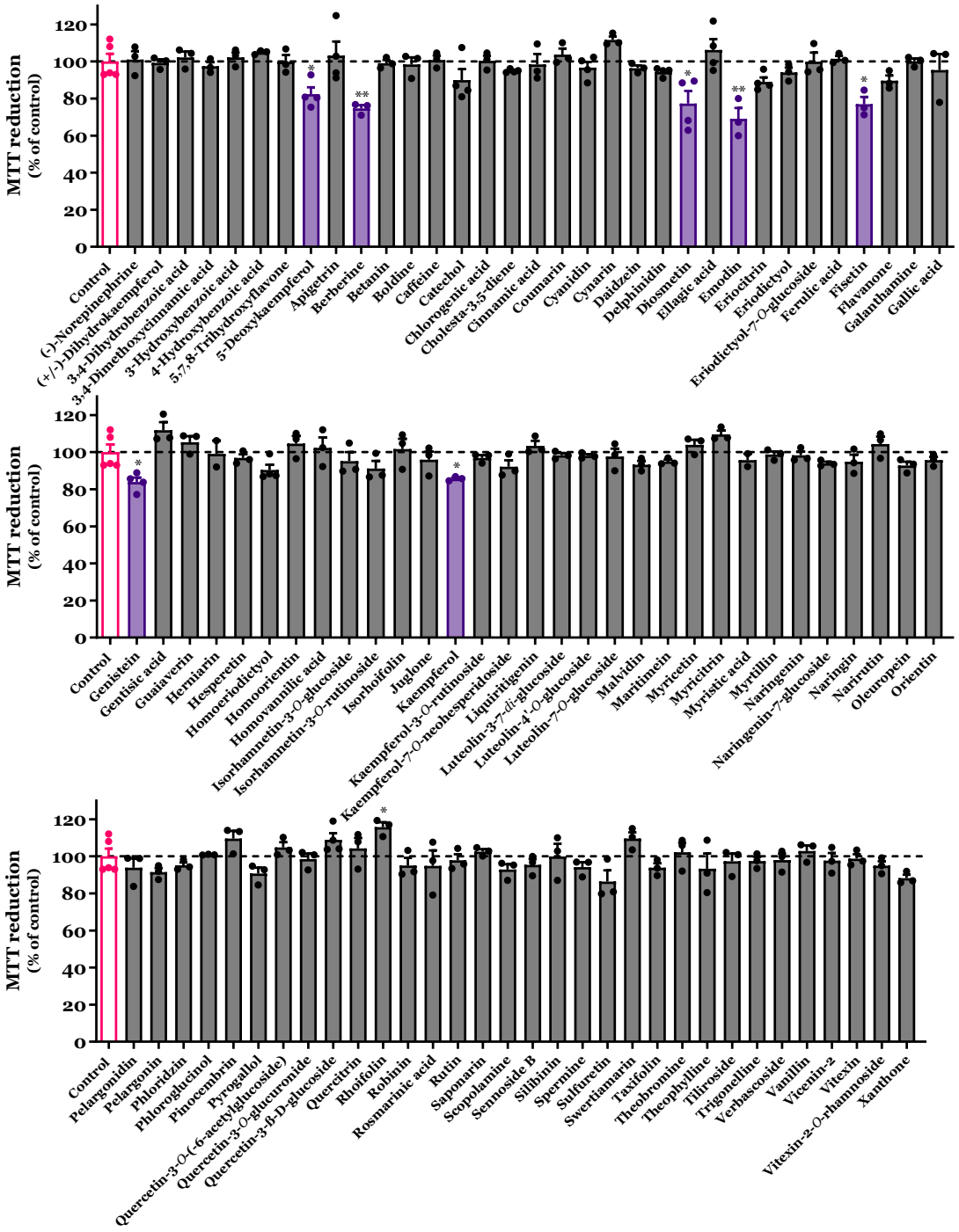

Supplementary Figure S6. Effect of a library of natural products upon A549 cell viability, as determined by MTT reduction assays. All compounds were tested at 50 μM. Results correspond to the mean ± standard error of the mean and represent, at least, three independent experiments, each performed in triplicate. *$p < 0.05$, **$p < 0.01$.

ORIGINAL ARTICLE #3

Naturally occurring small molecules with dual effect upon inflammatory signaling pathways and endoplasmic reticulum stress response

Daniela Correia da Silva, Patrícia Valentão, David M. Pereira

(Submitted)

Abstract

The endoplasmic reticulum (ER) is determinant to maintain cellular proteostasis. Upon unresolved ER stress, this organelle activates the unfolded protein response (UPR). Sustained UPR activates is known to occur in inflammatory processes, deeming the ER a potential molecular target for the treatment of inflammation. This work characterizes the inflammatory/UPR-related molecular machinery modulated by an in-house library of natural products, aiming to pave the way for the development of new selective drugs that act upon the ER to counter inflammation-related chronic diseases.

Starting from a library of 134 compounds of natural occurrence, mostly occurring in medicinal plants, nontoxic molecules were screened for their inhibitory capacity against LPS-induced nuclear factor kappa B (NF-κB) activation in a luciferase-based reporter gene assay. Since several natural products inhibited NF-κB expression in THP-1 macrophages, their effect on reactive oxygen species (ROS) production and inflammasome activation was assessed, as well as their transcriptional outcome regarding ER stress.

The bioactivities of several natural products are described herein for the first time. We report the anti-inflammatory potential of guaiazulene and describe 5-deoxykaempferol as a novel inhibitor of inflammasome activation. Furthermore, we describe the dual potential of 5-deoxykaempferol, berberine, guaiazulene, luteolin-4'-*O*-glucoside, myricetin, quercetagetin and sennoside B to modulate inflammatory signaling and ER stress. Our results show that natural products are promising molecules for the discovery and pharmaceutical development of chemical entities able to modulate the inflammatory response, as well as proteostasis and the UPR.

Keywords: IL-6, TNF-α, IL-1β, ATF4, CHOP, caspase-1

3.3.1. Introduction

The endoplasmic reticulum (ER) is responsible for most of the protein production of eukaryotic cells, and thus cells rely on tight proteostasis regulation to survive. A set of signaling pathways has evolved in this organelle, rendering it able to detect and respond to anomalies in protein folding. As a whole, these signaling pathways are known as the unfolded protein response (UPR) (329, 414).

Three major signaling branches constitute the UPR network, each possessing its respective transmembrane sensor. All of these sensors are bound to chaperones, the most expressive being the binding immunoglobulin protein (BiP or GRP78). BiP binds misfolded proteins on the ER lumen on its C-terminal domain, releasing the aforementioned transmembrane sensors from its N-terminal domain and initiating the UPR. These transmembrane proteins are: i) protein kinase RNA-like endoplasmic reticulum kinase (PERK), ii) inositol-requiring enzyme 1 (IRE1), and iii) activating transcription factor 6 (ATF6). The signaling cascades they initiate scale down global protein synthesis rates, while increasing the expression of selected genes and proteins that are involved in the expansion of the ER machinery or the UPR, ER-associated degradation (ERAD) or ultimately involved in cell death (329, 378, 379).

ER stress signaling pathway activation has been shown to occur in the pathogenesis of several types of diseases, being virtually omnipresent in chronic and age-related ones (414-416). ER stress and the UPR are implicated in the pancreatic β-cell dysfunction underlying types I and II diabetes mellitus, viral infection, in proteinopathy-associated neurodegenerative diseases, and in the death or survival of cancer cells (379, 414). Inflammatory signaling is traditionally associated to infectious diseases and mechanical trauma. However, not unlike ER stress, inflammation is deeply associated to chronic diseases, such as cancer, diabetes and neurodegenerative disorders (417). The most broadly reported mechanism connecting ER stress to inflammatory signaling pathways is related to the fact that the UPR both reduces the synthesis and promotes degradation of several short-lived proteins, including the nuclear factor kappa B (NF-κB) inhibitor (IκB). Its eventual depletion owing to its relatively short half-life, contributes to the activation of the NF-κB (128, 418). As so, ER stress and the resulting UPR directly potentiate the propagation of inflammatory processes. Furthermore, the UPR additionally results in the upregulation of several proinflammatory proteins. For instance, in intestinal cells ATF6 increases the expression of TNF-α and other inflammatory cytokines, leading to the hypothesis that inhibiting the activation of this signaling pathway may be useful to counter inflammatory bowel diseases (280).

Increased levels of the C/EBP homologous protein (CHOP), a UPR-associated transcription factor, induces the expression of IL-23, while ATF6 induces the transcription of acute phase proteins (419). We have shown before that treating M1 macrophages (pro-inflammatory phenotype) with marine-derived molecules, such as ergosta-7,22,dien-3-ol results in downregulation of CHOP and also cyclooxygenase-2 (COX-2) and inducible nitric oxide synthase (iNOS), simultaneously resulting in the upregulation of NF-κB inhibitor IκB-α (128).

Previous works have shown that many described ER stress modulators are naturally occurring small molecules (128, 219, 387). In this work, we compiled and assessed over 100 small molecules, aiming to repurpose previously characterized and commercially available natural products. We investigated if these molecules could exert inhibitory effects on both inflammatory and ER stress signaling on THP-1 macrophages, thus providing additional advantages versus single-target molecules.

3.3.2. Materials and Methods

3.3.2.1. Chemical library and reagents

Our chemical library consisted solely on commercially acquired natural products. (-)-Norepinephrine, (+/-)-dihydrokaempferol, 1,4-naphtoquinone, 18α-glycyrrhetinic acid, 3,4-dihydrobenzoic acid, 3,4-dimethoxycinnamic acid, 3-hydroxybenzoic acid, 4-hydroxybenzoic acid, 5-methoxypsoralen, ajmalicine, berberine, betanin, betulin, boldine, catechol, cholesta-3,5-diene, chrysin, cynarin, daidzein, emodin, galanthamine, genistein, guaiaverin, hesperetin, hydroquinone, lupeol, myristic acid, naringenin, naringin, *p*-coumaric acid, phloridzin, pinocembrin, plumbagin, quercetin, quercetin-3-*O*-β-D-glucoside, quercitrin, rosmarinic acid, rutin, and silibinin were purchased from Sigma-Aldrich (St. Louis, MO, USA). 5,7,8-Trihydroxyflavone, 5-deoxykaempferol, acacetin, apigenin, apigetrin, β-escin, chrysoeriol, chrysophanol, coumarin, cyanidin, delphinidin, diosmetin, diosmin, ellagic acid, eriocitrin, eriodictyol, eriodictyol-7-*O*-glucoside, eupatorin, ferulic acid, fisetin, flavanone, galangin, gallic acid, genkwanin, gentisic acid, guaiazulene, herniarin, hesperidin, homoeriodictyol, homoorientin, homovanillic acid, hyoscyamine, isorhamnetin, isorhamnetin-3-*O*-glucoside, isorhamnetin-3-*O*-rutinoside, isorhoifolin, juglone, kaempferide, kaempferol, kaempferol-3-*O*-rutinoside, kaempferol-7-*O*-glucoside, kaempferol-7-*O*-neohesperidoside, linarin, liquiritigenin, lutein, luteolin, luteolin tetramethylether, luteolin-3',7-di-*O*-glucoside, luteolin-4'-*O*-glucoside, luteolin-7-*O*-glucoside, malvidin, mangiferin, maritimein, myricetin, myricitrin, myrtillin,

naringenin-7-*O*-glucoside, narirutin, oleuropein, orientin, pelargonidin, pelargonin, phloroglucinol, pyrogallol, quercetin-3-*O*-(-6-acetylglucoside), quercetagetin, quercetin-3,3',4',7-tetramethylether, quercetin-3,4'-dimethylether, quercetin-3-methylether, quercetin-3-*O*-glucuronide, rhoifolin, robinin, saponarin, scopolamine, sennoside A, sennoside B, sulfuretin, tectochrysin, tiliroside, verbascoside, and vitexin were obtained from Extrasynthese (Genay, France). Chlorogenic acid was acquired from PhytoLab (Vestenbergsgreuth, Germany). Cinnamic acid was purchased from Biopurify (Chengdug, China). Swertiamarin was obtained from ChemFaces (Wuhan, China). 5,8-Dihydroxy-1,4-naphtoquinone and caffeine were supplied from Fluka (Buchs, Switzerland), vanillin was obtained from Vaz Pereira (Santarém, Portugal), and vicenin-2 from Honeywell (Charlotte, NC, USA).

Roswell Park Memorial Institute (RPMI) 1640 Medium, fetal bovine serum, penicillin/streptomycin solution (penicillin 5000 units/mL and streptomycin 5000 µg/mL), trypsin-EDTA (0.25%), Qubit® RNA IQ assay kit and Qubit® RNA HS assay kit and the SuperScript™ IV VILO™ MasterMix were obtained from Invitrogen (Grand Island, NE, USA). Dimethyl sulfoxide (DMSO) was acquired from Fisher Chemical (Loughborough, UK). Isopropanol was obtained from Merck (Darmstadt, Germany). Dichlorodihydrofluorescein diacetate (DCFH-DA), 3-(4,5-dimethylthiazol-2-yl)-2,5-diphenyltetrazolium bromide (MTT), RNAzol®, chloroform, isopropanol, diethyl pyrocarbonate (DEPC), KAPA SYBR® FAST qPCR Kit Master Mix (2X) Universal, protease inhibitor cocktail, sodium dodecylsulfate (SDS), Trizma® hydrochloride, sodium deoxycholate, sodium chloride, potassium phosphate monobasic, potassium chloride, sodium phosphate dibasic, sodium bicarbonate, D-glucose and Triton X-100 were purchased from Sigma-Aldrich (St. Louis, MO, USA). Formaldehyde was from Bio-Optica (Milan, Italy). The ELISA MAX™ Deluxe Set Human IL-6, ELISA MAX™ Deluxe Set Human TNF-α, and ELISA MAX™ Deluxe Set Human IL-1β were supplied by BioLegend (San Diego, CA, USA), while the Caspase-Glo® 1 Inflammasome Assay kit was obtained from Promega Corporation (Madison, WI, USA).

3.3.2.2. Cell culture conditions

THP-1 monocytes (American Type Culture Collection, LGC Standards S.L.U., Spain) were maintained in RPMI 1640 medium (p5-p20), containing 10% FBS and 1% penicillin/streptomycin and HEPES at 25 mM. THP-1 Lucia™ NF-κB monocytes (Invivogen, San Diego, CA, USA) were maintained in the same medium containing 100 µg/ml Normocin™ and a selective antibiotic, Zeocin™, was added every other passage at

100 µg/mL, as recommended by the supplier (p2-p8). Both cell lines were kept at 37 ºC with 5% CO_2.

3.3.2.3. MTT reduction assay

THP-1 monocytes were seeded at a density of 6 x 10^4 cells/well. PMA at 50 nM was added as a differentiation agent into macrophages. After 24 h, this medium was discarded and replaced by fresh PMA-free medium for another 24 h period, after which the differentiated macrophages were incubated with the compounds of interest. 24 h later, the wells are aspirated, and the medium replaced by MTT at 0.5 mg/mL and incubated for 2 h. At the end of this period, the solution was discarded and the formazan crystals in the well were dissolved in 200 µL of a 3:1 DMSO:isopropanol solution. The absorbance was read at 560 nm in a Thermo Scientific™ Multiskan™ GO microplate reader.

3.3.2.4. NF-κB luciferase assay

For the evaluation of the NF-κB activation status, a luciferase-based assay was used. THP-1 Lucia™ NF-κB monocytes were seeded on 96-well plates, differentiated into macrophages as described above for non-transfected THP-1 monocytes, and incubated with the selected compounds. After 2 h, LPS from *E. coli* was added to each well at a final concentration of 1 µg/mL, to induce polarization into M1 pro-inflammatory macrophages. 22 h later, 20 µL of supernatant were collected from each well and transferred to a white 96-well plate. Then, as indicated by the supplier, 50 µL of QUANTI-Luc™ assay solution were added to each well, the plate was shaken, and luminescence was immediately read in a Cytation™ 3 (BioTek) microplate reader.

3.3.2.5. Cytokine analysis by ELISA

THP-1 macrophages were obtained as described before on 96-well plates. After exposure to LPS on the presence of the molecules under study, supernatants were collected, and the cells were lysed in RIPA buffer containing 1% protease inhibitor cocktail for 30 min on ice. The concentration of tumor necrosis factor-α (TNF-α), interleukin-6 (IL-6) and interleukin-1β (IL-1β) in the supernatants was determined by ELISA, following the

instructions from the manufacturer of a specific kit for each of the pro-inflammatory cytokines under analysis (BioLegend Inc.; San Diego, CA, USA).

3.3.2.6. Detection of reactive oxygen species (ROS) production

THP-1 monocytes were seeded at a density of 6 x 10^4 cells/well on black-bottomed 96-well plates and the differentiation was carried out as mentioned before. The resulting macrophages were incubated with the compounds of interest and, 2 h later, LPS from *E. coli* was added to each well at a final concentration of 1 µg/mL. Cells were carefully washed with HBSS after 22 h and incubated with the fluorescent probe DCFH-DA at 25 µM for 30 min, in HBSS. Finally, fluorescence at 490/520 nm was read in a Cytation™ 3 (BioTek) microplate reader.

3.3.2.7. Caspase-Glo® 1 Inflammasome Assay

Cells were plated and incubated as above described for the NF-κB luciferase assay, yet directly on white 96-well plates. After the differentiation process, the cells were incubated with the molecules of interest and, 2 h later, LPS was added at a final concentration of 1 µg/mL and incubated for 90 min. Caspase-Glo® 1 Reagent was added to each well, in the absence and presence of the selective caspase-1 inhibitor Ac-YVAD-CHO, according to the instructions provided by the manufacturer. After a period of 60 min of incubation at room temperature, luminescence was read on a Cytation™ 3 (BioTek) microplate reader.

3.3.2.8. RNA extraction and quantification, conversion to cDNA and RT-qPCR

Cells were seeded at 4.8 x 10^5 cells/well in 12-well plates, left at 37 ºC for 24 h and then incubated with the molecules selected in previous assays. After 2 h, LPS from *E. coli* at 1 µg/mL was added. The plates were then left in the incubator for a period of 16 h. Samples were collected in 500 µL of PureZOL RNA isolation reagent. The lysate was kept at room temperature for 5 min and then RNA extraction was performed by phase separation by adding 100 µL of chloroform, shaking, incubating for 5 min and centrifuging at 12000 *g* for 15 min at 4ºC. The aqueous phase was collected and 250 µL of isopropyl alcohol were added, following 5 min of incubation and new centrifugation at 12000 *g* for 10 min at 4ºC. The supernatant was then discarded, and the pellet was washed with 75% ethanol, vortexed, centrifuged at 7500 *g* for 5 min at 4 ºC, air dried and resuspended in DEPC-treated water. The RNA in the solution was quantified resorting to the Qubit® RNA IQ assay kit. Sample

integrity was then evaluated with the Qubit® RNA IQ assay kit, and, if in appropriate conditions, 1 µg was converted to cDNA using the SuperScript™ IV VILO™ MasterMix. Primers for target genes were designed on Primer BLAST (NCBI, Bethesda, MD, USA) and synthesized by Thermo Fisher (Waltham, MA, USA). The respective nucleotide sequences are presented on **Table 7**. RT-qPCR cycles consisted in 3 min at 95 ºC, 40 cycles of 95 ºC for 3 s, gene-specific temperature for 20 s and 20 s at 72 ºC and took place in a qTOWER3 G (Analytik Jena AG, Germany), using the KAPA SYBR® FAST qPCR Kit Master Mix (2X) Universal mastermix. Data were analyzed resorting to the qPCRsoft 4.0 software. Product specificity was verified with melting curves. *Gapdh* was selected as reference genes for expression normalization.

Table 7. Genes studied by qPCR, NCBI accession numbers and respective primers, annealing temperatures and amplification product size.

Gene	Accession number	Primers	Annealing Temperature (ºC)	Amplicon length (bp)
gapdh	NM_002046.6	F: AGGTCGGAGTCAACGGATTT R: TGGAATTTGCCATGGGTGGA	60	157
hspa5	NM_005347.4	F: ACTCCTGAAGGGGAACGTCT R: TTTTCAACCACCTTGAACGGC	59.5	161
ddit3	NM_001195053.1	F: AAGTCTAAGGCACTGAGCGT R: TTGAACACTCTCTCCTCAGGT	59	93
hsp90β1	NM_003299.2	F: GCTCTATGTGCGCCGTGTAT R: ATCTGAGTCCACCACACCCTT	60.5	91
atf4	NM_001675.4	F: ACAACAGCAAGGAGGATGCC R: CCAACGTGGTCAGAAGGTCA	60	135
edem1	NM_014674.2	F: GCGGGGACCCTTCAAATCT R: CGGCTTTCTGGAACTCGGAT	60	117

3.3.2.9. Statistical analysis

Statistical analysis was performed in the GraphPad Prism 8 software. The unpaired Student's t-test was used to compare single treatments with control groups. Values of $p < 0.05$ were considered statistically significant. The Grubbs' test was resorted to in order to detect outliers.

3.3.3. Results

3.3.3.1. Selection of non-toxic molecules and their effect upon NF-κB signaling pathway

In the literature, THP-1 macrophages have been extensively used as a cell model of monocyte/macrophage signaling pathways (420). The first step of our work was to assess the impact of the molecules under study upon cell viability of THP-1 macrophages (**Figure 24 A**), as a strategy to identify and remove potentially toxic molecules early in the pipeline.

Due to the large number of molecules, all of them were tested at the single concentration of 50 μM. Among all compounds, 47 had a negative impact in cell viability, reason for which they were removed from the study. The remaining 87 molecules were kept and proceeded to subsequent studies (**Supplementary Table S5**).

Non-toxic molecules arising from the experiment described above were tested for their ability to decrease NF-κB signaling in LPS-activated macrophages, using a luciferase-based activity assay. NF-κB is a pivotal inflammatory mediator, inducing the expression of multiple downstream pro-inflammatory genes (260). From the set of compounds tested herein (**Figure 24 B**), around 40% (35 molecules) were able to reduce luciferase activity/NF-κB signaling in a significant manner.

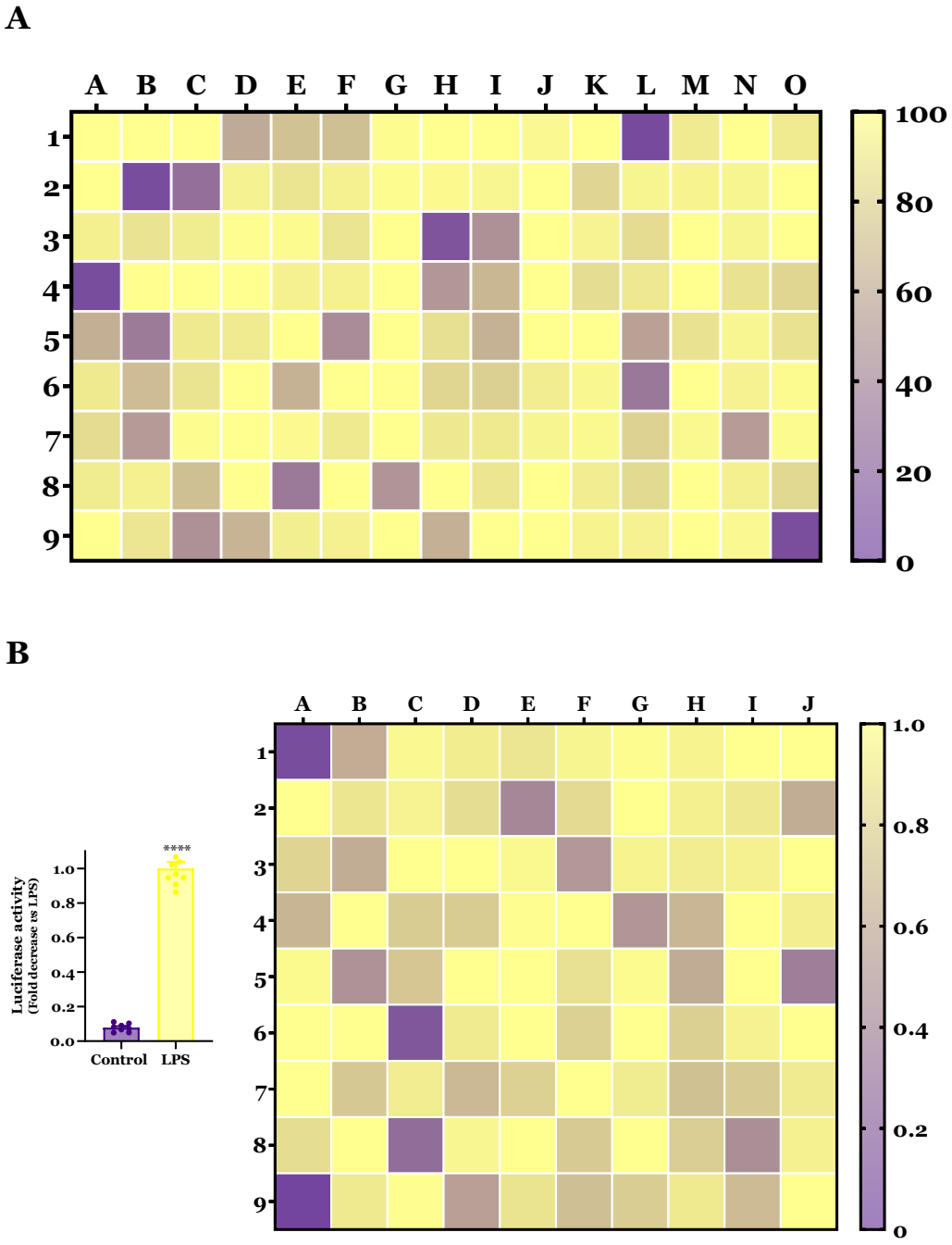

Figure 24. A: Impact of each molecule upon cell viability of THP-1 macrophages after 24 h, as determined by the MTT reduction assay. The yellow color stands for maximum cell viability, which translates to 100% of that of the control group, while purple color represents reduced cell viability. All molecules were tested at 50 μM. Results are expressed as percentage of the control (A1) and correspond to the mean of at least three independent experiments, individually performed in triplicate. The legend to this heatmap can be found in **Supplementary Table S5**. Bar charts for this data containing error bars can be found in **Supplementary Figure 7**. **B**: Effect of nontoxic natural products upon NF-κB gene expression on THP-1 Lucia™ NF-κB cells after 24 h, as determined by the QUANTI-Luc™ luciferase activity assay. The purple color represents minimum luminescent signal, closer to that of the control group (low NF-κB activation, represented as A1). The yellow color

represents maximum NF-κB activation, closer to the positive control (LPS-induced activation, represented by A2). Results express the relative change against the positive control (A2) and represent the mean of at least three independent experiments. ****$p < 0.0001$. The legend to this heatmap can be found in **Supplementary Table S6**. Bar charts for this data presenting standard errors can be found in **Supplementary Figure S8**.

Our set of molecules of interest to study subsequently in mechanistic studies was scaled down to 36 molecules (**Supplementary Table S6**) displaying the inhibition of NF-κB signaling, namely (-)-norepinephrine (A3), (+/-)-dihydrokaempferol (A4), 5,7,8-trihydroxyflavone (A8), 5-deoxykaempferol (A9), 5-methoxypsoralen (B1), berberine (B3), boldine (B5), catechol (B7), daidzein (C4), delphinidin (C5), diosmetin (C6), eriodictyol (C8), genistein (D4), guaiazulene (D7), hesperetin (D9), homoeriodictyol (E2), isorhamnetin-3-*O*-glucoside (E7), kaempferol-7-*O*-neohesperidoside (F2), liquiritigenin (F3), luteolin-4'-*O*-glucoside (F5), malvidin (F6), maritimein (F8), myricetin (F9), naringenin (G4), pelargonidin (G9), pinocembrin (H4), pyrogallol (H5), quercetagetin (H6), quercetin-3-β-D-*O*-glucoside (H7), quercetin-3-*O*-glucuronide (H8), sennoside B (I7), silibinin (I8), spermine (I9), taxifolin (J2), and tiliroside (J5). The molecules displaying the strongest activities were 5-deoxykaempferol (over 95% inhibition of LPS-induced NF-κB signaling), eriodictyol (about 70% inhibition), homoeriodictyol (around 60%), and diosmetin (over 80%).

3.3.3.2. Impact of anti-inflammatory molecules on inflammation-triggered ROS production

We evaluated whether our active compounds (i.e., those that inhibited NF-κB signaling in the previous experiment), could inhibit ROS overproduction in a context of inflammatory phenotype, namely M1 macrophages. The results narrowed down our group of target compounds from 36 to 22 (**Figure 25**) that inhibited ROS overproduction in LPS-activated macrophages, showing that 5,7,8-trihydroxyflavone (A5), 5-deoxykaempferol (B1), berberine (B3), boldine (B4), catechol (B5), delphinidin (C2), diosmetin (C3), eriodictyol (C4), guaiazulene (D1), kaempferol-7-*O*-neohesperidoside (E1), luteolin-4'-*O*-glucoside (E3), malvidin (E4), myricetin (F1), pelargonidin (F3), pyrogallol (F5), quercetagetin (G1), quercetin-3-β-D-*O*-glucoside (G2), quercetin-3-*O*-glucuronide (G3), sennoside B (G4), silibinin (G5), spermine (H1), and tiliroside (H3) mitigated the LPS-induced increased generation of ROS (**Supplementary Table S7**).

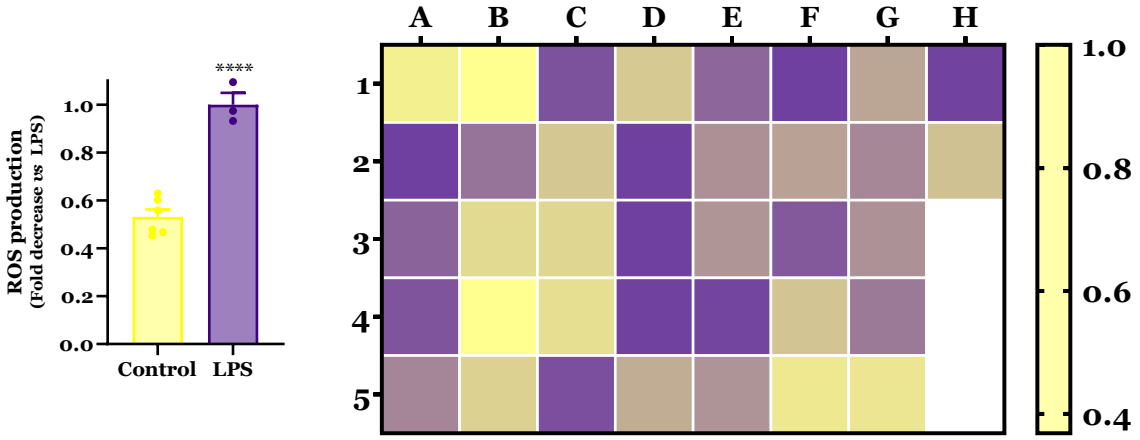

Figure 25. Effect of anti-inflammatory molecules on ROS production on THP-1 macrophages after 24 h of incubation, as determined with the fluorescent probe DCFH-DA. Results express the relative change against the positive control (A2) and represent the mean of at least three independent experiments. ****$p < 0.0001$. The legend to this heatmap can be found in **Supplementary Table S7**. Bar charts for this data presenting standard errors can be found in **Supplementary Figure S9**.

3.3.3.3. Effect of selected molecules upon proinflammatory cytokine secretion and impact upon inflammasome formation

Out of the 22 tested molecules, 15 displayed a capacity to significantly inhibit the expression of the IL-6 cytokine (**Figure 26 A**). 5-Deoxykaempferol, boldine, delphinidin, diosmetin, guaiazulene, myricetin, pelargonidin, pyrogallol, quercetagetin, quercetin-3-β-D-*O*-glucoside, quercetin-3-*O*-glucuronide, sennoside B, silibinin, spermine and tiliroside all resulted in the inhibition of IL-6 production in this incubation period, at a concentration of 50 μM. Seven compounds, mostly of phenolic nature, successfully inhibited the expression of TNF-α, namely 5-deoxykaempferol, delphinidin, diosmetin, eriodictyol, guaiazulene, pyrogallol, quercetagetin and spermine. At the same concentration of the molecules under study, dexamethasone was employed as a positive control, inhibiting the release of both pro-inflammatory cytokines. Thus, most of the selected compounds were able to inhibit LPS-mediated IL-6 upregulation, while this effect was less frequent at the level of the TNF-α production.

In our experimental model, the molecules tested were the least effective against the release of IL-1β. Only two molecules were effective against the production of all of the three major inflammatory cytokines, and those were 5-deoxykaempferol and spermine. Notably, the reference anti-inflammatory compound dexamethasone also failed to exert this effect under the stated experimental conditions, even though this molecule is employed in

therapeutics, implying that IL-1β *per se* is not a sufficiently robust parameter to assess anti-inflammatory activity. Furthermore, the same phenomenon has been described in mice (421).

On the other hand, 5,7,8-trihydroxyflavone, berberine, catechol, kaempferol-7-*O*-neohesperidoside, luteolin-4'-*O*-glucoside and malvidin did not reduce the secretion of the analyzed pro-inflammatory cytokines. We hypothesize the NF-κB inhibition is insufficient with this concentration of the molecule, and/or in the chosen experimental period, to allow the observation of the reduced cytokine expression that was expected, as hinted by a generally weaker activity of these compounds in the NF-κB activity assay presented above. Boldine, myricetin, pelargonidin, quercetin-3-β-D-*O*-glucoside, quercetin-3-*O*-glucuronide, sennoside B, silibinin, and tiliroside exclusively reduced the production of IL-6, while eriodictyol lead to a mitigated secretion of TNF-α only. Finally, delphinidin, diosmetin, guaiazulene, pyrogallol, and quercetagetin inhibited the release of both IL-6 and TNF-α.

Among the 22 molecules that build our library at this point, 8 were effective at significantly reducing the LPS-induced activation of caspase-1 under our experimental conditions. Thus, 5-deoxykaempferol, berberine, guaiazulene, luteolin-4'-*O*-glucoside, myricetin, quercetagetin, quercetin-3-*O*-glucuronide and sennoside B were shown to be inhibitors of NLRP3 inflammasome activation (**Figure 26 B**).

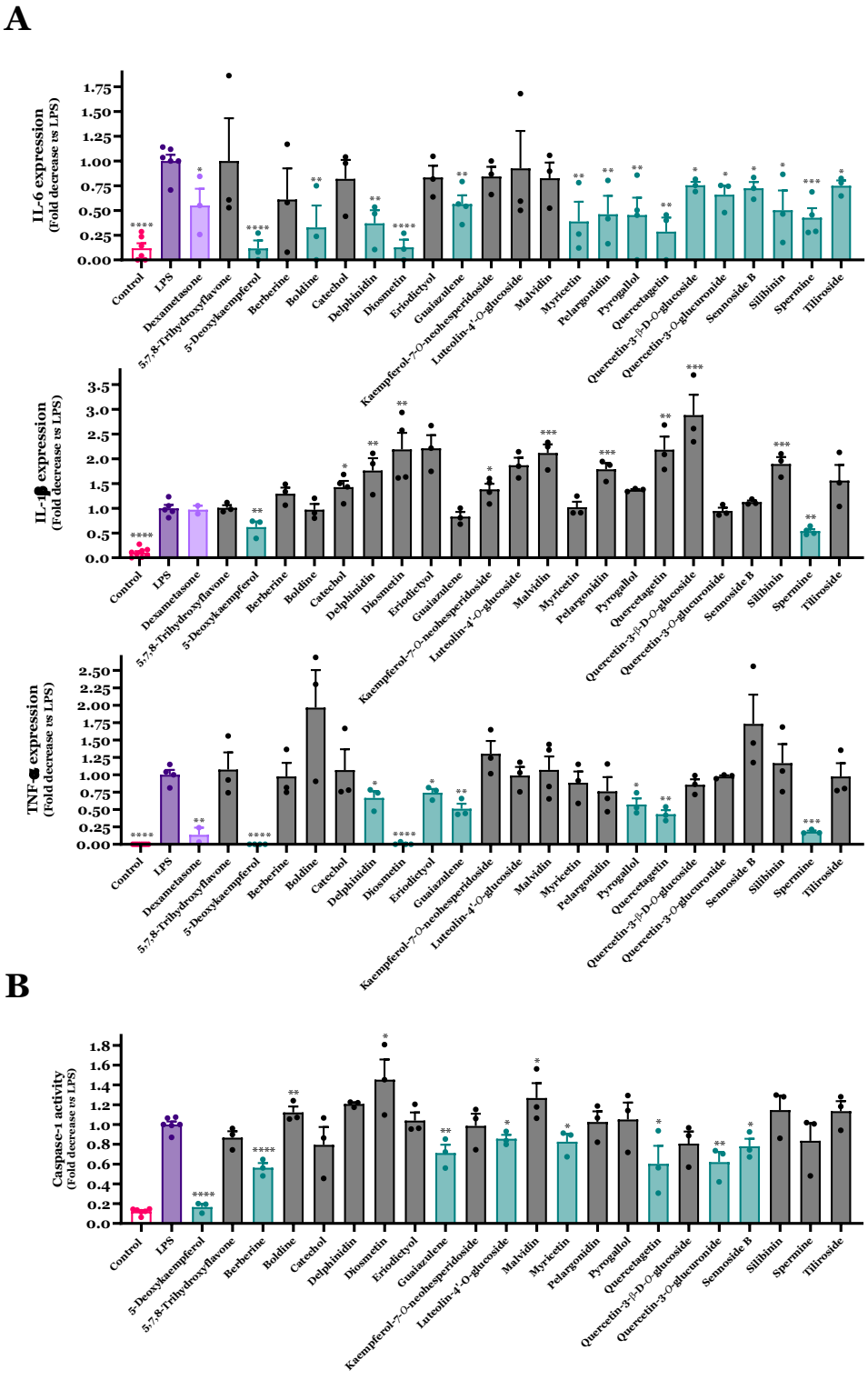

Figure 26. A: Influence of active molecules on the expression of IL-6, TNF-α and IL-1β, evaluated by ELISA. Results presented as mean ± standard deviation of the mean of at least three independent experiments, each conducted in triplicate. **B**: Effect of selected molecules on LPS-induced NLRP3 inflammasome activation, as determined by caspase-1 activation. Each column represents the mean ± standard error of the mean of at least three independent experiments, individually performed in duplicate. *$p < 0.05$, **$p < 0.01$, ***$p < 0.001$, ****$p < 0.0001$.

3.3.3.4. Effect of anti-inflammatory molecules on UPR-related gene expression

Incubation with LPS at 1 µg/mL for 16 h results in the upregulation UPR-related genes *atf4*, *ddit3* and *edem1* (**Figure 27**). However, the same conditions did not result in significant increases in the reticular chaperones *hspa5* and *hsp90β1* (data not shown). As it was mentioned before, activation of the UPR is characterized by the increased expression of multiple target genes, including *atf4*, *ddit3* and *edem1*, and thus this experimental model faithfully encompasses traits of inflammation (**Figure 26**) and UPR signaling (**Figure 27**).

The molecules displaying ability to downregulate cytokine release or NLRP3 inflammasome activation, as determined by the previous assay, were tested for their capacity to reduce the impact of LPS-induced UPR signaling on THP-1 macrophages. The results indicate that berberine is the only among these 8 molecules that can significantly inhibit *atf4* expression under the stated experimental conditions (**Figure 27**). Furthermore, this molecule also inhibited the expression of the other tested transcription factor, *ddit3*. 5-Deoxykaempferol and guaiazulene have resulted in a significant inhibition of both *ddit3* and *edem1* genes. Luteolin-4'-*O*-glucoside was the only compound revealing the ability to inhibit only the expression of *ddit3*. Finally, myricetin, quercetagetin, and sennoside B inhibited the LPS-induced increase in the expression of *edem1*.

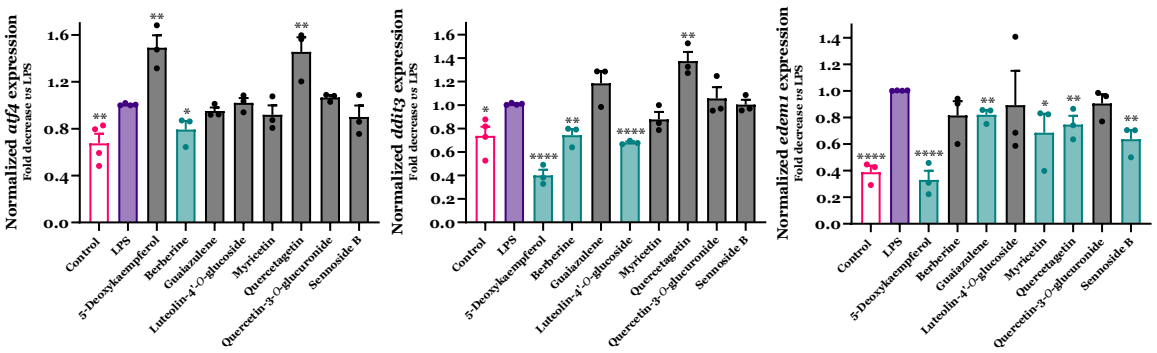

Figure 27. Effect of LPS on the expression of the UPR-related genes coding for *atf4*, *ddit3* and *edem1*, as determined by qPCR. *Gapdh* was the selected reference gene. Results represent the mean ± standard error of the mean of three independent experiments, individually performed in duplicate. *$p < 0.05$, **$p < 0.01$, ****$p < 0.0001$.

3.3.4. Discussion

Our library initially comprised 134 molecules and their detailed physico-chemical properties have been published elsewhere by us (387). The library comprised 65.9% of phenylpropanoids/polyketides, 14.4% of benzenoids and 6% of lipids and lipid-like molecules. Within phenylpropanoids/polyketides, the most prevalent subclass was flavonoids, followed by cinnamic acids and coumarins, all of which are widespread in vegetable species present in human diet.

The ability to counter or inhibit NF-κB signaling is an important indicator of anti-inflammatory activity. NF-κB is rendered inactive by negative regulation by IκBα, which is bound to the transcription factor under homeostatic conditions. Whenever a cytokine or pattern recognition receptor recognizes a ligand, the activation of a signaling cascade takes place, releasing NF-κB and allowing its activity as a transcription factor, and thus inducing inflammatory gene expression (259). For this reason, we excluded molecules that failed to inhibit NF-κB signaling from our library.

The relationship between oxidative stress and inflammation is a two-way street. One does not occur without the other, and the increase of one enhances the other (422). It is known that NF-κB signaling regulates ROS generation, and, conversely, that ROS can positively or negatively impact NF-κB signaling (423, 424). ROS overproduction leads to the phosphorylation of the IκBα, leading to its degradation by the proteasome, resulting in NF-κB activation (425). On the other hand, ROS production is inherent to protein folding, and ER stress implicates oxidative stress (426). Inhibiting ROS overproduction can therefore be of interest to ameliorate inflammatory processes, and for that reason this was the ensuing exclusion criterion. Molecules that failed to reduce LPS-induce ROS generation were excluded of further experiments. Notably, the past few years have witnessed the discovery of an additional crosstalk between oxidative stress and ER stress. The generation of ROS is inherent to protein folding (427) and, on the other hand, increased levels of ROS result in ionic calcium influx into the cytosol, triggering ER stress and further ROS generation (329, 426). Accordingly, the molecules identified herein as capable of countering ROS overproduction can be of interest when trying to mitigate ER stress.

Inflammatory signaling is largely regulated by cytokines. Interleukin-6 (IL-6), tumour necrosis factor (TNFα) and interleukin-1β (IL-1β) are key pro-inflammatory cytokines that signal *via* the type I cytokine receptors. All of these cytokines are abundantly secreted by M1 macrophages (428). For this reason, we were interested in studying the ability of the molecules under study to negatively modulate these cytokines in macrophages.

Innate immune cells contain the intracellular sensor NOD-, LRR- and pyrin domain-containing protein 3 (NLRP3), that detects danger signals (pathogens, environmental or

endogenous), acting as a sensor of cellular stress, leading to the assembly and activation of the NLRP3 inflammasome and subsequent processing of procaspase-1 into catalytically active caspase-1, which, in turn, results in the activation and release of cytokines IL-1β and IL-18, and in the occurrence of pyroptosis (293). There are reports linking the activation of all three major signaling branches of the UPR to inflammasome activation, mainly IRE1 and PERK. Briefly, UPR signaling promotes NF-κB signaling, increasing the expression of IL-1β and NLRP3. Additionally, UPR activation promotes ROS production and NLRP3 association to the mitochondria, leading to leakage of mitochondrial contents that, in turn, activate NLRP3 (295). A disturbance in Ca^{2+} levels is also reported to be linked to NLRP3 activation, being that it can occur both upstream or downstream of this event (293).

Inflammatory and ER stress signaling share the trait of being activated in order to protect cellular function. There are multiple signaling of crosstalk between these two molecular machineries. In fact, NF-κB activation may result from the activation of any of the three major signaling branches of the UPR, whereas inflammatory signaling results in UPR activation. Furthermore, both signaling pathways can be deleterious when intensely and/or chronically induced (158).

The gene *atf4* encodes the activating transcription factor 4 (ATF4), a transcription factor that is translated in response to the activation of the PERK branch of the UPR. Activation of PERK causes increased phosphorylation levels of the eIF2α, leading to an overall halt in protein synthesis. However, eIF2α phosphorylation promotes the synthesis of a few target proteins, such as the ATF4. In turn, ATF4 induces the expression of specific genes, including *ddit3*, the gene that codes for the CHOP transcription factor (429). The latter is involved in ER stress-associated regulated cell death mechanisms when the activation of the UPR fails to restore proteostasis (392).

The ER degradation-enhancing alpha-mannosidase-like protein 1 (EDEM1), the enzyme that corresponds to the *edem1* gene, participates in endoplasmic reticulum-associated degradation (ERAD) of misfolded glycoproteins, by removing them of the calnexin cycle. Enhancement of ERAD is known to be a downstream event of the activation of the ATF6 signaling branch of the UPR (35, 430).

As all of these molecules inhibited inflammatory signaling in previous assays, we can confirm the dual activity of 5-deoxykaempferol, berberine, guaiazulene, luteolin-4'-*O*-glucoside, myricetin, quercetagetin and sennoside B. Even though at different levels, these natural products can significantly mitigate inflammatory and UPR signaling. The genes *atf4* and *ddit3* are more associated to the deleterious effects of ER stress signaling, since, as mentioned before, ATF4 induces the expression of CHOP, that, in turn, is involved in ER stress-induced regulated cell death. For this reason, we hypothesize that berberine is the most promising molecule within our group, given that it was the only that significantly

inhibited the expression of both genes in our experimental model. However, *ATF4* can also be associated to the adaptive effects of UPR activation, unlike *ddit3*. Thus, the effects of luteolin-4'-*O*-glucoside should also be considered, even though it only inhibited the expression of *ddit3* in a significant manner. Increased EDEM1 expression enhances ERAD, promoting proteasome-mediated degradation of toxic misfolded proteins. Loss of mannoses in these peptides indicates that they have remained in the calnexin cycle for too long to endure several failed attempts at correct folding, and they should be forwarded for degradation (431). Diminished *edem1* expression might indicate a reduced presence of toxic misfolded proteins in the lumen of the ER, and, for this reason, 5-deoxykaempferol, guaiazulene, myricetin, quercetagetin, and sennoside B have shown to preserve homeostatic conditions in the organelle.

To our knowledge, this is the first report of 5-deoxykaempferol as an inhibitor of inflammasome or caspase-1 activation, even though its anti-inflammatory potential has already been described in a murine macrophage model. In RAW264.7 cells, this molecule inhibited NO production, TNF-α and IL-1β mRNA expression, as well as iNOS and COX-2 protein expression, at the same concentration that was employed in this study (50 μM) and lower concentrations (432). In concentrations up to 75 μM, albeit with a different incubation period, berberine inhibited inflammasome activation and IL-1β secretion in THP-1 macrophages (433). A similar effect has been observed in BV2 (434) and AML12 cells (435). Notably, NLRP3 inhibition and IL-1β downregulation by this compound have also been observed *in vivo* (436). In Caco-2 cells (intestinal epithelial cells), berberine seems to prevent tunicamycin- or proinflammatory cytokine-induced ER stress. Under these conditions, berberine reduced GRP78 expression and XBP-1 splicing, and downregulated JNK, caspase-12 and caspase-3, successfully preventing apoptosis. For these reasons, the authors hypothesise that berberine can be useful against the pathogenesis of the inflammatory bowel disease (339). Guaiazulene bioactivity in the scope of inflammation, to the extent of our knowledge, has not been characterized so far. Luteolin-4'-*O*-glucoside has reduced the levels of IL-1*β* and TNF-*α* and displayed the ability to reduced paw edema in mice (437). However, there are no other reports concerning the anti-inflammatory potential of this molecule, namely at the level of inflammasome activation. Myricetin was reported to inhibit NF-κB signaling in RAW264.7 macrophages (25-100 μM), as well as in mice. Interestingly, this effect results from suppressed degradation of the IκBα (438). Besides inhibiting NF-κB signaling, myricetin is described as a NLRP3 inflammasome activation inhibitor (25-75 μM), by inducing NLRP3 ubiquitination and reducing ASC ubiquitination, therefore blocking inflammasome assembly, in primary peritoneal macrophages (PMs) (294). To the extent of our knowledge, there are no other reports of quercetagetin as an inhibitor of inflammasome activation. However, its anti-inflammatory potential has been

evaluated before, albeit in cell models different than those we employed here. In H9c2 rat myoblasts, quercetagetin (10 μM) decreased COX-2 expression and decreased IκBα degradation (439). Furthermore, in HaCaT human keratinocytes, quercetagetin (12.5-50 μM) inhibited the production of the thymus and activation-regulated chemokine (TARC) and macrophage-derived chemokine (MDC) (440). Quercetin-3-*O*-glucuronide inhibited ROS overproduction in human umbilical vein endothelial cells (HUVECs), as well as IL-6 and TNF-α protein levels, at concentrations from 1 μM (441). In LPS-insulted RAW 264.7 macrophages, at concentrations from 50 μM, quercetin-3-*O*-glucuronide inhibited NO and PGE_2 production, as well as iNOS and COX-2 expressions at the protein level, while inhibiting JNK activation from 10 μM (442). Furthermore, this natural product has displayed its anti-inflammatory activity *in vivo*, inhibiting ear edema in mice (443). Recently, sennoside B was identified as a strong inhibitor of the activity of TNF-α on a competitive binding assay based on analytical size exclusion chromatography, even though the effect at the gene level expression is not reported (444).

The literature conveys no reports of the activity on 5-deoxykaempferol against ER stress besides our previous study, in which we describe this molecule's ability to counter thapsigargin-induced ER stress (387). As so, we hypothesize that the protective effect of this molecule against ER stress may be involved in the anti-inflammatory effect here reported. In HepG2 cells, berberine has demonstrated to inhibit ER stress, as evidenced by the decreased levels of phosphorylation PERK and eIF2α in tunicamycin-insulted cells after exposure to berberine up to 20 μM (327). In a mice model, this molecule was effective in reducing ER stress, as observed by the decrease in the expression of BiP, p-PERK and p-eIF2α, that resulted in the inhibition of tau hyperphosphorylation (445). Berberine was protective against palmitate-induced ER stress in a mouse podocyte cell line (MPC5), reducing the expression of multiple ER stress biomarkers (446). Myricetin triggered the efflux of Ca^{2+} into the cytosol, while increasing the expression of UPR markers in concentrations from 20 μM, in JAR and JEG-3 cells (both from placental choriocarcinomas) (447). This concurs with results observed on an ovarian cancer cell line (SKOV3), in which an increase of BiP expression was observed upon treatment with myricetin (40 μg/mL) (448). However, this molecule has also displayed protective potential against ER stress before (20 μM), protecting rat primary pancreatic β-cells from high glucose-induced apoptosis and preventing the abnormal expression of UPR biomarkers, such as BiP, p-PERK, p-eIF2α, ATF4 and CHOP (449). Regarding luteolin-4'-*O*-glucoside, quercetagetin and sennoside B, we find no accounts in the literature of their potential to modulate ER stress.

In the present day, a significant part of the most prevalent chronic diseases are of inflammatory nature (428). On the other hand, ER stress and activation of the UPR is deeply

associated with chronic diseases (450-452). Conversely, it is increasingly documented that inflammatory pathways are highly linked to UPR activation (**Figure 28**) (414). It has been suggested the foundation of chronic inflammatory disease may be the NLRP3 inflammasome activation triggered by ER stress. The two phenomena are deeply connected, since ER stress may trigger NLRP3 inflammasome activation *via* oxidative stress, Ca2+ signaling and NF-κB activation (453).

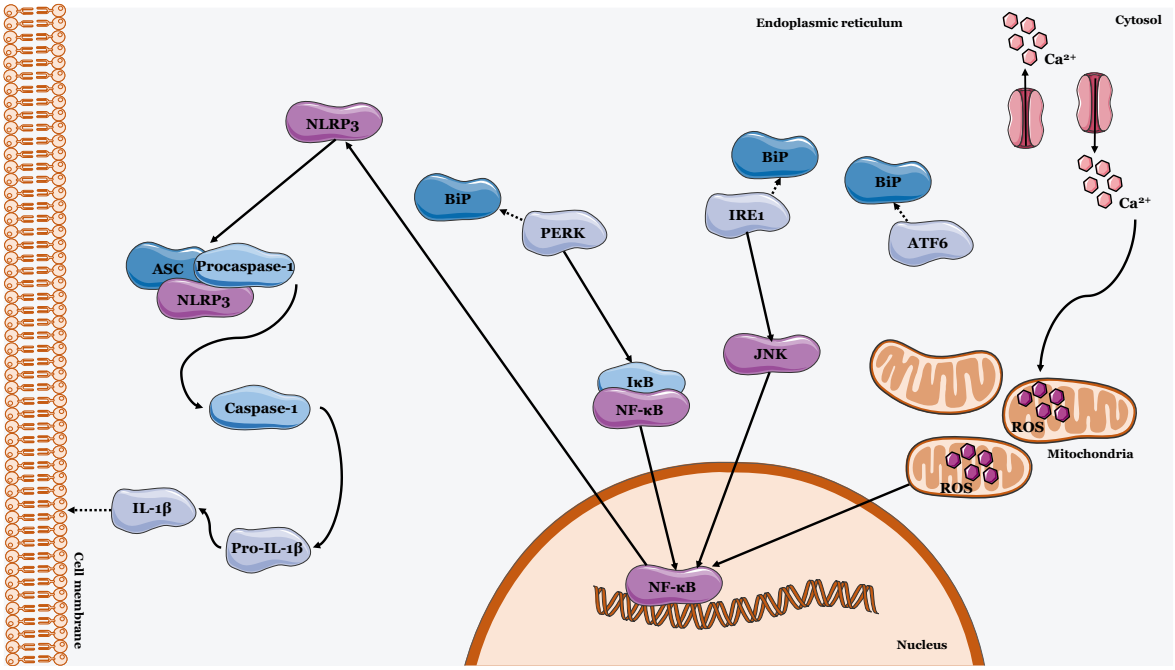

Figure 28. Crosstalk between ER stress and inflammatory signaling.

For this reason, there is a need for molecules that can display a dual effect against both inflammatory and UPR signaling. This work led to the identification of promising drug candidates against these diseases among a library of small molecules of natural origin, being that 5-deoxykaempferol stood out as the most auspicious molecule.

Supplementary Materials

Supplementary Table S5. List of compounds tested in the MTT reduction assays. Highlighted names represent the molecules that were excluded from subsequent experiments due to a significant decrease in cell viability.

	A	B	C	D	E
1	Control	5,7,8-Trihydroxyflavone	Betanin	Chrysophanol	Ellagic acid
2	(-)-Norepinephrine	5,8-Dihydroxy-1,4-naphtoquinone	Betulin	Cinnamic acid	Emodin
3	(+/-)-Dihydrokaempferol	5-Deoxykaempferol	Boldine	Coumarin	Eriocitrin
4	1,4-Naphtoquinone	5-Methoxypsoralen	Caffeine	Cyanidin	Eriodictyol
5	18α-Glycyrrhetinic acid	Acacetin	Catechol	Cynarin	Eriodictyol-7-*O*-glucoside
6	3,4-Dihydrobenzoic acid	Ajmalicine	Chlorogenic acid	Daidzein	Eupatorin
7	3,4-Dimethoxycinnamic acid	Apigenin	Cholesta-3,5-diene	Delphinidin	Ferulic acid
8	3-Hydroxybenzoic acid	Apigetrin	Chrysin	Diosmetin	Fisetin
9	4-Hydroxybenzoic acid	Berberine	Chrysoeriol	Diosmin	Flavanone

	F	G	H	I	J
1	Galangin	Hesperetin	Isorhamnetin-3-*O*-rutinoside	Liquiritigenin	Mangiferin trihydrate
2	Galanthamine	Hesperidin	Isorhoifolin	Lupeol	Maritimein
3	Gallic acid	Homoeriodictyol	Juglone	Lutein	Myricetin
4	Genistein	Homoorientin	Kaempferide	Luteolin	Myricitrin
5	Genkwanin	Homovannilic acid	Kaempferol	Luteolin tetramethylether	Myristic acid
6	Gentisic acid	Hydroquinone	Kaempferol-3-*O*-rutinoside	Luteolin-3',7-di-*O*-glucoside	Myrtillin
7	Guaiaverin	Hyoscyamine	Kaempferol-7-*O*-glucoside	Luteolin-4'-*O*-glucoside	Naringenin
8	Guaiazulene	Isorhamnetin	Kaempferol-7-*O*-neohesperidoside	Luteolin-7-*O*-glucoside	Naringenin-7-glucoside
9	Herniarin	Isorhamnetin-3-*O*-glucoside	Linarin	Malvidin chloride	Naringin

	K	L	M	N	O
1	Narirutin	Plumbagin	Quercetin-3-ß-D-*O*-glucoside	Sennoside B	Tiliroside
2	Oleuropein	Pyrogallol	Quercitrin	Silibinin	Trigonelline
3	Orientin	Quercetin-3-*O*-(-6-acetylglucoside)	Rhoifolin	Spermine	Vanillin
4	*p*-Coumaric acid	Quercetagetin	Robinin	Sulfuretin	Verbascoside
5	Pelargonidin	Quercetin	Rosmarinic acid	Swertiamarin	Vicenin-2
6	Pelargonin	Quercetin-3,3',4',7-tetramethylether	Rutin	Taxifolin	Vitexin
7	Phloridzin	Quercetin-3,4'-dimethylether	Saponarin	Tectochrysin	Vitexin-2-*O*-rhamnoside
8	Phloroglucinol	Quercetin-3-methylether	Scopolamine	Theobromine	Xanthone
9	Pinocembrin	Quercetin-3-*O*-glucuronide	Sennoside A	Theophylline	ß-escin

Supplementary Table S6. List of compounds tested in NF-κB reporter assays. Highlighted names represent molecules that significantly decreased NF-κB expression, as determined by this assay, and were selected for subsequent studies.

	A	B	C	D	E
1	Control	5-Methoxypsoralen	Coumarin	Ferulic acid	Hesperidin
2	LPS	Apigetrin	Cyanidin	Flavanone	Homoeriodictyol
3	(-)-Norepinephrine	Berberine	Cynarin	Galanthamine	Homoorientin
4	(+/-)-Dihydrokaempferol	Betanin	Daidzein	Genistein	Homovannilic acid
5	3,4-Dihydrobenzoic acid	Boldine	Delphinidin	Gentisic acid	Hydroquinone
6	3-Hydroxybenzoic acid	Caffeine	Diosmetin	Guaiaverin	Hyoscyamine
7	4-Hydroxybenzoic acid	Catechol	Eriocitrin	Guaiazulene	Isorhamnetin-3-*O*-glucoside
8	5,7,8-Trihydroxyflavone	Cholesta-3,5-diene	Eriodictyol	Herniarin	Isorhamnetin-3-*O*-rutinoside
9	5-Deoxykaempferol	Cinnamic acid	Eriodictyol-7-*O*-glucoside	Hesperetin	Isorhoifolin
	F	**G**	**H**	**I**	**J**
1	Kaempferol-7-*O*-glucoside	Myricitrin	Pelargonin	Rhoifolin	Swertiamarin
2	Kaempferol-7-*O*-neohesperidoside	Myristic acid	Phloridzin	Robinin	Taxifolin
3	Liquiritigenin	Myrtillin	Phloroglucinol	Rutin	Theobromine
4	Lupeol	Naringenin	Pinocembrin	Saponarin	Theophylline
5	Luteolin-4'-*O*-glucoside	Naringenin-7-glucoside	Pyrogallol	Scopolamine	Tiliroside
6	Malvidin	Naringin	Quercetagetin	Sennoside A	Trigonelline
7	Mangiferin	Narirutin	Quercetin-3-β-D-*O*-glucoside	Sennoside B	Vanillin
8	Maritimein	Orientin	Quercetin-3-*O*-glucuronide	Silibinin	Vitexin
9	Myricetin	Pelargonidin	Quercitrin	Spermine	Vitexin-2-*O*-rhamnoside

Supplementary Table S7. List of compounds tested in ROS production assay. Highlighted names represent molecules that significantly decreased ROS levels, as determined by this assay, and were selected for subsequent studies.

	A	B	C	D	E
1	Control	5-Deoxykaempferol	Daidzein	Guaiazulene	Kaempferol-7-*O*-neohesperidoside
2	LPS	5-Methoxypsoralen	Delphinidin	Hesperetin	Liquiritigenin
3	(-)-Norepinephrine	Berberine	Diosmetin	Homoeriodictyol	Luteolin-4'-*O*-glucoside
4	(+/-)-Dihydrokaempferol	Boldine	Eriodictyol	Hyperoside	Malvidin
5	5,7,8-Trihydroxyflavone	Catechol	Genistein	Isorhamnetin-3-*O*-glucoside	Maritimein
	F	**G**	**H**		
1	Myricetin	Quercetagetin	Spermine		
2	Naringenin	Quercetin-3-ß-D-*O*-glucoside	Taxifolin		
3	Pelargonidin	Quercetin-3-*O*-glucuronide	Tiliroside		
4	Pinocembrin	Sennoside B			
5	Pyrogallol	Silibinin			

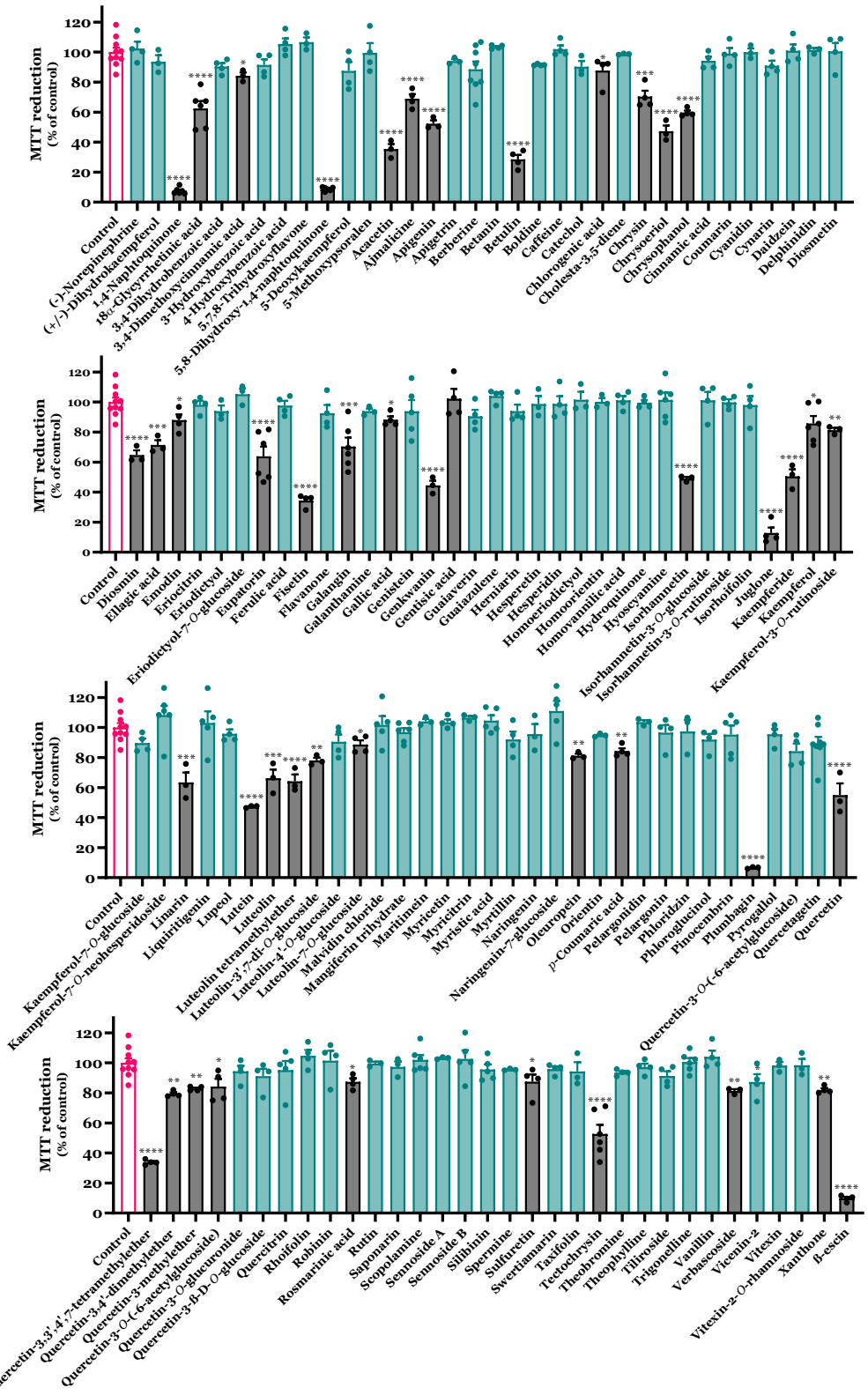

Supplementary Figure S7. Impact of the natural products upon cell viability after 24 h, as determined by the MTT reduction assay. All molecules were tested at 50 µM. Results correspond to the mean ± standard error of the mean of at least three independent experiments, each performed in triplicate. *$p < 0.05$, **$p < 0.01$, ***$p < 0.001$, ****$p < 0.0001$.

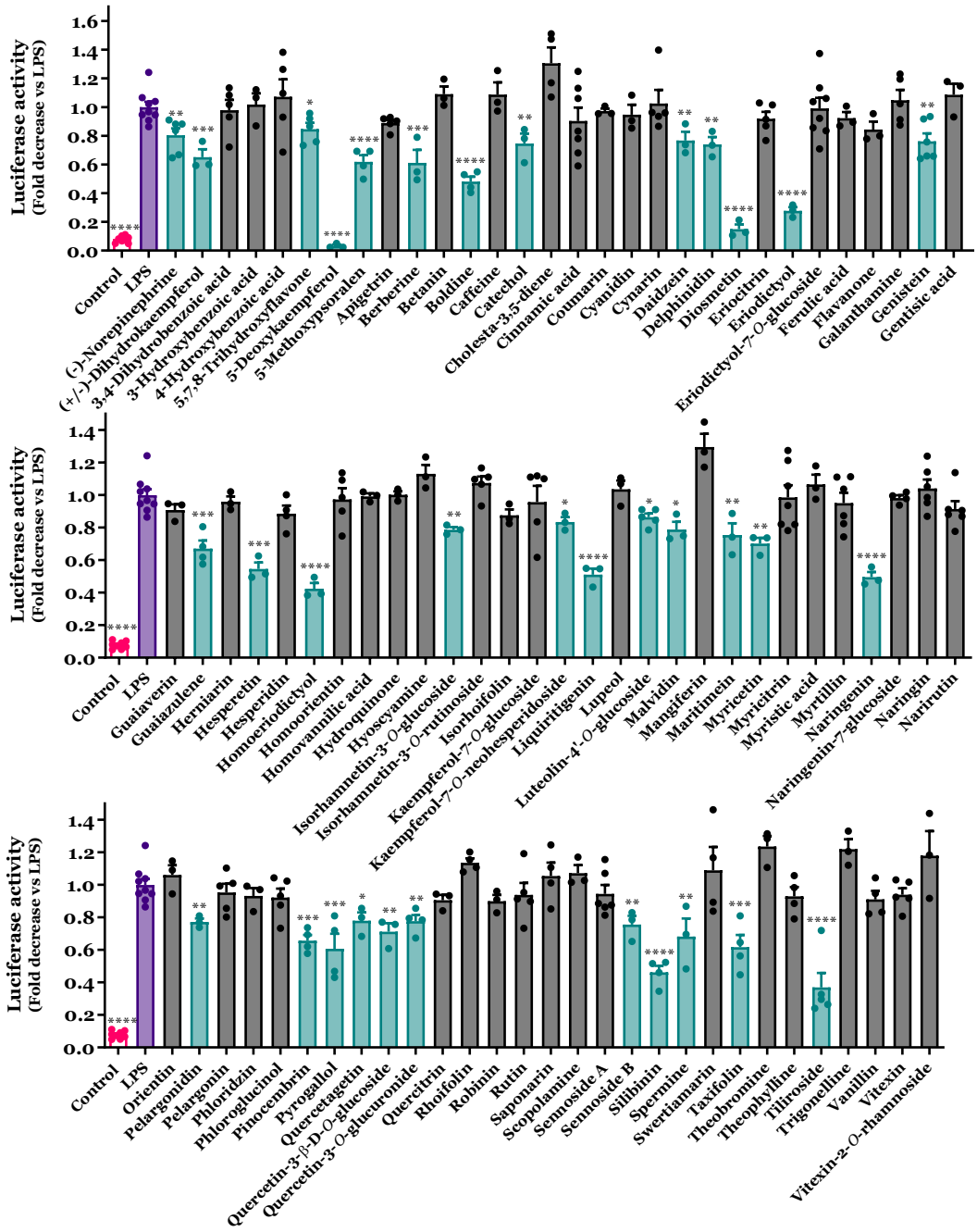

Supplementary Figure S8. Effect of nontoxic natural products upon NF-κB gene expression on THP-1 Lucia™ NF-κB after 24 h, determined by the QUANTI-Luc™ luciferase activity assay. Results express the relative change against the positive control and correspond to the mean of at least three independent experiments. *$p < 0.05$, **$p < 0.01$, ***$p < 0.001$, ****$p < 0.0001$.

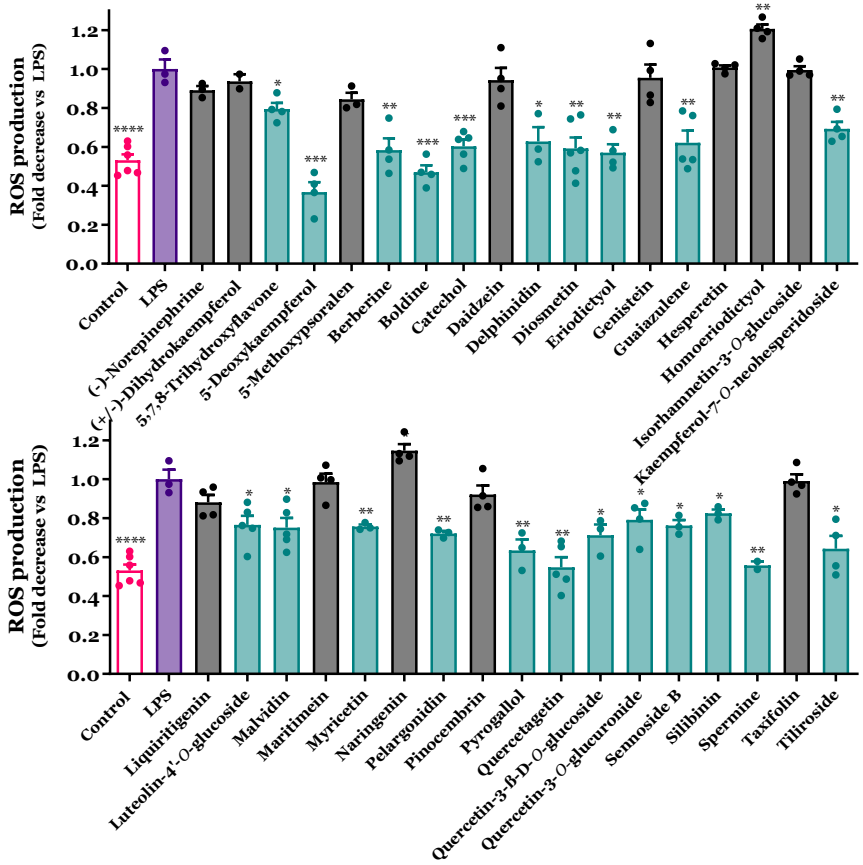

Supplementary Figure S9. Effect of anti-inflammatory molecules on ROS production on THP-1 macrophages after 24 h of incubation, as determined with the fluorescent probe DCFH-DA. Results express the relative change against the positive control and represent the mean of at least three independent experiments. *$p < 0.05$, **$p < 0.01$, ***$p < 0.001$, ****$p < 0.0001$.

3.4.1. Impact of fisetin derivatives upon cell viability and proteostasis in MRC-5 and SH-SY5Y cells

In light of the results presented in sections **3.1.** and **3.2.**, fisetin was considered a promising molecule in what concerns its potential against neurodegeneration and against cancer. Considering this, a set of derivatives of this molecule were synthesized and screened for these bioactivities.

To determine cellular viability after exposure to these molecules, MRC-5, AGS and A549 cells were seeded and incubated as it was described for MTT assays in sections **3.1.2.4.** and **3.2.2.3.**. After the incubation period, the Presto Blue™ reagent was added as according to the instructions from the supplier, and incubated for 30 min at 37 ºC, for AGS cells and 1 h for A549 cells. At this point, fluorescence was read at 560/590 nm on a Cytation™ 3 (BioTek) multifunctional microplate reader. This assay was selected considering the possibility to transition to a 3D cell model in subsequent experiments. The differences between the MTT reduction assays and the Presto Blue™ assays are summed up in **Figure 29**.

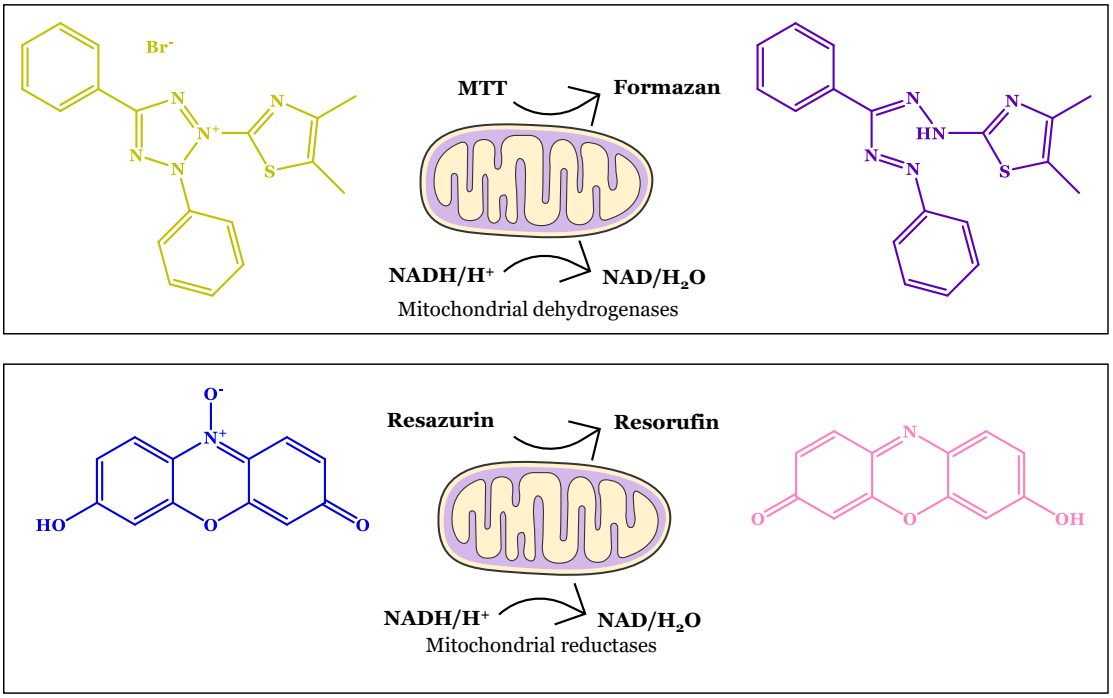

Figure 29. Reactions undergoing the MTT and resazurin reduction assays. MTT (yellow) is reduced to formazan (purple) by mitochondrial reductases of viable cells. Resazurin (blue) is reduced to resorufin (pink, fluorescent) by a similar mechanism.

When bound to amyloid fibrils and excited at 450 nm, ThT produces a fluorescent signal at 482 nm. It is hypothesized that this increased fluorescence is due to rotational immobilization of the central C-C bond connecting its benzothiazole and aniline rings. The

chemical structure of the compound in represented in **Figure 30** (454). Regarding the mechanism through which ThT binds amyloid fibrils, it is known that the can forms micelles, owing to its positive charge, and that these micelles bind the amyloid fibrils (455).

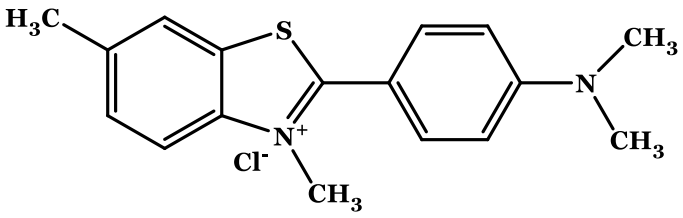

Figure 30. Chemical structure of thioflavin T.

Our results considering the potential of fisetin to inhibit protein aggregation in fibroblasts were promising, even though the molecule failed to inhibit protein aggregation in SH-SY5Y at subcytotoxic concentrations. Nonetheless, the neuroprotective potential of fisetin reported throughout the literature (456, 457). These facts prompted us to test a library of fisetin derivatives to screen for improved potential against neurodegeneration. However, the fisetin derivatives displayed poor to activity against protein aggregation in both MRC-5 and SH-SY5Y cells, as is evidenced by **Figure 31** and **Figure 32**, respectively.

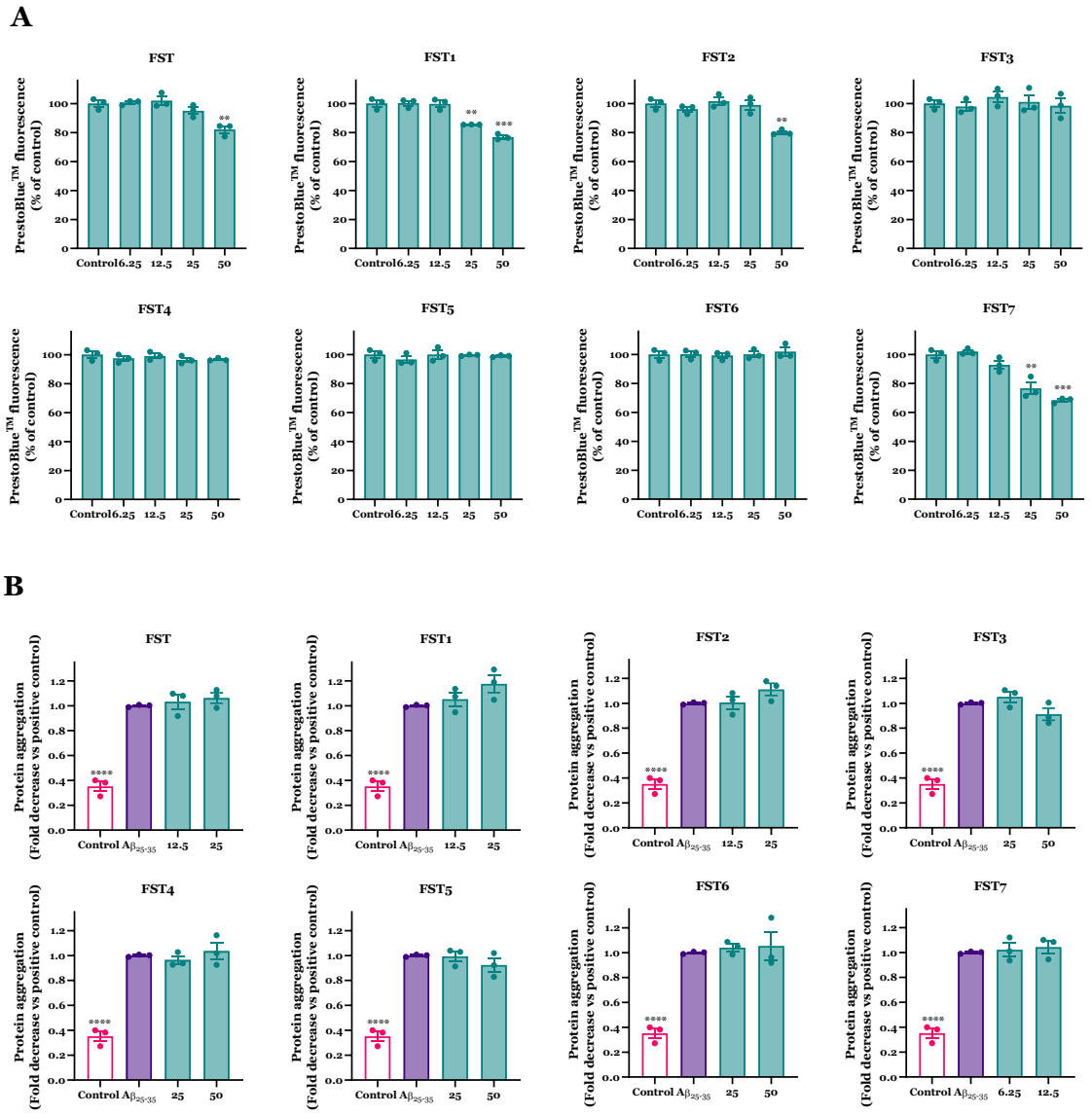

Figure 31. A: Cell viability of MRC-5 cells after 24 h of incubation with fisetin (FST) and its synthetic derivatives FST1-7, as determined by PrestoBlue™ cell viability assay. **B:** Effect the two highest nontoxic concentrations of FST and derivatives on $A\beta_{25-35}$-induced protein aggregation in MRC-5 cells, determined by the fluorescence of ThT. All experiments were individually conducted in triplicate. Results are presented as the percentage of the control and represent to the mean ± SEM of, at least, three independent experiments. $^{**}p < 0.01$, $^{***}p < 0.001$, $^{****}p < 0.0001$.

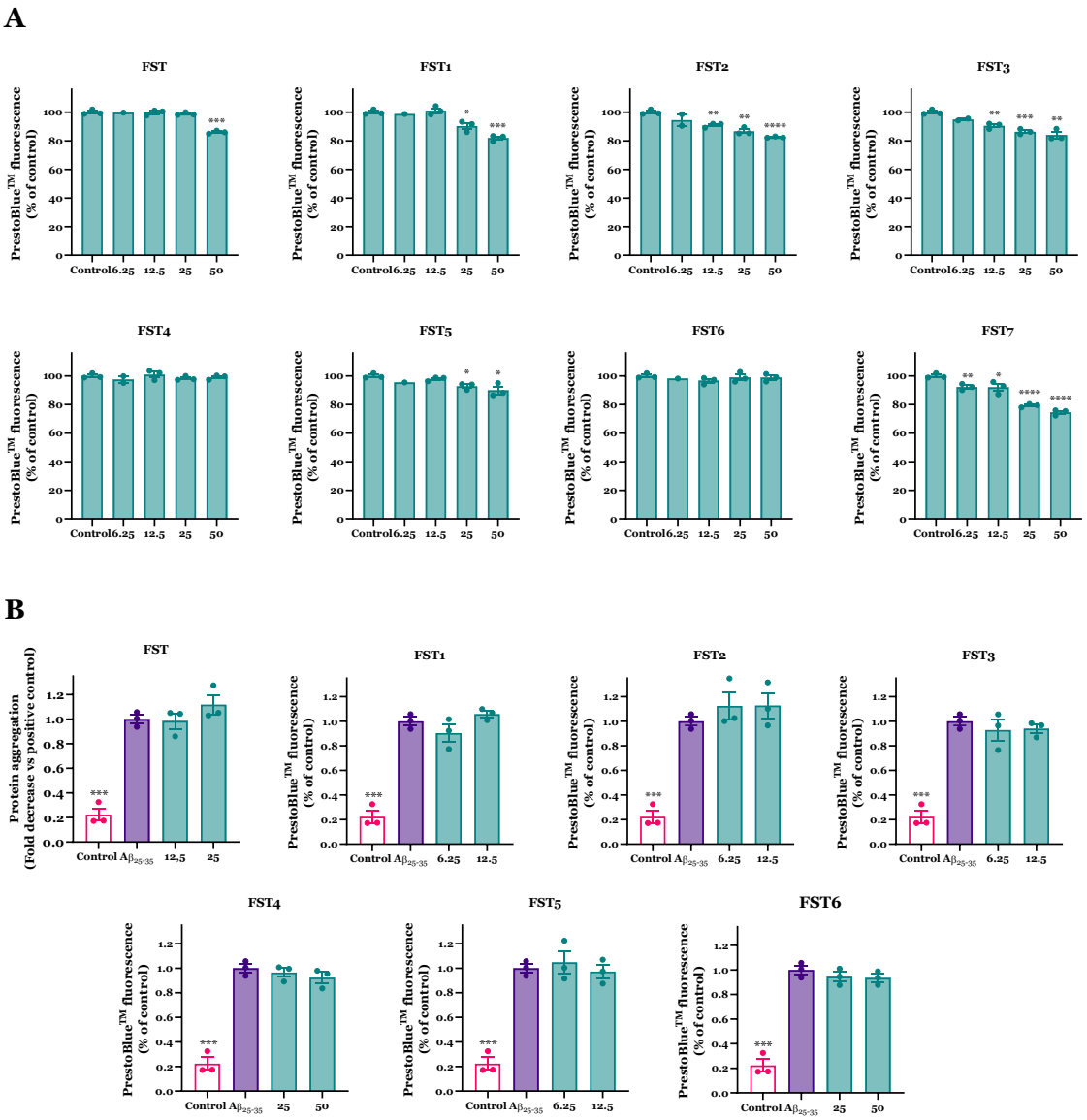

Figure 32. A: Cell viability of SH-SY5Y cells after 24 h of incubation with fisetin (FST) and its synthetic derivatives FST1-7, as determined by PrestoBlue™ cell viability assay. **B:** Effect the two highest nontoxic concentrations of FST and derivatives on $A\beta_{25-35}$-induced protein aggregation in SH-SY5Y cells, determined by the fluorescence of ThT. All experiments were individually conducted in triplicate. Results are presented as the percentage of the control and represent to the mean ± SEM of, at least, three independent experiments. *$p < 0.05$, **$p < 0.01$, ***$p < 0.001$, ****$p < 0.0001$.

3.4.2. Cytotoxicity of fisetin and derivatives upon MRC-5, AGS and A549 cells

The literature contains several reports concerning the potential of fisetin against malignant cells through induction of ER stress. One of those reports tests the compound against two very aggressive metastatic human melanoma cell lines (A375 and 451Lu), where it induced IRE1α, sXBP-1, ATF4 and GRP78 expression levels, and activated the intrinsic and extrinsic apoptotic mechanisms, while inducing autophagy. The authors also observed

the toxicity of fisetin against this type of cell to occur both dependent or independently of AMPK signalling (336). Fisetin was also effective against the oral cancer cell line HSC3, and the authors of the study propose that this potential was endoplasmic reticulum- and mitochondria-related, as they observed increased levels of Ca^{2+} and ROS. Furthermore, they observed increased activities of caspases -3, -8 and -9, chromatin condensation, and release of cytochrome c, apoptosis inducing factor (AIF) and endonuclease G (endoG) from the mitochondria (337). In the non-small cell lung cancer cell line NCI-H460, fisetin also induced MAPK-dependent ER stress. In this case, silencing this pathway actually prevented its effect. Upon the effect of the compound, the cells display increased cytosolic Ca^{2+} overload, as well as increases in several key UPR biomarkers, as are GRP78 and CHOP levels, IRE1, PERK and eIF2α phosphorylation, ATF6 cleavage and XBP-1 splicing (338). In light of this, the toxicity of fisetin against cancer cells seems to strongly rely on ER stress and MAPK signaling.

A survey of the literature regarding the anticancer potential of fisetin, along with our results, that indicate a selective cytotoxicity of the compound against both AGS and A549 cells, took us to test a library of fisetin derivatives to screen for improved potential. However, as evidenced by **Figure 33**, this attempt has resulted in poor activity of the derivatives regarding cytotoxicity.

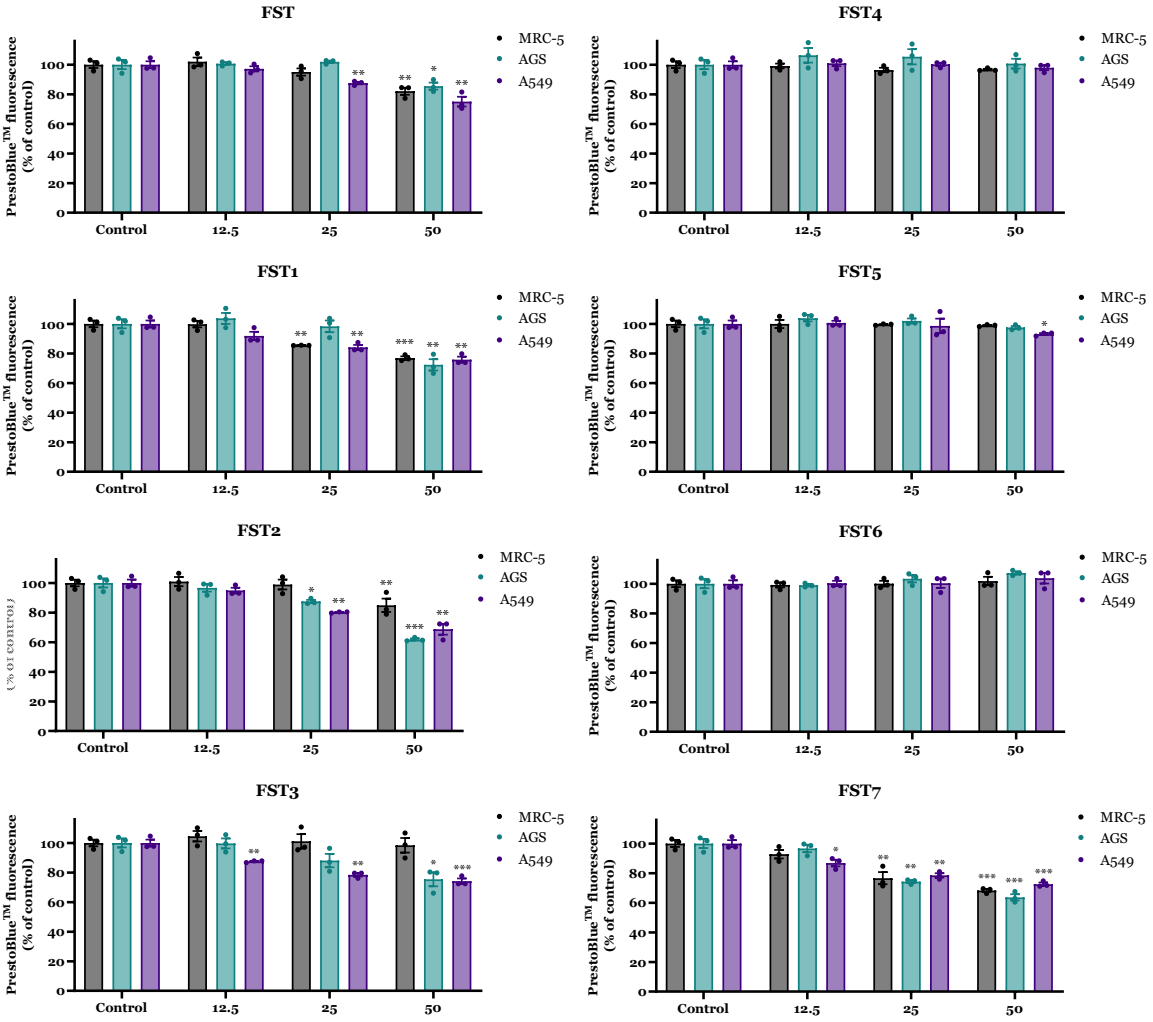

Figure 33. Cell viability of MRC-5, AGS and A549 cells after 24 h of incubation with FST and compounds FST1-7, as determined by PrestoBlue™ cell viability assay. Every experiment was performed in triplicate. Results are represented as the percentage of the control and express the mean ± SEM of, at least, three independent experiments. *$p < 0.05$, **$p < 0.01$, ***$p < 0.001$.

The anti-inflammatory potential of fisetin is often referred to throughout the scientific literature, regarding inflammation or even in different contexts such as anticancer activity (458) or neuroprotection (459). For this reason, we tested a library of fisetin derivatives to search for molecules with stronger anti-inflammatory and anti-ER stress activities, and also decreased cytotoxicity. This work is presented in the following section.

ORIGINAL ARTICLE #4

Fisetin derivatives exhibit enhanced anti-inflammatory activity and modulation of endoplasmic reticulum stress

Daniela Correia da Silva, Peter J. Jervis, José A. Martins, Patrícia Valentão, Paula M. T. Ferreira, David M. Pereira

International Immunopharmacology, 2023, 119, 110178

Abstract

Inflammation and endoplasmic reticulum (ER) stress are often hand in hand in the context of chronic disease. Both are activated upon perceived disturbances in homeostasis, being deleterious when intensely or chronically activated. Fisetin (FST) is a dietary flavonol that is known to possess multiple relevant bioactivities, raising the question of its potential health benefits and even its use in novel pharmacological approaches against ER stress and inflammation. To attain this prospect, some limitations to this molecule, namely its poor bioavailability and solubility, must be addressed.

In an attempt to improve the biological properties of the parent molecule, we have synthesized a set of FST derivatives. These new molecules were tested along with the original compound for their ability to mitigate the activation of the signaling pathways underlying inflammation and ER stress. By reducing LPS-induced nuclear factor-kappa B (NF-κB) activation, cytokine release, inflammasome activation and reactive oxygen species (ROS) generation, FST has proven to be effective against the onset of inflammation. The molecule also decreases the activation of the unfolded protein response (UPR), as evidenced by the reduced expression of relevant UPR-related genes upon ER stress induction. Some of the tested derivatives are novel inhibitors of targets associated to inflammation and ER stress signaling, in some cases more potent than the parent compound. Furthermore, the reduced cytotoxicity of some of these molecules enabled the use of higher concentrations than that of FST, resulting in the observation of enhanced bioactivities.

Keywords: natural products, fisetin, endoplasmic reticulum stress, inflammation, inflammasome, IL-6, TNF-α, IL-1β, ATF4, CHOP

3.5.1. Introduction

Inflammation encompasses the activation of several signaling cascades and the recruitment of specialized cells. This activation constitutes an attempt to restore homeostasis upon the detection of danger signals, arising either from injury or infection. Despite the importance of inflammatory signaling to solve these instances, its chronic activation is known to underlie several chronic diseases (233).

The endoplasmic reticulum (ER) is in charge of protein synthesis and folding of a substantial portion of the proteome of eukaryotes. The complexity of the protein folding process renders it error prone, and thus this organelle relies on signaling pathways to detect misfolded/unfolded protein in the ER lumen and attempt to restore homeostasis. These signaling pathways are known as the unfolded protein response (UPR) (460). Even though UPR signaling has evolved to promote cell survival, it can be deleterious. In fact, like inflammation, the UPR is chronically activated in the context of a number of chronic diseases (231, 415).

The flavonol fisetin (FST), or 3,3',4',7-tetrahydroxyflavone, was first isolated in 1833 from *Rhus cotinus* L., commonly known as venetian sumac. Its chemical structure was elucidated near the end of the century (461). This flavonol is synthesized as a specialized metabolite in leaves, stems, barks, hardwoods and fruits of multiple plants, including plants relevant to the human diet, such as strawberries (160 μg/g), apples (26.9 μg/g), persimmons (10.6 μg/g), onions (4.8 μg/g), grapes (3.9 μg/g) and kiwis (2.0 μg/g) (461, 462).

The average dietary intake of FST is estimated at 0.4 mg/day in geographies where this information is available, namely the Japanese population (463). Dietary supplements containing FST are available in the market, and are advertised as conveyers of multiple health benefits due to the multiple relevant bioactivities of the molecule, as well as its ability to cross the blood-brain-barrier (464). Even though no FST-based products are used for pharmacological purposes (461), there are several ongoing clinical trials, including phase III clinical trials (NCT05482672, NCT05505747).

FST is described as a free radical scavenger. This antioxidant potential is thought to be owed to the *o*-dihydroxy structure in the B ring, as well as the 3-hydroxy group and 2,3-double bond in the C ring (462). Additionally, FST has a possible therapeutic effect against cancer by exerting antiproliferative and apoptotic effects, while modulating key signaling pathways such as the nuclear factor-kappa B (NF-κB) and mitogen-activated protein kinase (MAPK) (465-467). FST has been described as neuroprotective by being antioxidant and anti-inflammatory, increasing intracellular glutathione levels and promoting synaptic plasticity (456, 457, 464, 468). Furthermore, it is described as being capable of modulating ER stress response, resulting in decreased protein aggregation under stress conditions

(387). Relevantly, FST has shown promise in areas that implicate both inflammation and ER stress signaling, such as neurodegeneration and cancer.

Low solubility in water and poor bioavailability may be limiting the use of this molecule in the pharmacological context (465, 469). For this reason, it is important to tailor this molecule into safer, more stable and active derivatives that can aid in the development of FST-based pharmacological strategies and also add to the current understanding of its bioactivities. In this work, we describe the bioactivity of several novel synthetic FST derivatives in the context of inflammatory and ER stress signaling. The discoveries published herein may contribute to provide new modulators of both signaling pathways into the current pharmacological arsenal.

3.5.2. Materials and Methods

3.5.2.1. Synthesis

FST derivatives FST1–7 were synthesized using methods developed in our laboratory, as outlined in **Figure 34**. The experimental procedures and characterization data for the compounds FST1–7 are presented in the Supplementary Material. FST was acquired from the Abcam chemical company (Cambridge, UK). All other reagents were purchased from Sigma-Aldrich or Acros and used without further purification. Analytical grade solvents were used, and dried by standard methods when required. Distilled water was used when aqueous medium was needed. Reactions were monitored by thin layer chromatography (TLC) on Merck-Kieselgel plates 60 F254 and detection was made by examination under UV light (240 nm) or by adsorption of iodine vapour. Chromatographic separations were performed on silica MN Kieselgel 60 M (230–400 mesh). NMR spectra were acquired on a Bruker Avance III 400 spectrometer. NMR spectra were recorded at 25 °C, using the residual solvent signals as reference. Deuterated dimethyl sulfoxide (DMSO-d_6) and deuterated chloroform ($CDCl_3$) were used as solvents. Chemical shifts are given in parts per million (ppm) and the coupling constants in Hertz (Hz). Mass spectrometry data were recorded by a ThermoFinnigan LxQ (Linear Ion Trap) mass detector with electrospray ionisation (ESI).

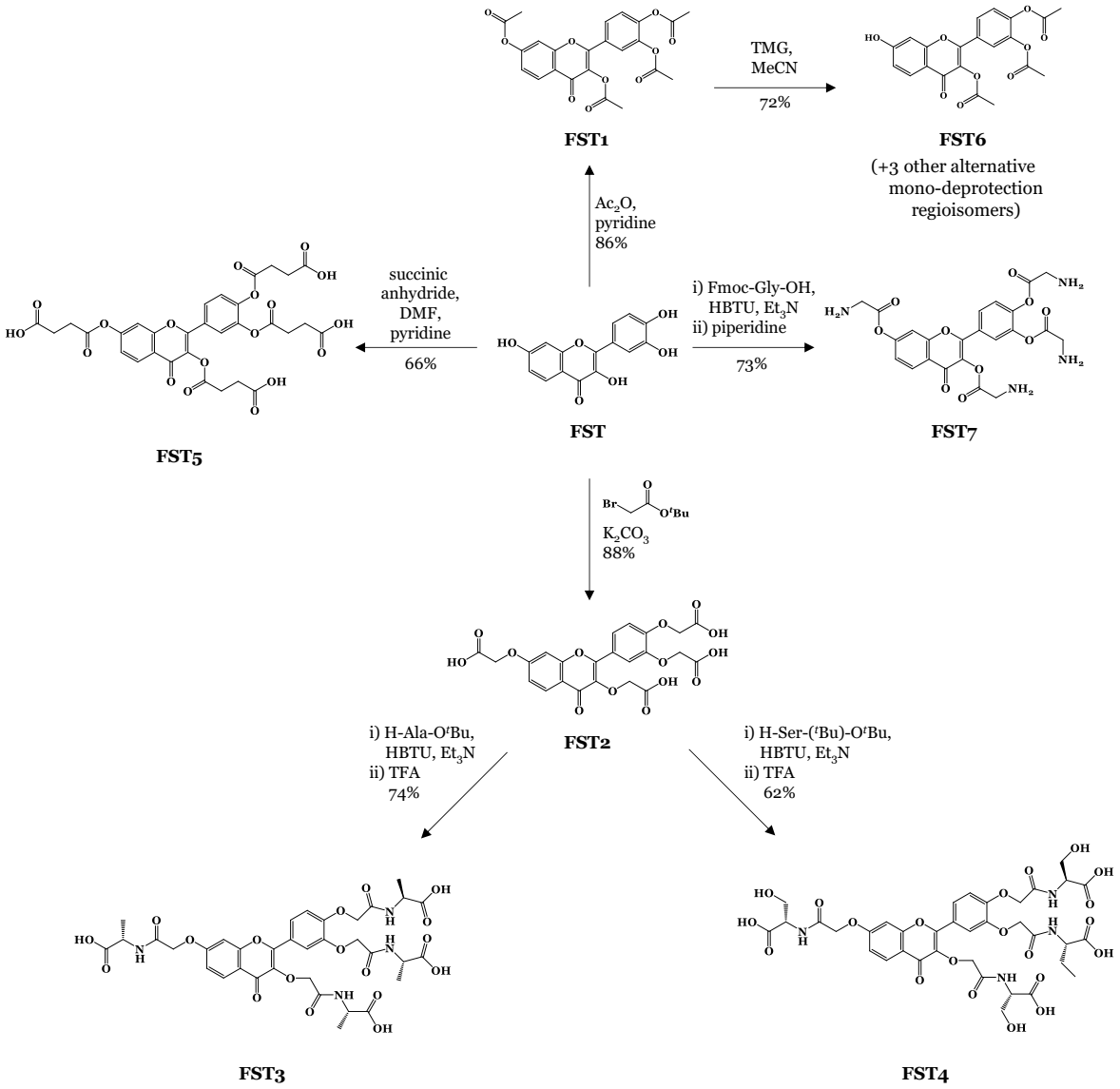

Figure 34. Synthetic routes to FST derivatives (FST1-7).

3.5.2.2. Cell culture conditions

THP-1 and THP-1 Lucia™ NF-κB monocytes were cultured at 37 ºC with 5% CO_2, in RPMI 1640 medium, with 10% FBS, 1% penicillin/streptomycin and HEPES at 25 mM. Additionally, as recommended by the supplier, medium for THP-1 Lucia™ NF-κB monocytes contained 100 µg/mL Normocin™. Zeocin™ (100 µg/mL) was included every other passage to ensure selective pression.

3.5.2.3. MTT reduction assays

Cellular viability was inferred according to the results of MTT reduction assays, carried out in 96-well plates. In these plates, THP-1 monocytes were seeded at a density of 6 x 10^4 cells/well. Differentiation of monocytes into macrophages was promoted with the addition of PMA at 50 nM when seeding. Medium contained PMA was discarded and replaced with fresh medium after 24 h. In the following day, differentiated macrophages were incubated with the solutions containing the molecules under analysis. After 24 h of incubation with the compounds, the medium was replaced with MTT at 0.5 mg/mL and incubated for 2 h. At this point, the MTT solution was discarded. The resulting crystals were dissolved in a 3:1 DMSO:isopropanol solution. Finally, the absorbance at 560 nm was read in a Thermo Scientific™ Multiskan™ GO microplate reader.

3.5.2.4. NF-κB activation assay

A luciferase based-assay was employed to determine the translation levels of the NF-κB transcription factor. The seeding of THP-1 Lucia™ NF-κB monocytes was performed as described above for the MTT reduction assays. 2 h after the incubation with the molecules of interest, LPS (from *E. coli*) was added at the final concentration of 1 μg/mL, in all wells except for the control group, promoting polarization of the macrophages into their pro-inflammatory phenotype, or M1. 24 h after the incubation with compounds, or 22 h after the addition of LPS, 20 μL of medium from each well was transferred to a clean 96-well plate, where 50 μL of QUANTI-Luc™ substrate solution was added each well, as according to the instructions from the supplier. The plate was shaken, and luminescence was immediately read in a Cytation™ 3 (BioTek) microplate reader.

3.5.2.5. Morphological analysis

In order to obtain fluorescence microscopy images, cells were seeded on clear bottomed-96-well plates at the aforementioned density and treated with the selected concentrations of the active molecules in the presence of LPS. Ended the incubation period, cells were fixed in 4% formaldehyde at room temperature for 15 min and incubated with DAPI at 0.25 μg/mL and a labeled phalloidin (CF543) at 5 U/mL. Finally, three washing steps with HBSS for 5 min were performed and cells were imaged under an inverted Eclipse Ts2R-FL (Nikon) fluorescence microscope equipped with a Retiga R1 camera. The DAPI staining was imaged using a DAPI filter, while phalloidin staining was visualized with the

TRITC filter. Fiji/ImageJ software version 1.51 (Fiji, Madison, WI, USA) was resorted to to analyze the images.

3.5.2.6. Pro-inflammatory cytokine release by ELISA

As described for the previous assays, THP-1 macrophages were seeded and differentiated in 96-well plates. After differentiation, cells were incubated with molecules of interest and LPS at 1 μg/mL was added after 2 h. Supernatants were collected 22 h after the addition of LPS. Concentrations of TNF-α, IL-6 and IL-1β were determined in the supernatant samples by ELISA. A specific kit for each cytokine was acquired, and the manufacturer's instructions (BioLegend Inc.; San Diego, CA, USA) were followed.

3.5.2.7. Quantification of ROS generation

THP-1 monocyte seeding was carried out as in the previous assays, only in black-bottomed 96-well plates. The molecules were once again incubated for a period of 24 h, including 22 h in the presence of LPS at 1 μg/mL. At this point, a washing step with HBSS ensued, followed by incubation with the fluorescent probe DCFH-DA at 25 μM for 30 min, in HBSS. Fluorescence at 490/520 nm was read in a Cytation™ 3 (BioTek) microplate reader.

3.5.2.8. Caspase-Glo® 1 Inflammasome Assay

Cells were seeded as mentioned above, only in white-bottomed 96-well plates. After the addition of LPS at 1 μg/mL, the incubation period was of 90 min. According to the instructions from the supplier, after these 90 min, Caspase-Glo® 1 Reagent was added to each well, in the absence and presence of the selective caspase-1 inhibitor Ac-YVAD-CHO, following a period of 60 min of incubation at room temperature. Finally, luminescence was read on a Cytation™ 3 (BioTek) microplate reader.

3.5.2.9. RNA extraction, quantification, conversion and RT-qPCR

In order to obtain mRNA samples, THP-1 monocytes were seeded in 12-well plates at a density of 4.8 x 10^5 cells/well. The compounds were incubated after differentiation of the monocytes into macrophages, as mentioned above. LPS was added after 2 h, and the plates were left in the incubator for 16 h. At this point, samples were obtained by resorting to the

PureZOL RNA isolation reagent. RNA extraction was performed by phase separation, according to the instructions provided by the supplier. After the extraction, RNA in the sample was quantified with the Qubit® RNA HS assay kit. The conversion to cDNA, using 1 µg of sample, was performed using the SuperScript™ IV VILO™ MasterMix. Our primers (**Table 8**) were designed on Primer BLAST (NCBI, Bethesda, MD, USA) and purchased to Thermo Fisher (Waltham, MA, USA).

The reaction was conducted with KAPA SYBR® FAST qPCR Kit Master Mix (2X) Universal, and took place in a qTOWER3 G (Analytik Jena AG, Germany), in the following conditions of thermal cycling: 3 min at 95 ºC, followed by 40 cycles of 95 ºC for 3 s (denaturation), gene-specific temperature for 20 s (annealing), and 20 s at 72 ºC (extension). Melting curves were observed to guarantee product specificity. Gene expression was normalized against the reference gene *GAPDH*. Data was analyzed in the qPCRsoft 4.0 software, supplied with the equipment.

Table 8. Analyzed genes, NCBI accession numbers, primers, annealing temperatures and amplification product size.

Gene	Accession number	Primers	Annealing Temperature (ºC)	Amplicon length (bp)
gapdh (GAPDH)	NM_002046.6	F: AGGTCGGAGTCAACGGATTT R: TGGAATTTGCCATGGGTGGA	60	157
ddit3 (CHOP)	NM_001195053.1	F: AAGTCTAAGGCACTGAGCGT R: TTGAACACTCTCTCCTCAGGT	59	93
atf4 (ATF4)	NM_001675.4	F: ACAACAGCAAGGAGGATGCC R: CCAACGTGGTCAGAAGGTCA	60	135
edem1 (EDEM1)	NM_014674.2	F: GCGGGGACCCTTCAAATCT R: CGGCTTTCTGGAACTCGGAT	60	117

3.5.2.10. Tanimoto coefficient

All molecules were drawn in RdKit having their SMILES strings as input. For the calculation of Tanimoto coefficients, SMILES were used to calculate extended-connectivity fingerprints (ECFP4) fragments which were then used as input for the calculation of Tanimoto coefficients in a pairwise fashion with FST, using the formula:

$$SIM_{AB} = \frac{c}{a + b - c}$$

in which ***c*** bits set in common in the two fingerprints and ***a*** and ***b*** are bits set in the fingerprints for molecules **A** and **B.**

3.5.2.11. Statistical analysis

GraphPad Prism 8 software was utilized for the statistical analysis, namely to perform unpaired Student's t-test to compare single treatments with control groups, with values of $p < 0.05$ considered statistically significant. Furthermore, outliers were detected with the Grubbs' test.

3.5.3. Results

3.5.3.1. Synthesis of FST derivatives

The parent molecule fisetin (FST) and the derivatives synthesized (FST1–7) were synthesized as shown in **Figure 34**. A number of molecular and topographical descriptors were also calculated, and can be found in **Table 9**. The Tanimoto coefficient was calculated for all derivatives (**Figure 35**), having FST in as the reference molecule, in order to assess the degree of chemical divergence introduced by the conducted modifications.

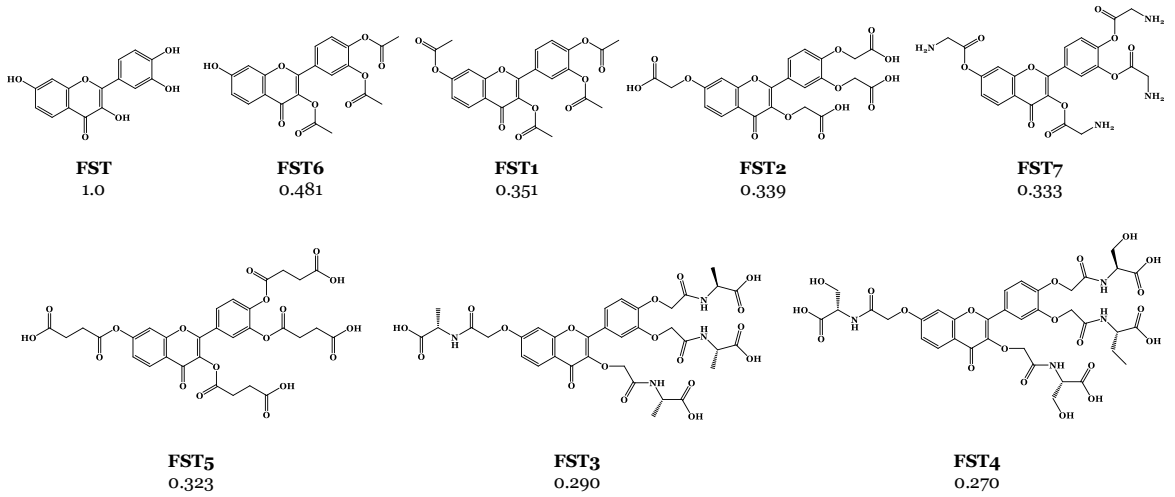

Figure 35. FST derivatives sorted according to their Tanimoto coefficient calculated using RdKit. FST was used as the reference molecule for pairwise calculation of the coefficient.

Table 9. Molecular and topographical descriptors of FST and derivatives. **BalabanJ**: Balaban's J value for a molecule; **BertzCT**: topological index meant to quantify complexity of molecules; **FractionCSP3**: fraction of carbons that are sp3 hybridized; **MolLogP**: Wildman-Crippen LogP value; **MolMR**: Wildman-Crippen MR value; **MolWt**: molecular weight; **NumValenceElectrons**: number of valence electrons; **qed**: quantitative estimation of drug-likeness; **TPSA**: topological polar surface area.

Molecule	FST	FST1	FST2	FST3	FST4	FST5	FST6	FST7
BalabanJ	2,34	2,27	2,16	2,1	2,12	2,15	2,28	2,24
BertzCT	909,92	1349,34	1420,95	2114,71	2189,64	1885,01	1237,19	1433,03
FractionCSP3	0	0,17	0,17	0,34	0,36	0,26	0,14	0,17
MolLogP	2,28	3,16	1,31	-0,67	-3,36	2,54	2,94	-1,08
MolMR	74,58	113,16	120,44	190,86	199,71	157,94	103,51	126,68
MolWt	286,24	454,38	518,38	802,7	864,72	686,53	412,35	514,45
NumValenceElectrons	106	170	194	306	330	258	154	194
qed	0,51	0,42	0,25	0,07	0,04	0,12	0,51	0,2
TPSA	111,13	135,41	216,33	332,73	393,42	284,61	129,34	239,49

3.5.3.2. Impact of fisetin derivatives on macrophage cell viability

This work began with the evaluation of the cytotoxic effect of FST and its 7 synthetic derivatives in order to define the concentrations that could be used in this experimental model without impacting cell viability. It is clear on **Figure 36** that FST and FST7 present the highest cytotoxicity, exerting a statistically significant effect from 25 µM. Two more molecules, FST1 and FST2, were cytotoxic at 50 µM. On the other hand, FST3, FST4, FST5 and FST6 were not cytotoxic up to 50 µM.

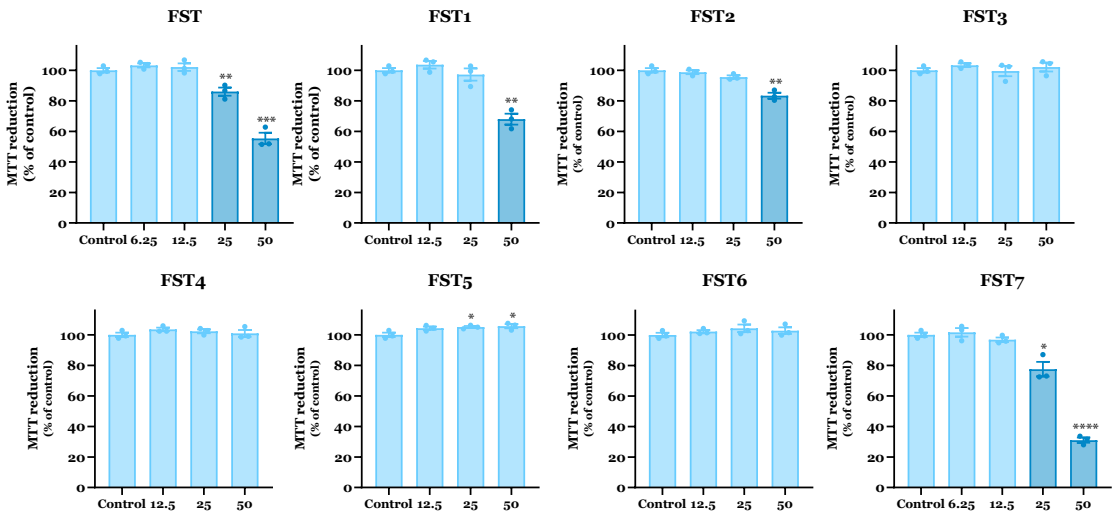

Figure 36. Effect of FST and each derivative upon cell viability of THP-1 macrophages after 24 h of incubation, determined by MTT reduction assays. Results as percentage of the

control correspond to the mean ± SEM of three independent experiments, individually conducted in triplicate. *$p < 0.05$, **$p < 0.01$, ***$p < 0.001$, ****$p < 0.0001$.

3.5.3.3. FST and derivatives inhibit LPS-mediated NF-κB activation

The results displayed in **Figure 37** show that FST derivatives FST4, FST5 and FST6 did not display any capacity to inhibit NF-κB activation in LPS-challenged macrophages in any of the tested concentrations. The parent compound, FST, as well as derivatives FST1, FST2, FST3 and FST7 were all remarkably effective at inhibiting the activation of NF-κB under our experimental conditions, being active in all concentrations tested. The images presented in **Supplementary Figure S10** confirm that the active molecules at effective concentrations and in the presence of LPS do not result in significant changes in cell density or morphology.

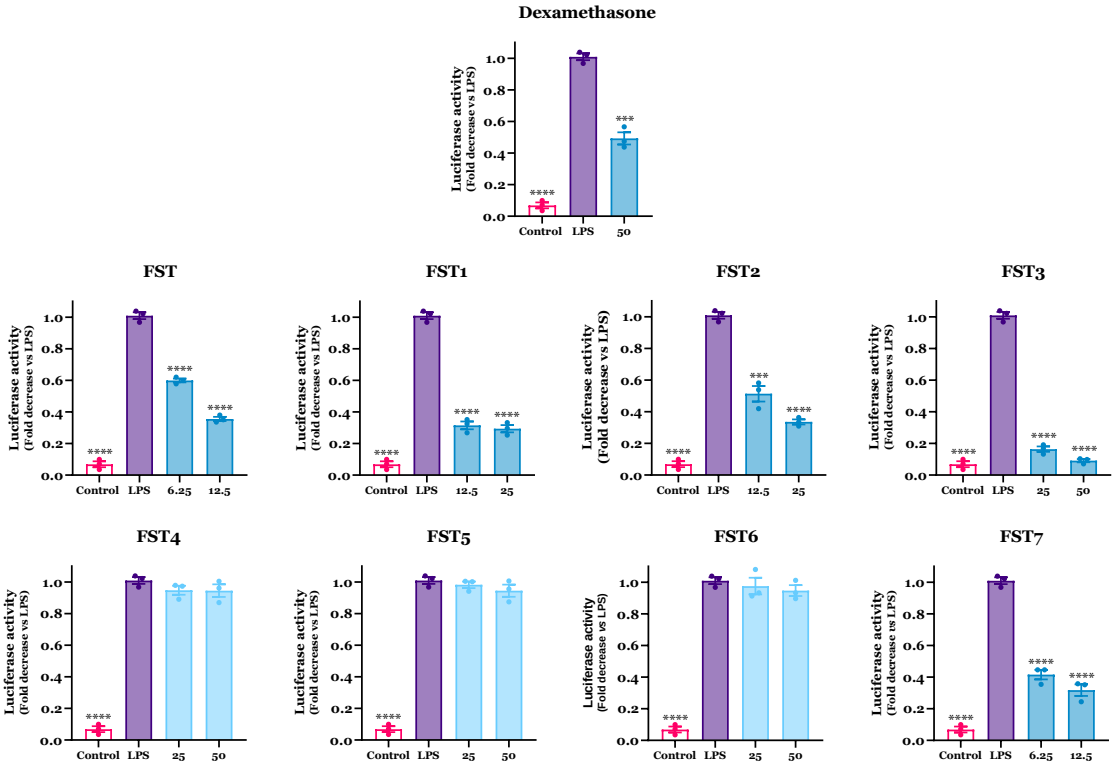

Figure 37. Effect of the two highest nontoxic concentrations of each molecule under study upon NF-κB activation after 22 h of LPS exposure, determined by the QUANTI-Luc™ luciferase activity assay in THP-1 Lucia™ NF-κB. The presented results express the relative NF-κB when compared to the positive control, including the mean ± SEM of three independent experiments, individually performed in duplicate. ***$p < 0.001$, ****$p < 0.0001$.

3.5.3.4. FST and some derivatives inhibit ROS generation

The results presented in **Figure 38** depict the evaluation of the ability of the molecules that had displayed anti-inflammatory potential in the previous assay to inhibit excessive ROS generation caused by LPS. With the exception of FST2, all molecules were effective in decreasing ROS generation in at least one of the tested concentrations. FST significantly inhibited ROS production only in the highest tested concentration (12.5 µM), the same being true for FST7. FST1, even though inactive at 12.5 µM, was also effective in its respective highest tested concentration (25 µM), displaying a stronger effect than that of FST and FST7. FST3 was the molecule displaying the stronger effect, reaching over 50% of inhibition at the highest tested concentrations.

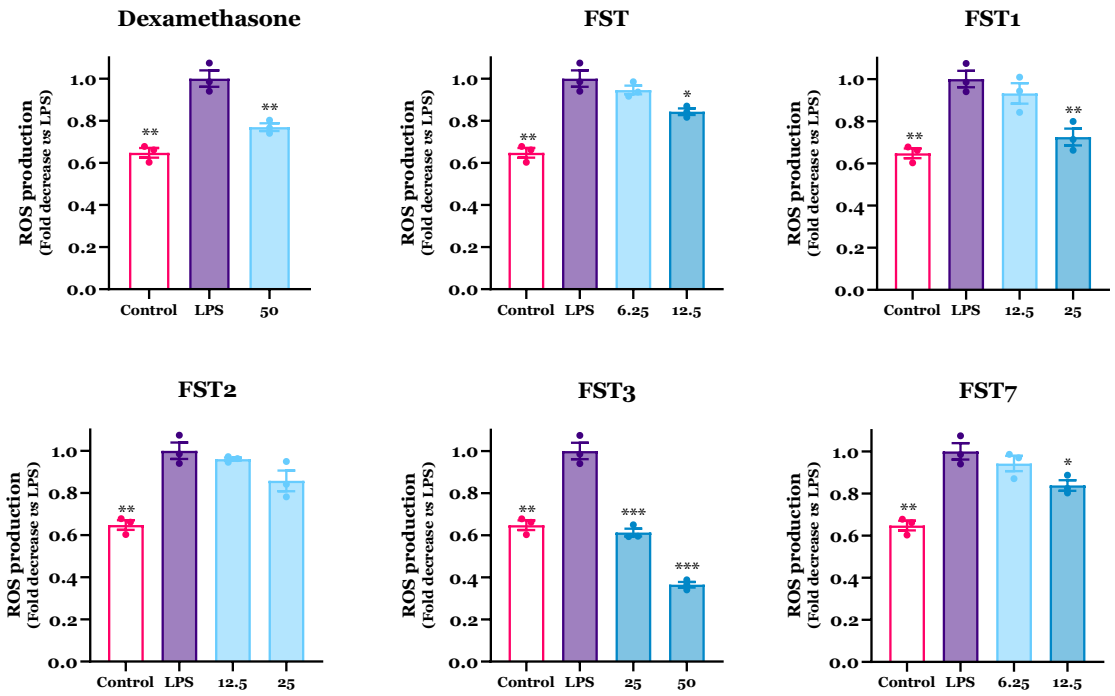

Figure 38. Impact of two highest concentrations of anti-inflammatory molecules on the generation of ROS by LPS-insulted THP-1 macrophages, determined by the fluorescence of DCFH-DA. Results express mean ± SEM of three independent experiments carried out in triplicate. *$p < 0.05$, **$p < 0.01$, ***$p < 0.001$.

3.5.3.5. FST and its derivatives decrease caspase-1 activation

The results obtained, displayed in **Figure 39**, show that every molecule under analysis was capable of inhibiting caspase-1 activation in its highest tested concentration. Only two molecules were effective at inhibiting NLRP3 inflammasome activation in both tested concentrations, specifically FST1 and FST3. The degree of inhibition is somewhat similar for both of these molecules at the concentration of 25 µM.

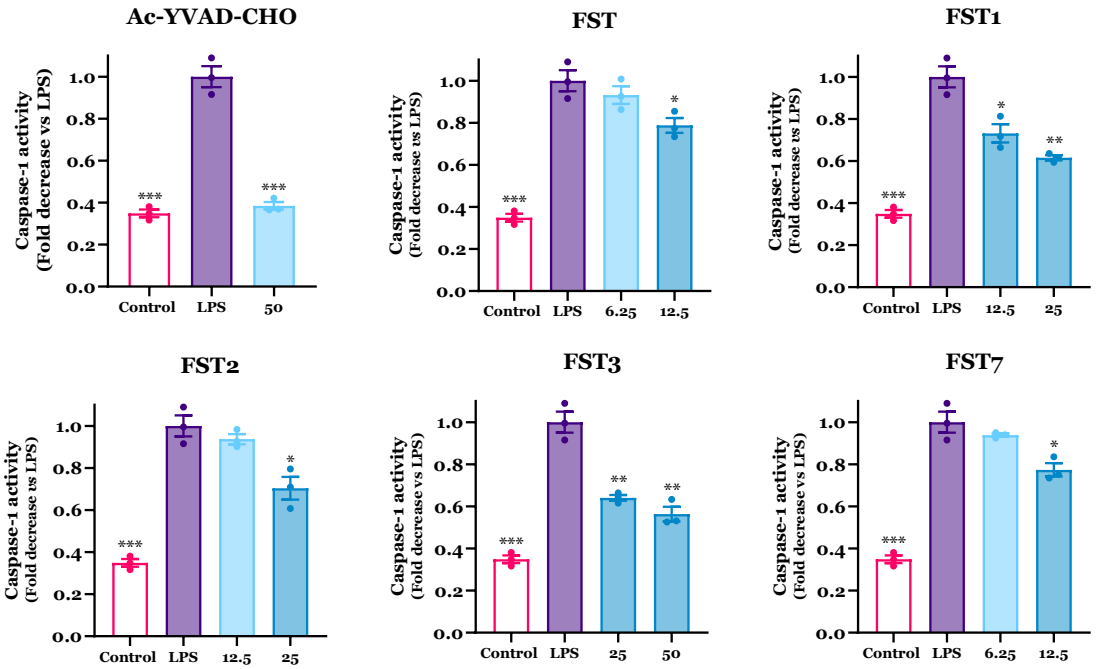

Figure 39. Effect of anti-inflammatory molecules on LPS-induced caspase-1 activation on THP-1 macrophages. Proteolytic activation of caspase-1 indicates NLRP3 inflammasome activation. Results are expressed as fold decrease *versus* maximum activation (on LPS-challenged cells) and stand for the mean ± SEM of three independent assays, with each performed in duplicate. *$p < 0.05$, **$p < 0.01$, ***$p < 0.001$.

3.5.3.6. FST and derivatives inhibit LPS-induced pro-inflammatory cytokine production

The impact of all molecules under study upon the production of the pro-inflammatory cytokines IL-6, TNF-α and IL-1β was assessed, with the steroid anti-inflammatory drug dexamethasone being used as a positive control for the inhibition of their release. Regarding the potential of FST and derivatives to inhibit LPS-induced IL-6 release, it is displayed in **Figure 40** that all tested FST derivatives significantly inhibit IL-6 release in both tested concentrations. FST is the only molecule under analysis that was effective only in the highest tested concentration. In the case of TNF-α, even though every molecule has shown to be active (**Figure 40**), the inhibitory potential was lower than in the case of IL-6. All molecules were effective at their highest tested concentration, while only FST3 was effective in both concentrations. This molecule was also the only capable of displaying any significant inhibition of IL-1β, albeit only at the highest tested concentration, or 50 μM (**Figure 40**).

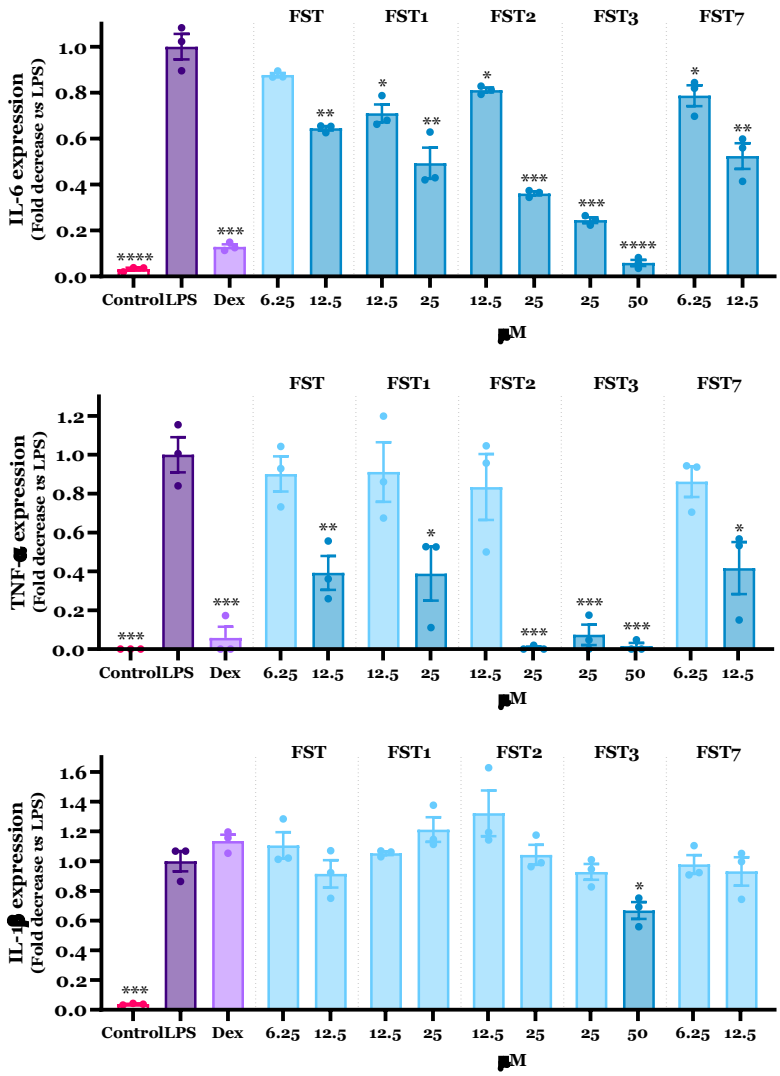

Figure 40. Influence of active molecules on the protein expression of the pro-inflammatory cytokines IL-6, TNF-α and IL-1β, as determined by ELISA. Results presented fold decrease against maximum activation, and represent the mean ± SEM of at least three independent experiments, individually performed in triplicate. *$p < 0.05$, **$p < 0.01$, ***$p < 0.001$, ****$p < 0.0001$.

3.5.3.7. Anti-inflammatory effect of FST and derivatives is concomitant with ER stress attenuation

The UPR-related genes *edem1*, *ddit3* and *atf4* saw their expression increased by incubation with LPS, as evidenced by the results presented in **Figure 41**. Incubation with FST resulted in significant inhibition of the LPS-induced overexpression of *edem1*. FST7 also exhibited a mild effect on this gene, while FST3 exerted a more pronounced effect. Notably, regarding *ddit3*, every molecule was effective at inhibiting its overexpression induced by LPS. On the other hand, FST and its derivative compounds failed to restore the expression levels of *atf4* to basal levels.

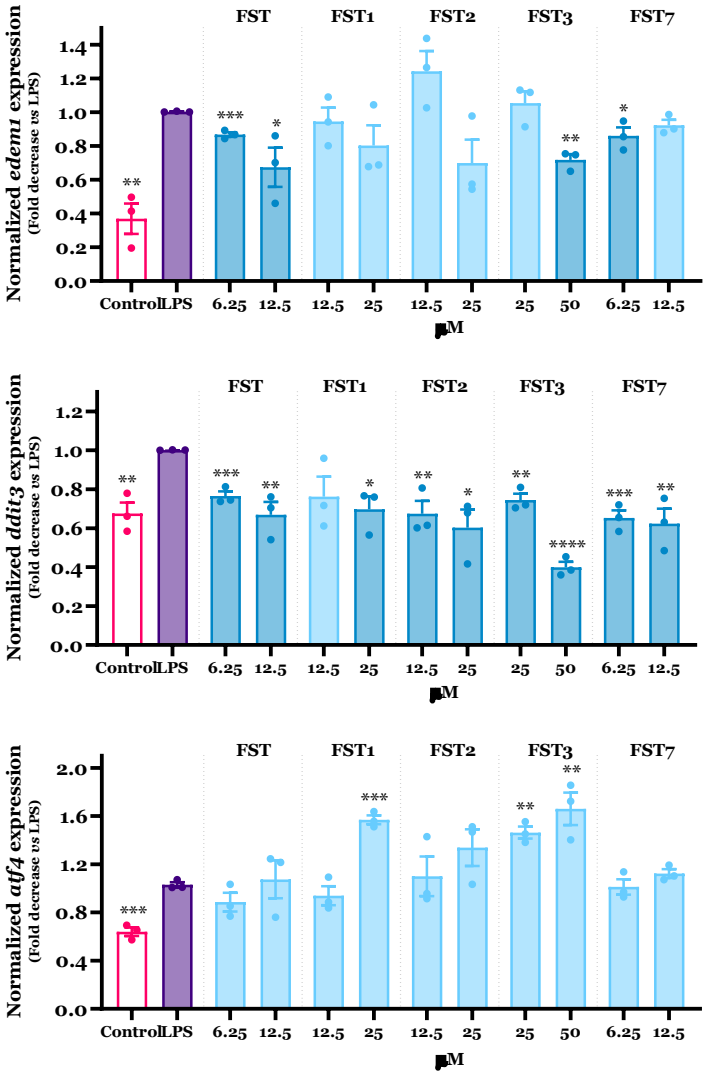

Figure 41. Effect of the anti-inflammatory molecules on gene expression of UPR target genes, namely *edem1*, *ddit3* and *atf4*, evaluated by RT-qPCR. Gene expression was normalized against *gapdh*. The results display the mean ± SEM of three independent assays, with each individually conducted in duplicate. *$p < 0.05$, **$p < 0.01$, ***$p < 0.001$, ****$p < 0.0001$.

3.5.4. Discussion

3.5.4.1. Similarity of FST derivatives to the parent molecule

FST6 is the closest molecule to the parent compound FST (**Figure 35**), followed by FST1 and FST2. FST3 and FST4 are the more chemically divergent molecules, owing not only to their complexity but also to the nature of their substituents. In fact, the BertzCT descriptor, which aims to quantify the complexity of a molecule, as expected, presents the highest values of the library for FST3 and FST4 (2114.7 and 2189.6, respectively, against 909.9 of FST, **Table 9**).

3.5.4.2. FST and derivatives ameliorate inflammation by inhibiting LPS-induced NF-κB activation

The evaluation of the cytotoxicity of the compounds under analysis in this cell model allowed the determination of the two highest nontoxic concentrations of each compound to be used in subsequent assays, in order to observe the strongest possible effect of FST and derivatives without compromising cell viability. THP-1 monocytes, when differentiated into M1 macrophages, are frequently used to assess the anti-inflammatory potential of small molecules, given their high expression pattern of relevant receptors such as the toll-like receptor 4 (TLR4) (470).

The NF-κB is a transcription factor that, upon activation, induces the expression of multiple pro-inflammatory cytokines and chemokines, as well as inflammasome assembly (260). As a major regulator of the inflammatory response, this transcription factor was chosen as a target to an initial evaluation of the anti-inflammatory potential of FST and derivatives. To infer NF-κB activation levels, we used THP-1 monocytes transfected with a NF-κB-inducible luciferase reporter construct (THP1-Lucia™ NF-κB). In light of the obtained results, three FST derivatives, namely FST4, FST5 and FST6, were dropped from the study and were not tested in the subsequent experiments, having failed to exert any inhibition of NF-κB activation under the tested experimental conditions. On the other hand, the parent compound and remaining derivatives exhibited a remarkable potential to inhibit NF-κB signaling. FST7 displays over 50% of inhibition at a concentration as low as 6.25 μM, thus being more active than the parent molecule. The same occurs with FST1 at 12.5 μM. The lowest concentration of FST3 results in NF-κB signaling near the basal levels, the most potent activity recorded for any of the derivatives. When examining the properties of the 3 molecules dropped due to lack of activity (FST 4-6), it is clear that they exhibit the most extreme logP values (FST4: -3.36, FST5: 2.54, FST6: 2.94), apart from FST1. In the case of the latter, it could be the case that the logP value of 3.16, the highest among all tested molecules, is relevant to the activity of the molecule.

3.5.4.3. Anti-inflammatory molecules inhibit LPS-induced ROS generation

The activation of NF-κB and other signaling pathways is a hallmark of M1 macrophage activation, as well as increased expression of proteins such as the matrix metalloproteinases (MMPs), induced expression of pro-inflammatory cytokines like TNF-α, IL-1α, IL-1β, IL-6, IL-12, IL-18, and IL-23, generation of nitric oxide (NO), reactive nitrogen species (RNS) and ROS (471). ROS are particularly well-established mediators of initiation, progression and resolution of inflammation. The oxidative burst is a broadly known phenomenon that

results from the extensive phagocytosis of pathogens and cell debris performed by neutrophils and macrophages that are recruited towards the inflammation site (264). It is, therefore, relevant to analyze what occurs at the level of ROS generation by the action of the NF-κB signaling inhibitors that we identified herein. In this regard, FST3 displayed the strongest activity among the FST derivatives, inhibiting LPS-induced ROS production in both tested concentrations. Even though the tested concentrations were higher (25 and 50 μM), both were observed before as not impactful towards cell viability, which may explain why we were able to achieve a higher inhibition of ROS generation with this molecule, when compared to the other active compounds. Notably, FST, FST1 and FST7 were only active in the respective highest tested concentrations.

3.5.4.4. FST and its bioactive derivatives inhibit NLRP3 inflammasome activation

The NLRP3 (NOD-, LRR- and pyrin domain-containing protein 3) inflammasome is a multimeric protein complex that consists of the innate immune receptor NLRP3, the adaptor protein ASC (apoptosis-associated speck-like protein containing CARD [caspase recruitment domain]) and the inflammatory caspase-1. Proteolytic cleavage of procaspase-1 in the inflammasome renders the active form of the protease. This event is used in this assay as a means to assess the activation of the NLRP3 inflammasome, that is known to be induced in the presence of microbe ligands, such as LPS, and result in caspase-1 activation and consequent cleavage of pro-IL-1β and release of its active form (472). Furthermore, NLRP3 inflammasome activation is one of the bridges connecting inflammatory and ER stress signaling, since it is known to mediate ER stress-induced inflammation (453). It is then justified to determine the ability of the molecules displaying an anti-inflammatory potential to impact caspase-1 activity, and, indirectly, on NLRP3 inflammasome activation.

Relevantly, NLRP3 inflammasome activation is often triggered by ER stress and UPR activation, deeming UPR modulation and NLRP3 inhibition a possible strategy to relieve inflammation (473). Currently, there are no approved drugs to modulate NLRP3 (474) or caspase-1 (475), since few molecules have entered clinical trials and they have failed. The need for modulators of inflammasome activation that are of low toxicity remains, and FST and derivatives are promising molecules to attain this goal. In fact, the parent compound FST has already been described as inhibitor of caspase-1 expression, as well as of IL-1β secretion *in vivo* (476). Besides describing the inhibitory effect of FST against caspase-1 activation in THP-1 macrophages, we add FST derivatives to the chemical space that comprises inhibitors of NLRP3 inflammasome activation.

3.5.4.5. FST and derivatives inhibit LPS-induced pro-inflammatory cytokine production

Immune cells, notably macrophages, recognize an infection through its pathogen-recognition receptors (PRRs), such as TLRs. Following NF-κB activation, the synthesis and release of pro-inflammatory mediators ensues, including the cytokines IL-6, TNF-α and IL-1β (263, 477). These three major cytokines, despite possessing potentially both pro- and anti-inflammatory properties, are mainly pro-inflammatory cytokines secreted by activated M1 macrophages, being involved in the modulation of the acute phase response (471, 478).

Unlike the parent compound, every molecule was able to inhibit IL-6 release in the two tested concentrations. FST was, nonetheless, effective at the highest tested concentration, of 12.5 μM. FST3 at the highest tested concentration inhibited IL-6 release almost completely. TNF-α release was at a basal level in the presence of this compound in both tested concentrations. Furthermore, this was the only molecule to inhibit the release of IL-1β, even though only at the highest concentration. When compared to FST or other derivatives, this is the molecule that presents the most promising anti-inflammatory potential, being able to strongly modulate every parameter analyzed.

3.5.4.6. Anti-inflammatory effect of FST and and derivatives is concomitant with ER stress attenuation

ER stress and the UPR activation that follows result in the enhanced expression of a battery of genes. Therefore, the evaluation of the transcriptional outcome at the level of ER stress in the presence of LPS and the compounds of interest was assessed. In order to facilitate the comprehension of the relevance of these results, it is fundamental to mention that UPR activation comprises the activation of three major signaling branches, that are initiated by the activation of a sensor protein that can be i) protein kinase R-like endoplasmic reticulum kinase (PERK), ii) inositol-requiring enzyme 1 (IRE1) or iii) activating transcription factor 6 (ATF6) (329).

The *edem1* gene encodes the EDEM1 (ER degradation enhancing-mannosidase-like protein), an important enzyme in ER-associated degradation (ERAD) of misfolded proteins (431). Inhibition of the overexpression of this gene indicates that ERAD is decreased, and thus ER stress is ameliorated. For this reason, we can conclude that FST, as well as FST3 and FST7, inhibit UPR signaling.

Furthermore, apart from FST1, which was still effective in the highest tested concentration, every molecule significantly inhibited LPS-induced overexpression of *ddit3* in a statistically significant manner in both tested concentrations, attesting for the ability of

FST and derivative compounds to reduce inflammation while restoring ER homeostasis. Increased *ddit3* expression is classically attributed to PERK/activating transcription factor 4 (ATF4) signaling, but this gene is a downstream target of every UPR signaling branch, including ATF6 and IRE1/X-box binding protein 1 (XBP1) (479). CCAAT-enhancer-binding protein homologous protein (CHOP) is a pro-apoptotic transcriptional factor, and thus the fact that every molecule inhibits its overexpression attests for their potential to preserve cellular homeostasis upon LPS insult (480). Similarly to what was observed in other evaluated parameters, FST3 was the molecule that displayed the most promising potential.

The *atf4* gene encodes the ATF4. This is a transcription factor that induces, among others, the expression of protein folding-related genes. Its expression is selectively enhanced upon UPR activation, that also being the case of *ddit3*. The translation of the latter results in the CHOP transcription factor, that governs processes of ER stress-induced regulated cell death (329). Every treatment was ineffective at inhibiting *atf4* overexpression, including FST3 at 50 μM, that had been active in every other parameter analyzed throughout this work. However, even though the mRNA expression did not decrease, the levels of the active transcription factor may be decreased, which could explain the enhanced *atf4* mRNA expression at this point. Furthermore, the activation and translocation to the nucleus of this transcription factor has been observed to be induced by TLR4 signaling in a JNK-dependent manner. ATF4 promotes inflammation by positively regulating the secretion of cytokines like IL-6. Furthermore, TLR4 signaling leads to increased protein stability of this protein (481). TLR4 signaling is decreased by effect of FST and derivatives, further adding to the hypothesis that ATF4 activation may be decreased independently of its mRNA levels.

3.5.5. Conclusions

Notwithstanding its wide coverage in scientific literature, the biological activities of FST have yet to be present in therapeutic approaches for any type of disease. In this work, we add to the knowledge on the bioactivity of this molecule, while presenting synthetic derivatives that present enhanced properties. Some of these bioactive derivatives are remarkably less cytotoxic towards the cell model employed herein than the parent compound itself. This enabled testing of higher concentrations without deleterious effects upon the cell, and resulted in the observation of a stronger biological activity on some or all of the analyzed parameters, being that FST3 was the molecule that resulted in the most promising observations.

In our experimental model, FST has significantly attenuated LPS-induced onset of inflammation and ER stress, simultaneously ameliorating NF-κB activation, ROS

generation, pro-inflammatory cytokine release, capase-1 and, consequently, inflammasome activation. Concurrently, the presence of FST impaired activation of the UPR signaling that was triggered in response to LPS, as observed by the decreased gene expression of relevant genes. Notably, FST and all its derivatives that could inhibit NF-κB signaling reduced inflammasome activation and cell death-oriented UPR signaling, adding to the connection between the molecular machineries that underlie inflammation and ER stress.

Supplementary Material

FST 1. Acetic anhydride (0.26 mL, 2.80 mmol) was added to a cooled (0 °C) solution of fisetin (80 mg, 0.28 mmol) in pyridine (1.0 mL). The resulting suspension was allowed to warm to room temperature and then stirred overnight. Filtration of the suspension provided a brown solid, which was recrystallized from chloroform/methanol (50:50) to afford **FST2** as a white solid (109 mg, 86%). ^{1}H NMR (400 MHz, DMSO-d_6, δ): 2.32 (3H, s, CH_3), 2.33 (6H, s 2 × CH_3), 2.34 (3H, s, CH_3), 7.36 (1H, dd, *J* 8.6, 2.2, ArH, 7.53 (1H, dd, *J* 8.6, 1.0, ArH), 7.70 (1H, d, *J* 2.2, ArH), 7.86 (1H, d, *J* 1.0, ArH), 7.87 (1H, dd, *J* 8.6, 2.2, ArH), 8.13 (1H, d, *J* 8.6, ArH). *m/z* (TOF ES+) 455.1 ([M + H]$^+$, 100%).

FST2. *tert*-Butyl bromoacetate (240 mg, 1.23 mmol) was added to a suspension of fisetin (70 mg, 0.25 mmol) and K_2CO_3 (170 mg, 1.23 mmol) in DMF (3.0 mL). The resulting suspension was stirred overnight, before EtOAc (20 mL) and H_2O (20 mL) were added. The phases were separated and the organic phase was washed with H_2O (2 × 20 mL) and brine (20 mL). The organic phase was then dried ($MgSO_4$), filtered and concentrated under reduced pressure to afford a white solid, which was immediately dissolved in TFA (2.0 mL) and stirred for 1 h. The TFA was then removed under reduced pressure. Residual TFA was removed by adding portions of chloroform (3 × 5.0 mL) and then removing under reduced pressure, to afford **FST2** as a white solid (114 mg, 88%). ^{1}H NMR (400 MHz, DMSO-d_6, δ): 4.78 (2H, s, CH_2CO$_2$H), 4.79 (2H, s, CH_2CO$_2$H), 4.82 (2H, s, CH_2CO$_2$H), 4.88 (2H, s, CH_2CO$_2$H), 7.06 (1H, d, *J* 8.8, ArH), 7.09 (1H, dd, *J* 8.8 2.2, ArH), 7.26 (1H, d, *J* 2.2, ArH), 7.76 (1H, dd, *J* 8.8, 2.2, ArH), 7.82 (1H, d, *J* 2.2, ArH), 7.97 (1H, d, *J* 8.8, ArH), 12.96 (4H, br s, 4 × CO_2H). *m/z* (TOF ES+) 541.1 ([M + Na]$^+$, 100%).

FST3. HBTU (148 mg, 0.39 mmol) was added to a solution of **FST2** (40 mg, 0.08 mmol), H-Ala-O^{t}Bu•HCl (71 mg, 0.39 mmol) and Et_3N (0.16 mL, 1.17 mmol) in MeCN (4.0 mL) The resulting solution was stirred at room temperature overnight. The solvent was removed under reduced pressure and then EtOAc (10 mL) was added. This solution was washed with $KHSO_4$ solution (1.0 M, 2 × 10 mL) and $NaHCO_3$ solution (1.0 M, 2 × 10 mL). The organic phase was dried ($MgSO_4$), filtered and concentrated under reduced pressure to afford a residue which was immediately dissolved in TFA (2.0 mL) and stirred for 1 h. The TFA was then removed under reduced pressure. Residual TFA was removed by adding portions of chloroform (3 × 5.0 mL) and then removing under reduced pressure, to afford **FST3** as a white solid (48 mg, 74%). ^{1}H NMR (400 MHz, DMSO-d_6, δ): 1.28–1.35 (12H, m, 4 × CH_3), 4.27–4.35 (4H, m 4 × CH), 4.61–4.77 (8H, m, 4 × CH_2), 7.11–7.19 (2H, m, 2 × ArH), 7.28 (1H, d, *J* 2.0, ArH), 7.75–7.84 (2H, m, 2 × ArH), 8.01 (1H, m, *J* 8.8, ArH), 8.28 (1H, br s, NH), 8.35 (1H, br s, NH), 8.47 (1H, br s NH), 8.51 (1H, br s, NH), 12.43 (4H, br s, 4 × CO_2H). *m/z* (TOF ES+) 803.2 ([M + H]$^+$, 100%).

FST4. HBTU (148 mg, 0.39 mmol) was added to a solution of **FST2** (40 mg, 0.08 mmol), H-Ser(^{t}Bu)-O^{t}Bu•HCl (99 mg, 0.39 mmol) and Et_3N (0.16 mL, 1.17 mmol) in MeCN (4.0 mL) The resulting solution was stirred at room temperature overnight. The solvent was removed under reduced pressure and then EtOAc (10 mL) was added. This solution was washed with $KHSO_4$ solution (1.0 M, 2 × 10 mL) and $NaHCO_3$ solution (1.0 M, 2 × 10 mL). The organic phase was dried ($MgSO_4$), filtered and concentrated under reduced pressure to afford a residue which was immediately dissolved in TFA (2.0 mL) and stirred for 1 h. The TFA was then removed under reduced pressure. Residual TFA was removed by adding portions of chloroform (3 × 5.0 mL) and then removing under reduced pressure, to afford **FST3** as a white solid (43 mg, 62%). ^{1}H NMR (400 MHz, DMSO-d_6, δ): 3.62–3.83 (12H, m, 4 × C*H*$_2$OH, 4 × CH), 4.53 (4H, br s, 4 × OH), 4.69–4.80 (8H, m, 4 × OCH_2CO), 7.12–7.17 (2H, m, ArH), 7.31 (1H, d, *J* 2.0, ArH), 7.77 (2H, m, ArH), 8.01 (1H, d, *J* 8.8, ArH), 8.11–8.27 (4H, m, 4 × NH). The exchangeable CO_2H protons were not observed. m/z (TOF ES+) 866.2 ([M – H]$^-$, 100%).

FST5. Succinic anhydride (55 mg, 0.55 mmol) was added to a stirred suspension of fisetin (32 mg, 0.11 mmol) and K_2CO_3 (76 mg, 0.55 mmol) in DMF (3.0 mL). The mixture was stirred at room temperature overnight before EtOAc (10 mL) and $KHSO_4$ solution (1.0 M, 10 mL) were added. The phases were separated and the aqueous phase was further extracted with EtOAc (3 × 10 mL). The combined organic phase was washed with brine (10 mL), dried ($MgSO_4$), filtered and concentrated under reduced pressure to afford **FST5** as a white solid (50 mg, 66%). ^{1}H NMR (400 MHz, DMSO-d_6, δ): 2.61–2.83 (16H, m, 4 × COC*H*$_2$C*H*$_2$CO$_2$H), 7.42 (1H, d, *J* 8.8, 2.2 ArH), 7.54 (1H, d, *J* 8.8, ArH), 7.72 (1H, d, *J* 2.2, ArH), 7.89 (1H, d, *J* 2.2, ArH), 7.91 (1H, d, *J* 8.8, 2.2 ArH), 8.14 (1H, d, *J* 8.8, ArH), 12.23 (4H, br s, 4 × CO_2H). *m/z* (TOF ES+) 709.1 ([M + Na]$^+$, 100%).

FST6. *N*,*N*,*N*',*N*'-Tetramethylguanidine (0.12 mL, 0.95 mmol) was added to cooled (0 °C) solution of **FST1** (45 mg, 0.10 mmol) in MeCN (3.0 mL). After 10 min, the reaction mixture was diluted with EtOAc and $KHSO_4$ solution (1.0 M, 10 mL). The phases were separated and the aqueous phase was further extracted with EtOAc (3 × 10 mL). The combined organic phase was washed with brine (10 mL), dried ($MgSO_4$), filtered and concentrated under reduced pressure. The resulting residue was purified by flash column chromatography (eluent: 10% MeOH in $CHCl_3$) to afford **FST6** as an isomeric mixture of three mono-deacetylated products (30 mg, 72%). ^{1}H NMR (400 MHz, $CDCl_3$, δ): 2.32–2.42 (9H, m, 3 × CH_3), 6.87–6.95 (1H, m, ArH), 7.12 (0.4H, d, *J* 8.8, ArH), 7.17–7.21 (0.6H, m, ArH), 7.33–7.47 (1H, m, ArH), 7.66–7.79 (2H, m, ArH), 8.08 (0.4H, *J* 8.8, ArH), 8.26 (0.6H, d, *J* 8.8, ArH). *m/z* (TOF ES+) 413.1 ([M + H]$^+$, 100%).

FST7. HBTU (228 mg, 0.60 mmol) was added to a solution of fisetin (35 mg, 0.12 mmol), Fmoc-Gly-OH (152 mg, 0.60 mmol) and Et_3N (0.13 mL, 1.80 mmol) in MeCN (4.0

mL) The resulting solution was stirred at room temperature overnight. The solvent was removed under reduced pressure and then EtOAc (10 mL) was added. This solution was washed with $KHSO_4$ solution (1.0 M, 2 × 10 mL) and $NaHCO_3$ solution (1.0 M, 2 × 10 mL). The organic phase was dried ($MgSO_4$), filtered and concentrated under reduced pressure to afford a residue which was immediately dissolved in a mixture of DMF/piperidine (3:1, 1.0 mL) and stirred for 2 h. Et_2O (3.0 mL) was added and the mixture was stirred for 5 min. The precipitate was collected by filtration and the filter cake was washed with more Et_2O (2 × 3.0 mL). The removal of residual Et_2O under reduced pressure afforded **FST7** as a white solid. (45 mg, 73%). ^{1}H NMR (400 MHz, DMSO-d_6, δ): 3.95–4.12 (8H, 4 × C*H*$_2$NH$_2$), 7.43 (1H, d, *J* 8.8, 2.2 ArH), 7.56 (1H, d, *J* 8.8, ArH), 7.76 (1H, d, *J* 2.2, ArH), 7.91 (1H, d, *J* 2.2, ArH), 7.93 (1H, d, *J* 8.8, 2.2 ArH), 8.17 (1H, d, *J* 8.8, ArH), 8.80 (8H, br s, 4 × NH_2). *m/z* (TOF ES+) 515.1 ($[M + H]^+$, 100%).

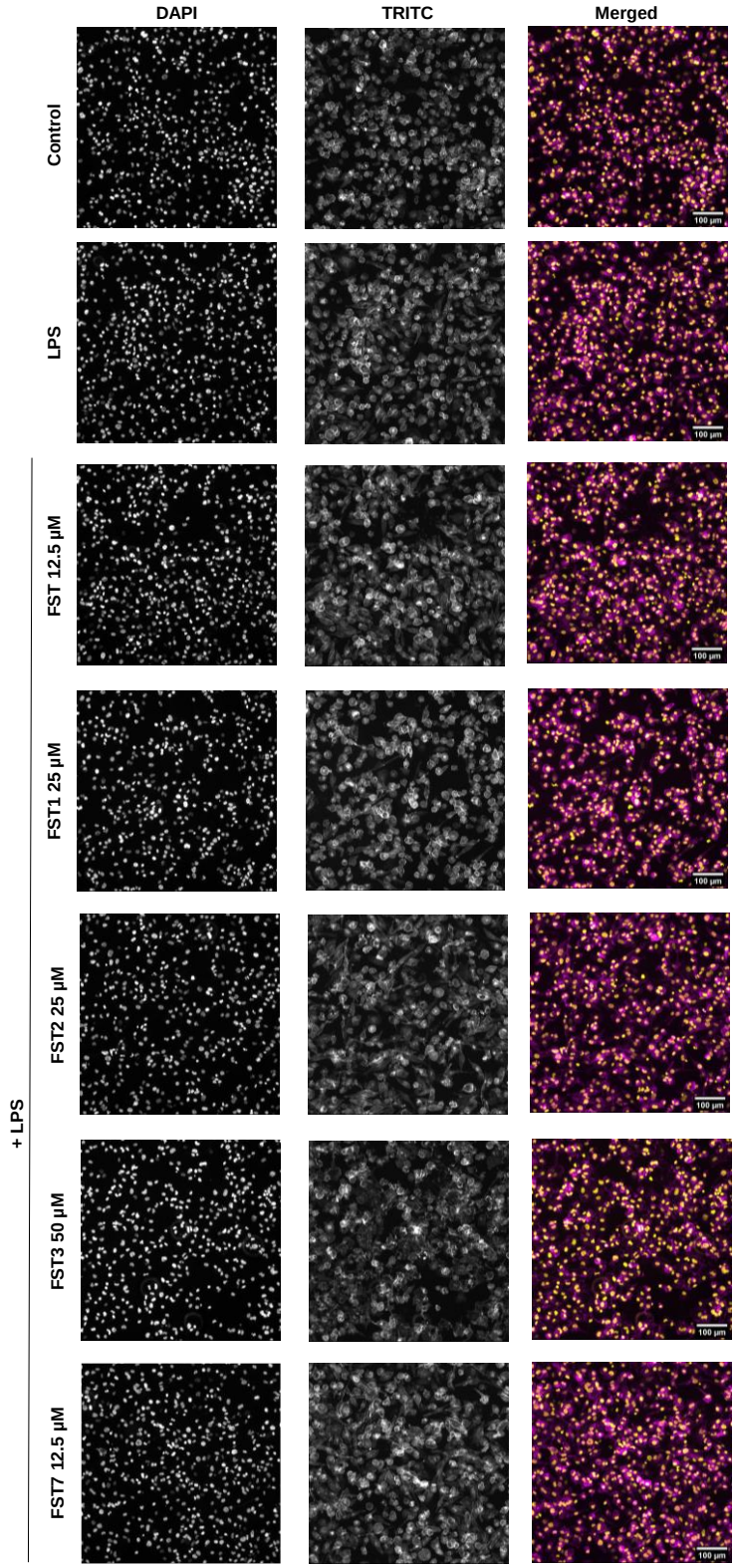

Supplementary Figure S10. Effect of the highest concentration of each active molecule, namely FST, FST1, FST2, FST3 and FST7, on cellular density and morphology, as observed under a fluorescence microscope. The DAPI channel shows cell nuclei, while the TRITC channel displays the cytoskeleton.

Chapter IV – Discussion, conclusions and future perspectives

4.1. Discussion

4.1.1. ER stress, protein aggregation and neurodegeneration

Proteins are complex macromolecules that, in order to function, must attain and maintain their so-called native state, while keeping conformational flexibility. Some proteins do not possess a stable three-dimensional conformation, acquiring their structure after performing their interactions. Proteins that behave like this include tau and α-synuclein, which renders them prone to aggregation. Misfolded proteins aggregate because they display hydrophobic amino-acid residues outwards, while properly folded proteins possess their hydrophobic residues inwards. This aggregation may result in amorphous or fibrillary aggregates (482).

A **molecular chaperone** is a protein that contributes to the successful folding of a given protein, not integrating its structure (483). Protein quality control and the homeostasis of the proteome is regulated by a network of molecular chaperones to promote protein folding and refolding and ubiquitin-proteasome system and autophagy to degrade aggregated and terminally misfolded proteins (482). Molecular chaperones ensure proteostasis by participating in *de novo* folding, refolding, assembly, trafficking and assistance in the degradation of proteins (482). A small molecule that assists the protein folding process is termed a **chemical chaperone**. Molecules of this kind are frequently unable to directly bind proteins. Accordingly, they enhance protein folding through different mechanisms. Chemical chaperones are further divided in osmolytes (e. g. glycerol) and hydrophobic compounds (e. g. 4-phenylbutyrate). If any molecule, regardless of its chemical class or origin, can bind a specific protein and aid it attain its functional conformation, this molecule is a **pharmacological chaperone** (34, 484).

In this work, we have described the ability of several natural molecules to counter ER stress. The chemical structures of those discussed in this section are presented in **Figure 42**.

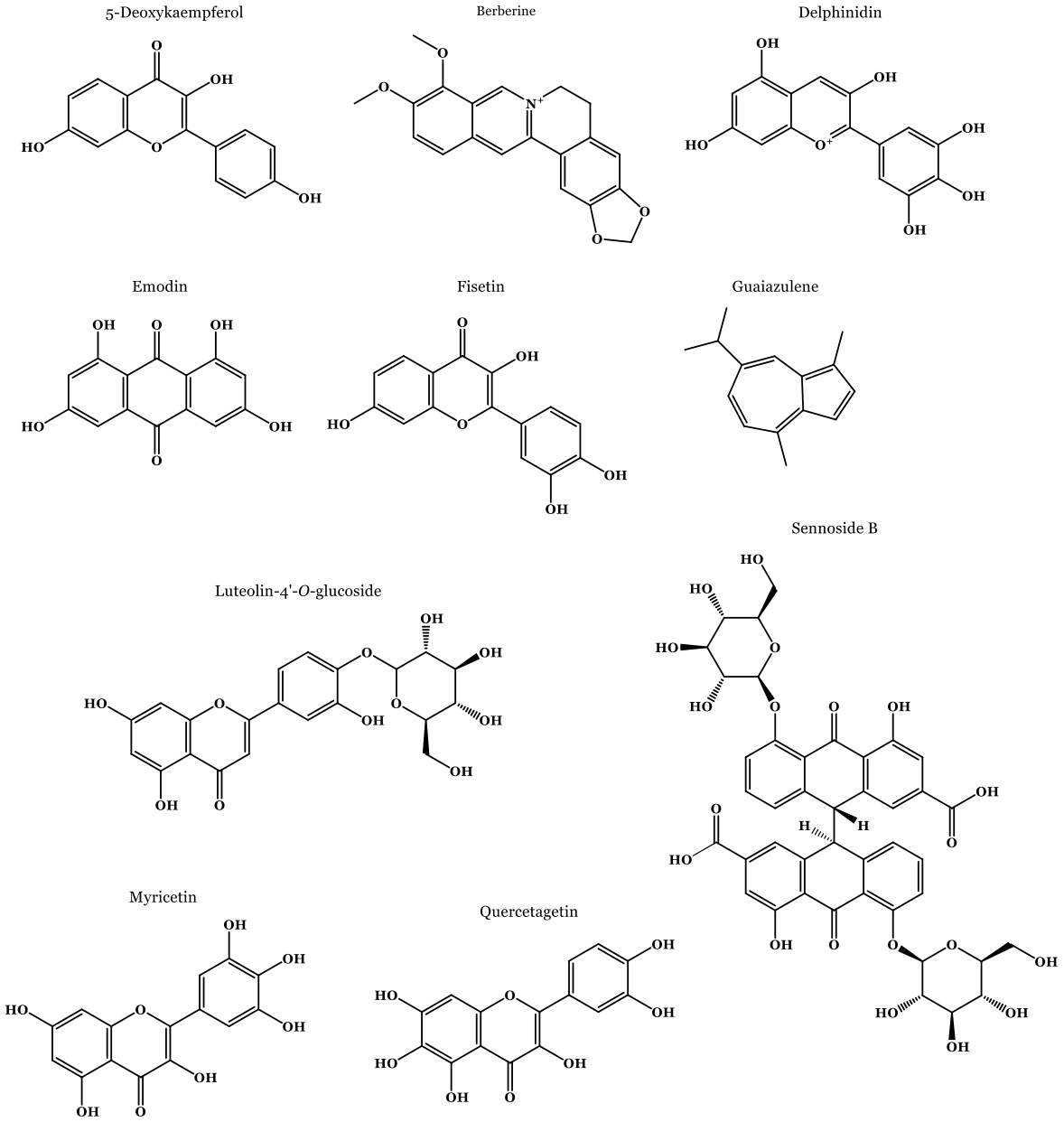

Figure 42. Chemical structures of the natural products discussed throughout this section.

Fisetin was effective at reducing protein aggregation in fibroblasts, and delphinidin proved to be effective in different contexts, since it could ameliorate the parameters under analysis in a cell model of neurodegeneration, but also in fibroblasts, hence having concluded that delphinidin could be a promising candidate to counter neurodegeneration. The observation of strongly reduced protein aggregation and concomitant normalization of chaperone expression hints that both natural molecules may act as chemical or pharmacological chaperones, although further studies would be necessary to confirm this hypothesis. At this point, it is not possible to classify them as such.

The literature refers the neuroprotective potential of **fisetin**. This molecule has been confirmed to inhibit tau aggregation by interacting with the protein, preventing the

formation of β-strands, approximately from 10 μM, in human embryonic kidney 293 (HEK293) cells (485). It has also been described as an inhibitor of β-amyloid fibrillation in HT22 murine neuroblastoma cells (≈ 40 μM) (375). Furthermore, this molecule has been described as neuroprotective due to its antioxidant and anti-inflammatory properties, as well as promoting neurotrophy (486, 487). By enhancing the antioxidant machinery of the cell and increasing glutathione levels, fisetin reduces intracellular ROS, leading to extended neuron lifespan (456, 468). In this thesis, this molecule proved to be effective against β-amyloid aggregation on MRC-5 fibroblasts at the tested concentration of 50 μM. However, when evaluated using the presented model of neurodegeneration, no beneficial effects of were detected. Even though reports of the literature are mentioned herein that describe otherwise, these studies have used shorter incubation periods and distinct cell models. This shortcoming of the molecule indicates that we could benefit from synthesizing less cytotoxic and/or more potent derivatives of this natural product. In fact, we have tested a library of fisetin derivatives towards this effect; however, the goal was not achieved as the molecules failed to produce significant results (data not shown).

Delphinidin has been described as a conveyor on multiple beneficial bioactivities, ranging from anticancer to antidiabetic, as reviewed elsewhere (488). Anthocyanins, the glycosylated counterparts of anthocyanidins, are biosynthesized by the phenylpropanoid pathway, glycosylated at C-3 or C-3 and C-5 (489). To this day, thirty-one anthocyanidins have been identified, along with more than five hundred anthocyanins (488). There are six dietary anthocyanidins, namely delphinidin, cyanidin, malvidin, pelargonidin, peonidin and petunidin, and they differ between one another solely in the substitution pattern at C-3' and C-5' by hydrogen, hydroxyl or methoxyl groups (488). It is thereby likely that at least some anthocyanidins can share the bioactivities of delphinidin described herein. In this regard, it is relevant to mention that malvidin and pelargonidin are herein reported as inactive against ER stress, since they failed to preserve Ca^{2+} homeostasis in MRC-5 cells. This hints at the relevance of the hydroxyl groups of delphinidin to its bioactivity. However, it remains to be clarified if these molecules could be active in higher concentrations, or if they can positively modulate ER stress signaling without impacting Ca^{2+} in the experimental conditions described herein.

Of particular relevance to the results obtained under the scope of this thesis is that anthocyanins have been observed before to cross the blood-brain-barrier, since they can accumulate and multiple organs, including the brain (489, 490). From 13 μM, delphinidin has inhibited $A\beta_{25-35}$ (10 μM) induced toxicity towards PC12 cells, and this neuroprotective effect was attributed to the preservation of Ca^{2+} levels upon insult. Tau phosphorylation was also observed to decrease (491). Delphinidin-3-*O*-glucoside, cyanidin-3-*O*-glucoside and petunidin-3-*O*-glucoside, the three major anthocyanins from *Glycine max* (L.) Merr., are

reported as neuroprotective in concentration from 2 to 25 μg/ml, having been effective against oxidative stress and the ROS-dependent activation of ASK1-JNK/p38 pathways is SK-N-SH cells (492). While there are no other accounts in literature of the potential of delphinidin to reduce ER stress apart from the work included in this thesis, delphinidin-3-*O*-galactoside is described as protective against ER stress in mouse hepatocytes, reducing *ddit3* expression and XBP1 splicing resulting from the effect of (–)-epigallocatechin-3-gallate (493).

There are, however, reports of very low blood-brain-barrier permeability of anthocyanins, and the suggestion that the neuroprotective effects of these molecules are merely a byproduct of improved brain circulation (494). On the other hand, the results discussed herein imply that delphinidin exerts a direct effect upon the preservation of neuronal fitness. Further studies are necessary to clarify the capacity of the anthocyanidin to cross the blood-brain-barrier, and, if its permeability falls short, to develop new strategies to aid the molecule reach its target.

It would be relevant to analyse the potential of fisetin and delphinidin as chemical or pharmacological chaperones, since the latter are seen as a potential new strategy to treat neurodegenerative diseases (484), and our results open that possibility.

Relevantly, it was determined that delphinidin occupies a rather distinct chemical space than that of the other elements of the chemical library. This is a valuable information to take into consideration when designing future studies, as the definition of this space constitutes a tool to select similar compounds to maximize the identification of active molecules while optimizing the use of resources.

4.1.2. ER stress and cancer

Cancer cells rely on protective UPR activation to counter the permanent stress that is inflicted on the ER by their aberrant metabolism. On the other hand, cell death resulting from deleterious UPR signaling has been shown to be elicited in cancer cells upon activation of each major signaling branch of the UPR (380). This renders the molecules berberine and emodin as promising to be leads in the development of new strategies against one of the heaviest burdens to modern society, since they display the ability to selectively induce deleterious UPR signaling in cancer cell models.

The isoquinoline alkaloid **berberine** has been proven to induce autophagy in cancer cells, and that the mechanism of action implicates increased expression of *HSPA5*, since, upon knockdown of this gene, autophagy was inhibited. In the results presented herein, the increase in the expression of this gene in AGS cells was not observed. However, the compound did increase said expression in A549 cells under these experimental conditions.

A possible explanation for this difference is that the referred study was conducted in a different cell model, namely HCT-116 cells (human colon carcinoma cells), suggesting that the effect may be cell type-specific (495). Furthermore, in the mentioned study, the tested concentration that produced this effect was much higher: 120 μM at an incubation period of 24 h, which by itself could explain why berberine at 50 μM failed to exert this effect on AGS cells after 16 h. Since berberine increased other ER stress related genes in these conditions (i. e. *atf4*, *ddit3* and *edem1*), it is plausible that it could also enhance the expression of *hspa5* in a different setting. Importantly, the molecule at 100 μm did not induce *hspa5* increase in the non-malignant HL-7702 cells, human liver cells (495). This further evidences the selectivity of the molecule to induce ER stress upon cancerous cells. In a different work, berberine (100 μM) induced apoptotic cell death in the human cervical epidermoid carcinoma cell line CaSki. In this cell model, the alkaloid disrupted Ca^{2+} homeostasis, increased ROS, lowered the $\Delta\Psi_m$ and activated caspase-3 (496). This mechanism of action shares the disruption of the $\Delta\Psi_m$ and Ca^{2+} homeostasis with our results. We did not, however, observe increased activity of caspase-3, but we did notice berberine-induced activation of caspase-4 in both tested cell models.

In the glioblastoma cell line T98G, berberine (from approximately 150 μM at 24 h of incubation) exacerbated ROS production, impacted Ca^{2+} levels and modulated several UPR-related proteins, namely BiP, CHOP, phosphorylated PERK and eIF2α. These authors also observed caspase-3 and -9 activation. Furthermore, the cytotoxic effect of berberine was reverted by co-incubation with salubrinal, as we observed in A549 cells. Salubrinal maintains eIF2α phosphorylation, and therefore can magnify the protective signaling of the UPR. In that case, it resulted in an increase in the level of Bcl-2 with a concomitant decrease in Bax and caspase and PARP activation (497). It is also described that caspase-4 can engage in regulated cell death mechanisms induced by ER stress with or without the activation of other caspases (498), and the latter mechanism of action is suggested by our results.

Whether caspase-3 can be induced by this molecule on AGS and A549 cells could be clarified with dose-response studies over multiple endpoints, in order to rule out the involvement of this protease in other experimental conditions. Furthermore, the involvement of other mitochondrial proteins in the organized cell death mechanisms could also be clarified, namely assessing Bcl-2 and Bax levels.

Finally, it is worth mentioning that there has been a considerable effort to investigate the potential of berberine against cancer, attributing it a myriad of other mechanisms of action, as is reviewed elsewhere (499).

Emodin occurs in free form or glycosylated in several plant families, namely Rhamnaceae, Polygonaceae, Fabaceae and Asteraceae, occurring also in fungi of the genuses *Aspergillus*, *Cladosporium*, *Chaetomium*, *Penicillium* and *Penicilliosis*. In plants,

it derives from acetate *via* the acetate-malonate pathway, while in fungi it derives from acetyl-CoA by the polyketide pathway (500). This anthraquinone presents preclinical potential against multiple cancer types, with several mechanisms of action reported, notably converging towards apoptosis through the mitochondrial pathway (501, 502). However, this was not the mechanism that we uncovered in A549 cells, since we did not detect increases in caspase activation. Emodin at 25-50 μM induced ROS-mediated, JNK- and RIP1-dependent necroptosis in several renal cancer cell lines without caspase activation (503), which is concurrent to the mechanism of action we have observed in A549 cells. In primary human T cells, emodin induced ER stress, as observed by upregulation of the UPR biomarkers GRP78, ATF4, XBP1 and CHOP, Ca^{2+} release, ROS production, compromised $\Delta\Psi_m$, and activating caspases -4, -9 and -3 (504). This occurred after 72 h of incubation and at higher concentrations (150 μM), and also in a different experimental model. At 72 h of incubation, Su et al. report caspase-3 activation by emodin from 20 μM in A549 and also in H1299 lung cancer cells. Notably, increased CHOP expression was detected, reinforcing that the effect of emodin is ER stress-dependent (505).

The results presented herein, along with these reports in the literature, warrant for a future for this compound as a drug lead.

4.1.3. ER stress and inflammation

The course of inflammation involves enhanced protein synthesis of inflammatory mediators, including cytokines, chemokines and transcription factors. This fact can, by itself, present a strain on the homeostasis of the ER. Concurrently, ER stress and inflammation are connected in a myriad of ways that remain to be fully understood (506, 507). In this scope, we identified natural products that can modulate both ER stress signaling and inflammation, by inhibiting NF-κB activation, ROS overproduction, caspase-1 activation, pro-inflammatory cytokine release and UPR-related gene expression. The model used in this work is based on the LPS-induced activation of the UPR, which has been observed before (508-511).

Most of the molecules described herein as dually active against inflammation and ER stress, namely 5-deoxykaempferol, berberine, guaiazulene, luteolin-4'-*O*-glucoside, myricetin, sennoside B and quercetagetin, are present in the human diet. **5-Deoxykaempferol** occurs in plants from the Fabaceae family, namely *Anthyllis vulneraria* L. (226) and *Astragalus beckari* (512). *Astragalus* species have been used as food supplements (513), while this genus is also important in traditional medicine (514). Furthermore, since the Fabaceae family is one of the most important in agriculture, it is likely that this compound may be identified in more dietary plants. **Berberine** has been

obtained from plants such as *Berberis vulgaris* L. (common barberry) and *Coptis chinensis* Franch. (Chinese goldthread) for use in traditional medicines for many years (515). The fruits of *B. vulgaris* are used for human consumption in many countries (516). Nowadays, this alkaloid is available in food supplements (517). Evidence of the versatility of the bioactivities of natural products is the described effect of berberine throughout this work, where this molecule decreased the activity of caspase-1, an inflammatory caspase, in THP-1 macrophages. The activation of this caspase indicates that the assembly of the multimeric complex known as the inflammasome has occurred (518-520). Along with cytokine release, this is a hallmark of inflammatory signaling. Furthermore, the ER plays a part in the process of inflammasome activation. It was for these reasons that the capacity of the selected molecules to inhibit pro-inflammatory cytokine release (namely of IL-6, TNF-α and IL-1β) and caspase-1 activation was evaluated.

On the other hand, we have discussed how this molecule induced the activation the of the inflammatory caspase-4 in AGS and A549 cells. Taken together, these results indicate that the cytotoxicity of berberine is exerted specifically against cancer cells. THP-1 macrophages derive from an acute monocytic leukemia. However, our experimental conditions implicated their differentiation to macrophages, and, in this process, they cease to multiply. This might be the reason why berberine was not toxic to this cell line in the same concentration (50 μM), and inhibited LPS-induced inflammatory caspases in these cells while it could activate caspase-4 in cancer cells. Considering this, it could be fruitful to further explore the potential of this molecule in the context of protein aggregation, since it was dropped in this study because it failed to preserve Ca^{2+} homeostasis.

The sesquiterpenoid **guaiazulene** occurs in *Matricaria chamomilla* L. (521), while the anthraquinone **sennoside B** naturally occurs in *Rheum* sp. (522). These plants are widely used as herbal medicines, while chamomile (*M. chamomilla*) oil is used by the food industry (523) and rhubarb (*Rheum* sp.) is consumed as food (524). **Myricetin** is present in the human diet through multiple sources, from fruits and berries to wine and tea, among others, being that the highest amounts have been observed in strawberries (*Fragaria* x *ananassa* (Weston) Duchesne ex Rozier) and spinach (*Spinacia oleracea* L.) (525, 526). This molecule is already established as a nutraceutical (525). **Quercetagetin** has been observed to occur in tangerines (*Citrus unshiu* Marcow.) (440). **Luteolin-4'-*O*-glucoside** has been identified in *Olea europaea* L. leaves, adding potential value to this agricultural byproduct even though, to the extent of our knowledge, the molecule is yet to be identified in the fruits (527). These facts deem these molecules suitable not only for drug development, but also as nutraceuticals that convey health benefits against inflammation and ER stress.

Fisetin, as mentioned in **Section 3.5.1.**, is present in vegetable species of high dietary relevance. Even though natural phenylpropanoids often occur in glycosylated forms, there

is little knowledge of glycosylated derivatives of fisetin in nature, unlike what occurs with analogs such as resokaempferol, liquiritigenin or fustin (461). Based on the knowledge of the remarkable bioactivity of this molecule, we synthesized derivatives proved to be a effective strategy to enhance the potential of this compound to be incorporated in strategies to counter inflammation and ER stress-related disorders.

4.1.4. Limitations of this work

As a final remark, it is important to pinpoint the main shortcomings of this work, since this identification will outline possible strategies to circumvent these limitations in future studies.

One of the barriers of this work can be identified early on in the process of molecule selection. The chemical library was assembled resorting to in-house available products, which resulted in the selection of compounds at random, and thus could have resulted in the obtainment of an entirely different set of molecules.

Considering logistical constraints resulting from the number of molecules involved, each experimental condition was tested solely at one time point, which may have been insufficient to detect the activity of some compounds.

Concurrently, for the same reason, the molecules were tested at the single concentration of 50 μM throughout most of this work, the exceptions being fisetin and derivatives. The latter were tested in more concentrations, since they composed a more limited group of molecules. In the future, selecting the elements of a chemical library with the aid of the definition of a target chemical space can mitigate all of the constraints mentioned above.

This work includes a model of LPS-induced inflammation and UPR activation. While it was shown that incubation with LPS results in UPR activation, it was not possible to determine if the observed anti-inflammatory effect of the molecules of interest was due to the ER stress inhibition potential or *vice-versa*.

Another limitation lies on the fact that experiments were performed solely in cell lines. Specifically, monocultures were used. In the future, and having identified the mechanisms of action in these cell models, co-cultures of different cell types could be implemented, since these models more closely mimic the *in vivo* environments. *In vivo* assessment would also be important to confirm the results obtained *in vitro*.

Furthermore, only two cancer cell lines were used. Even though they represent two of the most common cancer types, testing only two models does not allow to understand the potential of the compounds against overall cancer types.

Throughout this study, the ability of the molecules under study to cross the blood-brain-barrier was not analyzed. This is of particular relevance in the scope of neurodegenerative diseases and, thus, it would be ideal to assess the potential of delphinidin to permeate this barrier.

4.2. Conclusions and future perspectives

The aging of the global population increases the burden that chronic diseases represent to modern society, particularly in developed countries. The involvement of ER stress signaling in the pathogenesis of virtually any chronic disease is currently established, and since this area of research is currently seething, the years to come are expected to add to the current bulk of knowledge of how these signaling pathways can be modulated to improve our quality of life and even our life expectancy.

The obtained results indicate a role for natural products in attaining this goal, since it was possible to identify modulators of ER stress signaling in different contexts, namely neurodegeneration, cancer and inflammation. For each case, the mechanism of action was studied and the cellular and molecular targets identified. Notably, this concerns solely commercially available natural molecules. Some of these molecules have been known for decades, yet their potential has not been fully explored. The pool of bioactive molecules is expected to increase, both with the addition of currently known molecules and with the contribution of the significant portion of Nature's potential that remains untapped. Currently, computer-aided drug discovery approaches are enhancing the speed and increasing the cost efficiency of the drug discovery process. Taking this into account, this line of work can certainly benefit from approaches that allow experimenting with multitudes of compounds and molecular targets. These new strategies will certainly facilitate the arrival of new products to the shelves in the years to come.

CHAPTER V – References

1. Schwarz DS, Blower MD. The endoplasmic reticulum: structure, function and response to cellular signaling. Cellular and Molecular Life Sciences. 2016;73:79-94.

2. Lavoie C, Roy L, Lanoix J, Taheri M, Young R, Thibault G, et al. Taking organelles apart, putting them back together and creating new ones: Lessons from the endoplasmic reticulum. Progress in Histochemistry and Cytochemistry. 2011;46(1):1-48.

3. Shibata Y, Voeltz GK, Rapoport TA. Rough sheets and smooth tubules. Cell. 2006;126(3):435-9.

4. Du Y, Ferro-Novick S, Novick P. Dynamics and inheritance of the endoplasmic reticulum. Journal of Cell Science. 2004;117(14):2871.

5. Joensuu M, Belevich I, Vihinen H, Kumar D, Rämö O, Lak B, et al. Structure and dynamics of the endoplasmic reticulum in cultured mammalian cells. European Microscopy Congress 2016: Proceedings, (Ed)2016. p. 69-70.

6. Braakman I, Hebert DN. Protein folding in the endoplasmic reticulum. Cold Spring Harbor Perspectives in Biology. 2013;5(5):a013201.

7. Farhan H, Rabouille C. Signalling to and from the secretory pathway. Journal of Cell Science. 2011;124(2):171-80.

8. Lee AR, Seo MJ, Kim J, Lee DM, Kim IY, Yoon MJ, et al. Lercanidipine Synergistically Enhances Bortezomib Cytotoxicity in Cancer Cells via Enhanced Endoplasmic Reticulum Stress and Mitochondrial Ca(2+) Overload. International journal of molecular sciences. 2019;20(24):6112.

9. Ellis CE, Naicker D, Basson KM, Botha CJ, Meintjes RA, Schultz RA. A fluorescent investigation of subcellular damage in H9c2 cells caused by pavetamine, a novel polyamine. Toxicology in Vitro. 2010;24(4):1258-65.

10. Zhao P, Xiao X, Kim AS, Leite MF, Xu J, Zhu X, et al. c-Jun inhibits thapsigargin-induced ER stress through up-regulation of DSCR1/Adapt78. Experimental Biology and Medicine. 2008;233(10):1289-300.

11. Pallet N, Bouvier N, Bendjallabah A, Rabant M, Flinois JP, Hertig A, et al. Cyclosporine-induced endoplasmic reticulum stress triggers tubular phenotypic changes and death. American Journal of Transplantation. 2008;8(11):2283-96.

12. Cole L, Davies D, Hyde GJ, Ashford AE. Brefeldin A affects growth, endoplasmic reticulum, Golgi bodies, tubular vacuole system, and secretory pathway in *Pisolithus tinctorius*. Fungal Genetics and Biology. 2000;29(2):95-106.

13. Peshenko IV, Olshevskaya EV, Dizhoor AM. Binding of guanylyl cyclase activating protein 1 (GCAP1) to retinal guanylyl cyclase (RetGC1). The role of individual EF-hands. The Journal of Biological Chemistry. 2008;283(31):21747-57.

14. Peng T, Bonamy GMC, Glory-Afshar E, Rines DR, Chanda SK, Murphy RF. Determining the distribution of probes between different subcellular locations through automated unmixing of subcellular patterns. Proceedings of the National Academy of Sciences of the United States of America. 2010;107(7):2944-9.

15. Abodeely M, DuBois KN, Hehl A, Stefanic S, Sajid M, DeSouza W, et al. A contiguous compartment functions as endoplasmic reticulum and endosome/lysosome in Giardia lamblia. Eukaryot Cell. 2009;8(11):1665-76.

16. Yoo S-A, You S, Yoon H-J, Kim D-H, Kim H-S, Lee K, et al. A novel pathogenic role of the ER chaperone GRP78/BiP in rheumatoid arthritis. J Exp Med. 2012;209(4):871-86.

17. Macedo AA, Silva APC, Mol JPS, Costa LF, Garcia LNN, Araújo MS, et al. The abcEDCBA-encoded ABC transporter and the virB operon-encoded type IV secretion system of *Brucella ovis* are critical for intracellular trafficking and survival in ovine monocyte-derived macrophages. PLOS One. 2015;10(9):e0138131-e.

18. McDonald L, Liu B, Taraboletti A, Whiddon K, Shriver LP, Konopka M, et al. Fluorescent flavonoids for endoplasmic reticulum cell imaging. Journal of Materials Chemistry B. 2016;4(48):7902-8.

19. Meinig JM, Fu L, Peterson BR. Synthesis of fluorophores that target small molecules to the endoplasmic reticulum of living mammalian cells. Angewandte Chemie (International ed in English). 2015;54(33):9696-9.

20. Schips TG, Vanhoutte D, Vo A, Correll RN, Brody MJ, Khalil H, et al. Thrombospondin-3 augments injury-induced cardiomyopathy by intracellular integrin inhibition and sarcolemmal instability. Nat Commun. 2019;10(1):76-.

21. Xie Q, Xu Y, Gao W, Zhang Y, Su J, Liu Y, et al. TAT-fused IP3R-derived peptide enhances cisplatin sensitivity of ovarian cancer cells by increasing ER Ca2+ release. International Journal of Molecular Medicine. 2018;41(2):809-17.

22. Sander G, Konrad A, Thurau M, Wies E, Leubert R, Kremmer E, et al. Intracellular localization map of human herpesvirus 8 proteins. Journal of Virology. 2008;82(4):1908-22.

23. de la Vega M, Burrows JF, McFarlane C, Govender U, Scott CJ, Johnston JA. The deubiquitinating enzyme USP17 blocks N-Ras membrane trafficking and activation but leaves K-Ras unaffected. The Journal of Biological Chemistry. 2010;285(16):12028-36.

24. Liu P, Zhao L, Pol J, Levesque S, Petrazzuolo A, Pfirschke C, et al. Crizotinib-induced immunogenic cell death in non-small cell lung cancer. Nat Commun. 2019;10(1):1486.

25. Cassimeris L, Engiles JB, Galantino-Homer H. Detection of endoplasmic reticulum stress and the unfolded protein response in naturally-occurring endocrinopathic equine laminitis. BMC Vet Res. 2019;15(1):24-.

26. Abdullahi A, Stanojcic M, Parousis A, Patsouris D, Jeschke MG. Modeling acute ER stress *in vivo* and *in vitro*. Shock. 2017;47(4):506-13.

27. Beghein E, Gettemans J. Nanobody technology: A versatile toolkit for microscopic imaging, protein-protein interaction analysis, and protein function exploration. Front Immunol. 2017;8(771).

28. Kirmiz M, Gillies TE, Dickson EJ, Trimmer JS. Neuronal ER–plasma membrane junctions organized by Kv2–VAP pairing recruit Nir proteins and affect phosphoinositide homeostasis. Journal of Biological Chemistry. 2019.

29. Buser DP, Schleicher KD, Prescianotto-Baschong C, Spiess M. A versatile nanobody-based toolkit to analyze retrograde transport from the cell surface. Proceedings of the National Academy of Sciences. 2018;115(27):E6227-E36.

30. Prole DL, Taylor CW. A genetically-encoded toolkit of functionalized nanobodies against fluorescent proteins for visualizing and manipulating intracellular signalling. bioRxiv. 2019:544700.

31. Van Audenhove I, Gettemans J. Nanobodies as Versatile Tools to Understand, Diagnose, Visualize and Treat Cancer. EBioMedicine. 2016;8:40-8.

32. Muyldermans S. Nanobodies: Natural Single-Domain Antibodies. Annual Review of Biochemistry. 2013;82(1):775-97.

33. Hassanzadeh-Ghassabeh G, Devoogdt N, Pauw PD, Vincke C, Muyldermans S. Nanobodies and their potential applications. Nanomedicine. 2013;8(6):1013-26.

34. Pereira David M, Valentão P, Andrade PB. Tuning protein folding in lysosomal storage diseases: the chemistry behind pharmacological chaperones. Chemical Science. 2018;9(7):1740-52.

35. Halperin L, Jung J, Michalak M. The many functions of the endoplasmic reticulum chaperones and folding enzymes. IUBMB Life. 2014;66(5):318-26.

36. Otero JH, Lizák B, Hendershot LM. Life and death of a BiP substrate. Seminars in Cell & Developmental Biology. 2010;21(5):472-8.

37. Kraus A, Michalak M. Endoplasmic reticulum dynamics and calcium signaling. In: Krebs J, Michalak M, editors. New Comprehensive Biochemistry. 41: Elsevier; 2007. p. 199-218.

38. Schäfer A, Wolf DH. Sec61p is part of the endoplasmic reticulum-associated degradation machinery. The EMBO Journal. 2009;28(19):2874-84.

39. Eletto D, Dersh D, Argon Y. GRP94 in ER quality control and stress responses. Seminars in Cell & Developmental Biology. 2010;21(5):479-85.

40. Ross CA, Poirier MA. Protein aggregation and neurodegenerative disease. Nature Medicine. 2004;10(7):S10-S7.

41. Groenning M, Olsen L, van de Weert M, Flink JM, Frokjaer S, Jørgensen FS. Study on the binding of Thioflavin T to β-sheet-rich and non-β-sheet cavities. Journal of Structural Biology. 2007;158(3):358-69.

42. Beriault DR, Werstuck GH. Detection and quantification of endoplasmic reticulum stress in living cells using the fluorescent compound, Thioflavin T. Biochimica et Biophysica Acta (BBA) - Molecular Cell Research. 2013;1833(10):2293-301.

43. Jin H, Komita M, Aoe T. The role of BiP retrieval by the KDEL receptor in the early secretory pathway and its effect on protein quality control and neurodegeneration. Frontiers in Molecular Neuroscience. 2017;10:222.

44. Dewal MB, DiChiara AS, Antonopoulos A, Taylor RJ, Harmon CJ, Haslam SM, et al. XBP1s links the unfolded protein response to the molecular architecture of mature *N*-glycans. Chemistry & Biology. 2015;22(10):1301-12.

45. Fusakio ME, Willy JA, Wang Y, Mirek ET, Al Baghdadi RJT, Adams CM, et al. Transcription factor ATF4 directs basal and stress-induced gene expression in the unfolded protein response and cholesterol metabolism in the liver. Molecular Biology of the Cell. 2016;27(9):1536-51.

46. Giorgi C, Bonora M, Sorrentino G, Missiroli S, Poletti F, Suski JM, et al. p53 at the endoplasmic reticulum regulates apoptosis in a Ca^{2+}-dependent manner. Proceedings of the National Academy of Sciences of the United States of America. 2015;112(6):1779-84.

47. Graham RM, Hernandez F, Puerta N, De Angulo G, Webster KA, Vanni S. Resveratrol augments ER stress and the cytotoxic effects of glycolytic inhibition in neuroblastoma by downregulating Akt in a mechanism independent of SIRT1. Experimental & Molecular Medicine. 2016;48:e210.

48. Higa A, Taouji S, Lhomond S, Jensen D, Fernandez-Zapico ME, Simpson JC, et al. Endoplasmic reticulum stress-activated transcription factor ATF6α requires the disulfide isomerase PDIA5 to modulate chemoresistance. Molecular and Cellular Biology. 2014;34(10):1839-49.

49. Lajoie P, Moir RD, Willis IM, Snapp EL. Kar2p availability defines distinct forms of endoplasmic reticulum stress in living cells. Molecular Biology of the Cell. 2012;23(5):955-64.

50. Capitani M, Sallese M. The KDEL receptor: New functions for an old protein. FEBS Letters. 2009;583(23):3863-71.

51. Watanabe MM, Laurindo FRM, Fernandes DC. Methods of measuring protein disulfide isomerase activity: a critical overview. Frontiers in Chemistry. 2014;2:73.

52. Xu S, Sankar S, Neamati N. Protein disulfide isomerase: a promising target for cancer therapy. Drug Discovery Today. 2014;19(3):222-40.

53. Raturi A, Vacratsis PO, Seslija D, Lee L, Mutus B. A direct, continuous, sensitive assay for protein disulphide-isomerase based on fluorescence self-quenching. Biochem J. 2005;391(Pt 2):351-7.

54. Cai H, Wang CC, Tsou CL. Chaperone-like activity of protein disulfide isomerase in the refolding of a protein with no disulfide bonds. Journal of Biological Chemistry. 1994;269(40):24550-2.

55. Smith AM, Chan J, Oksenberg D, Urfer R, Wexler DS, Ow A, et al. A high-throughput turbidometric assay for screening inhibitors of protein disulfide isomerase activity. Journal of Biomolecular Screening. 2004;9(7):614-20.

56. Ogen-Shtern N, Ben David T, Lederkremer GZ. Protein aggregation and ER stress. Brain Research. 2016;1648:658-66.

57. Lewy TG, Grabowski JM, Bloom ME. BiP: master regulator of the unfolded protein response and crucial factor in flavivirus biology The Yale Journal of Biology and Medicine. 2017;90(2):291-300.

58. Shim SM, Choi HR, Sung KW, Lee YJ, Kim ST, Kim D, et al. The endoplasmic reticulum–residing chaperone BiP is short-lived and metabolized through *N*-terminal arginylation. Science Signaling. 2018;11(511).

59. Ren C, Li X, Li X, Xie Y, Fu H, Yan Z, et al. RNAi of Grp78 may disturb the fusion of ICR mouse palate cultured *in vitro*. Human & Experimental Toxicology. 2017;37(2):196-204.

60. Dey S, Savant S, Teske BF, Hatzoglou M, Calkhoven CF, Wek RC. Transcriptional repression of ATF4 gene by CCAAT/enhancer-binding protein β (C/EBPβ) differentially regulates integrated stress response. The Journal of Biological Chemistry. 2012;287(26):21936-49.

61. Dey S, Baird TD, Zhou D, Palam LR, Spandau DF, Wek RC. Both transcriptional regulation and translational control of ATF4 are central to the integrated stress response. The Journal of Biological Chemistry. 2010;285(43):33165-74.

62. Yi S, Shi W, Wang H, Ma C, Zhang X, Wang S, et al. Endoplasmic reticulum stress PERK-ATF4-CHOP pathway is associated with hypothalamic neuronal injury in different durations of stress in rats. Frontiers in Neuroscience. 2017;11:152.

63. Li Y, Guo Y, Tang J, Jiang J, Chen Z. New insights into the roles of CHOP-induced apoptosis in ER stress. Acta Biochimica et Biophysica Sinica. 2014;46(8):629-40.

64. Urra H, Dufey E, Lisbona F, Rojas-Rivera D, Hetz C. When ER stress reaches a dead end. Biochimica et Biophysica Acta (BBA) - Molecular Cell Research. 2013;1833(12):3507-17.

65. Ohoka N, Yoshii S, Hattori T, Onozaki K, Hayashi H. TRB3, a novel ER stress-inducible gene, is induced via ATF4–CHOP pathway and is involved in cell death. The EMBO Journal. 2005;24(6):1243-55.

66. Rozpędek W, Pytel D, Mucha B, Leszczyńska H, Diehl JA, Majsterek I. The role of the PERK/eIF2α/ATF4/CHOP signaling pathway in tumor progression during endoplasmic reticulum stress. Current Molecular Medicine. 2016;16(6):533-44.

67. Nishitoh H. CHOP is a multifunctional transcription factor in the ER stress response. The Journal of Biochemistry. 2012;151(3):217-9.

68. Adjibade P, Grenier St-Sauveur V, Bergeman J, Huot M-E, Khandjian EW, Mazroui R. DDX3 regulates endoplasmic reticulum stress-induced ATF4 expression. Scientific Reports. 2017;7(1):13832.

69. Halliday M, Radford H, Sekine Y, Moreno J, Verity N, le Quesne J, et al. Partial restoration of protein synthesis rates by the small molecule ISRIB prevents neurodegeneration without pancreatic toxicity. Cell Death Dis. 2015;6(3):e1672.

70. Matsuoka M, Komoike Y. Experimental evidence shows salubrinal, an eIF2α dephosphorylation inhibitor, reduces xenotoxicant-induced cellular damage. International Journal of Molecular Sciences. 2015;16(7):16275-87.

71. Gong T, Wang Q, Lin Z, Chen M-l, Sun G-z. Endoplasmic reticulum (ER) stress inhibitor salubrinal protects against ceramide-induced SH-SY5Y cell death. Biochemical and Biophysical Research Communications. 2012;427(3):461-5.

72. Correia da Silva D, Andrade PB, Valentão P, Pereira DM. Neurotoxicity of the steroidal alkaloids tomatine and tomatidine is RIP1 kinase- and caspase-independent and involves the eIF2α branch of the endoplasmic reticulum. The Journal of Steroid Biochemistry and Molecular Biology. 2017;171:178-86.

73. Hamamura K, Nishimura A, Iino T, Takigawa S, Sudo A, Yokota H. Chondroprotective effects of salubrinal in a mouse model of osteoarthritis. Bone & Joint Research. 2015;4(5):84-92.

74. Nakajima S, Chi Y, Gao K, Kono K, Yao J. eIF2α-independent inhibition of TNF-α-triggered NF-κB activation by salubrinal. Biological and Pharmaceutical Bulletin. 2015;38(9):1368-74.

75. Hamamura K, Nishimura A, Chen A, Takigawa S, Sudo A, Yokota H. Salubrinal acts as a Dusp2 inhibitor and suppresses inflammation in anti-collagen antibody-induced arthritis. Cellular Signalling. 2015;27(4):828-35.

76. Gao B, Zhang X-y, Han R, Zhang T-t, Chen C, Qin Z-h, et al. The endoplasmic reticulum stress inhibitor salubrinal inhibits the activation of autophagy and neuroprotection induced by brain ischemic preconditioning. Acta Pharmacologica Sinica. 2013;34(5):657-66.

77. Tan H-P, Guo Q, Hua G, Chen J-X, Liang J-C. Inhibition of endoplasmic reticulum stress alleviates secondary injury after traumatic brain injury. Neural Regeneration Research. 2018;13(5):827-36.

78. Rubovitch V, Barak S, Rachmany L, Goldstein RB, Zilberstein Y, Pick CG. The neuroprotective effect of salubrinal in a mouse model of traumatic brain injury. NeuroMolecular Medicine. 2015;17(1):58-70.

79. Wu CT, Sheu ML, Tsai KS, Chiang CK, Liu SH. Salubrinal, an eIF2α dephosphorylation inhibitor, enhances cisplatin-induced oxidative stress and nephrotoxicity in a mouse model. Free Radical Biology and Medicine. 2011;51(3):671-80.

80. Maurel M, Chevet E, Tavernier J, Gerlo S. Getting RIDD of RNA: IRE1 in cell fate regulation. Trends in Biochemical Sciences. 2014;39(5):245-54.

81. Tam Arvin B, Koong Albert C, Niwa M. Ire1 has distinct catalytic mechanisms for XBP1/HAC1 splicing and RIDD. Cell Reports. 2014;9(3):850-8.

82. Chen Y, Brandizzi F. IRE1: ER stress sensor and cell fate executor. Trends in Cell Biology. 2013;23(11):547-55.

83. Lee K, Tirasophon W, Shen X, Michalak M, Prywes R, Okada T, et al. IRE1-mediated unconventional mRNA splicing and S2P-mediated ATF6 cleavage merge to regulate XBP1 in signaling the unfolded protein response. Genes & Development. 2002;16(4):452-66.

84. Calfon M, Zeng H, Urano F, Till JH, Hubbard SR, Harding HP, et al. IRE1 couples endoplasmic reticulum load to secretory capacity by processing the XBP-1 mRNA. Nature. 2002;415:92.

85. Back SH, Schröder M, Lee K, Zhang K, Kaufman RJ. ER stress signaling by regulated splicing: IRE1/HAC1/XBP1. Methods. 2005;35(4):395-416.

86. Nakamura D, Tsuru A, Ikegami K, Imagawa Y, Fujimoto N, Kohno K. Mammalian ER stress sensor IRE1β specifically down-regulates the synthesis of secretory pathway proteins. FEBS Letters. 2011;585(1):133-8.

87. Hirota M, Kitagaki M, Itagaki H, Aiba S. Quantitative measurement of spliced XBP1 mRNA as an indicator of endoplasmic reticulum stress. The Journal of Toxicological Sciences. 2006;31(2):149-56.

88. Lee A-H, Iwakoshi NN, Glimcher LH. XBP-1 regulates a subset of endoplasmic reticulum resident chaperone genes in the unfolded protein response. Molecular and Cellular Biology. 2003;23(21):7448-59.

89. Bouchecareilh M, Caruso M-E, Roby P, Parent S, Rouleau N, Taouji S, et al. AlphaScreen®-based characterization of the bifunctional kinase/RNase IRE1α: a novel and atypical drug target. Journal of Biomolecular Screening. 2010;15(4):406-17.

90. Bouchecareilh M, Higa A, Fribourg S, Moenner M, Chevet E. Peptides derived from the bifunctional kinase/RNase enzyme IRE1α modulate IRE1α activity and protect cells from endoplasmic reticulum stress. The FASEB Journal. 2011;25(9):3115-29.

91. Lee H, Noh J-Y, Oh Y, Kim Y, Chang J-W, Chung C-W, et al. IRE1 plays an essential role in ER stress-mediated aggregation of mutant huntingtin via the inhibition of autophagy flux. Human Molecular Genetics. 2011;21(1):101-14.

92. Tufanli O, Telkoparan Akillilar P, Acosta-Alvear D, Kocaturk B, Onat UI, Hamid SM, et al. Targeting IRE1 with small molecules counteracts progression of atherosclerosis. Proceedings of the National Academy of Sciences. 2017;114(8):E1395-E404.

93. Shoulders Matthew D, Ryno Lisa M, Genereux Joseph C, Moresco James J, Tu Patricia G, Wu C, et al. Stress-independent activation of XBP1s and/or ATF6 reveals three functionally diverse ER proteostasis environments. Cell Reports. 2013;3(4):1279-92.

94. Iwawaki T, Akai R, Kohno K, Miura M. A transgenic mouse model for monitoring endoplasmic reticulum stress. Nature Medicine. 2003;10:98.

95. Dong H, Chen L, Chen X, Gu H, Gao G, Gao Y, et al. Dysregulation of unfolded protein response partially underlies proapoptotic activity of bortezomib in multiple myeloma cells. Leukemia & Lymphoma. 2009;50(6):974-84.

96. Hollien J, Weissman JS. Decay of endoplasmic reticulum-localized mRNAs during the unfolded protein response. Science. 2006;313(5783):104-7.

97. Drogat B, Auguste P, Nguyen DT, Bouchecareilh M, Pineau R, Nalbantoglu J, et al. IRE1 signaling is essential for ischemia-induced vascular endothelial growth factor-A expression and contributes to angiogenesis and tumor growth *in vivo*. Cancer Research. 2007;67(14):6700-7.

98. Cross BCS, Bond PJ, Sadowski PG, Jha BK, Zak J, Goodman JM, et al. The molecular basis for selective inhibition of unconventional mRNA splicing by an IRE1-binding small molecule. Proceedings of the National Academy of Sciences of the United States of America. 2012;109(15):E869-E78.

99. Jiang D, Niwa M, Koong AC. Targeting the IRE1α-XBP1 branch of the unfolded protein response in human diseases. Seminars in Cancer Biology. 2015;33:48-56.

100. Zhang L, Nosak C, Sollazzo P, Odisho T, Volchuk A. IRE1 inhibition perturbs the unfolded protein response in a pancreatic β-cell line expressing mutant proinsulin, but does not sensitize the cells to apoptosis. BMC Cell Biology. 2014;15:29-.

101. Stewart C, Estrada A, Kim P, Wang D, Wei Y, Gentile C, et al. Regulation of IRE1α by the small molecule inhibitor 4μ8C in hepatoma cells. Endoplasmic reticulum stress in diseases. 2017;4(1):1-10.

102. Chan SMH, Lowe MP, Bernard A, Miller AA, Herbert TP. The inositol-requiring enzyme 1 (IRE1α) RNAse inhibitor, 4μ8C, is also a potent cellular antioxidant. Biochemical Journal. 2018;475(5):923-9.

103. Qiu Q, Zheng Z, Chang L, Zhao Y-S, Tan C, Dandekar A, et al. Toll-like receptor-mediated IRE1α activation as a therapeutic target for inflammatory arthritis. The EMBO Journal. 2013;32(18):2477-90.

104. Abuaita BH, Burkholder KM, Boles BR, O'Riordan MX. The endoplasmic reticulum stress sensor inositol-requiring enzyme 1α augments bacterial killing through sustained oxidant production. mBio. 2015;6(4).

105. Chien W, Ding L-W, Sun Q-Y, Torres-Fernandez LA, Tan SZ, Xiao J, et al. Selective inhibition of unfolded protein response induces apoptosis in pancreatic cancer cells. Oncotarget. 2014;5(13):4881-94.

106. Papandreou I, Denko NC, Olson M, Van Melckebeke H, Lust S, Tam A, et al. Identification of an IRE1a endonuclease specific inhibitor with cytotoxic activity against human multiple myeloma. Blood. 2011;117(4):1311-4.

107. Ming J, Ruan S, Wang M, Ye D, Fan N, Meng Q, et al. A novel chemical, STF-083010, reverses tamoxifen-related drug resistance in breast cancer by inhibiting IRE1/XBP1. Oncotarget. 2015;6(38):40692-703.

108. Guo F-J, Xiong Z, Lu X, Ye M, Han X, Jiang R. ATF6 upregulates XBP1s and inhibits ER stress-mediated apoptosis in osteoarthritis cartilage. Cellular Signalling. 2014;26(2):332-42.

109. Yu Z, Sheng H, Liu S, Zhao S, Glembotski CC, Warner DS, et al. Activation of the ATF6 branch of the unfolded protein response in neurons improves stroke outcome. Journal of Cerebral Blood Flow & Metabolism. 2017;37(3):1069-79.

110. Wang Y, Shen J, Arenzana N, Tirasophon W, Kaufman RJ, Prywes R. Activation of ATF6 and an ATF6 DNA binding site by the ER stress response. Journal of Biological Chemistry. 2000.

111. Yoshida H, Okada T, Haze K, Yanagi H, Yura T, Negishi M, et al. ATF6 activated by proteolysis binds in the presence of NF-Y (CBF) directly to the cis-acting element responsible for the mammalian unfolded protein response. Molecular and Cellular Biology. 2000;20(18):6755-67.

112. Sommer T, Jarosch E. BiP binding keeps ATF6 at bay. Developmental Cell. 2002;3(1):1-2.

113. Dadey DYA, Kapoor V, Khudanyan A, Urano F, Kim AH, Thotala D, et al. The ATF6 pathway of the ER stress response contributes to enhanced viability in glioblastoma. Oncotarget. 2016;7(2):2080-92.

114. Galindo I, Hernáez B, Muñoz-Moreno R, Cuesta-Geijo MA, Dalmau-Mena I, Alonso C. The ATF6 branch of unfolded protein response and apoptosis are activated to promote African swine fever virus infection. Cell Death & Disease. 2012;3(7):e341.

115. Gallagher CM, Garri C, Cain EL, Ang KK-H, Wilson CG, Chen S, et al. Ceapins are a new class of unfolded protein response inhibitors, selectively targeting the ATF6α branch. eLife. 2016;5:e11878.

116. Plate L, Cooley CB, Chen JJ, Paxman RJ, Gallagher CM, Madoux F, et al. Small molecule proteostasis regulators that reprogram the ER to reduce extracellular protein aggregation. eLife. 2016;5:e15550.

117. Blackwood EA, Azizi K, Thuerauf DJ, Paxman RJ, Plate L, Kelly JW, et al. Pharmacologic ATF6 activation confers global protection in widespread disease models by reprograming cellular proteostasis. Nat Commun. 2019;10(1):187-.

118. Bommiasamy H, Popko B. Animal models in the study of the unfolded protein response. Methods in enzymology. 2011;491:91-109.

119. Shen J, Prywes R. ER stress signaling by regulated proteolysis of ATF6. Methods. 2005;35(4):382-9.

120. Wang S, Binder P, Fang Q, Wang Z, Xiao W, Liu W, et al. Endoplasmic reticulum stress in the heart: insights into mechanisms and drug targets. British Journal of Pharmacology. 2017;175(8):1293-304.

121. Teske BF, Wek SA, Bunpo P, Cundiff JK, McClintick JN, Anthony TG, et al. The eIF2 kinase PERK and the integrated stress response facilitate activation of ATF6 during endoplasmic reticulum stress. Molecular Biology of the Cell. 2011;22(22):4390-405.

122. Liu Z-W, Zhu H-T, Chen K-L, Dong X, Wei J, Qiu C, et al. Protein kinase RNA- like endoplasmic reticulum kinase (PERK) signaling pathway plays a major role in reactive oxygen species (ROS)- mediated endoplasmic reticulum stress- induced apoptosis in diabetic cardiomyopathy. Cardiovascular Diabetology. 2013;12:158-.

123. Rozpędek W, Markiewicz Ł, Diehl JA, Pytel D, Majsterek I. Unfolded protein response and PERK kinase as a new therapeutic target in the pathogenesis of Alzheimer's disease. Current Medicinal Chemistry. 2015;22(27):3169-84.

124. Goodall JC, Wu C, Zhang Y, McNeill L, Ellis L, Saudek V, et al. Endoplasmic reticulum stress-induced transcription factor, CHOP, is crucial for dendritic cell IL-23 expression. Proceedings of the National Academy of Sciences. 2010;107(41):17698-703.

125. Koyama M, Furuhashi M, Ishimura S, Mita T, Fuseya T, Okazaki Y, et al. Reduction of endoplasmic reticulum stress by 4-phenylbutyric acid prevents the development of hypoxia-induced pulmonary arterial hypertension. American Journal of Physiology-Heart and Circulatory Physiology. 2014;306(9):H1314-H23.

126. Fu J, Zhao L, Wang L, Zhu X. Expression of markers of endoplasmic reticulum stress-induced apoptosis in the placenta of women with early and late onset severe pre-eclampsia. Taiwanese Journal of Obstetrics and Gynecology. 2015;54(1):19-23.

127. Bian Z-M, Elner SG, Elner VM. Dual involvement of caspase-4 in inflammatory and ER stress-induced apoptotic responses in human retinal pigment epithelial cells. Investigative ophthalmology & visual science. 2009;50(12):6006-14.

128. Pereira DM, Valentao P, Correia-da-Silva G, Teixeira N, Andrade PB. Translating endoplasmic reticulum biology into the clinic: a role for ER-targeted natural products? Natural Product Reports. 2015;32(5):705-22.

129. Jung TW, Choi KM. Pharmacological modulators of endoplasmic reticulum stress in metabolic diseases. International Journal of Molecular Sciences. 2016;17(2):192.

130. Liu H, Yang J, Li L, Shi W, Yuan X, Wu L. The natural occurring compounds targeting endoplasmic reticulum stress. Evidence-Based Complementary and Alternative Medicine. 2016;2016:7831282-.

131. Gonzalez-Teuber V, Albert-Gasco H, Auyeung VC, Papa FR, Mallucci GR, Hetz C. Small Molecules to Improve ER Proteostasis in Disease. Trends in Pharmacological Sciences. 2019;40(9):684-95.

132. Hetz C, Axten JM, Patterson JB. Pharmacological targeting of the unfolded protein response for disease intervention. Nature Chemical Biology. 2019;15(8):764-75.

133. Kusama H, Kon K, Ikejima K, Arai K, Aoyama T, Uchiyama A, et al. Sodium 4-phenylbutyric acid prevents murine acetaminophen hepatotoxicity by minimizing endoplasmic reticulum stress. Journal of Gastroenterology. 2017;52(5):611-22.

134. Wiley JC, Meabon JS, Frankowski H, Smith EA, Schecterson LC, Bothwell M, et al. Phenylbutyric acid rescues endoplasmic reticulum stress-induced suppression of APP proteolysis and prevents apoptosis in neuronal cells. PLOS One. 2010;5(2):e9135.

135. Ayala P, Montenegro J, Vivar R, Letelier A, Urroz PA, Copaja M, et al. Attenuation of endoplasmic reticulum stress using the chemical chaperone 4-phenylbutyric acid prevents cardiac fibrosis induced by isoproterenol. Experimental and Molecular Pathology. 2012;92(1):97-104.

136. Romero-Ramírez L, Nieto-Sampedro M, Barreda-Manso MA. All roads go to Salubrinal: endoplasmic reticulum stress, neuroprotection and glial scar formation. Neural Regeneration Research. 2015;10(12):1926-7.

137. Boyce M, Bryant KF, Jousse C, Long K, Harding HP, Scheuner D, et al. A selective inhibitor of eIF2α dephosphorylation protects cells from ER stress. Science. 2005;307(5711):935-9.

138. Fujiwara T, Oda K, Yokota S, Takatsuki A, Ikehara Y. Brefeldin A causes disassembly of the Golgi complex and accumulation of secretory proteins in the endoplasmic reticulum. 1988;263(34):18545-52.

139. Moon JL, Kim SY, Shin SW, Park J-W. Regulation of brefeldin A-induced ER stress and apoptosis by mitochondrial NADP+-dependent isocitrate dehydrogenase. Biochemical and Biophysical Research Communications. 2012;417(2):760-4.

140. Ivessa NE, De Lemos-Chiarandini C, Gravotta D, Sabatini DD, Kreibich G. The brefeldin A-induced retrograde transport from the Golgi apparatus to the endoplasmic reticulum depends on calcium sequestered to intracellular stores. Journal of Biological Chemistry. 1995;270(43):25960-7.

141. Tatu U, Braakman I, Helenius A. Membrane glycoprotein folding, oligomerization and intracellular transport: effects of dithiothreitol in living cells. The EMBO Journal. 1993;12(5):2151-7.

142. Yin J, Wang Y, Gu L, Fan N, Ma Y, Peng Y. Palmitate induces endoplasmic reticulum stress and autophagy in mature adipocytes: Implications for apoptosis and inflammation. International Journal of Molecular Medicine. 2015;35(4):932-40.

143. Pillon NJ, Chan KL, Zhang S, Mejdani M, Jacobson MR, Ducos A, et al. Saturated fatty acids activate caspase-4/5 in human monocytes, triggering IL-1β and IL-18 release. American Journal of Physiology-Endocrinology and Metabolism. 2016;311(5):E825-E35.

144. Lytton J, Westlin M, Hanley MR. Thapsigargin inhibits the sarcoplasmic or endoplasmic reticulum Ca-ATPase family of calcium pumps. Journal of Biological Chemistry. 1991;266(26):17067-71.

145. Thastrup O, Cullen PJ, Drøbak BK, Hanley MR, Dawson AP. Thapsigargin, a tumor promoter, discharges intracellular Ca2+ stores by specific inhibition of the endoplasmic reticulum Ca2(+)-ATPase. Proceedings of the National Academy of Sciences of the United States of America. 1990;87(7):2466-70.

146. Wang H, Wang X, Ke Z-J, Comer AL, Xu M, Frank JA, et al. Tunicamycin-induced unfolded protein response in the developing mouse brain. Toxicology and Applied Pharmacology. 2015;283(3):157-67.

147. Bravo-Sagua R, Rodriguez AE, Kuzmicic J, Gutierrez T, Lopez-Crisosto C, Quiroga C, et al. Cell death and survival through the endoplasmic reticulum-mitochondrial axis. Current Molecular Medicine. 2013;13(2):317-29.

148. Wieckowski MR, Giorgi C, Lebiedzinska M, Duszynski J, Pinton P. Isolation of mitochondria-associated membranes and mitochondria from animal tissues and cells. Nature Protocols. 2009;4(11):1582-90.

149. Shamas-Din A, Brahmbhatt H, Leber B, Andrews DW. BH3-only proteins: Orchestrators of apoptosis. Biochimica et Biophysica Acta (BBA) - Molecular Cell Research. 2011;1813(4):508-20.

150. Rodriguez D, Rojas-Rivera D, Hetz C. Integrating stress signals at the endoplasmic reticulum: The BCL-2 protein family rheostat. Biochimica et Biophysica Acta (BBA) - Molecular Cell Research. 2011;1813(4):564-74.

151. Breckenridge DG, Germain M, Mathai JP, Nguyen M, Shore GC. Regulation of apoptosis by endoplasmic reticulum pathways. Oncogene. 2003;22(53):8608-18.

152. Obeng EA, Boise LH. Caspase-12 and caspase-4 are not required for caspase-dependent endoplasmic reticulum stress-induced apoptosis. Journal of Biological Chemistry. 2005;280(33):29578-87.

153. Binet F, Chiasson S, Girard D. Evidence that endoplasmic reticulum (ER) stress and caspase-4 activation occur in human neutrophils. Biochemical and Biophysical Research Communications. 2010;391(1):18-23.

154. Verma G, Datta M. The critical role of JNK in the ER-mitochondrial crosstalk during apoptotic cell death. Journal of Cellular Physiology. 2011;227(5):1791-5.

155. Csordás G, Weaver D, Hajnóczky G. Endoplasmic reticulum-mitochondrial contactology: structure and signaling functions. Trends in cell biology. 2018;28(7):523-40.

156. Chong WC, Shastri MD, Eri R. Endoplasmic Reticulum Stress and Oxidative Stress: A Vicious Nexus Implicated in Bowel Disease Pathophysiology. International journal of molecular sciences. 2017;18(4):771.

157. Sarkar DD, Edwards SK, Mauser JA, Suarez AM, Serowoky MA, Hudok NL, et al. Increased redox-sensitive green fluorescent protein reduction potential in the endoplasmic reticulum following glutathione-mediated dimerization. Biochemistry. 2013;52(19):3332-45.

158. Chaudhari N, Talwar P, Parimisetty A, Lefebvre d'Hellencourt C, Ravanan P. A molecular web: endoplasmic reticulum stress, inflammation, and oxidative stress. Front Cell Neurosci. 2014;8:213-.

159. Malhotra JD, Miao H, Zhang K, Wolfson A, Pennathur S, Pipe SW, et al. Antioxidants reduce endoplasmic reticulum stress and improve protein secretion. Proceedings of the National Academy of Sciences. 2008;105(47):18525-30.

160. Yuan Y, Xu X, Zhao C, Zhao M, Wang H, Zhang B, et al. The roles of oxidative stress, endoplasmic reticulum stress, and autophagy in aldosterone/mineralocorticoid receptor-induced podocyte injury. Laboratory Investigation. 2015;95(12):1374-86.

161. Hayashi T, Saito A, Okuno S, Ferrand-Drake M, Dodd RL, Nishi T, et al. Oxidative damage to the endoplasmic reticulum is implicated in ischemic neuronal cell death. Journal of Cerebral Blood Flow & Metabolism. 2003;23(10):1117-28.

162. Fujii J, Homma T, Kobayashi S, HG S. Mutual interaction between oxidative stress and endoplasmic reticulum stress in the pathogenesis of diseases specifically focusing on non-alcoholic fatty liver disease. World Journal of Biological Chemistry. 2018;9(1):1-15.

163. Li Y, Jiang W, Niu Q, Sun Y, Meng C, Tan L, et al. eIF2α-CHOP-BCl-2/JNK and IRE1α-XBP1/JNK signaling promote apoptosis and inflammation and support the proliferation of Newcastle disease virus. Cell Death & Disease. 2019;10(12):891.

164. Merksamer PI, Trusina A, Papa FR. Real-time redox measurements during endoplasmic reticulum stress reveal interlinked protein folding functions. Cell. 2008;135(5):933-47.

165. Kanekura K, Ishigaki S, Merksamer PI, Papa FR, Urano F. Establishment of a system for monitoring endoplasmic reticulum redox state in mammalian cells. Lab Invest. 2013;93(11):1254-8.

166. Hoseki J, Oishi A, Fujimura T, Sakai Y. Development of a stable ERroGFP variant suitable for monitoring redox dynamics in the ER. Bioscience reports. 2016;36(2):e00316.

167. Mekahli D, Bultynck G, Parys JB, De Smedt H, Missiaen L. Endoplasmic reticulum calcium depletion and disease. Cold Spring Harbor Perspectives in Biology. 2011;3(6):a004317.

168. McMullen DC, Kean WS, Verma A, Cole JT, Watson WD. A microplate technique to simultaneously assay calcium accumulation in endoplasmic reticulum and SERCA release of inorganic phosphate. Biological Procedures Online. 2012;14:4-.

169. Krebs J, Agellon LB, Michalak M. Ca^{2+} homeostasis and endoplasmic reticulum (ER) stress: An integrated view of calcium signaling. Biochemical and Biophysical Research Communications. 2015;460(1):114-21.

170. Katsuhiko M. IP3 receptor/Ca^{2+} channel: from discovery to new signaling concepts. Journal of Neurochemistry. 2007;102(5):1426-46.

171. Martinez NA, Ayala AM, Martinez M, Martinez-Rivera FJ, Miranda JD, Silva WI. Caveolin-1 regulates the P2Y2 receptor signaling in human 1321N1 astrocytoma cells. Journal of Biological Chemistry. 2016;291(23):12208-22.

172. Martínez M, Martínez NA, Silva WI. Measurement of the intracellular calcium concentration with Fura-2 AM using a fluorescence plate reader. Bio-Protocol 2017;7(14):e2411.

173. Roe MW, Lemasters JJ, Herman B. Assessment of Fura-2 for measurements of cytosolic free calcium. Cell Calcium. 1990;11(2):63-73.

174. Egnatchik RA, Leamy AK, Jacobson DA, Shiota M, Young JD. ER calcium release promotes mitochondrial dysfunction and hepatic cell lipotoxicity in response to palmitate overload. Molecular Metabolism. 2014;3(5):544-53.

175. Isomura M, Kotake Y, Masuda K, Miyara M, Okuda K, Samizo S, et al. Tributyltin-induced endoplasmic reticulum stress and its Ca^{2+}-mediated mechanism. Toxicology and Applied Pharmacology. 2013;272(1):137-46.

176. Cicek FA, Ozgur EO, Ozgur E, Ugur M. The interplay between plasma membrane and endoplasmic reticulum Ca^{2+}ATPases in agonist-induced temporal Ca^{2+} dynamics. Journal of Bioenergetics and Biomembranes. 2014;46(6):503-10.

177. Abcam. Fura 2 LeakRes K+ salt, fluorescent Ca2+ binding dye (ab142785) [Available from: https://www.abcam.com/fura-2-leakres-k-salt-fluorescent-ca2-binding-dye-ab142785.html.

178. Biotechnology SC. FURA-PE3/AM (CAS 172890-84-5) [Available from: https://www.scbt.com/scbt/product/fura-pe3-am-172890-84-5.

179. Yu L, Chen Y, Tooze SA. Autophagy pathway: Cellular and molecular mechanisms. Autophagy. 2018;14(2):207-15.

180. Metaxakis A, Ploumi C, Tavernarakis N. Autophagy in age-associated neurodegeneration. Cells. 2018;7(5):37.

181. Saha S, Panigrahi DP, Patil S, Bhutia SK. Autophagy in health and disease: A comprehensive review. Biomedicine & Pharmacotherapy. 2018;104:485-95.

182. Bento CF, Renna M, Ghislat G, Puri C, Ashkenazi A, Vicinanza M, et al. Mammalian autophagy: How does it work? 2016;85(1):685-713.

183. Doherty J, Baehrecke EH. Life, death and autophagy. Nature Cell Biology. 2018;20(10):1110-7.

184. Dikic I, Elazar Z. Mechanism and medical implications of mammalian autophagy. Nature Reviews Molecular Cell Biology. 2018;19(6):349-64.

185. Yorimitsu T, Nair U, Yang Z, Klionsky DJ. Endoplasmic reticulum stress triggers autophagy. The Journal of Biological Chemistry. 2006;281(40):30299-304.

186. Ogata M, Hino S-i, Saito A, Morikawa K, Kondo S, Kanemoto S, et al. Autophagy is activated for cell survival after endoplasmic reticulum stress. Molecular and Cellular Biology. 2006;26(24):9220.

187. Yan C, Liu J, Gao J, Sun Y, Zhang L, Song H, et al. IRE1 promotes neurodegeneration through autophagy-dependent neuron death in the Drosophila model of Parkinson's disease. Cell Death & Disease. 2019;10(11):800.

188. Kabir MF, Kim H-R, Chae H-J. Endoplasmic reticulum stress and autophagy. Endoplasmic Reticulum: Angel Català, IntechOpen; 2018.

189. Cai Y, Arikkath J, Yang L, Guo M-L, Periyasamy P, Buch S. Interplay of endoplasmic reticulum stress and autophagy in neurodegenerative disorders. Autophagy. 2016;12(2):225-44.

190. Hosoi T, Nomura J, Tanaka K, Ozawa K, Nishi A, Nomura Y. Link between endoplasmic reticulum stress and autophagy in neurodegenerative diseases. Endoplasmic Reticulum Stress in Diseases2017. p. 37.

191. Cheng X, Liu, H., Jiang, C., Fang, L., Chen, C., Zhang, X., Jiang, Z. Connecting endoplasmic reticulum stress to autophagy through IRE1/JNK/beclin-1 in breast cancer cells. International Journal of Molecular Medicine 2014;34(3):772-81.

192. Luhr M, Torgersen ML, Szalai P, Hashim A, Brech A, Staerk J, et al. The kinase PERK and the transcription factor ATF4 play distinct and essential roles in autophagy resulting from tunicamycin-induced ER stress. Journal of Biological Chemistry. 2019.

193. Liu Z, Lv Y, Zhao N, Guan G, Wang J. Protein kinase R-like ER kinase and its role in endoplasmic reticulum stress-decided cell fate. Cell Death & Disease. 2015;6(7):e1822-e.

194. Avivar-Valderas A, Salas E, Bobrovnikova-Marjon E, Diehl JA, Nagi C, Debnath J, et al. PERK integrates autophagy and oxidative stress responses to promote survival during extracellular matrix detachment. Molecular and Cellular Biology. 2011;31(17):3616-29.

195. Sharma M, Bhattacharyya S, Sharma KB, Chauhan S, Asthana S, Abdin MZ, et al. Japanese encephalitis virus activates autophagy through XBP1and ATF6 ER stress sensors in neuronal cells. Journal of General Virology. 2017;98:1027-39.

196. Gade P, Ramachandran G, Maachani UB, Rizzo MA, Okada T, Prywes R, et al. An IFN-γ–stimulated ATF6–C/EBP-β–signaling pathway critical for the expression of Death Associated Protein Kinase 1 and induction of autophagy. Proceedings of the National Academy of Sciences. 2012;109(26):10316-21.

197. Sun F, Xu X, Wang X, Zhang B. Regulation of autophagy by Ca^{2+}. Tumour Biology. 2016;37(12):15467-76.

198. Høyer-Hansen M, Jäättelä M. Connecting endoplasmic reticulum stress to autophagy by unfolded protein response and calcium. Cell Death & Differentiation. 2007;14(9):1576-82.

199. Yoshii SR, Mizushima N. Monitoring and measuring autophagy. International Journal of Molecular Sciences. 2017;18(9):1865.

200. Wang L, Liu L, Qin L, Luo Q, Zhang Z. Visualization of reticulophagy in living cells using an endoplasmic reticulum-targeted p62 mutant. Science China Life Sciences. 2017;60(4):333-44.

201. Islam F, Gopalan V, Lam AK-y. RETREG1 (FAM134B): A new player in human diseases: 15 years after the discovery in cancer. Journal of Cellular Physiology. 2018;233(6):4479-89.

202. Liao Y, Duan B, Zhang Y, Zhang X, Xia B. Excessive ER-phagy mediated by the autophagy receptor FAM134B results in ER stress, the unfolded protein response, and cell death in HeLa cells. Journal of Biological Chemistry. 2019.

203. Chiramel AI, Dougherty JD, Nair V, Robertson SJ, Best SM. FAM134B, the selective autophagy receptor for endoplasmic reticulum turnover, inhibits replication of ebola virus strains Makona and Mayinga. J Infect Dis. 2016;214(suppl 3):S319-S25.

204. Forrester A, De Leonibus C, Grumati P, Fasana E, Piemontese M, Staiano L, et al. A selective ER-phagy exerts procollagen quality control via a Calnexin-FAM134B complex. The EMBO journal. 2019;38(2):e99847.

205. Chen Q, Teng J, Chen J. ATL3, a cargo receptor for reticulophagy. Autophagy. 2019;15(8):1465-6.

206. Fitzmaurice C, Allen C, Barber RM, Barregard L, Bhutta ZA, Brenner H, et al. Global, regional, and national cancer incidence, mortality, years of life lost, years lived with disability, and disability-adjusted life-years for 32 cancer groups, 1990 to 2015: A systematic analysis for the Global Burden of Disease study. JAMA Oncol. 2017;3(4):524-48.

207. Vandewynckel Y-P, Laukens D, Geerts A, Bogaerts E, Paridaens A, Verhelst X, et al. The paradox of the unfolded protein response in cancer. Anticancer Res. 2013;33(11):4683-94.

208. Dejeans N, Glorieux C, Guenin S, Beck R, Sid B, Rousseau R, et al. Overexpression of GRP94 in breast cancer cells resistant to oxidative stress promotes high levels of cancer cell proliferation and migration: Implications for tumor recurrence. Free Radical Biology and Medicine. 2012;52(6):993-1002.

209. Huang LW, Lin CY, Lee CC, Liu TZ, Jeng CJ. Overexpression of GRP78 is associated with malignant transformation in epithelial ovarian tumors. Appl Immunohistochem Mol Morphol. 2012;20(4):381-5.

210. Zhang XX, Li HD, Zhao S, Zhao L, Song HJ, Wang G, et al. The cell surface GRP78 facilitates the invasion of hepatocellular carcinoma cells. Biomed Res Int. 2013;2013:917296.

211. Niu Z, Wang M, Zhou L, Yao L, Liao Q, Zhao Y. Elevated GRP78 expression is associated with poor prognosis in patients with pancreatic cancer. Sci Rep. 2015;5:16067.

212. Zheng Y-Z, Cao Z-G, Hu X, Shao Z-M. The endoplasmic reticulum stress markers GRP78 and CHOP predict disease-free survival and responsiveness to chemotherapy in breast cancer. Breast Cancer Research and Treatment. 2014;145(2):349-58.

213. Arap MA, Lahdenranta J, Mintz PJ, Hajitou A, Sarkis AS, Arap W, et al. Cell surface expression of the stress response chaperone GRP78 enables tumor targeting by circulating ligands. Cancer Cell. 2004;6(3):275-84.

214. Fang P, Xiang L, Huang S, Jin L, Zhou G, Zhuge L, et al. IRE1α-XBP1 signaling pathway regulates IL-6 expression and promotes progression of hepatocellular carcinoma. Oncol Lett. 2018;16(4):4729-36.

215. Hiramatsu N, Chiang W-C, Kurt TD, Sigurdson CJ, Lin JH. Multiple mechanisms of unfolded protein response–induced cell death. The American Journal of Pathology. 2015;185(7):1800-8.

216. Wang M, Kaufman RJ. The impact of the endoplasmic reticulum protein-folding environment on cancer development. Nature Reviews Cancer. 2014;14(9):581-97.

217. Wang WA, Groenendyk J, Michalak M. Endoplasmic reticulum stress associated responses in cancer. Biochim Biophys Acta. 2014;1843(10):2143-9.

218. Mimura N, Fulciniti M, Gorgun G, Tai YT, Cirstea D, Santo L, et al. Blockade of XBP1 splicing by inhibition of IRE1α is a promising therapeutic option in multiple myeloma. Blood. 2012;119(24):5772-81.

219. Ribeiro V, Andrade PB, Valentão P, Pereira DM. Benzoquinones from *Cyperus* spp. trigger IRE1α-independent and PERK-dependent ER stress in human stomach cancer cells and are novel proteasome inhibitors. Phytomedicine. 2019;63:153017.

220. Fan C, Yang Y, Liu Y, Jiang S, Di S, Hu W, et al. Icariin displays anticancer activity against human esophageal cancer cells via regulating endoplasmic reticulum stress-mediated apoptotic signaling. Scientific Reports. 2016;6(1):21145.

221. Cerezo M, Rocchi S. New anti-cancer molecules targeting HSPA5/BIP to induce endoplasmic reticulum stress, autophagy and apoptosis. Autophagy. 2017;13(1):216-7.

222. Mihailidou C, Chatzistamou I, Papavassiliou AG, Kiaris H. Improvement of chemotherapeutic drug efficacy by endoplasmic reticulum stress. Endocr Relat Cancer. 2015;22(2):229-38.

223. Xipell E, Aragón T, Martínez-Velez N, Vera B, Idoate MA, Martínez-Irujo JJ, et al. Endoplasmic reticulum stress-inducing drugs sensitize glioma cells to temozolomide through downregulation of MGMT, MPG, and Rad51. Neuro Oncol. 2016;18(8):1109-19.

224. Hoozemans JJM, van Haastert ES, Nijholt DAT, Rozemuller AJM, Eikelenboom P, Scheper W. The unfolded protein response is activated in pretangle neurons in Alzheimer's disease hippocampus. The American journal of pathology. 2009;174(4):1241-51.

225. Roussel BD, Kruppa AJ, Miranda E, Crowther DC, Lomas DA, Marciniak SJ. Endoplasmic reticulum dysfunction in neurological disease. Lancet Neurol. 2013;12(1):105-18.

226. Lee KM, Lee KW, Byun S, Jung SK, Seo SK, Heo Y-S, et al. 5-Deoxykaempferol plays a potential therapeutic role by targeting multiple signaling pathways in skin cancer. Cancer Prevention Research. 2010;3(4):454-65.

227. Hitomi J, Katayama T, Eguchi Y, Kudo T, Taniguchi M, Koyama Y, et al. Involvement of caspase-4 in endoplasmic reticulum stress-induced apoptosis and Aβ-induced cell death. The Journal of Cell Biology. 2004;165(3):347-56.

228. Mercado G, Valdés P, Hetz C. An ERcentric view of Parkinson's disease. Trends Mol Med. 2013;19(3):165-75.

229. Mercado G, Castillo V, Soto P, Sidhu A. ER stress and Parkinson's disease: Pathological inputs that converge into the secretory pathway. Brain Res. 2016;1648(Pt B):626-32.

230. Colla E, Coune P, Liu Y, Pletnikova O, Troncoso JC, Iwatsubo T, et al. Endoplasmic reticulum stress is important for the manifestations of α-synucleinopathy in vivo. J Neurosci. 2012;32(10):3306-20.

231. Libby P. Inflammatory mechanisms: the molecular basis of inflammation and disease. Nutr Rev. 2007;65(12 Pt 2):S140-6.

232. Kany S, Vollrath JT, Relja B. Cytokines in inflammatory disease. International Journal of Molecular Sciences. 2019;20(23):6008.

233. Chen L, Deng H, Cui H, Fang J, Zuo Z, Deng J, et al. Inflammatory responses and inflammation-associated diseases in organs. Oncotarget. 2017;9(6):7204-18.

234. Zhang K, Kaufman RJ. From endoplasmic-reticulum stress to the inflammatory response. Nature. 2008;454(7203):455-62.

235. Boehm T, Swann JB. Origin and evolution of adaptive immunity. Annual Review of Animal Biosciences. 2014;2(1):259-83.

236. Stanley AC, Lacy P. Pathways for cytokine secretion. Physiology. 2010;25(4):218-29.

237. Das A, Sinha M, Datta S, Abas M, Chaffee S, Sen CK, et al. Monocyte and macrophage plasticity in tissue repair and regeneration. The American journal of pathology. 2015;185(10):2596-606.

238. Gordon S, Taylor PR. Monocyte and macrophage heterogeneity. Nature Reviews Immunology. 2005;5(12):953-64.

239. Collin M, Bigley V. Human dendritic cell subsets: an update. Immunology. 2018;154(1):3-20.

240. Théry C, Amigorena S. The cell biology of antigen presentation in dendritic cells. Current Opinion in Immunology. 2001;13(1):45-51.

241. Galli SJ, Gaudenzio N, Tsai M. Mast cells in inflammation and disease: recent progress and ongoing concerns. Annual Review of Immunology. 2020;38(1):49-77.

242. Lichterman JN, Reddy SM. Mast cells: a new frontier for cancer immunotherapy. Cells. 2021;10(6):1270.

243. Shea-Donohue T, Stiltz J, Zhao A, Notari L. Mast cells. Curr Gastroenterol Rep. 2010;12(5):349-57.

244. Zitti B, Bryceson YT. Natural killer cells in inflammation and autoimmunity. Cytokine & Growth Factor Reviews. 2018;42:37-46.

245. Portales-Cervantes L, Dawod B, Marshall JS. Mast cells and natural killer cells - a potentially critical interaction. Viruses. 2019;11(6):514.

246. O'Sullivan TE, Sun JC, Lanier LL. Natural killer cell memory. Immunity. 2015;43(4):634-45.

247. Liew PX, Kubes P. The neutrophil's role during health and disease. Physiological Reviews. 2019;99(2):1223-48.

248. Silvestre-Roig C, Fridlender ZG, Glogauer M, Scapini P. Neutrophil diversity in health and disease. Trends Immunol. 2019;40(7):565-83.

249. Mayadas TN, Cullere X, Lowell CA. The multifaceted functions of neutrophils. Annual Review of Pathology: Mechanisms of Disease. 2014;9(1):181-218.

250. Kolaczkowska E, Kubes P. Neutrophil recruitment and function in health and inflammation. Nature Reviews Immunology. 2013;13(3):159-75.

251. Fulkerson PC, Rothenberg ME. Targeting eosinophils in allergy, inflammation and beyond. Nat Rev Drug Discov. 2013;12(2):117-29.

252. Klion AD, Ackerman SJ, Bochner BS. Contributions of eosinophils to human health and disease. Annu Rev Pathol. 2020;15:179-209.

253. Ishikawa H, Ma Z, Barber GN. STING regulates intracellular DNA-mediated, type I interferon-dependent innate immunity. Nature. 2009;461(7265):788-92.

254. Chieosilapatham P, Kiatsurayanon C, Umehara Y, Trujillo-Paez JV, Peng G, Yue H, et al. Keratinocytes: innate immune cells in atopic dermatitis. Clin Exp Immunol. 2021;204(3):296-309.

255. Song Y, Shen H, Schenten D, Shan P, Lee PJ, Goldstein DR. Aging enhances the basal production of IL-6 and CCL2 in vascular smooth muscle cells. Arteriosclerosis, Thrombosis, and Vascular Biology. 2012;32(1):103-9.

256. Tupin E, Kinjo Y, Kronenberg M. The unique role of natural killer T cells in the response to microorganisms. Nature Reviews Microbiology. 2007;5(6):405-17.

257. Bonilla FA, Oettgen HC. Adaptive immunity. Journal of Allergy and Clinical Immunology. 2010;125(2, Supplement 2):S33-S40.

258. Padron JG, Saito Reis CA, Kendal-Wright CE. The role of danger associated molecular patterns in human fetal membrane weakening. Frontiers in Physiology. 2020;11.

259. Dorrington MG, Fraser IDC. NF-κB signaling in macrophages: dynamics, crosstalk, and signal integration. Front Immunol. 2019;10.

260. Liu T, Zhang L, Joo D, Sun S-C. NF-κB signaling in inflammation. Signal transduction and targeted therapy. 2017;2:17023.

261. Kim EK, Choi EJ. Compromised MAPK signaling in human diseases: an update. Arch Toxicol. 2015;89(6):867-82.

262. Zhang J-M, An J. Cytokines, inflammation, and pain. Int Anesthesiol Clin. 2007;45(2):27-37.

263. Tanaka T, Narazaki M, Kishimoto T. IL-6 in inflammation, immunity, and disease. Cold Spring Harbor perspectives in biology. 2014;6(10):a016295-a.

264. Chelombitko MA. Role of reactive oxygen species in inflammation: a minireview. Moscow University Biological Sciences Bulletin. 2018;73(4):199-202.

265. Mittal M, Siddiqui MR, Tran K, Reddy SP, Malik AB. Reactive oxygen species in inflammation and tissue injury. Antioxid Redox Signal. 2014;20(7):1126-67.

266. Forrester SJ, Kikuchi DS, Hernandes MS, Xu Q, Griendling KK. Reactive oxygen species in metabolic and inflammatory signaling. Circulation Research. 2018;122(6):877-902.

267. Paiva CN, Bozza MT. Are reactive oxygen species always detrimental to pathogens? Antioxid Redox Signal. 2014;20(6):1000-37.

268. Cook-Mills JM, Marchese ME, and Abdala-Valencia H. Vascular cell adhesion molecule-1 expression and signaling during disease: Regulation by reactive oxygen species and antioxidants. Antioxidants & Redox Signaling. 2011;15(6):1607-38.

269. Mattaj IW. Sorting out the nuclear envelope from the endoplasmic reticulum. Nature Reviews Molecular Cell Biology. 2004;5(1):65-9.

270. Bravo-Sagua R, Torrealba N, Paredes F, Morales PE, Pennanen C, López-Crisosto C, et al. Organelle communication: Signaling crossroads between homeostasis and disease. The International Journal of Biochemistry & Cell Biology. 2014;50:55-9.

271. Phillips MJ, Voeltz GK. Structure and function of ER membrane contact sites with other organelles. Nature Reviews Molecular Cell Biology. 2016;17(2):69-82.

272. Liu J, Du L. PERK pathway is involved in oxygen-glucose-serum deprivation-induced NF-kB activation via ROS generation in spinal cord astrocytes. Biochemical and Biophysical Research Communications. 2015;467(2):197-203.

273. Huang W, Liao C-C, Han Y, Lv J, Lei M, Li Y, et al. Co-activation of Akt, Nrf2, and NF-κB signals under UPRER in torpid Myotis ricketti bats for survival. Communications Biology. 2020;3(1):658.

274. Ma Q. Role of nrf2 in oxidative stress and toxicity. Annu Rev Pharmacol Toxicol. 2013;53:401-26.

275. Liu Q, Turner KM, Alfred Yung WK, Chen K, Zhang W. Role of AKT signaling in DNA repair and clinical response to cancer therapy. Neuro Oncol. 2014;16(10):1313-23.

276. Tam AB, Mercado EL, Hoffmann A, Niwa M. ER stress activates NF-κB by integrating functions of basal IKK activity, IRE1 and PERK. PloS one. 2012;7(10):e45078-e.

277. Dong H, Adams NM, Xu Y, Cao J, Allan DSJ, Carlyle JR, et al. The IRE1 endoplasmic reticulum stress sensor activates natural killer cell immunity in part by regulating c-Myc. Nature Immunology. 2019;20(7):865-78.

278. Darling NJ, Cook SJ. The role of MAPK signalling pathways in the response to endoplasmic reticulum stress. Biochimica et Biophysica Acta (BBA) - Molecular Cell Research. 2014;1843(10):2150-63.

279. Nakajima S, Hiramatsu N, Hayakawa K, Saito Y, Kato H, Huang T, et al. Selective abrogation of BiP/GRP78 blunts activation of NF-κB through the ATF6 branch of the UPR: involvement of C/EBPβ and mTOR-dependent dephosphorylation of Akt. Mol Cell Biol. 2011;31(8):1710-8.

280. Stengel ST, Fazio A, Lipinski S, Jahn MT, Aden K, Ito G, et al. Activating transcription factor 6 mediates inflammatory signals in intestinal epithelial cells upon endoplasmic reticulum stress. Gastroenterology. 2020;159(4):1357-74.e10.

281. Romero-Garcia S, Prado-Garcia H. Mitochondrial calcium: Transport and modulation of cellular processes in homeostasis and cancer (Review). Int J Oncol. 2019;54(4):1155-67.

282. Hann J, Bueb J-L, Tolle F, Bréchard S. Calcium signaling and regulation of neutrophil functions: Still a long way to go. Journal of Leukocyte Biology. 2020;107(2):285-97.

283. Hasiakos S, Gwack Y, Kang M, Nishimura I. Calcium signaling in T cells and chronic inflammatory disorders of the oral cavity. J Dent Res. 2021;100(7):693-9.

284. Kaufmann U, Kahlfuss S, Yang J, Ivanova E, Koralov SB, Feske S. Calcium signaling controls pathogenic Th17 cell-mediated inflammation by regulating mitochondrial function. Cell Metab. 2019;29(5):1104-18.e6.

285. Ye Z, Shen Y, Jin K, Qiu J, Hu B, Jadhav RR, et al. Arachidonic acid-regulated calcium signaling in T cells from patients with rheumatoid arthritis promotes synovial inflammation. Nat Commun. 2021;12(1):907.

286. Dalal PJ, Muller WA, Sullivan DP. Endothelial cell calcium signaling during barrier function and inflammation. Am J Pathol. 2020;190(3):535-42.

287. Zumerle S, Calì B, Munari F, Angioni R, Di Virgilio F, Molon B, et al. Intercellular calcium signaling induced by ATP potentiates macrophage phagocytosis. Cell Rep. 2019;27(1):1-10.e4.

288. Lv Z, Xu X, Sun Z, Yang YX, Guo H, Li J, et al. TRPV1 alleviates osteoarthritis by inhibiting M1 macrophage polarization via $Ca^{(2+)}$/CaMKII/Nrf2 signaling pathway. Cell Death Dis. 2021;12(6):504.

289. Sipka T, Peroceschi R, Hassan-Abdi R, Groß M, Ellett F, Begon-Pescia C, et al. Damage-induced calcium signaling and reactive oxygen species mediate macrophage activation in zebrafish. Front Immunol. 2021;12.

290. Yu T, Huang D, Wu H, Chen H, Chen S, Cui Q. Navigating calcium and reactive oxygen species by natural flavones for the treatment of heart failure. Frontiers in Pharmacology. 2021;12.

291. Sarbadhikary P, George BP, Abrahamse H. Inhibitory role of berberine, an isoquinoline alkaloid, on NLRP3 inflammasome activation for the treatment of inflammatory diseases. Molecules. 2021;26(20).

292. Sun Z, Gong W, Zhang Y, Jia Z. Physiological and pathological roles of mammalian NEK7. Frontiers in Physiology. 2020;11.

293. Swanson KV, Deng M, Ting JPY. The NLRP3 inflammasome: molecular activation and regulation to therapeutics. Nature Reviews Immunology. 2019;19(8):477-89.

294. Chen H, Lin H, Xie S, Huang B, Qian Y, Chen K, et al. Myricetin inhibits NLRP3 inflammasome activation via reduction of ROS-dependent ubiquitination of ASC and promotion of ROS-independent NLRP3 ubiquitination. Toxicology and Applied Pharmacology. 2019;365:19-29.

295. Zhou Y, Tong Z, Jiang S, Zheng W, Zhao J, Zhou X. The roles of endoplasmic reticulum in NLRP3 inflammasome activation. Cells. 2020;9(5):1219.

296. Cragg GM, Newman DJ. Natural product drug discovery in the next millennium. Pharmaceutical Biology. 2001;39(sup1):8-17.

297. Newman DJ, Cragg GM. Natural products as sources of new drugs over the nearly four decades from 01/1981 to 09/2019. J Nat Prod. 2020;83(3):770-803.

298. Martucciello S, Masullo M, Cerulli A, Piacente S. Natural products targeting ER stress, and the functional link to mitochondria. Int J Mol Sci. 2020;21(6).

299. Chen D, Evans PA. A concise, efficient and scalable total synthesis of thapsigargin and nortrilobolide from (R)-(–)-carvone. Journal of the American Chemical Society. 2017;139(17):6046-9.

300. Hom Jennifer R, Gewandter Jennifer S, Michael L, Sheu SS, Yoon Y. Thapsigargin induces biphasic fragmentation of mitochondria through calcium-mediated mitochondrial fission and apoptosis. Journal of Cellular Physiology. 2007;212(2):498-508.

301. Baumgartner HK, Gerasimenko JV, Thorne C, Ferdek P, Pozzan T, Tepikin AV, et al. Calcium elevation in mitochondria is the main Ca^{2+} requirement for mitochondrial permeability transition pore (mPTP) opening. Journal of Biological Chemistry. 2009;284(31):20796-803.

302. Atta HM. Biochemical studies on antibiotic production from *Streptomyces* sp.: Taxonomy, fermentation, isolation and biological properties. Journal of Saudi Chemical Society. 2015;19(1):12-22.

303. Hamada J, Onuma H, Ochi F, Hirai H, Takemoto K, Miyoshi A, et al. Endoplasmic reticulum stress induced by tunicamycin increases resistin messenger ribonucleic acid through the pancreatic endoplasmic reticulum eukaryotic initiation factor 2α kinase–activating transcription factor 4–CAAT/enhancer binding protein-α homologous protein pathway in THP-1 human monocytes. Journal of Diabetes Investigation. 2016;7(3):312-23.

304. Lefterova MI, Mullican SE, Tomaru T, Qatanani M, Schupp M, Lazar MA. Endoplasmic Reticulum Stress Regulates Adipocyte Resistin Expression. Diabetes. 2009;58(8):1879-86.

305. Nami B, Donmez H, Kocak N. Tunicamycin-induced endoplasmic reticulum stress reduces in vitro subpopulation and invasion of CD44+/CD24- phenotype breast cancer stem cells. Experimental and Toxicologic Pathology. 2016;68(7):419-26.

306. Guha P, Kaptan E, Gade P, Kalvakolanu DV, Ahmed H. Tunicamycin induced endoplasmic reticulum stress promotes apoptosis of prostate cancer cells by activating mTORC1. Oncotarget. 2017;8(40):68191-207.

307. Tsai H-Y, Ho C-T, Chen Y-K. Biological actions and molecular effects of resveratrol, pterostilbene, and 3′-hydroxypterostilbene. Journal of Food and Drug Analysis. 2017;25(1):134-47.

308. Chen L, Wang T, Chen G, Wang N, Gui L, Dai F, et al. Influence of resveratrol on endoplasmic reticulum stress and expression of adipokines in adipose tissues/adipocytes induced by high-calorie diet or palmitic acid. Endocrine. 2017;55(3):773-85.

309. Gaballah HH, Zakaria SS, Elbatsh MM, Tahoon NM. Modulatory effects of resveratrol on endoplasmic reticulum stress-associated apoptosis and oxido-inflammatory markers in a rat model of rotenone-induced Parkinson's disease. Chemico-Biological Interactions. 2016;251:10-6.

310. Park J, Woo KJ, Lee J, Lim, J. H., , Lee T, Kim SH, Choi YH, et al. Resveratrol induces pro-apoptotic endoplasmic reticulum stress in human colon cancer cells. Oncology Reports. 2007;18(5):1269-73.

311. Tabata Y, Takano K, Ito T, Iinuma M, Yoshimoto T, Miura H, et al. Vaticanol B, a resveratrol tetramer, regulates endoplasmic reticulum stress and inflammation. American Journal of Physiology-Cell Physiology. 2007;293(1):C411-C8.

312. Navarrete C, Sancho R, Caballero FJ, Pollastro F, Fiebich BL, Sterner O, et al. Basiliolides, a class of tetracyclic C19 dilactones from *Thapsia garganica*, release Ca^{2+} from the endoplasmic reticulum and regulate the activity of the transcription factors nuclear factor of activated T cells, nuclear factor-κB, and activator protein 1 in T lymphocytes. Journal of Pharmacology and Experimental Therapeutics. 2006;319(1):422.

313. Patel K, Singh RB, Patel DK. Pharmacological and analytical aspects of withaferin A: A concise report of current scientific literature. Asian Pacific Journal of Reproduction. 2013;2(3):238-43.

314. Choi MJ, Park EJ, Min KJ, Park J-W, Kwon TK. Endoplasmic reticulum stress mediates withaferin A-induced apoptosis in human renal carcinoma cells. Toxicology in Vitro. 2011;25(3):692-8.

315. Khan S, Rammeloo AW, Heikkila JJ. Withaferin A Induces Proteasome Inhibition, Endoplasmic Reticulum Stress, the Heat Shock Response and Acquisition of Thermotolerance. PLOS ONE. 2012;7(11):e50547.

316. Chen C-M, Chung Y-P, Liu C-H, Huang K-T, Guan S-S, Chiang C-K, et al. Withaferin A protects against endoplasmic reticulum stress-associated apoptosis, inflammation, and fibrosis in the kidney of a mouse model of unilateral ureteral obstruction. Phytomedicine. 2020;79:153352.

317. Pimentel AA, Felibertt P, Sojo F, Colman L, Mayora A, Silva ML, et al. The marine sponge toxin agelasine B increases the intracellular Ca^{2+} concentration and induces apoptosis in human breast cancer cells (MCF-7). Cancer Chemotherapy and Pharmacology. 2012;69(1):71-83.

318. Dirsch VM, Müller IM, Eichhorst ST, Pettit GR, Kamano Y, Inoue M, et al. Cephalostatin 1 selectively triggers the release of Smac/DIABLO and subsequent apoptosis that is characterized by an increased density of the mitochondrial matrix. Cancer Research. 2003;63(24):8869.

319. López-Antón N, Rudy A, Barth N, Schmitz LM, Pettit GR, Schulze-Osthoff K, et al. The marine product cephalostatin 1 activates an endoplasmic reticulum stress-specific and apoptosome-independent apoptotic signaling pathway. Journal of Biological Chemistry. 2006;281(44):33078-86.

320. Tahtamouni LH, Nawasreh MM, Al-Mazaydeh ZA, Al-Khateeb RA, Abdellatif RN, Bawadi RM, et al. Cephalostatin 1 analogues activate apoptosis via the endoplasmic reticulum stress signaling pathway. European Journal of Pharmacology. 2018;818:400-9.

321. Briante R, Patumi M, Febbraio F, Nucci R. Production of highly purified hydroxytyrosol from *Olea europaea* leaf extract biotransformed by hyperthermophilic β-glycosidase. Journal of Biotechnology. 2004;111(1):67-77.

322. Giordano E, Davalos A, Nicod N, Visioli F. Hydroxytyrosol attenuates tunicamycin-induced endoplasmic reticulum stress in human hepatocarcinoma cells. Molecular Nutrition & Food Research. 2013;58(5):954-62.

323. Grüneberg WJ, Goffman FD, Velasco L. Characterization of yam bean (*Pachyrhizus* spp.) seeds as potential sources of high palmitic acid oil. Journal of the American Oil Chemists' Society. 1999;76(11):1309-12.

324. Zhang Y, Xue R, Zhang Z, Yang X, Shi H. Palmitic and linoleic acids induce ER stress and apoptosis in hepatoma cells. Lipids in Health and Disease. 2012;11:1-.

325. Chen T-C, Chien C-C, Wu M-S, Chen Y-C. Evodiamine from *Evodia rutaecarpa* induces apoptosis via activation of JNK and PERK in human ovarian cancer cells. Phytomedicine. 2016;23(1):68-78.

326. Ma B, Zhang H, Wang Y, Zhao A, Zhu Z, Bao X, et al. Corosolic acid, a natural triterpenoid, induces ER stress-dependent apoptosis in human castration resistant prostate cancer cells via activation of IRE-1/JNK, PERK/CHOP and TRIB3. J Exp Clin Cancer Res. 2018;37(1):210.

327. Wang Z-s, Lu F-e, Xu L-j, Dong H. Berberine reduces endoplasmic reticulum stress and improves insulin signal transduction in Hep G2 cells. Acta Pharmacologica Sinica. 2010;31(5):578-84.

328. Zhang Z, Li B, Meng X, Yao S, Jin L, Yang J, et al. Berberine prevents progression from hepatic steatosis to steatohepatitis and fibrosis by reducing endoplasmic reticulum stress. Scientific Reports. 2016;6:20848.

329. Correia da Silva D, Valentão P, Andrade PB, Pereira DM. Endoplasmic reticulum stress signaling in cancer and neurodegenerative disorders: Tools and strategies to understand its complexity. Pharmacological Research. 2020;155:104702.

330. Xiang C, Wang Y, Zhang H, Han F. The role of endoplasmic reticulum stress in neurodegenerative disease. Apoptosis. 2017;22(1):1-26.

331. Taalab YM, Ibrahim N, Maher A, Hassan M, Mohamed W, Moustafa AA, et al. Mechanisms of disordered neurodegenerative function: concepts and facts about the different roles of the protein kinase RNA-like endoplasmic reticulum kinase (PERK). Rev Neurosci. 2018;29(4):387-415.

332. Cissé M, Duplan E, Checler F. The transcription factor XBP1 in memory and cognition: Implications in Alzheimer disease. Mol Med. 2017;22:905-17.

333. Duran-Aniotz C, Cornejo VH, Espinoza S, Ardiles Á O, Medinas DB, Salazar C, et al. IRE1 signaling exacerbates Alzheimer's disease pathogenesis. Acta Neuropathol. 2017;134(3):489-506.

334. O'Connor T, Sadleir KR, Maus E, Velliquette RA, Zhao J, Cole SL, et al. Phosphorylation of the translation initiation factor eIF2alpha increases BACE1 levels and promotes amyloidogenesis. Neuron. 2008;60(6):988-1009.

335. Shen B. A new golden age of natural products drug discovery. Cell. 2015;163(6):1297-300.

336. Syed DN, Lall RK, Chamcheu JC, Haidar O, Mukhtar H. Involvement of ER stress and activation of apoptotic pathways in fisetin induced cytotoxicity in human melanoma. Archives of biochemistry and biophysics. 2014;563:108-17.

337. Shih Y-L, Hung F-M, Lee C-H, Yeh M-Y, Lee M-H, Lu H-F, et al. Fisetin induces apoptosis of HSC3 human oral cancer cells through endoplasmic reticulum stress and dysfunction of mitochondria-mediated signaling pathways. In Vivo. 2017;31(6):1103-14.

338. Kang KA, Piao MJ, Madduma Hewage SRK, Ryu YS, Oh MC, Kwon TK, et al. Fisetin induces apoptosis and endoplasmic reticulum stress in human non-small cell lung cancer through inhibition of the MAPK signaling pathway. Tumor Biology. 2016;37(7):9615-24.

339. Hao X, Yao A, Gong J, Zhu W, Li N, Li J. Berberine ameliorates pro-inflammatory cytokine-induced endoplasmic reticulum stress in human intestinal epithelial cells *in vitro*. Inflammation. 2012;35(3):841-9.

340. Sorokina M, Merseburger P, Rajan K, Yirik MA, Steinbeck C. COCONUT online: Collection of Open Natural Products database. J Cheminform. 2021;13(1):2.

341. Pedregosa F, Varoquaux G, Gramfort A, Michel V, Thirion B, Grisel O, et al. Scikit-learn: Machine Learning in Python. J Mach Learn Res. 2011;12(null):2825–30.

342. McInnes LH, J. UMAP: Uniform manifold approximation and projection for dimension reduction. ArXiv e-prints 2018;1802.03426.

343. Vanii Jayaseelan K, Moreno P, Truszkowski A, Ertl P, Steinbeck C. Natural product-likeness score revisited: an open-source, open-data implementation. BMC Bioinformatics. 2012;13(1):106.

344. Djoumbou Feunang Y, Eisner R, Knox C, Chepelev L, Hastings J, Owen G, et al. ClassyFire: automated chemical classification with a comprehensive, computable taxonomy. J Cheminform. 2016;8:61-.

345. Carreras-Sureda A, Pihán P, Hetz C. Calcium signaling at the endoplasmic reticulum: fine-tuning stress responses. Cell Calcium. 2018;70:24-31.

346. Coe H, Michalak M. Calcium binding chaperones of the endoplasmic reticulum. Gen Physiol Biophys. 2009;28 Spec No Focus:F96-f103.

347. Bhattarai KR, Riaz TA, Kim H-R, Chae H-J. The aftermath of the interplay between the endoplasmic reticulum stress response and redox signaling. Experimental & Molecular Medicine. 2021;53(2):151-67.

348. Verma A, Bhatt AN, Farooque A, Khanna S, Singh S, Dwarakanath BS. Calcium ionophore A23187 reveals calcium related cellular stress as “I-Bodies”: An old actor in a new role. Cell Calcium. 2011;50(6):510-22.

349. Castillero E, Akashi H, Pendrak K, Yerebakan H, Najjar M, Wang C, et al. Attenuation of the unfolded protein response and endoplasmic reticulum stress after mechanical unloading in dilated cardiomyopathy. Am J Physiol Heart Circ Physiol. 2015;309(3):H459-H70.

350. Shinde V, Kotla P, Strang C, Gorbatyuk M. Unfolded protein response-induced dysregulation of calcium homeostasis promotes retinal degeneration in rat models of autosomal dominant retinitis pigmentosa. Cell death & disease. 2016;7(2):e2085-e.

351. Jung ES, Hong H, Kim C, Mook-Jung I. Acute ER stress regulates amyloid precursor protein processing through ubiquitin-dependent degradation. Scientific Reports. 2015;5(1):8805.

352. Doyle KM, Kennedy D, Gorman AM, Gupta S, Healy SJ, Samali A. Unfolded proteins and endoplasmic reticulum stress in neurodegenerative disorders. J Cell Mol Med. 2011;15(10):2025-39.

353. Kim D-K, Kim TH, Lee S-J. Mechanisms of aging-related proteinopathies in Caenorhabditis elegans. Experimental & Molecular Medicine. 2016;48(10):e263-e.

354. Zhou W, Chang L, Fang Y, Du Z, Li Y, Song Y, et al. Cerebral dopamine neurotrophic factor alleviates Aβ25-35-induced endoplasmic reticulum stress and early synaptotoxicity in rat hippocampal cells. Neuroscience Letters. 2016;633:40-6.

355. Liu Y-Q, Jia M-Q, Xie Z-H, Liu X-F, Hui Y, Zheng X-L, et al. Arrestins contribute to amyloid beta-induced cell death via modulation of autophagy and the α7nAch receptor in SH-SY5Y cells. Scientific reports. 2017;7(1):3446-.

356. Boileau P, Hejazi NS, Dudoit S. Exploring high-dimensional biological data with sparse contrastive principal component analysis. Bioinformatics. 2020;36(11):3422-30.

357. Meglen RR. Examining large databases: a chemometric approach using principal component analysis. Marine Chemistry. 1992;39(1):217-37.

358. Weidner J, Jarenbäck L, Åberg I, Westergren-Thorsson G, Ankerst J, Bjermer L, et al. Endoplasmic reticulum, Golgi, and lysosomes are disorganized in lung fibroblasts from chronic obstructive pulmonary disease patients. Physiol Rep. 2018;6(5):e13584.

359. Dai X, Kuang Q, Sun Y, Xu M, Zhu L, Ge C, et al. Fisetin represses oxidative stress and mitochondrial dysfunction in NAFLD through suppressing GRP78-mediated endoplasmic reticulum (ER) stress. Journal of Functional Foods. 2022;90:104954.

360. Ahmad A, Ali T, Park HY, Badshah H, Rehman SU, Kim MO. Neuroprotective effect of fisetin against amyloid-beta-induced cognitive/synaptic dysfunction, neuroinflammation, and neurodegeneration in adult mice. Molecular Neurobiology. 2017;54(3):2269-85.

361. Jia S, Xu X, Zhou S, Chen Y, Ding G, Cao L. Fisetin induces autophagy in pancreatic cancer cells via endoplasmic reticulum stress- and mitochondrial stress-dependent pathways. Cell Death & Disease. 2019;10(2):142.

362. Gorbatyuk MS, Gorbatyuk OS. The molecular chaperone GRP78/BiP as a therapeutic target for neurodegenerative disorders: a mini review. J Genet Syndr Gene Ther. 2013;4(2):128.

363. Ghemrawi R, Khair M. Endoplasmic reticulum stress and unfolded protein response in neurodegenerative diseases. International journal of molecular sciences. 2020;21(17):6127.

364. Hoozemans JJM, Veerhuis R, Van Haastert ES, Rozemuller JM, Baas F, Eikelenboom P, et al. The unfolded protein response is activated in Alzheimer's disease. Acta Neuropathologica. 2005;110(2):165-72.

365. Hamos JE, Oblas B, Pulaski-Salo D, Welch WJ, Bole DG, Drachman DA. Expression of heat shock proteins in Alzheimer's disease. Neurology. 1991;41(3):345-50.

366. Moreno JA, Halliday M, Molloy C, Radford H, Verity N, Axten JM, et al. Oral treatment targeting the unfolded protein response prevents neurodegeneration and clinical disease in prion-infected mice. Sci Transl Med. 2013;5(206):206ra138.

367. Radford H, Moreno JA, Verity N, Halliday M, Mallucci GR. PERK inhibition prevents tau-mediated neurodegeneration in a mouse model of frontotemporal dementia. Acta Neuropathol. 2015;130(5):633-42.

368. Nonaka T, Watanabe ST, Iwatsubo T, Hasegawa M. Seeded aggregation and toxicity of α-synuclein and tau. Journal of Biological Chemistry. 2010;285(45):34885-98.

369. Xicoy H, Wieringa B, Martens GJM. The SH-SY5Y cell line in Parkinson's disease research: a systematic review. Molecular Neurodegeneration. 2017;12(1):10.

370. Rcom-H'cheo-Gauthier AN, Meedeniya AC, Pountney DL. Calcipotriol inhibits α-synuclein aggregation in SH-SY5Y neuroblastoma cells by a Calbindin-D28k-dependent mechanism. J Neurochem. 2017;141(2):263-74.

371. Sang JC, Hidari E, Meisl G, Ranasinghe RT, Spillantini MG, Klenerman D. Super-resolution imaging reveals α-synuclein seeded aggregation in SH-SY5Y cells. Commun Biol. 2021;4(1):613.

372. Lee JH, Won SM, Suh J, Son SJ, Moon GJ, Park UJ, et al. Induction of the unfolded protein response and cell death pathway in Alzheimer's disease, but not in aged Tg2576 mice. Exp Mol Med. 2010;42(5):386-94.

373. Santos LE, Ferreira ST. Crosstalk between endoplasmic reticulum stress and brain inflammation in Alzheimer's disease. Neuropharmacology. 2018;136:350-60.

374. Sharma R, Srivastava T, Pandey AR, Mishra T, Gupta B, Reddy SS, et al. Identification of natural products as potential pharmacological chaperones for protein misfolding diseases. ChemMedChem. 2021;16(13):2146-56.

375. Kim H, Park B-S, Lee K-G, Choi CY, Jang SS, Kim Y-H, et al. Effects of naturally occurring compounds on fibril formation and oxidative stress of β-amyloid. Journal of Agricultural and Food Chemistry. 2005;53(22):8537-41.

376. Miller KD, Nogueira L, Mariotto AB, Rowland JH, Yabroff KR, Alfano CM, et al. Cancer treatment and survivorship statistics, 2019. CA: A Cancer Journal for Clinicians. 2019;69(5):363-85.

377. Global Burden of Disease Cancer C, Fitzmaurice C, Dicker D, Pain A, Hamavid H, Moradi-Lakeh M, et al. The Global Burden of Cancer 2013. JAMA Oncol. 2015;1(4):505-27.

378. Bravo R, Parra V, Gatica D, Rodriguez AE, Torrealba N, Paredes F, et al. Endoplasmic reticulum and the unfolded protein response: dynamics and metabolic integration. Int Rev Cell Mol Biol. 2013;301:215-90.

379. Hetz C. The unfolded protein response: controlling cell fate decisions under ER stress and beyond. Nature Reviews Molecular Cell Biology. 2012;13(2):89-102.

380. Kim C, Kim B. Anti-cancer natural products and their bioactive compounds inducing ER stress-mediated apoptosis: a review. Nutrients. 2018;10(8):1021.

381. King AP, Wilson JJ. Endoplasmic reticulum stress: an arising target for metal-based anticancer agents. Chemical Society Reviews. 2020;49(22):8113-36.

382. Cheimonidi C, Samara P, Polychronopoulos P, Tsakiri EN, Nikou T, Myrianthopoulos V, et al. Selective cytotoxicity of the herbal substance acteoside against tumor cells and its mechanistic insights. Redox Biol. 2018;16:169-78.

383. Berning L, Scharf L, Aplak E, Stucki D, von Montfort C, Reichert AS, et al. *In vitro* selective cytotoxicity of the dietary chalcone cardamonin (CD) on melanoma compared to healthy cells is mediated by apoptosis. PLOS ONE. 2019;14(9):e0222267.

384. Kim JH, Jung CH, Jang B-H, Go HY, Park J-H, Choi Y-K, et al. Selective cytotoxic effects on human cancer cell lines of phenolic-rich ethyl-acetate fraction from *Rhus verniciflua* stokes. The American Journal of Chinese Medicine. 2009;37(03):609-20.

385. Oakes SA. Endoplasmic reticulum stress signaling in cancer cells. Am J Pathol. 2020;190(5):934-46.

386. Oakes SA. Endoplasmic reticulum proteostasis: a key checkpoint in cancer. Am J Physiol Cell Physiol. 2017;312(2):C93-C102.

387. Correia da Silva D, Valentão P, Andrade PB, Pereira DM. A pipeline for natural small molecule inhibitors of endoplasmic reticulum stress. Frontiers in Pharmacology. 2022;13.

388. Wang Y, Biswas G, Prabu SK, Avadhani NG. Modulation of mitochondrial metabolic function by phorbol 12-myristate 13-acetate through increased mitochondrial translocation of protein kinase Cα in C2C12 myocytes. Biochemical Pharmacology. 2006;72(7):881-92.

389. Badisa RB, Darling-Reed SF, Joseph P, Cooperwood JS, Latinwo LM, Goodman CB. Selective cytotoxic activities of two novel synthetic drugs on human breast carcinoma MCF-7 cells. Anticancer Res. 2009;29(8):2993-6.

390. Gupta S, Cuffe L, Szegezdi E, Logue SE, Neary C, Healy S, et al. Mechanisms of ER stress-mediated mitochondrial membrane permeabilization. International journal of cell biology. 2010;2010:170215-.

391. Rzymski T, Milani M, Pike L, Buffa F, Mellor HR, Winchester L, et al. Regulation of autophagy by ATF4 in response to severe hypoxia. Oncogene. 2010;29(31):4424-35.

392. Hu H, Tian M, Ding C, Yu S. The C/EBP homologous protein (CHOP) transcription factor functions in endoplasmic reticulum stress-induced apoptosis and microbial infection. Front Immunol. 2019;9.

393. Hetz C, Zhang K, Kaufman RJ. Mechanisms, regulation and functions of the unfolded protein response. Nature Reviews Molecular Cell Biology. 2020;21(8):421-38.

394. Marzec M, Eletto D, Argon Y. GRP94: An HSP90-like protein specialized for protein folding and quality control in the endoplasmic reticulum. Biochimica et Biophysica Acta (BBA) - Molecular Cell Research. 2012;1823(3):774-87.

395. Kim RS, Hasegawa D, Goossens N, Tsuchida T, Athwal V, Sun X, et al. The XBP1 arm of the unfolded protein response induces fibrogenic activity in hepatic stellate cells through autophagy. Scientific Reports. 2016;6(1):39342.

396. Määttänen P, Gehring K, Bergeron JJM, Thomas DY. Protein quality control in the ER: The recognition of misfolded proteins. Seminars in Cell & Developmental Biology. 2010;21(5):500-11.

397. van Ziel AM, Scheper W. The UPR in neurodegenerative disease: not just an inside job. Biomolecules. 2020;10(8):1090.

398. Duchen MR. Mitochondria and calcium: from cell signalling to cell death. J Physiol. 2000;529 Pt 1(Pt 1):57-68.

399. Srivastava SP, Davies MV, Kaufman RJ. Calcium depletion from the endoplasmic reticulum activates the double-stranded RNA-dependent protein kinase (PKR) to inhibit protein synthesis. Journal of Biological Chemistry. 1995;270(28):16619-24.

400. Li Y, Yan Y, Liu F, Wang M, Feng F, Xiao Y. Effects of calcium ionophore A23187 on the apoptosis of hepatic stellate cells stimulated by transforming growth factor-β(1). Cell Mol Biol Lett. 2018;23:1-.

401. Boya P, Cohen I, Zamzami N, Vieira HLA, Kroemer G. Endoplasmic reticulum stress-induced cell death requires mitochondrial membrane permeabilization. Cell Death & Differentiation. 2002;9(4):465-7.

402. Momoi T. Caspases involved in ER stress-mediated cell death. Journal of Chemical Neuroanatomy. 2004;28(1):101-5.

403. Stepczynska A, Lauber K, Engels IH, Janssen O, Kabelitz D, Wesselborg S, et al. Staurosporine and conventional anticancer drugs induce overlapping, yet distinct pathways of apoptosis and caspase activation. Oncogene. 2001;20(10):1193-202.

404. Musaogullari A, Mandato A, Chai Y-C. Role of glutathione depletion and reactive oxygen species generation on caspase-3 activation: a study with the kinase inhibitor staurosporine. Frontiers in Physiology. 2020;11.

405. Yang R-Q, Guo P-F, Ma Z, Chang C, Meng Q-N, Gao Y, et al. Effects of simvastatin on iNOS and caspase-3 levels and oxidative stress following smoke inhalation injury. Molecular medicine reports. 2020;22(4):3405-17.

406. Egger L, Madden DT, Rhême C, Rao RV, Bredesen DE. Endoplasmic reticulum stress-induced cell death mediated by the proteasome. Cell Death & Differentiation. 2007;14(6):1172-80.

407. Feldman D, Koong AC. Irestatin, a potent inhibitor of IRE1α and the unfolded protein response, is a hypoxia-selective cytotoxin and impairs tumor growth. Journal of Clinical Oncology. 2007;25(18_suppl):3514-.

408. Ron D, Walter P. Signal integration in the endoplasmic reticulum unfolded protein response. Nature Reviews Molecular Cell Biology. 2007;8(7):519-29.

409. Feldman DE, Chauhan V, Koong AC. The unfolded protein response: a novel component of the hypoxic stress response in tumors. Molecular Cancer Research. 2005;3(11):597-605.

410. Fennema E, Rivron N, Rouwkema J, van Blitterswijk C, de Boer J. Spheroid culture as a tool for creating 3D complex tissues. Trends Biotechnol. 2013;31(2):108-15.

411. Sun T, Jackson S, Haycock JW, MacNeil S. Culture of skin cells in 3D rather than 2D improves their ability to survive exposure to cytotoxic agents. J Biotechnol. 2006;122(3):372-81.

412. Edmondson R, Broglie JJ, Adcock AF, Yang L. Three-dimensional cell culture systems and their applications in drug discovery and cell-based biosensors. Assay Drug Dev Technol. 2014;12(4):207-18.

413. Lv D, Hu Z, Lu L, Lu H, Xu X. Three-dimensional cell culture: A powerful tool in tumor research and drug discovery. Oncol Lett. 2017;14(6):6999-7010.

414. Lin JH, Walter P, Yen TSB. Endoplasmic reticulum stress in disease pathogenesis. Annu Rev Pathol. 2008;3:399-425.

415. Yoshida H. ER stress and diseases. The FEBS Journal. 2007;274(3):630-58.

416. Chakrabarti A, Chen AW, Varner JD. A Review of the Mammalian Unfolded Protein Response. Biotechnology and bioengineering. 2011;108(12):2777-93.

417. Hunter P. The inflammation theory of disease: The growing realization that chronic inflammation is crucial in many diseases opens new avenues for treatment. EMBO Reports. 2012;13(11):968-70.

418. Kitamura M, Hiramatsu N. Chapter Five - Real-Time Monitoring of ER Stress in Living Cells and Animals Using ESTRAP Assay. In: Conn PM, editor. Methods in Enzymology. 490: Academic Press; 2011. p. 93-106.

419. Garg AD, Kaczmarek A, Krysko O, Vandenabeele P, Krysko DV, Agostinis P. ER stress-induced inflammation: does it aid or impede disease progression? Trends Mol Med. 2012;18(10):589-98.

420. Chanput W, Mes JJ, Wichers HJ. THP-1 cell line: an *in vitro* cell model for immune modulation approach. Int Immunopharmacol. 2014;23(1):37-45.

421. Takeshige T, Harada N, Harada S, Ishimori A, Katsura Y, Sasano H, et al. Chitin induces steroid-resistant airway inflammation and airway hyperresponsiveness in mice. Allergology International. 2021;70(3):343-50.

422. Rimessi A, Previati M, Nigro F, Wieckowski MR, Pinton P. Mitochondrial reactive oxygen species and inflammation: Molecular mechanisms, diseases and promising therapies. The International Journal of Biochemistry & Cell Biology. 2016;81:281-93.

423. Morgan MJ, Liu Z-g. Crosstalk of reactive oxygen species and NF-κB signaling. Cell Res. 2011;21(1):103-15.

424. Lingappan K. NF-κB in oxidative stress. Curr Opin Toxicol. 2018;7:81-6.

425. Zhang J, Wang X, Vikash V, Ye Q, Wu D, Liu Y, et al. ROS and ROS-mediated cellular signaling. Oxid Med Cell Longev. 2016;2016:4350965-.

426. Zeeshan HMA, Lee GH, Kim H-R, Chae H-J. Endoplasmic reticulum stress and associated ROS. International Journal of Molecular Sciences. 2016;17(3):327-.

427. Shimizu Y, Hendershot LM. Oxidative folding: cellular strategies for dealing with the resultant equimolar production of reactive oxygen species. Antioxidants & redox signaling. 2009;11(9):2317-31.

428. Turner MD, Nedjai B, Hurst T, Pennington DJ. Cytokines and chemokines: At the crossroads of cell signalling and inflammatory disease. Biochimica et Biophysica Acta (BBA) - Molecular Cell Research. 2014;1843(11):2563-82.

429. B'chir W, Maurin A-C, Carraro V, Averous J, Jousse C, Muranishi Y, et al. The eIF2α/ATF4 pathway is essential for stress-induced autophagy gene expression. Nucleic Acids Research. 2013;41(16):7683-99.

430. Barrera MJ, Aguilera S, Castro I, Cortés J, Bahamondes V, Quest AFG, et al. Pro-inflammatory cytokines enhance ERAD and ATF6α pathway activity in salivary glands of Sjögren's syndrome patients. Journal of Autoimmunity. 2016;75:68-81.

431. Olivari S, Cali T, Salo KEH, Paganetti P, Ruddock LW, Molinari M. EDEM1 regulates ER-associated degradation by accelerating de-mannosylation of folding-defective polypeptides and by inhibiting their covalent aggregation. Biochemical and Biophysical Research Communications. 2006;349(4):1278-84.

432. Yu Q, Zeng K, Ma X, Song F, Jiang Y, Tu P, et al. Resokaempferol-mediated anti-inflammatory effects on activated macrophages via the inhibition of JAK2/STAT3, NF-κB and JNK/p38 MAPK signaling pathways. International Immunopharmacology. 2016;38:104-14.

433. Jiang Y, Huang K, Lin X, Chen Q, Lin S, Feng X, et al. Berberine attenuates NLRP3 inflammasome activation in macrophages to reduce the secretion of interleukin-1β. Annals of Clinical & Laboratory Science. 2017;47(6):720-8.

434. Huang S, Liu H, Lin Y, Liu M, Li Y, Mao H, et al. Berberine protects against NLRP3 inflammasome via ameliorating autophagic impairment in MPTP-induced Parkinson's disease model. Frontiers in pharmacology. 2021;11:618787-.

435. Mai W, Xu Y, Xu J, Zhao D, Ye L, Yu G, et al. Berberine inhibits NOD-like receptor family pyrin domain-containing 3 inflammasome activation and pyroptosis in nonalcoholic steatohepatitis via the ROS/TXNIP axis. Frontiers in Pharmacology. 2020;11.

436. Vivoli E, Cappon A, Milani S, Piombanti B, Provenzano A, Novo E, et al. NLRP3 inflammasome as a target of berberine in experimental murine liver injury: interference with P2X7 signalling. Clinical Science. 2016;130(20):1793-806.

437. Lin Y, Liu P-G, Liang W-Q, Hu Y-J, Xu P, Zhou J, et al. Luteolin-4′-O-glucoside and its aglycone, two major flavones of Gnaphalium affine D. Don, resist hyperuricemia and acute gouty arthritis activity in animal models. Phytomedicine. 2018;41:54-61.

438. Cho BO, Yin HH, Park SH, Byun EB, Ha HY, Jang SI. Anti-inflammatory activity of myricetin from Diospyros lotus through suppression of NF-κB and STAT1 activation and Nrf2-mediated HO-1 induction in lipopolysaccharide-stimulated RAW264.7 macrophages. Bioscience, Biotechnology, and Biochemistry. 2016;80(8):1520-30.

439. Gutiérrez-Venegas G, Torras-Ceballos A, Gómez-Mora JA, Fernández-Rojas B. Luteolin, quercetin, genistein and quercetagetin inhibit the effects of lipopolysaccharide obtained from *Porphyromonas gingivalis* in H9c2 cardiomyoblasts. Cell Mol Biol Lett. 2017;22:19-.

440. Kang G-J, Han S-C, Ock J-W, Kang H-K, Yoo E-S. Anti-inflammatory effect of quercetagetin, an active component of immature *Citrus unshiu*, in HaCaT human keratinocytes. Biomol Ther (Seoul). 2013;21(2):138-45.

441. Guo X-D, Zhang D-Y, Gao X-J, Parry J, Liu K, Liu B-L, et al. Quercetin and quercetin-3-*O*-glucuronide are equally effective in ameliorating endothelial insulin resistance through inhibition of reactive oxygen species-associated inflammation. Molecular Nutrition & Food Research. 2013;57(6):1037-45.

442. Park J-Y, Lim M-S, Kim S-I, Lee HJ, Kim S-S, Kwon Y-S, et al. Quercetin-3-*O*-β-D-glucuronide suppresses lipopolysaccharide-induced JNK and ERK phosphorylation in LPS-challenged RAW264.7 cells. Biomol Ther (Seoul). 2016;24(6):610-5.

443. Fan D, Zhou X, Zhao C, Chen H, Zhao Y, Gong X. Anti-inflammatory, antiviral and quantitative study of quercetin-3-*O*-β-D-glucuronide in *Polygonum perfoliatum* L. Fitoterapia. 2011;82(6):805-10.

444. Peng L, Durai P, Park K, Pyo JJ, Choi Y. A novel competitive binding screening assay reveals sennoside B as a potent natural product inhibitor of TNF-α. Biomedicines. 2021;9(9):1250.

445. Wu Y, Chen Q, Wen B, Wu N, He B, Chen J. Berberine reduces Aβ42 deposition and tau hyperphosphorylation *via* ameliorating endoplasmic reticulum stress. Frontiers in Pharmacology. 2021;12.

446. Xiang X-Y, Liu T, Wu Y, Jiang X-S, He J-L, Chen X-M, et al. Berberine alleviates palmitic acid-induced podocyte apoptosis by reducing reactive oxygen species-mediated endoplasmic reticulum stress. Molecular Medicine Reports. 2021;23(1):3.

447. Yang C, Lim W, Bazer FW, Song G. Myricetin suppresses invasion and promotes cell death in human placental choriocarcinoma cells through induction of oxidative stress. Cancer Letters. 2017;399:10-9.

448. Xu Y, Xie Q, Wu S, Yi D, Yu Y, Liu S, et al. Myricetin induces apoptosis via endoplasmic reticulum stress and DNA double-strand breaks in human ovarian cancer cells. Molecular medicine reports. 2016;13(3):2094-100.

449. Karunakaran U, Elumalai S, Moon JS, Jeon JH, Kim ND, Park KG, et al. Myricetin protects against high glucose-induced β-cell apoptosis by attenuating endoplasmic reticulum stress *via* inactivation of cyclin-dependent kinase 5. Diabetes Metab J. 2019;43(2):192-205.

450. Hetz C, Papa FR. The unfolded protein response and cell fate control. Molecular Cell. 2018;69(2):169-81.

451. Walter P, Ron D. The unfolded protein response: From stress pathway to homeostatic regulation. Science. 2011;334(6059):1081.

452. Khanna M, Agrawal N, Chandra R, Dhawan G. Targeting unfolded protein response: a new horizon for disease control. Expert Rev Mol Med. 2021;23:e1.

453. Li W, Cao T, Luo C, Cai J, Zhou X, Xiao X, et al. Crosstalk between ER stress, NLRP3 inflammasome, and inflammation. Applied Microbiology and Biotechnology. 2020;104(14):6129-40.

454. Xue C, Lin TY, Chang D, Guo Z. Thioflavin T as an amyloid dye: fibril quantification, optimal concentration and effect on aggregation. Royal Society Open Science. 2017;4(1):160696.

455. Khurana R, Coleman C, Ionescu-Zanetti C, Carter SA, Krishna V, Grover RK, et al. Mechanism of thioflavin T binding to amyloid fibrils. Journal of Structural Biology. 2005;151(3):229-38.

456. Elsallabi O, Patruno A, Pesce M, Cataldi A, Carradori S, Gallorini M. Fisetin as a senotherapeutic agent: Biopharmaceutical properties and crosstalk between cell senescence and neuroprotection. Molecules. 2022;27(3).

457. Ravula AR, Teegala SB, Kalakotla S, Pasangulapati JP, Perumal V, Boyina HK. Fisetin, potential flavonoid with multifarious targets for treating neurological disorders: An updated review. Eur J Pharmacol. 2021;910:174492.

458. Farooqi AA, Naureen H, Zahid R, Youssef L, Attar R, Xu B. Cancer chemopreventive role of fisetin: Regulation of cell signaling pathways in different cancers. Pharmacological Research. 2021;172:105784.

459. Cui J, Fan J, Li H, Zhang J, Tong J. Neuroprotective potential of fisetin in an experimental model of spinal cord injury: via modulation of NF-κB/IκBα pathway. Neuroreport. 2021;32(4):296-305.

460. Karagöz GE, Acosta-Alvear D, Walter P. The unfolded protein response: detecting and responding to fluctuations in the protein-folding capacity of the endoplasmic reticulum. Cold Spring Harb Perspect Biol. 2019;3(11).

461. Grynkiewicz G, Demchuk OM. New perspectives for fisetin. Front Chem. 2019;7:697.

462. Khan N, Syed DN, Ahmad N, Mukhtar H. Fisetin: a dietary antioxidant for health promotion. Antioxid Redox Signal. 2013;19(2):151-62.

463. Kimira M, Arai Y, Shimoi K, Watanabe S. Japanese intake of flavonoids and isoflavonoids from foods. Journal of Epidemiology. 1998;8(3):168-75.

464. Maher P. Protective effects of fisetin and other berry flavonoids in Parkinson's disease. Food Funct. 2017;8(9):3033-42.

465. Rengarajan T, Yaacob NS. The flavonoid fisetin as an anticancer agent targeting the growth signaling pathways. European Journal of Pharmacology. 2016;789:8-16.

466. Imran M, Saeed F, Gilani SA, Shariati MA, Imran A, Afzaal M, et al. Fisetin: An anticancer perspective. Food Sci Nutr. 2021;9(1):3-16.

467. Kashyap D, Sharma A, Sak K, Tuli HS, Buttar HS, Bishayee A. Fisetin: A bioactive phytochemical with potential for cancer prevention and pharmacotherapy. Life Sci. 2018;194:75-87.

468. Maher P. How fisetin reduces the impact of age and disease on CNS function. Front Biosci (Schol Ed). 2015;7(1):58-82.

469. Lorthongpanich N, Mahalapbutr P, Rungrotmongkol T, Charoenwongpaiboon T, Prousoontorn MH. Fisetin glycosides synthesized by cyclodextrin glycosyltransferase from Paenibacillus sp. RB01: characterization, molecular docking, and antioxidant activity. PeerJ. 2022;10:e13467.

470. Jakopin Ž, Corsini E. THP-1 cells and pro-inflammatory cytokine production: an *in vitro* tool for functional characterization of NOD1/NOD2 antagonists. International journal of molecular sciences. 2019;20(17):4265.

471. Shapouri-Moghaddam A, Mohammadian S, Vazini H, Taghadosi M, Esmaeili S-A, Mardani F, et al. Macrophage plasticity, polarization, and function in health and disease. Journal of Cellular Physiology. 2018;233(9):6425-40.

472. Franchi L, Eigenbrod T, Muñoz-Planillo R, Nuñez G. The inflammasome: a caspase-1-activation platform that regulates immune responses and disease pathogenesis. Nature Immunology. 2009;10(3):241-7.

473. Chong WC, Shastri MD, Peterson GM, Patel RP, Pathinayake PS, Dua K, et al. The complex interplay between endoplasmic reticulum stress and the NLRP3 inflammasome: a potential therapeutic target for inflammatory disorders. Clinical & Translational Immunology. 2021;10(2):e1247.

474. Mangan MSJ, Olhava EJ, Roush WR, Seidel HM, Glick GD, Latz E. Targeting the NLRP3 inflammasome in inflammatory diseases. Nature Reviews Drug Discovery. 2018;17(8):588-606.

475. Dhani S, Zhao Y, Zhivotovsky B. A long way to go: caspase inhibitors in clinical use. Cell Death & Disease. 2021;12(10):949.

476. Ding H, Li Y, Chen S, Wen Y, Zhang S, Luo E, et al. Fisetin ameliorates cognitive impairment by activating mitophagy and suppressing neuroinflammation in rats with sepsis-associated encephalopathy. CNS Neuroscience & Therapeutics. 2022;28(2):247-58.

477. Yao C, Narumiya S. Prostaglandin-cytokine crosstalk in chronic inflammation. Br J Pharmacol. 2019;176(3):337-54.

478. Opal SM, DePalo VA. Anti-inflammatory cytokines. Chest. 2000;117(4):1162-72.

479. Iurlaro R, Muñoz-Pinedo C. Cell death induced by endoplasmic reticulum stress. The FEBS Journal. 2016;283(14):2640-52.

480. Sano R, Reed JC. ER stress-induced cell death mechanisms. Biochimica et Biophysica Acta (BBA) - Molecular Cell Research. 2013;1833(12):3460-70.

481. Zhang C, Bai N, Chang A, Zhang Z, Yin J, Shen W, et al. ATF4 is directly recruited by TLR4 signaling and positively regulates TLR4-trigged cytokine production in human monocytes. Cellular & Molecular Immunology. 2013;10(1):84-94.

482. Hartl FU, Bracher A, Hayer-Hartl M. Molecular chaperones in protein folding and proteostasis. Nature. 2011;475(7356):324-32.

483. Smith HL, Li W, Cheetham ME. Molecular chaperones and neuronal proteostasis. Semin Cell Dev Biol. 2015;40:142-52.

484. Chaudhuri TK, Paul S. Protein-misfolding diseases and chaperone-based therapeutic approaches. Febs j. 2006;273(7):1331-49.

485. Xiao S, Lu Y, Wu Q, Yang J, Chen J, Zhong S, et al. Fisetin inhibits tau aggregation by interacting with the protein and preventing the formation of β-strands. Int J Biol Macromol. 2021;178:381-93.

486. Maher P. A comparison of the neurotrophic activities of the flavonoid fisetin and some of its derivatives. Free Radic Res. 2006;40(10):1105-11.

487. Chiruta C, Schubert D, Dargusch R, Maher P. Chemical modification of the multitarget neuroprotective compound fisetin. J Med Chem. 2012;55(1):378-89.

488. Chen Z, Zhang R, Shi W, Li L, Liu H, Liu Z, et al. The multifunctional benefits of naturally occurring delphinidin and its glycosides. J Agric Food Chem. 2019;67(41):11288-306.

489. Fernandes I, Faria A, Calhau C, de Freitas V, Mateus N. Bioavailability of anthocyanins and derivatives. Journal of Functional Foods. 2014;7:54-66.

490. Andres-Lacueva C, Shukitt-Hale B, Galli RL, Jauregui O, Lamuela-Raventos RM, Joseph JA. Anthocyanins in aged blueberry-fed rats are found centrally and may enhance memory. Nutritional Neuroscience. 2005;8(2):111-20.

491. Kim HS, Sul D, Lim JY, Lee D, Joo SS, Hwang KW, et al. Delphinidin ameliorates beta-amyloid-induced neurotoxicity by inhibiting calcium influx and tau hyperphosphorylation. Biosci Biotechnol Biochem. 2009;73(7):1685-9.

492. Kim SM, Chung MJ, Ha TJ, Choi HN, Jang SJ, Kim SO, et al. Neuroprotective effects of black soybean anthocyanins via inactivation of ASK1–JNK/p38 pathways and mobilization of cellular sialic acids. Life Sciences. 2012;90(21):874-82.

493. Inoue H, Maeda-Yamamoto M, Nesumi A, Murakami A. Delphinidin-3-*O*-galactoside protects mouse hepatocytes from (−)-epigallocatechin-3-gallate–induced cytotoxicity via up-regulation of heme oxygenase-1 and heat shock protein 70. Nutrition Research. 2012;32(5):357-64.

494. Shimazu R, Anada M, Miyaguchi A, Nomi Y, Matsumoto H. Evaluation of blood–brain barrier permeability of polyphenols, anthocyanins, and their metabolites. Journal of Agricultural and Food Chemistry. 2021;69(39):11676-86.

495. La X, Zhang L, Li Z, Yang P, Wang Y. Berberine-induced autophagic cell death by elevating GRP78 levels in cancer cells. Oncotarget. 2017;8(13):20909-24.

496. Lin J-P, Yang J-S, Chang N-W, Chiu T-H, Su C-C, Lu K-W, et al. GADD153 mediates berberine-induced apoptosis in human cervical cancer Ca Ski cells. Anticancer Res. 2007;27(5A):3379-86.

497. Eom KS, Kim H-J, So H-S, Park R, Kim TY. Berberine-induced apoptosis in human glioblastoma T98G cells is mediated by endoplasmic reticulum stress accompanying reactive oxygen species and mitochondrial dysfunction. Biological and Pharmaceutical Bulletin. 2010;33(10):1644-9.

498. Gao J, Wells JA. Chapter 510 - Caspase-4 and Caspase-5. In: Rawlings ND, Salvesen G, editors. Handbook of Proteolytic Enzymes (Third Edition): Academic Press; 2013. p. 2265-9.

499. Ortiz LM, Lombardi P, Tillhon M, Scovassi AI. Berberine, an epiphany against cancer. Molecules. 2014;19(8):12349-67.

500. Semwal RB, Semwal DK, Combrinck S, Viljoen A. Emodin - A natural anthraquinone derivative with diverse pharmacological activities. Phytochemistry. 2021;190:112854.

501. Wei WT, Lin SZ, Liu DL, Wang ZH. The distinct mechanisms of the antitumor activity of emodin in different types of cancer. Oncol Rep. 2013;30(6):2555-62.

502. Dong X, Fu J, Yin X, Cao S, Li X, Lin L, et al. Emodin: a review of its pharmacology, toxicity and pharmacokinetics. Phytother Res. 2016;30(8):1207-18.

503. Wang KJ, Meng XY, Chen JF, Wang KY, Zhou C, Yu R, et al. Emodin induced necroptosis and inhibited glycolysis in the renal cancer cells by enhancing ROS. Oxid Med Cell Longev. 2021;2021:8840590.

504. Qu K, Shen N-y, Xu X-s, Su H-b, Wei J-c, Tai M-h, et al. Emodin induces human T cell apoptosis in vitro by ROS-mediated endoplasmic reticulum stress and mitochondrial dysfunction. Acta Pharmacologica Sinica. 2013;34(9):1217-28.

505. Su J, Yan Y, Qu J, Xue X, Liu Z, Cai H. Emodin induces apoptosis of lung cancer cells through ER stress and the TRIB3/NF-κB pathway. Oncol Rep. 2017;37(3):1565-72.

506. Smith JA. Regulation of cytokine production by the unfolded protein response; Implications for infection and autoimmunity. Front Immunol. 2018;9.

507. Kemp K, Poe C. Stressed: The unfolded protein response in T cell development, activation, and function. International Journal of Molecular Sciences. 2019;20(7):1792.

508. Wang Y, Gong J, Zeng H, Liu R, Jin B, Chen L, et al. Lipopolysaccharide activates the unfolded protein response in human periodontal ligament fibroblasts. Journal of Periodontology. 2016;87(5):e75-e81.

509. Gass JN, Jiang H-Y, Wek RC, Brewer JW. The unfolded protein response of B-lymphocytes: PERK-independent development of antibody-secreting cells. Mol Immunol. 2008;45(4):1035-43.

510. Kim HJ, Jeong JS, Kim SR, Park SY, Chae HJ, Lee YC. Inhibition of endoplasmic reticulum stress alleviates lipopolysaccharide-induced lung inflammation through modulation of NF-κB/HIF-1α signaling pathway. Scientific Reports. 2013;3(1):1142.

511. Ayaub EA, Tandon K, Padwal M, Imani J, Patel H, Dubey A, et al. IL-6 mediates ER expansion during hyperpolarization of alternatively activated macrophages. Immunol Cell Biol. 2019;97(2):203-17.

512. Hasan A, Sadiq A, Abbas A, Mughal E, Khan KM, Ali M. Isolation and synthesis of flavonols and comparison of their antioxidant activity. Natural Product Research. 2010;24(11):995-1003.

513. Ratajczak M, Kaminska D, Światły-Błaszkiewicz A, Matysiak J. Quality of dietary supplements containing plant-derived ingredients reconsidered by microbiological approach. Int J Environ Res Public Health. 2020;17(18).

514. Bratkov VM, Shkondrov AM, Zdraveva PK, Krasteva IN. Flavonoids from the genus *Astragalus*: Phytochemistry and biological activity. Pharmacogn Rev. 2016;10(19):11-32.

515. McCubrey JA, Lertpiriyapong K, Steelman LS, Abrams SL, Yang LV, Murata RM, et al. Effects of resveratrol, curcumin, berberine and other nutraceuticals on aging, cancer development, cancer stem cells and microRNAs. Aging (Albany NY). 2017;9(6):1477-536.

516. Rahimi-Madiseh M, Lorigoini Z, Zamani-Gharaghoshi H, Rafieian-Kopaei M. *Berberis vulgaris*: specifications and traditional uses. Iran J Basic Med Sci. 2017;20(5):569-87.

517. Marcheluzzo S, Faggian M, Zancato M, Peron G. Analysis of monacolins and berberine in food supplements for lipid control: An overview of products sold on the italian market. Molecules. 2021;26(8).

518. Vande Walle L, Lamkanfi M. Inflammasomes: caspase-1-activating platforms with critical roles in host defense. Frontiers in Microbiology. 2011;2.

519. Yang Y, Wang H, Kouadir M, Song H, Shi F. Recent advances in the mechanisms of NLRP3 inflammasome activation and its inhibitors. Cell Death & Disease. 2019;10(2):128.

520. Shi J, Zhao Y, Wang K, Shi X, Wang Y, Huang H, et al. Cleavage of GSDMD by inflammatory caspases determines pyroptotic cell death. Nature. 2015;526(7575):660-5.

521. Vinholes J, Rudnitskaya A, Gonçalves P, Martel F, Coimbra MA, Rocha SM. Hepatoprotection of sesquiterpenoids: A quantitative structure–activity relationship (QSAR) approach. Food Chemistry. 2014;146:78-84.

522. Koyama J, Morita I, Kobayashi N. Simultaneous determination of anthraquinones in rhubarb by high-performance liquid chromatography and capillary electrophoresis. Journal of Chromatography A. 2007;1145(1):183-9.

523. Singh O, Khanam Z, Misra N, Srivastava MK. Chamomile (*Matricaria chamomilla* L.): An overview. Pharmacogn Rev. 2011;5(9):82-95.

524. Barceloux DG. Rhubarb and xalosis (*Rheum* species). Disease-a-Month. 2009;55(6):403-11.

525. Taheri Y, Suleria HAR, Martins N, Sytar O, Beyatli A, Yeskaliyeva B, et al. Myricetin bioactive effects: moving from preclinical evidence to potential clinical applications. BMC Complement Med Ther. 2020;20(1):241.

526. Sultana B, Anwar F. Flavonols (kaempeferol, quercetin, myricetin) contents of selected fruits, vegetables and medicinal plants. Food Chemistry. 2008;108(3):879-84.

527. Orak HH, Karamać M, Amarowicz R, Orak A, Penkacik K. Genotype-related differences in the phenolic compound profile and antioxidant activity of extracts from olive (Olea europaea L.) leaves. Molecules. 2019;24(6).